The Effect of Matrix Molecular Weight on the Dispersion of Nanoclay in Unmodified High Density Polyethylene

David Chu

Thesis submitted to the faculty of the Virginia Polytechnic Institute and State University
in partial fulfillment of the requirements for the degree of

Master of Science
In
Chemical Engineering

Dr. Donald G. Baird, Committee Chair

Dr. Richey M. Davis

Dr. Aaron S. Goldstein

June 26, 2006
Blacksburg, VA

Keywords: Nanoclay, High Density Polyethylene, Molecular Weight

The Effect of Matrix Molecular Weight on the Dispersion of Nanoclay in Unmodified High Density Polyethylene

David Chu

ABSTRACT

The effect of molecular weight on the dispersion of relatively polar montmorillonite (MMT) in non polar, unmodified high density polyethylene (HDPE) was examined. Polymer layered silicate (PLS) nanocomposites were compounded using three unmodified HDPE matrices of differing molecular weight and an organically modified MMT in concentrations ranging from 2 wt% to 8 wt% via single screw extrusion. The weight average molecular weights ($\overline{M}_w$) of the HDPE matrices used in this study ranged from 87,000 g/mol to 460,000 g/mol. X-ray diffraction (XRD), mechanical testing, dynamic mechanical thermal analysis (DMTA), as well as dynamic and capillary rheometry were performed on the nanocomposites. Nanocomposites generated from the high molecular weight (HMW) HDPE matrix exhibited increased intercalation of the MMT as shown by XRD as well as greater improvements in the Young's modulus compared to nanocomposites generated from both the low (LMW) and middle molecular weight (MMW) matrices. This was attributed to higher shear stress imparted to MMT during compounding from the more viscous matrix facilitating their separation and orientation during injection molding. DMTA showed that the torsional response of the HMW nanocomposites was not as great compared to their LMW and MMW counterparts as observed from a lower percentage enhancement in the storage modulus (G') and estimated heat distortion temperature (HDT) due to anisotropy in mechanical properties. Dynamic rheology indicated that a percolated network did not exist in any of the

nanocomposites as shown by no change in the terminal behavior of G’ upon addition of clay.

Acknowledgments

The author would like to express his appreciation to Dr. Donald G. Baird for his guidance and support throughout the completion of this work both intellectually and financially. In addition, the author wishes to extend special thanks to Dr. Rick Davis and Dr. Aaron Goldstein for serving on his research committee.

The author would also like to recognize the following individuals for their additional support during his graduate studies:

- Linxia, for providing me with motivation for my work here as well as reminding me of what lies ahead in future.
- My family: Mom, Dad, Felix, Roger, and Jessie for their love during my time in Blacksburg.
- Dr. Garth Wilkes for useful discussions on XRD as well as enabling SEC work for my thesis.
- Lab Mates: Wade for showing me how to use the Instron, extruder, injection molder, and DMTA experiments, Aaron for providing training (and repair) on the RMS, Quang for performing XRD work for me, Matt for training me on the capillary rheometer, Desmond, Chris, Chris, Dave, Brent, Gregorio, Myoungbae, Jianhua, Joe, and Travis for providing the author with much entertainment during his short time in the lab.
- Chris, Lindsay, Jason, Sukit, Joe, and Will for being good friends during my stay here.

- Department of Chemical Engineering Staff: Chris Moore, Diane Cannaday, Jane Price, Riley Chan, and Mike Vaught for all the assistance needed to facilitate successful completion of my Masters work.

Original Contributions

The following are considered to be significant original contributions of this research:

1. A HMW, high viscosity polymer matrix positively influences the degree of dispersion in a polymer/layered silicate nanocomposite. This was demonstrated by increased separation of the galleries of montmorillonite in the 8 wt% HMW nanocomposite. It was concluded that a polymer matrix with a high shear viscosity is able to impart higher levels of shear stress onto aggregates of montmorillonite during melt compounding in a single screw extruder and injection molder enabling more uniform dispersion of the nanoclay particles. Consequently, mechanical properties are significantly enhanced for the nanocomposites generated from the HMW HDPE matrix.
2. Significant enhancement of mechanical properties such as the Young's Modulus has been shown to occur *without* the use of a compatibilizer between the hydrophobic high density polyethylene and hydrophilic polyethylene, especially for HMW HDPE. This is again attributed to the high shear viscosity of the HMW HDPE matrix leading to greater dispersion of the nanoclay particles within the polymer matrix as well as inducing orientation of the clay particles during injection molding leading to increased property enhancement in the flow direction of the test specimens.
3. The use of a single screw extruder combined with injection molding has been demonstrated as a viable option for producing intercalated polymer/layered silicate nanocomposites. Previous work has shown only the use of twin screw extruders and melt blenders in producing these nanocomposites. The shear stress produced in a

single screw extruder, while not as large as that found in a twin screw extruder, appears to be sufficient for intercalating HDPE within the galleries of montmorillonite clay. This was observed especially for the HMW HDPE due to its increased shear viscosity enabling increased separation of nanoclay platelets relative to the LMW and MMW nanocomposites at constant processing conditions.

Format of Thesis

This thesis is written in journal format. Chapter 3 is a self-contained paper that separately describes the experiments, results and conclusions pertinent to that chapter. With the exception of the literature review, the figures and tables are inserted after the reference section of each chapter.

Attribution

The co-author for the paper which comprises Chapter 3 of this thesis, Dr. Donald G. Baird, is the research advisor of David Chu who provided much guidance throughout the completion of this work. Dr. Donald G. Baird is the Henry C. Wyatt Professor of Chemical Engineering at the Virginia Polytechnic Institute and State University.

Table of Contents

List of Figures

List of Tables

1.0 Introduction

Preparation of polymer/layered silicate nanocomposites (PLS) via melt blending is an economically friendly method of generating materials with improved strength and stiffness [1]. However, property enhancements obtained by this method are not as dramatic as those seen from PLS nanocomposites generated by in-situ polymerization due to less homogeneity in the dispersion of the clay particles within the polymer matrix [1]. In the in-situ polymerization method, a monomer solution and nanoclay are swollen together and the polymerization reaction takes place directly in between the sheets of clay, while melt blending relies on polymer chains penetrating in between the clay platelets typically with the aid of shear [1].

Much academic as well as industrial research has been focused in the area of the preparation of (PLS) nanocomposites thanks in large part to work done by the Toyota research group in Japan who synthesized nylon 6/montmorillonite (MMT) nanocomposites via the in-situ polymerization technique [2]. A 55% increase in the tensile modulus and 87°C increase in the heat distortion temperature were reported [2]. However, the in-situ polymerization technique as well as solution blending technique, which utilize organic solvents to swell the MMT, are both environmentally as well as economically unfriendly due to the use and cost of organic solvents and chemical reagents. Vaia et al. [3] were among the first researchers who reported the possibility to generate these nanocomposites by simple melt compounding and, thus, providing a "green" approach to forming these materials. Past work on PLS nanocomposites included a wide variety of polymers including polyethylene, polypropylene, polyimide, polystyrene, polycarbonate, and a polystyrene/polyisoprene block copolymer [4-24].

Filling polymer matrices with these nanoclays has been shown to yield materials with dramatically increased mechanical [25-43], gas barrier [45, 46], and thermal stability properties [47, 48] with low loadings of clay (i.e less than 5 wt%).

The main reason for these marked improvements stem from the large aspect ratio of montmorillonite (MMT). Each individual layer of clay has a thickness on the order of 1 nanometer (nm) with lengths ranging from 100 nm to 300 nm [1, 49]. The high aspect ratio leads to a high contact surface area and, thus, physical interactions between the polymer and layered silicates with only a small concentration of clay. However, because the layered silicates typically exist as aggregates due to attractive van der Waals forces [50], the contact surface area available and, thus, improvements in physical properties are not as high as they could possibly be. Achieving a nanocomposite with an exfoliated morphology in which each individual layered silicate has been separated from its initial stack and dispersed uniformly throughout a given polymer matrix is the key to generating the full potential of to enhance mechanical, thermal, and barrier properties.

There are three main influences thought to be responsible for determining the amount of exfoliation that is able to be achieved when making PLS nanocomposites. First, the attractive interactions between the polymer matrix and the layered silicates determine, in large part, the degree of miscibility between the two separate phases. Layered silicates are naturally hydrophilic while many polymers such as polyolefins are hydrophobic and, thus, the surface energies between the two materials can be vastly different prohibiting any significant degree of dispersion of nanoclay within the polymer. Modification of layered silicates via ion exchange reactions through which quaternary alkyl ammonium cations replace the existing cations (Ca^{+}, Na^{+}, Li^{+} etc.) residing in the

interlayer of the silicates help to make the layered silicates more organophilic. Non-polar polymers such as polyolefins can also be modified to where the polar maleic anhydride is grafted onto the backbone of polymers such as various polyethylenes or polypropylenes [51-54] increasing the hydrophilicity of the polymer matrix.

The next two factors which influence the level of exfoliation in a PLS nanocomposite both depend on the molecular weight of the polymer matrix, but in opposing manners. The size of a polymer chain increases as the molecular weight of the polymer sample increases. Larger polymers have more difficulty in penetrating the interlayer gap of the layered silicates whose distance from each other typically range from 15 Å to 35 Å [55]. Thus, increased molecular weight is seen to have a negative influence on exfoliating the clays in this respect as shown previously [56-63]. On the other hand, with increasing polymer molecular weight, the viscosity of the material increases as well. Increased viscosity leads to an increased amount of shear force available to be exerted by the polymer matrix onto the aggregates of nanoclay and assists in separating each individual clay platelet apart from one another through what has been postulated to be a "peeling" mechanism [64, 65].

Much work has been performed on the effect that varying the molecular weight of either a polymer matrix or a compatibilizer has on the dispersion of nanoclays within a given polymer [56-65]. A variety of polymers have been studied ranging from relatively non-polar polyolefins such as polyisoprene to polar polyamides such as nylon 6 which contain many sites for hydrogen bonding to occur. However, mixed results have been found in the literature concerning the role matrix molecular weight plays [56-65]. There are benefits to using both a low molecular weight polymer as there are in using a high

molecular weight polymer, and the extent to which these two competing factors influence the degree of clay dispersion and enhancement in mechanical properties remains unclear. Only in Kaempfer's [64] study of syndiotactic polypropylene/fluorohectorite nanocomposites and Fornes' [65] examination of nylon 6/MMT nanocomposites was it found that increasing the molecular weight of the matrix (or of maleated polypropylene compatibilizer in Kaempfer's case) increased the degree of exfoliation of the nanocomposites.

It is the purpose of this work to determine if nanoclays can be exfoliated in non-polar, unmodified HDPE of various molecular weights via single screw extrusion. The molecular weights of the HDPE used are approximately 87,000 g/mol, 155,000 g/mol, and 460,000 g/mol. This range of molecular weights is as large if not larger than has been used in past work concerning matrix molecular weight on the dispersion of nanoclays. The degree of exfoliation or intercalation will be assessed by x-ray diffraction. The change in mechanical and rheological properties as a function of matrix molecular weight and MMT concentration will be examined as well in order to assess the tradeoff between property enhancement and processability.

1.1 References

1. Ray, Suprakas S. and Okamoto, Masami, "Polymer/layered silicate nanocomposites: a review from preparation to processing," *Progress in Polymer Science* **28** (2003), pp.1539-1641.

2. A. Okada, M. Kawasumi, A. Usuki, Y. Kojima, T. Kurauchi, O. Kamigaito. Polymer Based Molecular Composites, D.W. Schaefer, J.E. Mark, MRS Symposium Proceedings, Pittsburgh **171** (1990) pp 45-50

3. R.A. Vaia, H. Ishii, E.P. Gianelis, *Chem. Mater*. **5** (1993) pp. 1694-1696

4. A. Usuki, M. Kato, A. Okada, T. Kurauchi, *J. Applied Polymer Sci.*, **63** (1997), pp 137

5. M. Kawasumi, N. Hasegawa, M. Kato, A. Okada, A. Usuki, *Macromolecule*s, **30** (1997), pp 6333-6338

6. K. H. Wang, M.H. Choi, C.S. Koo, Y.S. Choi, I.J. Chung, *Polymer*, **42** (2001), pp 9819-9826

7. Y.T Lim, O.O. Park, *Rheologica Acta,* **40** (2001) pp 220-229

8. T.G. Gopakumar, J.A. Lee, M. Kontopoulou, J.S. Parent, *Polymer*, **43** (2002) pp 5483-5491

9. S. G. Hatzikiriakos, N. Rathod, E.B. Muliawan, *Polym. Eng. Sci*. **45** (2005) pp 1098-1107

10. K.H Wang, M.H. Choi, C.M. Koo, M. Xu, I.J. Chung, M.C. Jang, S.W. Cho i, H.H. Song, *J. Applied Polymer Sci. Part B: Polym. Phys*., **40** (2002) pp 1454-1463

11. P. Mederic, T. Razafinimaro, T. Aubry, M Moan, M.H. Klopffer, *Macromol. Symp*., **221** (2005) pp 75-84

12. Y.T. Lim, O.O. Park, *Rheol. Acta,* **40** (2001) pp 220-229

13. J.A. Lee, M. Kontopoulou, J.S. Parent, *Polymer* **45** (2004) 6595-6600

14. W. Lertwimolnun, B. Vergnes, *Polymer* **46** (2005) pp 3462-3471

15. G. Galgali, C. Ramesh, A. Lele *Macromolecules* **34** (2001) pp 852-858

16. L. Zhu, M. Xanthos, *J. App. Polym. Sci* **93** (2004) pp 1891-1899

17. M.J. Solomon, A.S Almusallam, K.F. Seefeldt, A. Somwangthanaroj, P. Varadan, *Macromolecules* **34** (2001) pp 1854-1872

18. V.E. Yudin, G.M. Divoux, J.U. Otaigbe, V.M. Svetlichnyi, *Polymer* **46** (2005) pp 10866-10872

19. T.H. Kim, S.T. Lim, C.H. Lee, H.J. Choi, M.S. Jhon, *J. App. Polym. Sci*. **87** (2003) pp 2106-2112

20. R. Qi, X. Jin, J. Nie, W. Yu, C. Zhou, *J. App. Polym. Sci* **97** (2005) pp 201-207

21. Y. Zhong, Z. Zhu, S-Q. Wang, *Polymer* **46** (2005) pp 3006-3013

22. A.J. Hsieh, P. Moy, F.L. Beyer, P. Madison, E. Napadensky, *Polym. Eng. Sci* **44** (2004) pp 825-837

23. K.M. Lee, C.D. Han, *Polymer* **44** (2003) pp 4573-4588

24. J. Ren, A.S. Silva, R. Krishnamoorti, *Macromolecules* **33** (2000) pp 3739-3746

25. A. Dasari, Z-Z. Yu, Y-W. Mai, G-H. Hu, J. Varlet, *Composites Sci. Tech*. **65** (2005) 2314-2328

26. W.S. Chow, Z.A. Mohd, U.S. Ishiaku, J. Karger-Kocsis, A.A. Apostolov, *J. Appl. Polym. Sci*. **91** (2004) pp 175-189

27. M. Yuan, A. Winardi, S. Gong, L-S. Turng, *Polym. Eng. Sci*. **45** (2005) pp 773-788

28. T.D. Fornes, P.J. Yoon, D.R. Paul, *Polymer* **44** (2003) pp 7545-7556

29. T.D. Fornes, D.L. Hunter, D.R. Paul, *Polymer* **45** (2004) pp 2321-2331

30. T.D. Fornes, P.J. Yoon, D.L. Hunter, H. Keskkula, D.R. Paul, *Polymer* **43** (2002) pp 5915-5933

31. T.D. Fornes, D.L. Hunter, D.R. Paul, *Macromolecule*s **37** (2004) pp 1793-1798

32. L. Chen, S-C. Wong, S. Pisharath, *J. Appl. Polym. S*ci. **88** (2003) pp 3298-3305

33. G. Galgali, S. Agarwal, A. Lele, *Polymer* **45** (2004) pp 6059-6069

34. Y.T. Vu, G.S. Rajan, J.E. Mark, C.L. Myers, *Polym. Int*. **53** (2004) pp 1071-1077

35. A. Leuteritz, D. Pospiech, B. Kretzschmar, M. Willeke, D. Jehnichen, U. Jentzsch, K. Grundke, A. Janke, *Macromol. Symp*. **221** (2005) pp 53-61

36. A.J. Hsieh, P. Moy, F.L. Beyer, P. Madison, E. Napadensky, *Polym. Eng. Sci* **44** (2004) pp 825-837

37. M.A. Osman, J.E.P. Rupp, U.W. Sutter, *Polymer* **46** (2005) pp 1653-1660

38. M. Mehrabzadeh, M.R. Kamal, *Polym. Eng. Sci*, **44** (2004) pp 1152-1161

39. T.G. Gopakumar, J.A. Lee, M. Kontopoulou, J.S. Parent, *Polymer* **43** (2002) pp 5483-5491

40. G. Liang, J. Xu, S. Bao, W. Xu, *J. Applied Polymer Sci.* **91** (2004) pp 3974-3980

41. J. Heinemann, P. Reichert, R. Thomann, R. Mulhaupt, *Macromol. Rapid Commun*. **20** (1999) pp 423-430

42. J. Morawiec, A. Pawlak, M. Slouf, A. Galeski, E. Piorkowska, N. Krasnikowa, *European Polymer Journal*, **41** (2005) pp 1115-1122

43. Y. Zhong, D. De Kee, *Polym. Eng. Sci*. **45** (2005) pp 469-477

44. E.C. Lee, D.F. Mielewski, R.J. Baird, *Polym. Eng. Sci* **44** (2004) pp 1773-1782

45. M.A. Osman, V. Mittal, M. Morbidelli, U.W. Suter, *Macromolecules* **36** (2003) pp 9851-9858

46. M.A. Osman, J.E.P Rupp, U.W. Sutter, *J. Mat. Chem*. **15** (2005) pp 1298-1304

47. M. Valera-Zaragoza, E. Ramirez-Vargas, F.J. Melellin-Rodriquez, B.M. Huerta-Martinez, *Polym. Degrad. Stab*. (2005) pp 1-7

48. J.W. Gilman, C.L. Jackson, A.B. Morgan, R. Harris Jr., *Chem. Mater* **12** (2000) pp 1866-1873

49. T. Pinnavaia and G. Beall, "Polymer-Clay Nanocomposites", John Wiley & Sons, Ltd., New York (2000)

50. M. Zanetti, S. Lomakin, G. Camino, Polymer layered silicate nanocomposites. *Macromol. Mater. Eng.* **279** (2000) p. 1-9

51. A. Usuki, M. Kato, A. Okada, T. Kurauchi, *J. Applied Polymer Sci.*, **63** (1997), pp 137-138

52. M. Kawasumi, N. Hasegawa, M. Kato, A. Okada, A. Usuki, *Macromolecule*s, **30** (20) (1997), pp 6333

53. K. H. Wang, M.H. Choi, C.S. Koo, Y.S. Choi, I.J. Chung, *Polymer*, **42** (2001), pp 9819

54. Y.T Lim, O.O. Park, *Rheologica Acta*, **40** (2001) pp 220-229

55. Southern Clay Products Inc., Technical Data Sheets, www.nanoclay.com

56. Y. Zhong, D. De Kee, *Polym. Eng. Sci*. **45** (2005) pp 469-477

57. E.C. Lee, D.F. Mielewski, R.J. Baird, *Polym. Eng. Sci* **44** (2004) pp 1773-1782

58. R.A. Vaia, K.D. Jandt, E.J. Kramer, E.P. Giannelis, *Macromolecules* **28** (1995) pp 8080-8085

59. Z. Shen, G.P. Simon, Y. Cheng, *Polym. Eng. Sci*. **42** (2002) pp 2369-2382

60. H.S. Jeon, J.K. Rameshwaram, *Computational Methods in Materials Characterisation*, Edited by A.A. Mammoli, C.A. Brebbia, Computational Mechanics, Boston, MA (2004) pp 255-263

61. S. Tanoue, L.A. Utracki, A. Garcia-Rejon, J. Tatibouet, M.R. Kamal, *Polym. Eng. Sci*, **45** (2005) pp 827-837

62. S. Tanoue, L.A. Utracki, A. Garcia-Rejon, P. Sammut, M-T. Ton-That, I. Pesneau, M.R. Kamal, J.Lyngaae-Jorgensen, *Polym. Eng. Sci* **44** (2004) pp 1061-1076

63. S. Tanoue, L.A. Utracki, A. Garcia-Rejon, J. Tatibouet, K.C. Cole, M.R. Kamal, *Polym. Eng. Sci* **44** (2004) pp 1046-1060

64. D. Kaempfer, R. Thomann, R. Mulhaupt, *Polymer* **43** (2002) pp 2909-2916

65. T.D. Fornes, P.J. Yoon, H.Keskkula, D.R. Paul, *Polymer* **42** (2001) pp 9929-9940

2.0 Literature Review

2.1 Structure and Properties of Layered Silicates

The most commonly used types of layered silicates in the formation of polymer/layered silicate (PLS) nanocomposites belong to the 2:1 phyllosilicate family. Structurally, the crystals consist of two tetrahedrally coordinated silicon atoms fused to an edge shared octahedral sheet of either aluminum or magnesium hydroxide [1]. Layer thickness is on the order of 1 nanometer (nm) while the lateral dimension can vary from 30 nm to 200 nm [1, 2]. Montmorillonite (MMT) is the most common type of layered silicate currently used in research, while mica, talc, hectorite and saponite are examples of lesser used 2:1 phyllosilicates [3, 4]. These clays typically exist as stacks of individual silicate layers held together by van der Waals forces resulting in gap spacings on the order of 1 nm [5]. These gaps are also referred to as the interlayer spacing or gallery. Electric charges can exist in these galleries in the form of cations residing in the space between the layers leading to the ability of the layered silicates such as MMT to be modified as needed through what are known as ion exchange reactions. Talc is an example of a phyllosilicate composed of electrically neutral silicate layers and empty galleries while mica contains a negative charge on its layers which is electrically neutralized by mainly potassium cations residing in the interlayer [6].

For the case of MMT, an excess of negative charge is present on the surface of the silicate layers resulting from isomorphic substitution. For example, Al^{3+} is replaced by Mg^{2+} or Mg^{2+} is replaced by Li^{+} [1]. As with mica, cations must reside in the interlayer to neutralize this charge. For MMT these cations include Ca^{2+}, Mg^{2+}, K^{+}, Na^{+}, etc. A characteristic parameter known as the cation exchange capacity (CEC) is often used to

describe this type of layered silicate. It is a measure of the surface charge on the silicate and is expressed as mequiv/100 grams of clay. The chemical formula and values of the CEC for MMT, hectorite, and saponite are given in Table 2.1.

2.2 Organically Modified Layered Silicate (OMLS)

For successful nanocomposite formation, the dispersion of the individual silicate layers within a chosen polymer matrix must be complete. Accomplishing this goal requires that the individual layered silicates residing in a stack as described above be "peeled" apart and distributed throughout the polymer matrix. However, since MMT is hydrophilic, miscibility with organic materials such as polymers is difficult to achieve without modifying MMT. Ion exchange reactions are utilized to render the layered silicates organophilic. The initial cations residing in the galleries of the layered silicates, namely Ca^{2+}, Mg^{2+}, K^{+}, Na^{+}, etc. are replaced by cationic surfactants usually in the form of quaternary alkylammonium cations [1]. The quaternary alkylammonium cations usually have at least one tallow or hydrogenated tallow group attached to it which are long alkyl chains derived from animal fat composed of roughly 18 carbon atoms [7]. Typically this process involves dispersing the clay in hot water at concentrations of approximately 1% [8]. A second solution is then added which contains the required amount of cation to be exchanged which is based on the CEC described above. The alkylammonium cations act to lower the surface energy of the layered silicate and enhance wetting with the polymer matrix [1]. Increased gallery spacings are also obtained due to the length associated with the tallow groups. It is this long alkyl chain of tallow which makes the layered silicate organophilic and thus promotes dispersion throughout

the polymer matrix. Representative quaternary alkylammonium salt modifiers are shown in Figure 2.1.

2.3 Nanocomposite Morphology

Three distinct arrangements of the layered silicates may exist in a polymer matrix depending on the degree of interfacial attractions between the polymer and clay as shown in Figure 2.2. First, there are intercalated composites which occur when the polymer chains are inserted in the galleries of the layered silicate in a regular repeating fashion. Next, there are flocculated nanocomposites. These occur when intercalated layered silicates are pulled together by intermolecular attractive forces at the hydroxylated edges of the silicate layers. Lastly there are exfoliated structures in which each individual silicate layer is separated and dispersed throughout the polymer matrix. The clay content required to achieve an exfoliated structure is usually less than the intercalated nanocomposites [1]. An exfoliated morphology is the most desirable as it provides the most contact surface area available for interactions between the layered silicate and polymer and offers optimum property improvements [9].

2.4 Current Methods for Nanocomposite Formation

Three methods are most commonly used for incorporating polymer chains between layers of silicate. First, there is intercalation of polymer from solution. In this method a solvent is chosen which will dissolve the polymer and swell the silicate layers. The clay is initially swollen in the solvent and then the polymer is added and displaces the solvent in the clay galleries leading to an intercalated structure [1]. High density polyethylene (HDPE) has been intercalated by this method using xylene and benzonitrile

Table 2.1. Summary of Various Clay Properties.

2:1 Phyllosilicates	Chemical Formula	CEC (meq/100g clay)	Particle Length (nm)
Montmorillonite	$Mx(Al_{4-x}Mg_x)Si_8O_{20}(OH)_4$	110	100 – 150
Hectorite	$Mx(Mg_{6-x}Li_x)Si_8O_{20}(OH)_4$	120	200 – 300
Saponite	$Mx(Si_{8-x}Al_x)Si_8O_{20}(OH)_4$	87	50 - 60

M, monovalent cation; x, degree of isomorphous substitution (between 0.5 and 1.3). Adapted from Ray et al. [1].

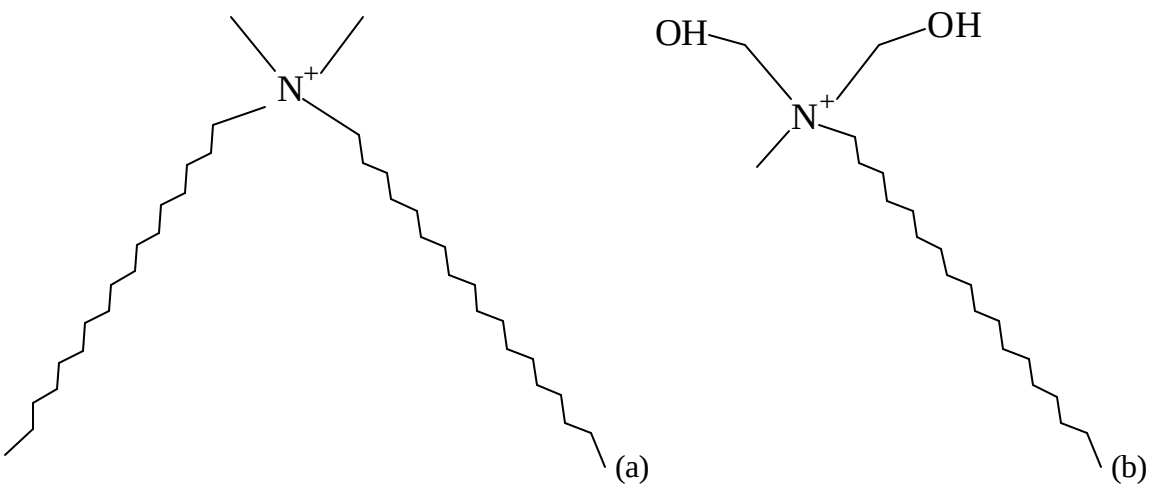

Figure 2.1. Structure of quaternary alkylammonium salt: (a) dimethyl, dihydrogenated tallow quaternary alkylammonium cation, (b) methyl, tallow, bis-2-hydroxyethyl alkylammonium cation.

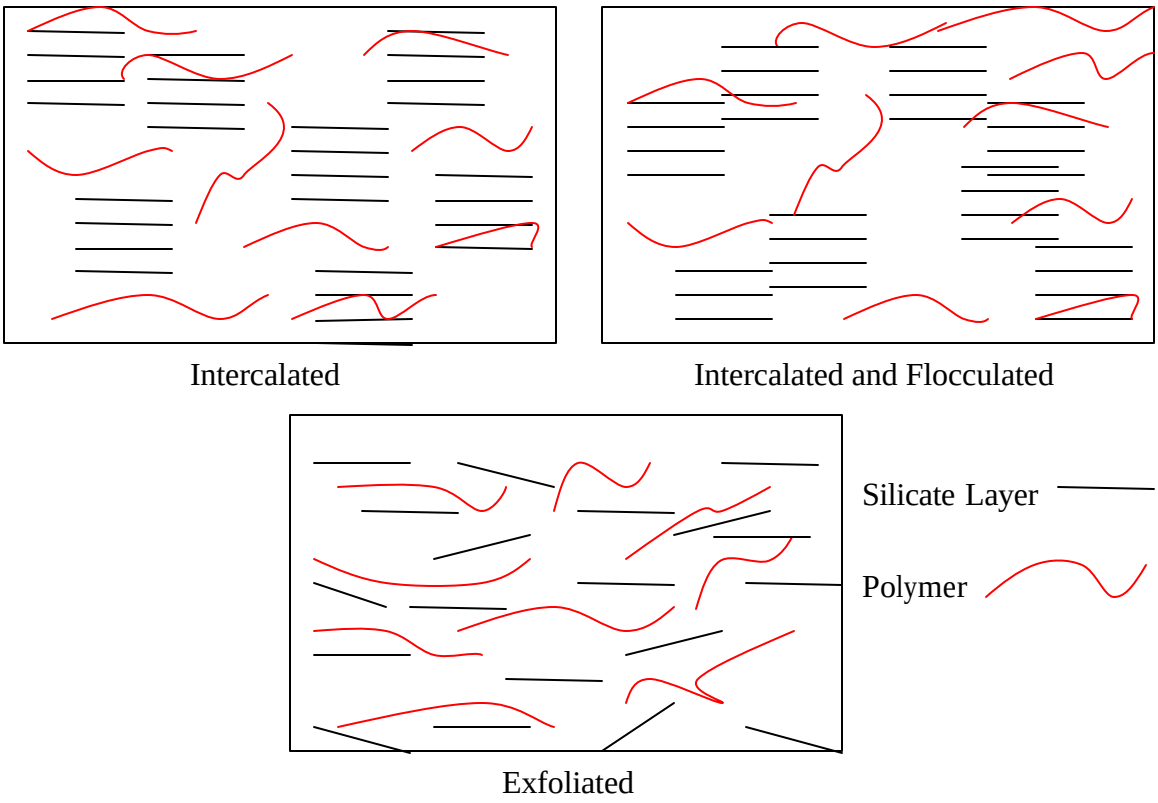

Figure 2.2. Schematic of three types of nanocomposite morphologies.

as solvents [10]. Second, there is the in situ polymerization method. Here a monomer or monomer solution is used to swell the layered silicates. Polymerization is then initiated by an energy input in the form of heat or radiation or a suitable reagent. The reaction initiator can either be added in separately or can already exist in the galleries of the layered silicates via ion exchange reaction [1]. PLS nanocomposite is obtained upon the removal of the solvent, either by solvent evaporation or polymer precipitation [11-12]. Alexandre et al. [13] used this technique to synthesize polyethylene/hectorite nanocomposites whose Young's modulus showed an increase of 259% (2,480 MPa) for an 11.4 wt% clay sample over its corresponding unfilled matrix (690 MPa). The drawbacks in these two previously mentioned methods are the requirement of suitable monomer/solvent or polymer solvent pairs and the high costs associated with the solvents, their disposal, and their impact on the environment. Third, melt intercalation involves melting a mixture of polymer and clay and applying some shear force usually in the form of a blender or extruder. Melt intercalation offers several advantages to both solvent intercalation and in situ polymerization. There is no need for chemical solvents or reagents in this process and, thus, it is the most environmentally friendly process. Also, melt intercalation utilizes commonly available polymer processing equipment such as an extruder facilitating easier adoption into present research labs and industry. However, it has been shown that melt intercalation does not give improvements in tensile properties comparable to in-situ polymerization. An 85.5% increase in Young's modulus was observed for 3.4 wt% clay loading for a nanocomposite synthesized via in-situ polymerization [13] compared to only a 41% increase in modulus obtained via melt

intercalation using a twin-screw extruder for a 3.5 wt% clay loading as shown by Kato et al. [14]

2.5 Characterization Methods

In forming PLS nanocomposites achieving an exfoliated morphology is regarded as the end goal as it is this state which provides the greatest improvements in physical properties. X-ray diffraction (XRD) analysis and transmission electron microscopy (TEM) are the two methods that have been used to typically establish the structure of nanocomposites. Due to its ease of use and wide availability XRD is most commonly used to probe the nanocomposite structure. The nanocomposite structure, namely intercalated or exfoliated, may be identified by monitoring the position, shape, and intensity of the basal reflections from the distributed silicate.

The XRD spectrum of an immiscible system is exemplified when the distance between the interlayers of the clay galleries has not changed from its initial state prior to synthesizing the nanocomposite. The mean interlayer spacing, d, between silicate layers is calculated by Bragg's Law given by

$$d = \frac{l}{2\sin q} \tag{1}$$

where l is the wavelength of the x-ray used and q is half the diffraction angle. An intercalated system occurs when the peak of the spectrum has broadened and shifted to the left indicating an increase in interlayer spacing of the clay. As seen in Equation 1, a decrease in the angle q corresponds to an increase in the interlayer spacing of the clay. The exfoliated nanocomposite shows the complete disappearance of the peak

corresponding to the basal reflection indicating a loss of order within the nanocomposite due to the separation of the individual clay platelets.

XRD can offer a convenient method to determine the interlayer spacing of the silicate layers in the original layered silicates and in the intercalated nanocomposites (1-4 nm), but little can be concluded about the spatial distribution of the silicate layers [16]. Additionally, because some layered silicates initially do not exhibit well-defined basal reflections, peak broadening and intensity decreases are very difficult to study systematically. Thus, conclusions based solely on XRD patterns are only tentative when concerning the mechanism of nanocomposites formation and their structure. To complete the results provided by XRD, TEM can be used. TEM allows a qualitative understanding of the internal structure, spatial distribution of the various phases, and views of the defect structure through direct visualization [16]. Together, TEM and XRD are essential tools for evaluating nanocomposite structure [17]. TEM is time-intensive, and gives only qualitative information on a localized portion of the sample analyzed instead of the entire sample, while low-angle peaks in XRD allow quantification of changes in layer spacing. Occasionally, small angle x-ray scattering (SAXS) can also be used to characterize structure of nanocomposites. SAXS is useful when layer spacings exceed 6-7 nm in intercalated nanocomposites or when the layers become relatively disordered in exfoliated nanocomposites.

2.6 Rheology of Polymer/Layered Silicate Nanocomposite Systems

2.6.1 Small Amplitude Oscillatory Flow

Besides XRD and TEM, rheology can and has been used to assess the degree of exfoliation in PLS nanocomposites including polypropylene [18-21], polyimide [22],

polystyrene [23-25], polycarbonate [26], and polystyrene/polyisoprene block copolymers [27, 28]. Specifically, small amplitude oscillatory flow as applied by a rotational rheometer in which a polymer sample is subjected to a periodic deformation in the form of a sinusoidal strain can be used to find two characteristic parameters, namely the complex viscosity ($|h^*|$) and the storage modulus (G'). When a nanocomposite exhibits exfoliation, the complex viscosity shows a stronger non-Newtonian, shear thinning slope in the lower frequency region of oscillation when compared to the complex viscosity of the neat polymer. G' of an exfoliated PLS nanocomposite shows what is often referred to as a "tail" or flattening plateau in the lower frequency region as opposed to being directly proportional to the square of the oscillation frequency, i.e. $G' \propto w^2$, which is normally observed in polymers with liquid-like behavior [29]. These characteristic changes are attributed to the formation of a solid network within the polymer by interacting with the layered silicates. This behavior can be elucidated by small amplitude oscillatory flow because the deformation or strain is so small that the solid network remains intact during the test leading to a plateau in G' [29].

2.6.2 Polyethylene

Studies involving polyethylene typically utilize samples that have been grafted with maleic anhydride to increase the polar character and thus hydrophilicity of non-polar polyethylene. Maleic anhydride containing polymers show improved compatibility, i.e. increased dispersion, with layered silicates [30-33]. In a study by Gopakumar et al. [34], maleated polyethylene nanocomposites prepared by melt compounding showed a larger non-Newtonian slope in the lower frequency region of $|h^*|$ compared to unmodified high density polyethylene. Two types of clay were used: unmodified montmorillonite clay

with the Na^+ ion remaining unexchanged in the interlayer of the silicates and a modified montmorillonite clay ion-exchanged with a dimethyl, distearyl ammonium salt. The molecular weight of the HDPE used was not given. The Newtonian plateau began to disappear at clay loadings of 5 weight (wt) % and showed the greatest viscosity enhancement at a clay level of 10 wt % from approximately 3,500 Pa*s for the unfilled maleated HDPE to 50,000 Pa*s at an oscillation frequency of 0.04 rad/sec for the 10 wt% nanocomposite. They attributed this behavior to the formation of weak structures that remain intact at very low oscillation frequencies. The level of exfoliation of the maleated HDPE/dimethyldistearylammonium montmorillonite nanocomposite as determined by x-ray diffraction showed that the characteristic peaks associated with the interlayer distance between silicate layers disappeared at levels below 5 wt %, but remained for the nanocomposite containing 10 wt % clay indicating incomplete exfoliation. It was also shown by x-ray diffraction that unmodified montmorillonite could not be exfoliated to any degree in either unmodified or maleated HDPE. Thus it was concluded that chemical modification of HDPE was essential for producing exfoliated nanocomposites and that even with compatibilized HDPE, there was a limit to the amount of clay that could be incorporated, specifically below 10 wt %.

Even though $|h^*|$ showed non-Newtonian, shear thinning behavior in the terminal region for the 10 wt% nanocomposite made from modified MMT the XRD data showed that there was no appreciable change in the interlayer spacing of the clay. The authors attributed the rheological behavior presented above to the formation a weak physical network between exfoliated clay platelets, but XRD analysis shows that conclusions based solely on rheology are incomplete.

Hatzikiriakos et al. [35] performed dynamic oscillatory flow studies on an unmodified Zeigler-Natta linear low density polyethylene (LLDPE) and found that a melt blended PLS nanocomposite containing 0.1 wt% MMT clay modified with a dimethyl, distearyl ammonium cation had $|h^*|$, G' and G" values that were less than the neat LLDPE throughout the entire frequency range of 0.1 rad/sec to 700 rad/sec. Specifically at w = 0.1 rad/sec, $|h^*|$=21,000 Pa*s for unfilled LLDPE and 19,000 Pa*s for 0.1 wt% filled LLDPE, G'=200 Pa for both filled and 0.1 wt% filled LLDPE, and G"=2,000 Pa and 1,900 Pa for the unfilled and 0.1 wt% filled LLDPE, respectively. This unconventional behavior was attributed to the high aspect ratio of the clay which was given to be greater than 500. The authors reasoned that the high aspect ratio of the clay may have caused a reduction in the entanglement density of the polymer by disrupting the entanglement network of the polymer chains. Also noted was that such small amounts of filler typically do not affect shear rheological properties of polymers. The authors concluded that the nanoclay could be easily incorporated into the LLDPE matrix, but no XRD characterization was performed so a quantitative measure of the MMT incorporation could not be made.

Wang et al. [36] studied melt intercalated nanocomposites composed of maleated LLDPE with two clays with different aspect ratios – montmorillonite with aspect ratio between 100-200 and laponite with aspect ratio between 20-30. Both clays were organically modified with dimethyl, dihydrogenated tallow and the clay content was varied from 0 wt % to 5 wt % for all composites formed. The G' of both composites increased with clay loading indicating the formation of a solid-like network, but the higher aspect ratio montmorillonite nanocomposite showed a smaller terminal slope, i.e.

G' $\propto w^{a}$, where a < 2, or a flat plateau in the low frequency region than the lower aspect ratio laponite. G' values at 0.01 rad/sec and 210°C were shown to be 6,500 Pa and 425 Pa for 3 vol% MMT and laponite nanocomposites, respectively, compared to 10 Pa for the unfilled LLDPE. This difference was attributed to the increased contact surface area between the montmorillonite and polymer matrix and greater interfacial adhesion. $|h^*|$ was also increased throughout the entire frequency region tested from 0.01 rad/sec to 100 rad/sec for all nanocomposites relative to the neat matrix. Specifically at 0.01 rad/sec and 210°C, $|h^*|$ was equal to 700,000 Pa*s and 85,000 Pa*s for the 3 vol% MMT and laponite nanocomposites, respectively, compared to 7,000 Pa*s for the unfilled LLDPE. The large increases in both G' and $|h^*|$ were attributed to the complete separation of the individual clay platelets and the formation of a solid-like network as shown by XRD which confirmed the existence of exfoliated nanocomposites for both clays used at 3 vol% by the disappearance of the characteristic basal reflections of the clays. Thus, there was satisfactory evidence from both rheology and XRD to support the authors claims of achieving exfoliation of the clay for the maleated LLDPE.

In yet another study involving maleated LLDPE, Mederic et al. [37] prepared, through melt mixing, a nanocomposite containing 2.5 vol% clay, 13 vol% maleated polyethylene and 84.5 vol% LLDPE. The clay used was MMT modified with a dimethyl, dihydrogenated tallow ammonium cation and the LLDPE had a weight average molecular weight of 140,000 g/mol. Higher values of G' were obtained over the entire frequency range tested from 0.02 rad/sec to 100 rad/sec with values increasing with frequency from 800 Pa to 15,000 Pa compared to a range of 5 Pa to 15,000 Pa for the unfilled matrix. A solid-like response in the low frequency region was also observed in agreement with x-

ray diffraction results which indicate an exfoliated morphology due to the complete disappearance of the basal reflection peak of the MMT in the nanocomposite. Thus, the behavior of G' was correctly attributed to the formation of a percolated network of individual clay platelets throughout LLDPE rather than being due to clay aggregates in contact with each other which could also lead to similar rheological behavior.

Lim et al. [33] studied melt blended maleic anhydride grafted polyethylene nanocomposites with clay loadings ranging from 3-10 wt %. Montmorillonite was used which was modified with dimethyl, dihydrogenated tallow ammonium cation and the weight average molecular weight of the maleated polyethylene used was given to be 212,000 g/mol. They found solid-like behavior in G' for all clay levels used. This was attributed to the polar interaction between the layered silicates and maleated polyethylene. For a frequency range of 0.03 rad/sec to 300 rad/sec, G' increased from 50 Pa to 60,000 Pa for the unfilled nanocomposite compared to a G' range from 900 Pa to 80,000 Pa for the 5 wt% clay loading for which XRD data was presented. Exfoliation was confirmed via x-ray diffraction as shown by the complete disappearance of the diffraction peak of MMT in the 5 wt% composite.

Small amplitude oscillatory measurements were also made on a 10 wt % clay sample of maleated polyethylene *after* the application of a large amplitude oscillatory shear (LAOS) with a strain percent of 120% and frequency of 1 rad/s. The intent of applying LAOS to the 10 wt % sample was to induce orientation or alignment of the high aspect ratio layered silicates within the polymer matrix and measure G' in small amplitude oscillatory flow to discern any changes in the elasticity of the nanocomposite. It was found that G' for the pre-sheared sample decreased throughout the entire

frequency range tested and that this decrease was not as dramatic as that found for pre-sheared polystyrene nanocomposites that exhibited little to no exfoliation as shown by x-ray diffraction. Specifically, G' started at 10,000 Pa and increased to 200,000 Pa with increasing frequency for the unsheared 10 wt% PE sample compared to a G' range of 9,000 Pa to 65,000 Pa for the pre-sheared 10 wt% PE sample. The authors attributed this observation to the fact that because the maleated polyethylene composites were completely exfoliated, each individual silicate layer formed a percolated network structure and this structure of randomly oriented, anisotropic particles could not be destroyed by LAOS resulting in less of a decrease in G' compared to polystyrene.

Lee et al. [38] studied the behavior of maleated HDPE and its melt mixed nanocomposite formed from 5 wt % montmorillonite ion-exchanged with a dimethyl, distearyl ammonium cation. An oscillation time sweep experiment where G' was measured as a function of time showed that for unfilled maleated HDPE a physical network existed as demonstrated by a crossover point in G' and G". The authors attributed this network to intermolecular dipole-dipole attractions and hydrogen bonding associated with the maleic anhydride functional groups. When the corresponding nanocomposite was studied no crossover point existed between G' and G" but both G' and G" were enhanced in the nanocomposite. For the unfilled matrix, G' grew from 10 Pa to 1,650 Pa over a time span of 3,600 seconds while G" grew from 500 Pa to 1350 Pa. The nanocomposite exhibited G' values increasing from 200 Pa to 600 Pa over the time span of 3,600 seconds while G" increased from 1,000 Pa to 1,400 Pa. It was suggested that the clay platelets reduced the polymer/polymer interactions of maleated HDPE as x-ray diffraction showed the existence of exfoliation. However, the XRD data presented

indicated that for the 5 wt% clay nanocomposite did not exhibit complete exfoliation as the diffraction peak was still noticeable. Thus, it is questioned whether individual clay platelets are responsible for the observed rheological behavior or whether the enhancement of G' and G" were due to attractions between aggregates of clay flocculated together.

In another test, two different amplitudes of stress oscillation were applied to unfilled maleated HDPE equal to 10 Pa and 10,000 Pa. When 10,000 Pa was applied to the sample G' did not grow as large as that for the 10 Pa stress amplitude indicating the break down of interactions between maleic anhydride functional groups when more stress was applied [38]. Specifically, at 10 Pa, G' increased from 50 Pa to 1,700 Pa, while at 10,000 Pa, G' grew from 50 Pa to 300 Pa. The ephemeral nature of the intermolecular interactions was further demonstrated when the growth of G' of maleated HDPE was monitored during an hour long oscillation at 3.764 Pa and 0.007 Hz followed by steady shear at 23,000 Pa. Once the high shear was applied, G' immediately fell to very low values indicating network destruction. This cycle was repeated three times with each cycle exhibiting the same modulus growth and destruction behavior confirming that the reversible nature of network formation and increased G' for maleated HDPE were due to physical associations rather than chemical crosslinking of maleic anhydride functional groups.

Current literature has shown dynamic rheological characterization to be extremely useful in providing a means to assess the degree of exfoliation in PLS nanocomposites. The majority of work involving polyethylene/clay nanocomposites utilizes maleic anhydride grafted onto the polyethylene backbone in order to increase compatibility with

the hydrophilic layers of silicate. However, the use of quaternary alkylammonium salt modifiers typically involves four alkyl substituents with no polarity whatsoever. The question arises then why alkylammonium cations with polar groups such as hydroxyl ethyl attached to the nitrogen atom are not seen more in the literature when nanocomposites formed from maleated polyethylene are made. The only reason with which this author can provide is that commercially available quaternary ammonium salt modifiers containing two hydroxyethyl groups have smaller d-spacings or interlayer distances between silicate layers than do the more commonly used modifiers containing two long hydrogenated tallow chains. Typical d-spacings are given as 18.5 Å for the hydroxyethyl modifier compared to 31.5 Å for the tallow modified salt [7]. This larger gap between silicate layers could allow easier penetration of the polymer chain in between the clay platelets promoting exfoliation. It is assumed then that this would have a greater impact on the degree of dispersion of clays than would increased polar attractions between polymer and clay. However, since the research described here in this thesis involves unmodified HDPE, the polarity of the alkylammonium salt is of little concern.

2.7 Mechanical Properties

2.7.1 Polyethylene

Many studies have been performed on the changes in tensile properties by the addition of layered silicates of a variety of polymers including nylon 6 [39-44], polypropylene [45-48], polycarbonate [26], as well as polyethylene [13, 14, 34, 36, 49-53]/OMLS nanocomposites. Stress versus strain curves are usually generated like the one shown below in Figure 2.3.

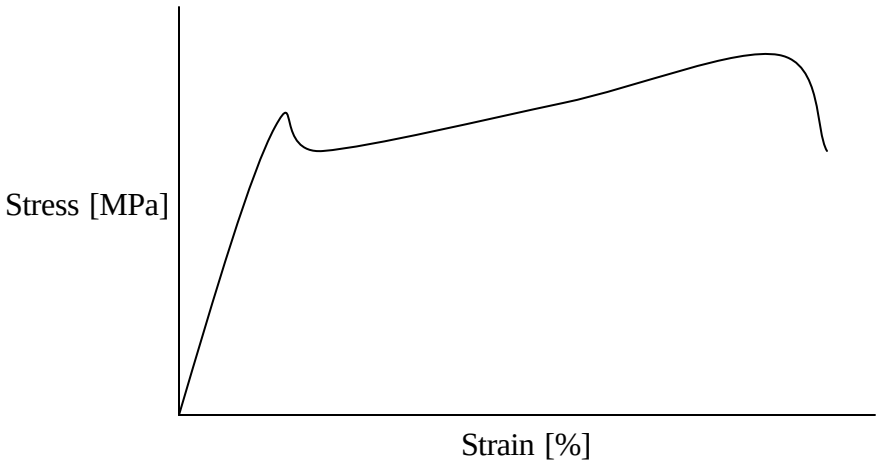

Figure 2.3. Example stress versus strain curve for tensile tests.

From these curves can be calculated the Young's or elastic modulus (from the initial slope of the stress vs. strain curve), yield stress or tensile strength, stress at break, and elongation at break.

Osman et al. [49] studied unmodified HDPE and the effect of varying the CEC and number of octadecyl chains attached to the nitrogen atom on the alkyl ammonium modifier had on the tensile properties of the resulting nanocomposites. They found that only partial exfoliation was achieved with the unmodified HDPE as shown by XRD. For a constant clay content, namely 2.8 vol %, it was shown that as the d-spacing of the clay increased via increased octadecyl chains on the alkyl ammonium cation modifier, so did the elastic modulus of the nanocomposite compared to that of the neat polyethylene. The CEC's of the clays used were 680, 880, 900, and 1000 μeq/g and the number of octadecyl chains on the alkyl ammonium modifier varied from between 1 and 4 chains. The amount of increase in the modulus for the nanocomposites compared to the unfilled matrix (1020 MPa) ranged from between 6.9 % (1090 MPa) for a CEC of 680 μeq/g and 1 octadecyl chain to a maximum increase of 39 % (1420 MPa) for a CEC of 880 μeq/g and 3 octadecyl chains. The d-spacing of the montmorillonite increased with both increased number of octadecyl chains attached to the nitrogen atom of the clay modifier as well as increasing CEC for clays with the same number of octadecyl chains. The increased d-spacing of the clay platelets was postulated to decrease the amount of attraction between the silicate layers facilitating their separation during composite formation and thus increase the level of exfoliation, which enhanced the modulus. The yield stress showed slight changes, by both positive and negative deviations from the neat HDPE, with increased d-spacing of the clays used, while the stress at break and yield strain both

decreased from 36 MPa for the neat HDPE to as low as 15 MPa with increased d-spacing indicating that the composites became more brittle with increasing levels of exfoliation. The changes in yield stress, a measure of strength or toughness, were attributed to varying levels of weak attraction forces between the clay and HDPE matrix. The nanocomposites showing the decrease in yield stress contained clays of smaller d-spacing, typically below 2.5 nm, indicating that clays with smaller interlayer gaps were less exfoliated and, thus, showed little to no improvement in toughness. The decrease in yield strain was said to be caused by local strain amplification in the polymer [49].

The tensile properties for one type of clay, CEC=900 μeq/g and 2 octadecyl chains, were studied with varying clay volume fraction ranging from 0 to 4%. The composites became stiffer as shown by an increase in elastic modulus from 1020 MPa for the unfilled matrix to 1360 MPa for the 4 vol% nanocomposite. Yield stress, yield strain, and stress at break all decreased from 27 MPa (0 vol% clay) to 25 MPa (4 vol% clay), 9.6 % (0 vol% clay) to 6.3 % (4 vol% clay), and 36 MPa (0 vol% clay) to 15 MPa (4 vol% clay), respectively with increasing volume fraction of clay possibly due to disabled strain hardening of the polymer in the presence of clay tactoids according to the authors [49]. That is, the clay aggregates acted as stress concentrators within the nanocomposites making them more brittle. Thus, while only partial exfoliation was achieved with these unmodified HDPE/clay composites, increased modulus resulted nonetheless.

Mehrabzadeh et al. [50] studied maleated HDPE/MMT composites formed in a twin screw extruder and the effect of using two different screw configurations on the level of exfoliation and changes in tensile properties. The HDPE used had a M_w given to be 142,000 g/mol and 20% maleated HDPE compatibilizer was blended into all HDPE

samples. The concentration of maleic anhydride contained in the compatibilizer was not given. One screw configuration had a shorter residence time as well as less mixing, kneading, and blistering elements than the other. For a 5 wt % MMT concentration the modulus was increased for both types of screws used, but there was a greater increase in modulus for the screw with the longer residence time and greater mixing from 1040 MPa to 1360 MPa compared to 1100 MPa for the configuration with less mixing. XRD analysis showed that the screw used to form the composite with the higher modulus showed almost complete disappearance of the clay's characteristic diffraction peak indicating the existence of an exfoliated composite. Both tensile strength and elongation at break decreased for the PLS nanocomposites relative to the neat HDPE but the nanocomposite formed from the screw with the higher residence time and mixing level showed properties which decreased to a lesser extent than that of the other extruder suggesting that clay tactoids, which often exist as stress concentrators within a polymer acting to decrease the tensile strength and elongation at break, were less prevalent in the extruder with higher residence time and mixing levels. Specifically, the tensile strength of the unfilled matrix was 24.5 MPa compared to 23.2 MPa and 23.5 MPa for the lower and higher mixing screws, respectively. Elongation at break decreased from 89% for the unfilled matrix to 80% and 88% for the lower and higher mixing screws, respectively.

Gopakumar et al. [34] used a melt mixer to generate PLS nanocomposites containing maleated HDPE and 0 to 10 wt % dimethyl, distearyl alkyl ammonium exchanged MMT and performed tensile tests on compression molded sheets. It was found that for uncompatibilized HDPE with a melt flow index (MFI) of 4.9, the Young's modulus increased by 9% (200 MPa) for a 5 wt % clay level when compared to unfilled

unmodified HDPE (183 MPa). However, this uncompatiblized sample showed little signs of exfoliation from XRD. In contrast, the maleated HDPE sample containing 5 wt% clay, which showed near complete disappearance of its diffraction peak, had its Young's modulus increase by 30% to 220 MPa over the unfilled maleated HDPE matrix which had a modulus value of 169 MPa. Addition of 10 wt% clay to the maleated HDPE increased the Young's modulus by 53% (258 MPa); however there were little signs of exfoliation as shown by the existence of a large diffraction peak corresponding to the presence of nanoclay. Improvements in the modulus when HDPE was grafted with maleic anhydride were attributed to the enhanced exfoliation which increased the contact surface area between clay and polymer thus enhancing reinforcement ability of the clay. Also, even though the modulus increased with increasing clay content, XRD analysis showed no sign of exfoliation past a clay concentration of 5 wt% indicating that increases in modulus beyond this point may be misleading when determining the success of nanocomposite formation. The tensile stress at yield showed only marginal increase with a maximum increase of 15% for the 10 wt% clay loading according to the authors but actual values were not presented [34].

Liang et al. [51] performed mechanical tests on compression molded maleated HDPE/MMT composites prepared by melt blending in a roller mill and studied the effect of varying the amount of maleic anhydride grafted polyethylene had on these properties. The MMT used was modified through ion exchange reaction with an octadecyl, trimethyl ammonium cation, polyethylene with 1.09 wt% maleic anhydride content was used as compatibilizer, and the M_w of the HDPE matrix used was not given. For a constant clay concentration of 3 wt % the tensile strength initially increased with maleic anhydride

content, from a value of 22.4 MPa for the uncompatibilized matrix to a maximum value of 23.3 MPa at 6 wt % compatibilizer. The Izod impact strength increased with increasing maleic anhydride content for all levels of compatibilizer (up to 9 wt %) from 78 J/m to 122.2 J/m. The authors reasoned that exfoliation was increased as compatibilizer was added and the separation of the interlayers during exfoliation increased the free volume in the composite allowing the polymer segments to move when subjected to a force [51]. Exfoliation was shown to exist according to XRD data presented for this composite.

Heinemann et al. [52] compared the tensile properties of various HDPE and LLDPE PLS nanocomposites formed by melt compounding and in-situ polymerization with a hectorite clay ion exchanged with either a dimethyl, distearyl ammonium (DMDS) or dimethyl, stearyl, benzyl ammonium (DMSB) cation. The in-situ polymerization was either an ethene homopolymerization or a ethene/1-octene copolymerization. It was found that for a constant clay content of 3.3 wt% the Young's modulus was 59% higher (700 MPa vs. 440 MPa) and tensile strength was 94% higher (33 MPa vs. 17 MPa) for nanocomposites formed by in-situ polymerization compared to melt compounding. XRD analysis showed that melt compounding actually reduced the interlayer spacing of the clays compared to their state prior to compounding attributed to compression of the silicate layers due to incompatibility. The in-situ polymerized sample showed a complete disappearance of a diffraction peak indicating an increase of interlayer spacing of the clays in the nanocomposite. Thus it can be seen that when exfoliation has been achieved as confirmed by XRD, a much more dramatic increase in mechanical properties occurs compared to a state of intercalation.

Kato et al. [14] prepared maleated LLDPE/MMT nanocomposites in a twin screw extruder with a clay content between 0 to 5.4 wt%. The MMT was modified with an octadecyl amine cation. The LLDPE had a MFI of 4 g/10 min and the maleated LDPE with 0.9% maleic anhydride grafting level and a MFI of 1.5 g/10 min was used. The tensile properties presented indicate that for the compatibilized systems, tensile modulus and tensile yield strength increased with increasing clay loading while yield strain decreased with increasing clay content. Specifically, unfilled maleated LLDPE exhibited a modulus of 99 MPa while nanocomposites containing 3.5 and 5.4 wt% clay showed tensile modulus values of 140 MPa and 180 MPa, respectively. These property changes were attributed to the existence of exfoliated clays throughout the polymer matrix as shown by XRD. A nanocomposite containing 5.7 wt % of unmodified MMT was shown to have no significant dispersion within the maleated LLDPE from XRD analysis. This was exhibited in the tensile properties by no change in the modulus, yield strength, or yield strain. As shown again, greater increases in tensile properties are achieved when silicate layers have been exfoliated.

Wang et al. [36] studied melt intercalated nanocomposites composed of maleated LLDPE (0.85 wt% maleic anhydride) with two clays with different aspect ratios – montmorillonite with aspect ratio between 100-200 and laponite with aspect ratio between 20-30. Both clays were organically modified with dimethyl, dihydrogenated tallow and the clay content was varied from 0 wt % to 5 vol% for all composites formed. Both yield stress and 1% secant modulus, which is defined as the slope of the stress vs. strain curve after 1% elongation of the sample, increased with increasing clay content with the greatest increase observed in the MMT nanocomposite. The 1% secant modulus

increased from 270 MPa for the unfilled matrix to 440 MPa for the 5 vol% clay nanocomposite representing a 63% increase from the neat LLDPE. The authors attributed this behavior of the high aspect ratio MMT to orientation of the clay which occurred during tensile drawing as observed by TEM images. Also, stronger interfacial adhesion of the MMT with the polymer matrix was seen by a lack of voids or cavities in SEM micrographs of specimens after tensile testing. Complete exfoliation was also found in the 3 wt% composite according to XRD results. The elongation at break decreased with increasing filler content with the greatest percentage decrease, 42% at 5 vol%, occurring for the high aspect ratio MMT. Thus, a high aspect ratio clay was seen to have greater reinforcing effects within the polymer matrix increasing both modulus and yield stress.

Morawiec et al. [53] studied LDPE/MMT nanocomposites that were melt blended. MMT was modified with an octadecyl group on the alkylammonium cation, the LDPE matrix used had a M_w = 450,000 g/mol, and maleic anhydride grafted ultra low density polyethylene (ULDPE) containing 0.5 - 1 wt% maleic anhydride was used as a compatibilizer between clay and LDPE. The clay content was varied from 0, 3, or 6 wt % and the amount of compatibilizer varied between 0, 6, and 12 wt %. The tensile properties indicate that non-compatibilized LDPE/MMT nanocomposites are more brittle than their compatibilized counterparts as shown by increased modulus and decreased elongation at break. Specifically, at for a clay concentration of 6 wt%, the Young's modulus and elongation at break for the uncompatibilized sample were 108.4 MPa and 363%, respectively, compared to 101.8 MPa and 630 % for a nanocomposite containing 12% maleated ULDPE and 6% clay. The modulus decrease upon addition of maleated ULDPE could possibly be due to a plasticizing effect of the less viscous compatibilizer

exemplified in a higher MI of 1.6 g/10 min at 190°C compared to 0.3 g/10 min at 190°C for the LDPE matrix. The decrease in elongation at break in the non-compatibilized composites was attributed to decohesion of the composite matrix around the clay particles causing samples to break prematurely. Scanning electron microscopy (SEM) revealed more cavities around the clay for systems that did not contain any maleated ULDPE compared to the compatibilized samples.

In their studies of the effects of clay concentration on tensile properties, Morawiec et al. [53] used clay loadings of 0, 6, and 12 wt%. However, as clay content was increased so too was the amount of maleated ULDPE in the nanocomposite, thus the effects of clay concentration and compatibilizer concentration are convoluted. Compositions of the nanocomposites tested given as wt% LDPE: wt% compatibilizer: wt% clay are 87:13:0, 91:6:3, and 82:12:6. The Young's moduli for these 3 materials were found to be 92.0 MPa, 100.8 MPa, and 101.8 MPa in order of increasing clay content. XRD data showed that the compatibilized samples had diffraction peaks shifted to lower angles corresponding to larger interlayer spacings of the clay with the 3 wt% clay composite showing more exfoliation than the 6 wt% sample. The modulus increase was expected as clay was introduced to the polymer, but only a slight increase was found when increasing from 3 wt% to 6 wt% clay. This may be due to a plasticizing effect the compatibilizer had on the polymer since the amount of maleated ULDPE was increased as well.

Alexandre et al. [13] synthesized PE/clay composites via in situ polymerization where the polymerization catalyst was attached directly to the silicate surface in between layers. Two clays were used, namely unmodified MMT and unmodified hectorite. Both

ultra-high molecular weight polyethylene (UHMWPE) and lower molecular weight PE were synthesized by controlled use of hydrogen as a chain transfer agent during polymerization to control the length and, thus, molecular weight of the polymer chain. It was found that the UHMWPE specimens were so brittle that no tensile yield or necking during tensile testing was observed thus values of strain at yield and stress at yield could not be measured. Lower elongation at break and higher stress at break were also observed for UHMWPE compared to lower molecular weight samples. The Young's modulus for the UHMWPE nanocomposites ranged from 350 MPa to 720 MPa. These properties were found to be independent of filler content and determined solely by the matrix itself [13]. When the molecular weight was decreased by hydrogen addition, both strain at break and Young's modulus increased for the nanocomposites. Clay content was varied from 3.4 to 13.0 wt%. The 3.4 wt% sample was shown to have an exfoliated morphology as found by XRD, and it showed the highest strain at break (467%) and stress at yield (27.4 MPa) out of all the nanocomposites relative to the unfilled matrix which exhibited strain at break and stress at yield values of 244% and 23 MPa, respectively. It is interesting to note that the 3.4 wt% nanocomposite exhibited a higher strain at break than did the unfilled matrix. It was expected that as clay is added to the polymer, the matrix becomes more brittle and thus breaks at lower strains than the neat matrix which was found to be the case for the 4.5, 11,4 and 13.0 wt% nanocomposites. XRD data was not presented for the 4.5, 11.4 and 13.0 wt% samples, and so no statement can be made concerning the effect nanoclay dispersion had on mechanical properties.

The thermodynamic stability of the nanocomposites was also examined. The authors used one UHMWPE nanocomposite and a low molecular weight polyethylene

nanocomposite sample after formation and reprocessed them by compression molding. For the low molecular weight sample, XRD analysis showed that the diffraction peak corresponding to the interlayer spacing between silicate layers, which disappeared after the initial in situ polymerization, reappeared upon compression molding. The authors attributed this to the collapse of the exfoliated structure due to the possibility that composites formed from clay and non-polar polymers like polyethylene are thermodynamically unstable and revert to their original state once melted [13]. This collapsed structure showed poorer mechanical properties as evidenced by a drop in Young's modulus and decrease in strain at break from 1280 MPa and 467%, respectively, for the initial nanocomposite to 890 MPa and 458%, respectively, for the compression molded sample. The authors then reasoned that if the viscosity of the polymer matrix were increased, loss of the exfoliated morphology could possibly be prevented by decreased mobility of the clays. This was experimentally shown for an UHMWPE sample which was compression molded after polymerization. No significant change in the XRD pattern indicated preservation of the exfoliated morphology.

2.7.2 Theoretical Modeling of the Young's Modulus

The observed increase in the Young's modulus with addition of layered silicates into a polymer matrix is of obvious practical benefit to many applications where improved strength and stiffness may be utilized. Realizing the full potential of mechanical property increase remains unclear even when fully exfoliated nanocomposite morphologies are shown by XRD. Evaluation of the expected modulus increase for polymer composites presented here will be based on two separate theories developed by Halpin and Tsai [54, 55] and Ji et al. [56].

The effectiveness of these two models to predict actual experimental values of Young's modulus depend on the assumptions each theory is based upon. Halpin and Tsai's model shown below in Equation 2 assumes unidirectional, i.e. well oriented filler particles as well as a high degree of adhesion of the filler particles to the surrounding polymer matrix,

$$E_c = E_m \left[\frac{1 + z h f_f}{1 - h f_f} \right], \tag{2}$$

where E_c = composite modulus, E_m = unfilled matrix modulus, f_f = filler volume fraction,

$$h = \frac{E_f / E_m - 1}{E_f / E_m + z}, \tag{3}$$

$$z = 2(l / t), \tag{4}$$

E_f = filler modulus taken to be 178 GPa for MMT [57], and l/t = aspect ratio of MMT taken here to be approximately 100 [57].

For PLS nanocomposites synthesized from non polar polyolefins such as polyethylene the assumption of the degree of bonding between MMT and the polyethylene matrix would be invalid due to differences in the surface energies of hydrophilic MMT and hydrophobic polyethylene. The level of adhesion could be increased the by use of organic modifiers such as long alkyl chains on the surface of MMT to increase the organophilic character of the nanoclay. Maleic anhydride could also be used as a compatibilizer with the clay when grafted onto polyethylene by increasing the polarity of the polymer matrix, thus making it more hydrophilic.

Orientation of nanoclays within a polymer matrix has been shown experimentally through TEM image analysis for injection molded nanocomposites [57], however, only one author performed tensile tests on injection molded specimens of polyethylene

composites surveyed above [57]. Compression molding was found to be the most common method of preparing samples for tensile testing, and no conclusion concerning the state of clay orientation could be made upon examination of TEM images.

The model developed by Ji et al. takes into account three phases present in a PLS nanocomposite: the matrix, filler, and the interphase region between the clay platelets with the polymer matrix residing within it. Ji's model shown below in Equation 5 makes no assumption as to the state of clay orientation and so is valid for randomly oriented systems compared to that of Halpin and Tsai,

$$\frac{1}{E_c} = \frac{1-a}{E_m} + \frac{a-b}{(1-a)E_m + a(k-1)E_m/\ln k} + \frac{b}{(1-a)E_m + (a-b)(k+1)E_m/2 + E_f b}, \quad (5)$$

where

$$a = \sqrt{[2(t/t_c)+1]f_f}, \quad (6)$$

t = thickness of the interphase region taken to be the d-spacing given by XRD analysis, t_c = thickness of MMT taken to be approximately 1nm [2], $b = \sqrt{f_f}$, and $k = E_f/E_m$.

The dependence of Ji's model on the interphase separation between clay particles further generalizes the model by making no assumption to the state of intercalation or exfoliation of the clay platelets. If d-spacing data are available then the dependence of Young's modulus on the degree of exfoliation may be examined. Table 2.2 below summarizes expected modulus increase from both the Halpin and Tsai equation as well as Ji et al.'s equation compared to that obtained from experiment for the polyethylene nanocomposites surveyed above. The upper and lower bounds of the expected modulus increase are given by the rule of mixtures and inverse rule of mixtures, respectively, as shown by Equations 7 and 8.

$$E_c = f_f E_f + f_m E_m \tag{7}$$

$$\frac{1}{E_c} = \frac{f_f}{E_f} + \frac{f_m}{E_m} \tag{8}$$

Table 2.2. Summary of Young's Modulus Increase for Various Polyethylene/MMT Nanocomposites Based on Experiment and Theoretical Predictions.

Authors	Matrix	Preparation Method	Clay Fraction	Nanocomposite Morphology	Experimental Modulus (MPa)	Ji et al. (MPa)	Halpin and Tsai (MPa)	Low/Upp. Bound (MPa)
Gopakumar et al.	HDPE, MI=4.9 g/10min	Melt Blender, 190°C, 60 rpm, 7 min	5 wt%	Intercalated	200	340	1100	190/5420
"	PE-g-MAn (1wt%), MI=9.6 g/10min	"	5 wt%	Intercalated	220	320	1030	170/5410
"	"	"	10 wt%	Intercalated	258	520	1940	180/10600
Wang et al.	LLDPE-g-MAn	Melt Blender, 140°C, 60 rpm, 20 min	0.5 – 5 vol%	Exfoliated	320	N/A	460	270/2050
Osman et al.	HDPE, MI=0.5 g/10min	Melt Blender, 160°C, 20 min	2.8 vol%	Intercalated	1060	1120	1880	190/5420
Mehrabzadeh et al.	HDPE, Mw=142K, MI=43 g/10min + 20% PE-g-MAn	Twin-screw extruder, 220°C	5 wt%	Intercalated	1100	1820	3900	1070/6250
Heinemann et al.	HDPE, Mw=500K	Melt Blender, 190°C, 5 min	3.3 wt%	Intercalated	700	570	1580	430/3970
Kato et al.	PE (MI=4 g/10min) + 30 wt% LLDPE-g-MAn (.9wt%), MI=1.5 g/10min	Twin-screw extruder, 220°C, 300 rpm	3.5 and 5.4 wt%	Both samples Exfoliated	140 (3.5%), 180 (5.4%)	N/A	460 (3.5%), 670 (5.4%)	101/3660 (3.5%) 102/5610 (5.4%)
Morawiec et al.	LDPE (Mw=450K, MI=0.3 g/10min	Melt Blender, 160°C, 60 rpm, 20 min	6 wt%	Intercalated	108.4	N/A	644	102/5384
"	LDPE (Mw=450K, MI=0.3 g/10min) + 6 or 12wt% ULDPE (0.5-1wt%)	"	3 or 6 wt%	Both samples Exfoliated	101 (3%), 102 (6%)	N/A	345 (3%), 603 (6%)	93/2740 (3%), 95/5380 (6%)
Alexandre et al.	PE	In-situ polymerization	3.4 wt%	Exfoliated	1280	N/A	2260	700/4240

As can be seen from Table 2.2, all of the experimental Young's moduli presented are below those predicted by the Halpin-Tsai model. The discrepancies between experiment and theory are attributed to the assumptions of significant bonding occurring between the polyethylene matrix and MMT particles, exfoliation of the silicate layers, as well as well oriented nanoclay particles in the direction of tensile testing which leads to an overestimation of the Young's modulus [54, 55].

Ji et al.'s model provides a closer approximation of the Young's modulus as shown in Table 2.2. By taking into account the separation of nanoclay particles directly in the model, a more accurate description of the nanocomposite morphology is related to the predicted Young's modulus. It is noted that when d-spacing data was not provided by the author, either due to lack of experimental data or exfoliation being achieved, and, thus no d-spacing data could be calculated, no attempt at determining the Young's modulus from Ji et al.'s model was made.

Current literature concerning the mechanical properties of polyethylene nanocomposites indicates that as the level of clay exfoliation is increased, improvements in the stiffness of the composites is attained as seen from increased values of the Young's modulus by 85.5% for in-situ polymerization [13] and 41% for melt intercalation [14] at similar clay concentrations (3.5 wt%). Increased strength also leads to increased brittleness in the samples quantified by decreased values of elongation at break and the stress at break. Exfoliation was seen to increase due to multiple factors including increased mixing during composite processing in the form of extruders with more blending elements [50], increased d-spacing of clays before addition to a polymer matrix [49], and use of maleic anhydride grafted onto polyethylene backbone as a compatibilizer

between hydrophilic layered silicates and hydrophobic polyethylene [50-53]. Use of compatibilizer was seen to have two effects on the mechanical properties of polyethylene/clay nanocomposites. While low levels of compatibilizer concomitantly increased the level of exfoliation and Young's modulus, a maximum then drop in tensile modulus has been seen as maleic anhydride content was increased due to a plasticizing effect of the maleic anhydride [45, 48]. The majority of the work surveyed utilized compression molded specimens for tensile testing. Exceptions include one author who reported the use of ribbons extruded from a slit die extruder [50] while another author used injection molded specimens for tensile testing [14].

2.8 Past Work on Molecular Weight Effects on Nanoclay Dispersion

2.8.1 Maleated Polyethylene

Zhong et al. [58] studied maleated LDPE as well as maleated HDPE nanocomposites prepared by melt intercalation in a twin screw extruder. The molecular weight of maleic anhydride grafted LLDPE and HDPE were varied in this study with the maleated LLDPE being used as a compatibilizer for LDPE and maleated HDPE used as the compatibilizer for HDPE. The grafting level on all maleated polyethylenes used was 1%. Each nanocomposite formed contained 5 wt% of the maleated polyethylene. Montmorillonite clay was used which was modified with a dimethyl, dihydrogenated tallow alkylammonium salt in varying amounts ranging from 0 to 5 wt %. Mechanical tests were performed on blown films of the nanocomposites, and for LDPE nanocomposites it was found that for the higher molecular weight compatibilizer, designated by a melt index (MI) and zero shear viscosity (h_0) of 1.5 g/10 min and 5.26 X 10^4 Pa*s at 190°C, respectively, compared to that of the low molecular weight

compatibilizer which had a MI and h_0 of 30 g/10 min and 1879 Pa*s at 190°C, respectively, the 1% secant modulus increased with clay loading from 73.28 MPa for the unfilled matrix to 100.26 MPa for the 5 wt% clay nanocomposite. However, the tensile strength decreased with clay loading from 14.28 MPa for the unfilled matrix to 12.97 MPa for the 5 wt% clay nanocomposite and, thus, the composite is getting stiffer and more brittle. However, the lower molecular weight LLDPE compatibilizer shows both an increase in tensile strength and modulus with increasing clay content. Specifically, the tensile strength increased from 12.97 MPa for the unfilled matrix to 16.70 MPa for the 5 wt% clay nanocomposite and the 1% secant modulus increased from 62.79 MPa for the unfilled matrix to 91.22 MPa for the 5 wt% clay nanocomposite. Increased exfoliation was suggested by XRD for the low molecular weight compatibilizer, and this could account for the improvement in tensile strength as well as the greater percentage increase in modulus for the low molecular weight compatibilizer (45.3%) relative to the high molecular weight compatibilizer (36.8%) by increased clay reinforcing effects. The authors attributed this to the fact that lower molecular weight polymers are smaller and can penetrate the interlayer gap of the clays more readily than the high molecular weight compatibilizer. In addition, the moduli for the low molecular weight compatibilized samples are lower than when the high molecular weight compatibilizer is used for all clay contents. This may be due to a plasticizing effect the low molecular weight compatibilizer has on the LDPE matrix.

In their studies of HDPE nanocomposites, Zhong et al. [58] found that HDPE blended with the high molecular weight compatibilizer showed increased yield stress and modulus compared to the uncompatibilized matrix, but these properties all decreased

upon addition of clay. Yield stress decreased from 25.60 MPa to 19.32 MPa and 1% secant modulus decreased from 478.52 MPa to 421.45 MPa for the unfilled and 5 wt% clay nanocomposites, respectivley. Despite these decreases in properties, the nanocomposites are still comparable to that of neat HDPE without compatibilizer or clay which exhibited a yield stress of 20.29 MPa and a modulus of 456.92 MPa. When the low molecular weight compatibilizer was used, the yield stress increased slightly from 19.80 MPa to 21.39 MPa with addition of clay as seen before with LDPE nanocomposites even though there was no increase in d-spacing as shown from XRD analysis. It is questionable then to attribute this increase in yield stress to enhanced exfoliation when using the low molecular weight compatibilizer. Reasoning that the low molecular weight compatibilizer has penetrated in between the silicate layers more easily than its high molecular weight counterpart does not seem likely because there is no difference in d-spacings between composites formed from each compatibilizer.

2.8.2 Polypropylene

Lee et al. [59] studied isotactic polypropylene of 3 different molecular weights each containing 5 wt% maleated polypropylene and 5 wt% montmorillonite modified with a dimethyl, dihydrogenated tallow ammonium salt melt blended in a twin screw extruder. The molecular weights were not specified but were correlated to the MI of the 3 samples given to be 37.0, 4.0, and 0.5 g/10min at 230°C for the low, medium, and high molecular weights, respectively. The MI of the maleated polypropylene was given to be 110 g/10min at 190°C. It was found that the flexural modulus of all nanocomposites increased relative to the corresponding neat matrix with the greatest increase, from 1,277 MPa to 1,968 MPa or 54.1%, occurring in the medium molecular weight polypropylene

followed by a 42.7% increase from 1,340 MPa to 1,912 MPa for the low molecular weight polypropylene composite while the smallest increase, 0.82%, was observed in the high molecular weight matrix from 1,466 MPa to 1,478 MPa. XRD analysis was not performed for these composites, and so no correlation can be made concerning the state of exfoliation and the molecular weight of the matrix. However, the method of ultrasonication was also used to disperse the nanoclays throughout the different molecular weight polypropylenes. Samples of each molecular weight were compounded in a twin screw extruder with 5 wt% montmorillonite *without* any compatibilizer. Each sample was then subjected to ultrasonic sound waves at a frequency of 20,000 Hz while in the melt phase. XRD analysis was performed for these samples and showed that the extent to which the d-spacings of the silicate layers increased depended on the molecular weight of the polymer with the greatest increases occurring at lower molecular weights. The authors attributed this dependence to increased diffusivity of the lower molecular weight molecules into the clay galleries due to lower melt viscosities. Mechanical properties were not performed in this study due to limited sample size produced during batch processing [59]. It is interesting to note that no compatibilizer was necessary to increase attractive interactions between the non-polar polypropylene and the polar clay to bring about increased exfoliation for these composites. An effective means of mixing was shown to dramatically increase the basal spacing of the clay up to 53%, from 23.6 Å to 36 Å, for the low molecular weight sample.

Kaempfer et al. [60] performed studies on syndiotactic polypropylene - fluorohectorite nanocomposites compounded via twin screw extrusion. The fluorohectorite was rendered organophilic via ion exchange reaction with an octadecyl

ammonium cation. The polypropylene used had a melt flow index of 4.4g/10min and two maleic anhydride grafted isotactic polypropylenes were used as compatibilizers with M_n given to be 7,500 g/mol and 2,900 g/mol, maleic anhydride contents of 4.2 wt% and 3.5 wt%, and polydispersities (M_w/M_n) given to be 3.9 and 4.1 for the high and low molecular weight compatibilizers, respectively. It was found that the Young's modulus was enhanced for a 20 wt% concentration of the high molecular weight compatibilizer at all clay concentrations from 0 to 20 wt% increasing from 670 MPa to 2640 MPa or 294% and from 520 MPa 1560 MPa or 200% for 20 wt% of the low molecular weight compatibilizer at clay concentrations ranging from 0 to 13 wt%. A larger increase in the basal spacing of the nanoclays was observed for the high molecular weight compatibilizer as shown by XRD for nanocomposites containing 5 wt% clay and 10 wt% of each compatibilizer. No reason was given to account for the larger increase in the interlayer gap of the clays when the higher molecular weight compatibilizer was used, but it could be due to greater shear force available from the higher molecular weight compatibilizer to separate the silicate layers. However, no XRD data was presented for 20 wt% clay nanocomposites for the high molecular weight compatibilizer so the observed increase in Young's modulus cannot be attributed to increased distance of the interlayer of the clays.

2.8.3 Polyisoprene

Jeon et al. [61] studied two polyisoprene samples with molecular weights of 40,000 g/mol and 95,000 g/mol and η_0 of 27 Pa*s and 720 Pa*s respectively at 50°C. Solvent intercalation with toluene was used to form the nanocomposites. There was confusion in the clay the authors chose to use for this study. They wrote that they used a modified MMT from Southern Clay Products termed Cloisite 10A which is modified

with a dimethyl, benzyl, hydrogenated tallow ammonium salt [7], but they later described that the clay used was modified with a methyl, tallow, bis-2-hydroxyethyl ammonium salt. Thus, it remains unclear exactly which modification was used on the clay. X-ray diffraction was performed on the composites containing 5 wt% clay and the results indicate that the low molecular weight sample was exfoliated as shown by the complete disappearance of its diffraction peak indicating the basal spacing of the nanoclay was greater than 40 Å. This was confirmed via small angle x-ray scattering (SAXS) where no characteristic peak was seen to correspond to distances of 30 to 140 Å. The high molecular weight sample displayed a shifted diffraction peak corresponding to an increase in the clay gallery but the existence of this peak suggests that an intercalated rather than exfoliated morphology exists.

Dynamic rheology experiments were also performed and G' was presented for 5 wt% clay loading. It was shown that the low molecular weight sample showed the greatest enhancement in G' compared to the neat polymer at low frequencies, with over 5 orders of magnitude at a value of 20,300 Pa. The composite made from the high molecular weight polymer showed an increase in G' of 3 orders of magnitude to a value of 4,690 Pa relative to the unfilled matrix. An enhanced h_0 was also observed for the 5 wt% nanocomposites at 0.1 rad/sec with the low molecular weight sample increasing from 27 Pa*s to 49,000 Pa*s and the high molecular weight sample increasing from 720 Pa*s to 67,400 Pa*s. This was attributed to exfoliation of the nanoclays causing the formation of a physically connected or percolated network due to their large aspect ratios and high surface areas. The high molecular weight sample was shown to have an intercalated morphology as shown by XRD and the reasoning provided by the authors

was that the large polymer chains with a radius of gyration of 90 Å could not diffuse in between the silicate layers separated by a distance of 20 Å [61]. Also shown was the independence of G' with clay loading at low frequencies ranging from 0.1 rad/sec to 0.3 rad/sec as the clay content increased in the low molecular weight polymer via a plot of G'(w =0.3 rad/sec)/G'(w =0.1 rad/sec) vs. volume fraction. The elastic percolation threshold was found to be 2 vol% of clay, where the transition from liquid to solid-like network behavior occurred.

2.8.4 Polystyrene

Tanoue et al. [62-64] melt compounded montmorillonite/polystyrene nanocomposites at 200°C in a twin screw extruder using three different molecular weight polystyrene matrices with molecular weights given to be 230,000 g/mol, 270,000 g/mol, and 310,000 g/mol and corresponding h_0 given to be 4,450 Pa*s, 8,860 Pa*s, and 17,900 Pa*s. The montmorillonite used was ion exchanged with a dimethyl, benzyl, hydrogenated tallow ammonium cation. Mechanical properties were found, and the results indicate that Young's modulus was nearly independent of matrix molecular weight, but did increase with increasing organoclay loading (up to 11 wt%) from approximately 3,400 MPa to 4,100 MPa. The independence of Young's modulus on molecular weight may be due to the fact that the differences in the molecular weights of polystyrene samples used did not differ much. Both stress at break and Izod impact strength were shown to increase with molecular weight and decrease with clay content, but their dependence on clay content was the same regardless of molecular weight. In other words the relative value of the stress at break of the nanocomposites at a given concentration of clay to that of the neat matrix was the same irrespective of the molecular

weight used. The elongation at break showed a dependence on the grade of polystyrene used, decreasing more with increasing clay content for the high molecular weight sample than the other two samples.

Tanoue et al. [63] also investigated dynamic rheological properties for these nanocomposites. Strain sweeps were performed with strains ranging from 0 to 80% to determine the linear viscoelastic range of the unfilled matrices as well as the nanocomposites. Data was presented for the unfilled polystyrene matrices and their corresponding nanocomposite containing 10 wt% of clay. The storage moduli for neat polystyrenes were found to be constant for the high, middle, and low molecular weight matrices up to strains of 24%, 28%, and 36%, respectively. However, the storage moduli for the 10 wt% nanocomposites decreased over the entire strain range applied. Thus the clays act to dissipate the energy applied from oscillation at all strains. The enhancement of both storage and loss moduli was analyzed as a function of clay concentration. It was shown that while the ratios of both nanocomposite storage and loss moduli to the of the corresponding neat matrix increased with increasing clay concentration, that increase was relatively independent of the matrix molecular weight. The highest molecular weight sample showed the least enhancement as clay concentration increased indicating that exfoliation process may be dominated by diffusion of smaller size polymer chains.

Also presented were changes in the initial slope, i.e. in the lower frequency or terminal region, of the storage and loss moduli on a log-log plot as a function of clay content. For a linear viscoelastic liquid $G' \propto w^2$ and $G'' \propto w^1$, while for lightly crosslinked gels both G'and G" should be proportional to w^0 [63]. Thus the position between these limiting values for which the storage and loss moduli of the

nanocomposites exist gives an indication of the structure i.e. dispersion of the clays within the polymer matrix. The initial slopes for both storage and loss moduli decreased with increasing clay concentration for all three molecular weights used and their dependence on clay content were similar as well. Decreases in the initial slope of the storage moduli were greatest for the middle molecular weight polystyrene nanocomposites going from 1.93 for the neat matrix to 1.67 for the 10 wt% clay composite. Nanocomposites formed from the high and low molecular weight matrices showed decreases in the slope from 1.78 to 1.60 and 1.85 to 1.73, respectively. The authors attributed this observed decrease in the terminal slope of G' to the formation of a three-dimensional structure between the clay platelets and polystyrene matrices [63]. However, XRD data indicated that a mixed structure was formed with some intercalation and some exfoliation [62]. A shift to higher $2q$ angles indicated an actual reduction in the interlayer spacing of the clays for all clay compositions from 1 to 10 wt%. This was attributed to thermal degradation of the organic modifier used on the MMT which was shown by FTIR. It seemed unlikely then that a percolated network structure was formed during the compounding since a reduction in the gallery spacing of the clay was shown to occur for all molecular weights and compositions.

Vaia et al. [65] studied octadecyl ammonium exchanged fluorohectorite/polystyrene nanocomposites using five matrices of different molecular weight ranging from 30,000 g/mol to 300,000 g/mol and a clay content of 25 wt%. Composites were prepared by mechanically mixing the clay and polystyrene then pressing the samples under 70 MPa of force. Intercalation of the fluorohectorite was accomplished by annealing the samples at a temperature of 180°C which is above the

glass transition of polystyrene. The fraction of clay which became intercalated into the polystyrene matrix was measured as a function of anneal time for each of the five matrices. This was done by taking the ratio of the intensities of the diffraction peaks for the composite at a given time to the intensity of the diffraction peak at long times where complete exfoliation is believed to have occurred. The authors concluded that while the rate of intercalation decreases with increasing matrix molecular weight due to increased melt viscosity, the final morphology of the composite does not. That is, given enough time, all nanocomposites will exhibit the same exfoliated or intercalated structure regardless of matrix molecular weight. However, this author finds the data presented to be too inconclusive to make such statements. The high molecular weight sample showed a leveling off of the fraction of intercalated clay in the nanocomposite occurring at lower fractions than the lower molecular weight samples indicating that less exfoliation was reached in the high molecular weight sample in the time period studied. Additional measurements of the amount of intercalated clay in the high molecular weight sample at longer times would make this clearer.

2.8.5 Nylon 6

Fornes et al. [66] studied the effect matrix molecular weight had on the formation of nylon 6/MMT nanocomposites. Using a twin screw extruder they melt blended three different molecular weight nylon 6 samples with M_n given to be 16,400 g/mol, 22,000 g/mol, and 29,300 g/mol and corresponding h_0 given to be 350 Pa*s, 1,700 Pa*s and 2,500 Pa*s at 240°C. The montmorillonite was modified with bis(hydroxyethyl)-(methyl)-rapseed quaternary ammonium cation, and the clay content in the nanocomposites ranged from 0 to 8 wt%. XRD results for 1.5 wt% clay nanocomposites

indicated that both the middle and high molecular weight samples had an exfoliated structure due to disappearance of the clay's characteristic basal reflection. However, the nanocomposite synthesized from the low molecular weight sample did show a broad and diffuse diffraction peak similar to that of the pure nanoclay suggesting that the system is composed of both intercalated and exfoliated clay platelets. The authors attributed differences in the melt rheology of each matrix in determining the level of exfoliation achieved. Higher molecular weight polymers have higher melt viscosities which enable the transfer of more shear stress to a stack of clay platelets to achieve separation of each individual platelet.

Mechanical properties were also examined in this work. The Young's modulus exhibited an increase with increasing clay content as well as with matrix molecular weight. Specifically, the low, middle, and high molecular weight nanocomposites containing approximately 7.0 wt% clay showed increases in modulus by 74.5%, 107%, and 107%, respectively. It is noted that the unfilled matrices had similar values of modulus given to be 2,820 MPa, 2,710 MPa, and 2,750 MPa for the low, middle and high molecular weight samples, respectively. XRD was performed for the high molecular weight nanocomposite at this clay loading and showed disappearance of the clay's characteristic diffraction peak indicating an exfoliated morphology according to the authors [66]. However, XRD results were not presented for the middle and low molecular weight nanocomposites containing the higher loading of clay, and so it is unclear whether the increases in modulus are due to the existence of clay aggregates or exfoliated clay platelets. The same trends were found for the yield strength of the nanocomposites. Elongation at break decreased with increasing clay content for all three molecular

weights but composites made from the low molecular weight matrix showed a greater decrease in elongation at break as clay content increased. Decreased ductility was expected to occur as more clay was added to the polymer, but the presence of unexfoliated clay aggregates in the low molecular weight composites may act as stress concentrators reducing the elongation at break at a greater rate than the for the higher molecular weight matrices. The notched Izod impact strength was found to be independent of clay concentration for the high and middle molecular weight nanocomposites, but decreased with increasing clay content for the low molecular weight sample.

Linear dynamic rheological experiments were also performed in a parallel plate rheometer under oscillatory shear. Complex viscosity data shows increasing non-Newtonian behavior of 3.0 wt% nanocomposites as the molecular weight of the matrix is increased with values at w = 0.06 rad/sec of 9,000 Pa*s, 4,500 Pa*s, and 800 Pa*s for the high, middle, and low molecular weight samples, respectively. G' data for the 3.0 wt% nanocomposites showed a decreased dependence on w in the lower frequency region as the matrix molecular weight increased. Specifically, the slopes of G' on a log-log plot were 0.6, 0.8, and 1.0 for the high, middle and low molecular weight nanocomposites, respectively, where a value of 2.0 indicates liquid-like behavior and 0 indicates solid like behavior. This increasing solid-like behavior was attributed greater levels of exfoliation being achieved in the higher molecular weight composites due to more shear stress being exerted onto the clay platelets to separate them and facilitate more particle-polymer interactions [66].

2.8.6 Poly(Ethylene Oxide)

Shen et al. [67] studied the effect molecular weight has on nanocomposite formation for two poly(ethylene oxide) samples of M_n equal to 103,600 g/mol and 172,700 g/mol. Melt intercalation was performed by mechanically mixing polymer and unmodified montmorillonite clay with a mortar and pestle, pressing into pellets, and then annealing the pellets at 85°C for up to 15 hours. A clay loading of 28 wt% was used for this study. The fraction of intercalation was measured as a function of time in the same manner as that described in the study of polystyrene conducted by Vaia and coworkers [65]. Shen et al. found that molecular weight did not affect the final structure of poly(ethylene oxide)/montmorillonite nanocomposite since the d-spacings of the final intercalated structure for both molecular weights were the same, but it only influenced the kinetics of nanocomposite formation just as Vaia et al. found. The low molecular weight composite was found to intercalate at a greater rate than that formed from high molecular weight poly(ethylene oxide). The authors attributed this behavior to a decrease in melt viscosity of the low molecular weight nanocomposite which leads to faster diffusion into the clay, but values of viscosity were not presented in this study making it difficult to assess the role melt viscosity plays.

It has been shown that much work has been performed on the effects that varying the molecular weight of either a polymer matrix or a compatibilizer has on the dispersion of nanoclays within a given polymer. A variety of polymers have been studied ranging from relatively non-polar polyolefins such as polyisoprene to polyamides such as nylon 6 which contains many sites for hydrogen bonding to occur. However, mixed results have been found in the literature concerning the role matrix molecular weight plays. It is

believed that lower molecular weight polymers can penetrate more easily between the galleries of layered silicates due to their smaller sizes as well as increased diffusivity due to the less viscous nature lower molecular weight matrix. Also believed to occur is that when molecular weight is increased the polymers become larger and less mobile but the more viscous matrix is able to apply more force to shear the individual clay platelets apart from one another. Thus, there are benefits to using both a low molecular weight polymer as well as in using a high molecular weight polymer and the extent to which these two competing factors influence the degree of clay dispersion and enhancement in mechanical properties remains unclear. Only in Kaempfer's [60] study of syndiotactic polypropylene/fluorohectorite nanocomposites and Fornes' [66] examination of nylon 6 was it found that increasing the molecular weight of the matrix (or of maleated polypropylene compatibilizer in Kaempfer's case) increased the degree of exfoliation of the nanocomposites. The method used to compound nanoclay and polymer also affects the final conclusion as shown in Vaia [65] and Shen's [67] studies on polystyrene and poly(ethylene oxide), respectively. In those studies a static mixing procedure was utilized to form the nanocomposites by which the clay and solid polymer pellets were dry mixed together then statically annealed at a temperature above where the glass transition occurs. Vaia and Shen both concluded that there is no difference in the final state of clay exfoliation when different molecular weight matrices are used and that only the rate at which exfoliation occurs is controlled by the polymer's molecular weight. The other studies presented show that by using mechanical mixing procedures in the form of a twin screw extruder, differences in the state of exfoliation were achieved for different

molecular weight polymers with exfoliation either increasing or decreasing with increasing molecular weight.

2.9 Research Objectives

2.9.1 Research Objective #1

It is unclear as to the effect of matrix molecular weight on intercalating and exfoliating nanoclays with a polymer. At low molecular weights its is believed that penetration of small polymer chains in between clay platelets enables separation of individual silicate layers, while at high molecular weights it is thought that the higher shear stress available from the more viscous matrix can facilitate separation of the nanoclays during compounding. Current studies for a wide variety of polymers have shown conflicting results as to the role molecular weight plays. Additionally, most studies on polyethylene have utilized maleic anhydride grafted onto the polymer backbone to increase its polarity and thus attraction for the nanoclays. Also, the studies involving the relatively non-polar compounds polyisoprene and polystyrene did not use a wide range of molecular weights [61-65], and one study of polystyrene which did use a wide range of molecular weights compounded the nanocomposites by a static mixing procedure [65]. The first research objective is then to:

> **Determine if nanoclays can be exfoliated in non-polar, unmodified HDPE of varying molecular weight. The molecular weights of the HDPE used are approximately 87,000 g/mol, 160,000 g/mol, and 460,000 g/mol. This range of molecular weights is as large if not larger than has been found to have been used in past work concerning matrix molecular weight on the dispersion of nanoclays.**

2.9.2 Research Objective #2

It has been found that most methods used to melt intercalate nanoclays with polymer matrices have been accomplished by use of a melt blender or twin screw

extruder. These two devices are known to impart a significant degree of mixing to the composite mixtures. The single screw extruder has not been reported to be used in the literature for being used to attempt melt intercalation. Thus, the second objective of this research is to:

> **Determine the viability of a single screw extruder as an effective means for compounding PLS nanocomposites. The effectiveness of the mixing method employed will be determined by monitoring any changes in the spectra provided by x-ray diffraction to analyze any changes in the basal spacing of the clay platelets. The effect of the nanoclay on the mechanical properties for these composites will also be determined.**

2.10 References

1. Ray, Suprakas S. and Okamoto, Masami, "Polymer/layered silicate nanocomposites: a review from preparation to processing," *Progress in Polymer Science* **28** (2003), pp.1539-1641

2. T. Pinnavaia and G. Beall, "Polymer-Clay Nanocomposites," John Wiley & Sons, Ltd., New York (2000)

3. S. Bridley, G. Brown, "Crystal Structure of Clay Minerals and Their X-ray Diffraction", Mineralogical Society, London (1980)

4. T. Pinnavaia, "Intercalated clay catalysts," *Science* **220**, (1983) pp. 365-371

5. M. Zanetti, S. Lomakin, G. Camino, "Polymer layered silicate nanocomposites," *Macromol. Mater. Eng.* **279** (2000) p. 1-9

6. L. Pauling. General Chemistry. Dover Publications, Inc., New York, (1970) pp. 643

7. Southern Clay Products Inc., Technical Data Sheets, www.nanoclay.com (2006).

8. K. Jordens. "Hybrid Inorganic-Organic Materials: Novel Poly(propylene oxide) Based Ceramers, Abrasion Resistant Sol-Gel Coatings for Metals, and Epoxy-Clay Nanocomposites," PhD Dissertation, Virginia Polytechnic Institute and State University, Blacksburg, VA., (1999) pp. 51-60

9. G. Jimenez, N. Ogata, H. Kawai, T. Ogihara, "Structure and thermal/mechanical properties of poly(*l*-lactide)-clay blend," *J Polym Sci*: *Part B: Polym*. *Phys.* **35**, (1997) pp.389-96.

10. N. Ogata, S. Kawakage, T. Ogihara, "Poly(vinyl alcohol)-clay and poly(ethylene oxide)-clay blends prepared using water as solvent," *J Appl Polym Sci*., **66 (**1997), pp 573-581.

11. N. Ogata, G. Jimenez, H. Kawai, T. Ogihara, "Structure and thermal/mechanical properties of poly(*l*-lactide)-clay blend," *J Polym Sci: Part B: Polym Phys*., **35**, (1997) 389-396.

12. K. Masenelli-Varlot, E. Reynaud, G. Vigier, and J. Varlet, "Mechanical properties of clay-reinforced polyamide," *J. Polymer. Sci., Part B: Polymer. Phys*., **40** (2002) pp. 272-283

13. M. Alexandre, P. Dubois, T. Sun, J.M. Garces, R. Jerome, "Polyethylene-layered silicate nanocomposites prepared by the polymerization-filling technique: synthesis and mechanical properties," *Polymer*, **43,** (2002) pp. 2123-2132

14. M. Kato, H. Okamoto, N. Hasegawa, A. Tsukigase, A. Usuki, "Preparation and Properties of Polyethylene-Clay Hybrids," *Polym. Eng. Sci*., **43,** (2003) pp. 1312-1316

15. R. Vaia and E.P. Giannelis, "Polymer Melt Intercalation in Organically-Modified Layered Silicates: Model Predictions and Experiment," *Macromolecules*, **30** (1997), pp. 8000-8009

16. B. Yalcin and M. Cakmak, "The role of plasticizer on the exfoliation and dispersion and fracture behavior of clay particles in PVC matrix: a comprehensive morphological study" *Polymer*, **45,** (2004), pp. 6623-6638

17. A.B. Morgan and J.W. Gilman, "Characterization of poly-layered silicate (clay) nanocomposites by transmission electron microscopy and X-ray diffraction: a comparative study," *J. Appl. Polym. Sci.,* **87,** (2003) pp. 1329–1338

18. W. Lertwimolnun, B. Vergnes, "Influence of compatibilizer and processing conditions on the dispersion of Nanoclay in a polypropylene matrix," *Polymer*, **46,** (2005) pp. 3462-3471

19. G. Galgali, C. Ramesh, A. Lele, "A Rheological Study on the Kinetics of Hybrid Formation in Polypropylene Nanocomposites," *Macromolecules* **34** (2001) pp. 852-858

20. L. Zhu, M. Xanthos, "Effects of Process Conditions and Mixing Protocols on Structure of Extruded Polypropylene Nanocomposites," *J. App. Polym. Sci* **93** (2004) pp. 1891-1899

21. M.J. Solomon, A.S Almusallam, K.F. Seefeldt, A. Somwangthanaroj, P. Varadan, "Rheology of Polypropylene/Clay Hybrid Materials," *Macromolecules* **34** (2001) pp. 1854-1872

22. V.E. Yudin, G.M. Divoux, J.U. Otaigbe, V.M. Svetlichnyi, "Synthesis and rheological properties of oligoimide/montmorillonite nanocomposites," *Polymer* 46 (2005) pp. 10866-10872

23. T.H. Kim, S.T. Lim, C.H. Lee, H.J. Choi, M.S. Jhon, "Preparation and Rheological Characterization of Intercalated Polystyrene/Organophilic Montmorillonite Nanocomposite,"*J. App. Polym. Sci*. **87** (2003) pp. 2106-2112

24. R. Qi, X. Jin, J. Nie, W. Yu, C. Zhou, "Synthesis and Properties of Polystyrene-Clay Nanocomposites via In Situ Intercalative Polymerization," *J. App. Polym. Sci.,* **97,** (2005) pp. 201-207

25. Y. Zhong, Z. Zhu, S-Q. Wang, "Synthesis and rheological properties of polystyrene/layered silicate nanocomposite," *Polymer*, **46,** (2005) pp. 3006-3013

26. A.J. Hsieh, P. Moy, F.L. Beyer, P. Madison, E. Napadensky, "Mechanical Response and Rheological Properties of Polycarbonate Layered-Silicate Nanocomposites," *Polym. Eng. Sci.,* **44,** (2004) pp. 825-837

27. K.M. Lee, C.D. Han, "Linear Dynamic Viscoelastic Properties of Functionalized Block Copolymer/Organoclay Nanocomposites," *Polymer*, **44,** (2003) pp. 4573-4588

28. J. Ren, A.S. Silva, R. Krishnamoorti, "Linear Viscoelasticity of Disordered Polystyrene-Polyisoprene Block Copolymer Based Layered-Silicate Nanocomposites," *Macromolecules,* **33,** (2000) pp. 3739-3746

29. J.M. Dealy, "Rheometers for Molten Plastics", Van Nostrand Reinhold Company. New York, (1982) pp. 41-56

30. A. Usuki, M. Kato, A. Okada, T. Kurauchi, "Synthesis of polypropylene-clay hybrid," *J. Applied Polymer Sci.*, **63**, (1997), pp. 137-138

31. M. Kawasumi, N. Hasegawa, M. Kato, A. Okada, A. Usuki, **"**Preparation and Mechanical Properties of Polypropylene-Clay Hybrids," *Macromolecule*s, **30**, (1997) pp. 6333-6338

32. K. H. Wang, M.H. Choi, C.S. Koo, Y.S. Choi, I.J. Chung, "Synthesis and characterization of maleated polyethylene/clay nanocomposites," *Polymer*, **42**, (2001) pp. 9819

33. Y.T. Lim, O.O. Park, "Phase morphology and rheological behavior of polymer/layered silicate nanocomposites," *Rheol. Acta,* **40** (2001), pp. 220-229

34. T.G. Gopakumar, J.A. Lee, M. Kontopoulou, J.S. Parent, "Influence of clay exfoliation on the physical properties of montmorillonite/polyethylene composites," *Polymer*, **43,** (2002) pp. 5483-5491

35. S. G. Hatzikiriakos, N. Rathod, E.B. Muliawan, "The Effect of Nanoclays on the Processibility of Polyolefins," *Polym. Eng. Sci*., **45,** (2005) pp. 1098-1107

36. K.H Wang, M.H. Choi, C.M. Koo, M. Xu, I.J. Chung, M.C. Jang, S.W. Choi, H.H. Song, "Morphology and Physical Properties of Polyethylene/Silicate Nanocomposite Prepared by Melt Intercalation," *J. Applied Polymer Sci. Part B: Polym. Phys*., **40,** (2002) pp. 1454-1463

37. P. Mederic, T. Razafinimaro, T. Aubry, M Moan, M.H. Klopffer, "Rheological and Structural Investigation of Layered Silicate Nanocomposites Based on Polyamide or Polyethylene: Influence of Processing Conditions and Volume Fraction Effects," *Macromol. Symp*., **221,** (2005) pp. 75-84

38. J.A. Lee, M. Kontopoulou, J.S. Parent, "Time and shear dependent rheology of maleated polyethylene and its nanocomposites," *Polymer,* **45,** (2004) pp. 6595-6600

39. W.S. Chow, Z.A. Mohd, U.S. Ishiaku, J. Karger-Kocsis, A.A. Apostolov, "The Effect of Organoclay on the Mechanical Properties and Morphology of Injection-Molded Polyamide 6/Polypropylene Nanocomposites," *J. Appl. Polym. Sci.,* **91,** (2004) pp. 175-189

40. M. Yuan, A. Winardi, S. Gong, L-S. Turng, "Effects of Nano- and Micro-fillers and Processing Parameters on Injection-Molded Microcellular Composites," *Polym. Eng. Sci*., **45,** (2005) pp. 773-788

41. T.D. Fornes, P.J. Yoon, D.R. Paul, "Polymer matrix degradation and color formation in melt processed nylon 6/clay nanocomposites," *Polymer,* **44,** (2003) pp. 7545-7556

42. T.D. Fornes, D.L. Hunter, D.R. Paul, "Effect of sodium montmorillonite source on nylon 6/clay nanocomposites," *Polymer,* **45**, (2004) pp. 2321-2331

43. T.D. Fornes, P.J. Yoon, D.L. Hunter, H. Keskkula, D.R. Paul, "Effect of organoclay structure on nylon 6 nanocomposite morphology and properties," *Polymer*, **43,** (2002) pp. 5915-5933

44. T.D. Fornes, D.L. Hunter, D.R. Paul, "Nylon-6 Nanocomposites from Alkylammonium-Modified Clay: The Role of Alkyl Tails on Exfoliation," *Macromolecule*s, **37**, (2004) pp. 1793-1798

45. L. Chen, S-C. Wong, S. Pisharath, "Fracture Properties of Nanoclay-Filled Polypropylene," *J. Appl. Polym. S*ci., **88,** (2003) pp. 3298-3305

46. G. Galgali, S. Agarwal, A. Lele, "Effect of clay orientation on the tensile modulus of polypropylene–nanoclay composites," *Polymer,* **45,** (2004) pp. 6059-6069

47. Y.T. Vu, G.S. Rajan, J.E. Mark, C.L. Myers, "Reinforcement of elastomeric polypropylene by nanoclay fillers," *Polym. Int*., **53,** (2004) pp. 1071-1077

48. A. Leuteritz, D. Pospiech, B. Kretzschmar, M. Willeke, D. Jehnichen, U. Jentzsch, K. Grundke, A. Janke, "Polypropylene-Clay Nanocomposites: Comparison of Different Layered Silicates," *Macromol. Symp*., **221,** (2005) pp. 53-61

49. M.A. Osman, J.E.P. Rupp, U.W. Sutter, "Tensile Properties of polyethylene-layered silicate nanocomposites," *Polymer,* **46,** (2005) pp. 1653-1660

50. M. Mehrabzadeh, M.R. Kamal, "Melt Processing of PA-66/Clay, HDPE/Clay and HDPE/PA-66/Clay Nanocomposites," *Polym. Eng. Sci*., **44,** (2004) pp. 1152-1161

51. G. Liang, J. Xu, S. Bao, W. Xu, "Polyethylene/Maleic Anhydride Grafted Polyethylene/Organic-Montmorillonite Nanocomposites. I. Preparation, Microstructure, and Mechanical Properties," *J. Applied Polymer Sci.*, **91,** (2004) pp. 3974-3980

52. J. Heinemann, P. Reichert, R. Thomann, R. Mulhaupt, "Polyolefin nanocomposites formed by melt compounding and transition metal catalyzed ethane homo- and copolymerization in the presence of layered silicates," *Macromol. Rapid Commun*., **20,** (1999) pp. 423-430

53. J. Morawiec, A. Pawlak, M. Slouf, A. Galeski, E. Piorkowska, N. Krasnikowa, "Preparation and properties of compatibilized LDPE/organo-modified montmorillonite nanocomposites," *European Polymer Journal*, **41,** (2005) pp. 1115-1122

54. J. C. Halpin and J. L. Kardos, "The Halpin-Tsai Equations: A Review," *Polym. Eng. Sci*, **16,** (1976) pp. 344-352

55. R.F. Gibson, *Principles of Composite Material Mechanics*, McGraw-Hill, New York (1994)

56. X.L. Ji, J.K. Jing, W. Jiang, B.Z. Jiang, **"**Tensile modulus of polymer nanocomposites," *Polym. Eng. Sci*, **42,** (2002) pp. 983-993

57. T.D. Fornes, D.R. Paul, "Modeling properties of nylon 6/clay nanocomposites using composite theories," *Polymer*, **44,** (2003) pp. 4993-5013

58. Y. Zhong, D. De Kee, "Morphology and Properties of Layered Silicate-Polyethylene Nanocomposite Blown Films," *Polym. Eng. Sci*., **45,** (2005) pp. 469-477

59. E.C. Lee, D.F. Mielewski, R.J. Baird, "Exfoliation and Dispersion Enhancement in Polypropylene Nanocomposites by In-Situ Melt Phase Ultrasonication," *Polym. Eng. Sci*., **44,** (2004) pp. 1773-1782

60. D. Kaempfer, R. Thomann, R. Mulhaupt, "Melt compounding of syndiotactic polypropylene nanocomposites containing organophilic layered silicates and in situ formed core/shell nanoparticles," *Polymer*, **43,** (2002) pp. 2909-2916

61. H.S. Jeon, J.K. Rameshwaram, "Fabrication and characterization of intercalated/exfoliated polydiene polymers-clay nanocomposites," *Computational Methods in Materials Characterisation*, Edited by A.A. Mammoli, C.A. Brebbia, Computational Mechanics, Boston, MA, (2004) pp. 255-263

62. S. Tanoue, L.A. Utracki, A. Garcia-Rejon, J. Tatibouet, M.R. Kamal, "Melt Compounding of Different Grades of Polystyrene With Organoclay. Part 3: Mechanical Properties," *Polym. Eng. Sci.*, **45,** (2005) pp. 827-837

63. S. Tanoue, L.A. Utracki, A. Garcia-Rejon, P. Sammut, M-T. Ton-That, I. Pesneau, M.R. Kamal, J.Lyngaae-Jorgensen, "Melt Compounding of Different Grades of Polystyrene With Organoclay. Part 2: Rheological Properties," *Polym. Eng. Sci.,* **44,**(2004) pp. 1061-1076

64. S. Tanoue, L.A. Utracki, A. Garcia-Rejon, J. Tatibouet, K.C. Cole, M.R. Kamal, "Melt Compounding of Different Grades of Polystyrene With Organoclay. Part 1: Compounding and Characterization," *Polym. Eng. Sci.*, **44,** (2004) pp. 1046-1060

65. R.A. Vaia, K.D. Jandt, E.J. Kramer, E.P. Giannelis, "Kinetics of Polymer Melt Intercalation," *Macromolecules,* **28,** (1995) pp. 8080-8085

66. T.D. Fornes, P.J. Yoon, H.Keskkula, D.R. Paul, "Nylon 6 nanocomposites: the effect of matrix molecular weight," *Polymer,* **42,** (2001) pp. 9929-9940

67. Z. Shen, G.P. Simon, Y. Cheng, "Effects of Molecular Weight and Clay Organo-Ions on the Melt Intercalation of Poly(Ethylene Oxide) Into Layered Silicates," *Polym. Eng. Sci*., **42,** (2002) pp. 2369-2382

3.0 Effect of Matrix Molecular Weight on the Dispersion of Nanoclay in Unmodified High Density Polyethylene

David Chu and Donald G. Baird

Department of Chemical Engineering, Virginia Polytechnic Institute and State University, 131 Randolph Hall, Blacksburg, VA 24061

Abstract

The effect that polymer molecular weight has on the dispersion of relatively polar montmorillonite (MMT) in non-polar, unmodified high density polyethylene (HDPE) was examined. Polymer layered silicate (PLS) nanocomposites were prepared via melt compounding in a single screw extruder using three unmodified HDPE matrices of differing molecular weight and organically modified MMT (organoclay) in concentrations ranging from 2 wt% to 8 wt%. The weight average molecular weights ($\overline{M}_w$) of the HDPE matrices used ranged from 87,000 g/mol to 460,000 g/mol. X-ray diffraction (XRD), tensile testing, dynamic mechanical thermal analysis (DMTA), and dynamic rheometry were performed on these nanocomposites. Nanocomposites generated from the high molecular weight (HMW) HDPE matrix exhibited increased intercalation of the MMT as shown by XRD and greater improvements in the Young's modulus compared to nanocomposites generated from the low (LMW) and middle molecular weight (MMW) matrices. DMTA measurements carried out in torsion showed that the increase in shear modulus of the HMW nanocomposites was not as great as that of the LMW and MMW counterparts as observed from a lower percentage enhancement in the storage modulus (G') and estimated heat distortion temperature (HDT). This was attributed to the higher degree of mechanical anisotropy in the HMW nanocomposites.

Dynamic rheology indicated that a percolated network did not exist in any of the nanocomposites as shown by no change in the terminal behavior of G' upon addition of clay.

3.1 Introduction

Preparation of polymer/layered silicate nanocomposites (PLS) via melt blending is an economically friendly method of generating materials with improved strength and stiffness [1]. However, property enhancements obtained by this method are not as dramatic as those seen from PLS nanocomposites generated by in-situ polymerization due to less homogeneity in the dispersion of the clay particles within the polymer matrix [1]. In the in-situ polymerization method, monomer and nanoclay are combined leading to the swelling of the clay, and the polymerization reaction takes place directly in between the sheets of clay, while melt blending relies on polymer chains penetrating in between the clay platelets typically with the aid of shear [1].

Much academic as well as industrial research focused in the area of the preparation of (PLS) nanocomposites was motivated in large part by the work done by the Toyota research group in Japan who synthesized nylon 6/montmorillonite (MMT) nanocomposites via the in-situ polymerization technique [2]. A 55% increase in the tensile modulus and 87°C increase in the heat distortion temperature were reported [2]. However, the in-situ polymerization technique as well as solution blending technique, which utilizes organic solvents to swell the MMT, are both environmentally as well as economically unfriendly due to the use of organic solvents and chemical reagents. Vaia et al. [3] were among the first researchers who reported the possibility to generate these nanocomposites by simple melt compounding and, thus, providing a "green" approach to forming these materials. Past work on PLS nanocomposites included a wide variety of polymers including polyethylene, polypropylene, polyimide, polystyrene, polycarbonate, and a polystyrene/polyisoprene block copolymer [4-9]. Filling polymer matrices with

these nanoclays has been shown to yield materials with dramatically increased mechanical [10, 11], gas barrier [12, 13], and thermal stability properties [14, 15] with low loadings of clay (i.e less than 5 wt%).

The main reason for these marked improvements stem from the large aspect ratio of montmorillonite (MMT). Each individual layer of clay has a thickness on the order of 1 nanometer (nm) with lengths ranging from 100 nm to 300 nm [11, 16]. The high aspect ratio leads to a high contact surface area and, thus, physical interactions between the polymer and layered silicates with only a small concentration of clay. However, because the layered silicates typically exist as aggregates due to attractive van der Waals forces [17], the contact surface area available and, thus, improvements in physical properties do not reach theoretical expectations. Achieving a nanocomposite with an exfoliated morphology in which each individual layered silicate has been separated from its initial stack and dispersed uniformly throughout a given polymer matrix is the key to reaching the full potential of the nanoclays to enhance mechanical, thermal, and barrier properties of a polymeric matrix.

There are three main factors thought to be responsible for determining the amount of exfoliation that is able to be achieved when making PLS nanocomposites. First, the attractive interactions between the polymer matrix and the layered silicates determine, in large part, the degree of compatibility between the two separate phases. Layered silicates are naturally hydrophilic while many polymers such as polyolefins are hydrophobic and, thus, the surface energies between the two materials can be vastly different prohibiting any significant degree of dispersion of nanoclay within the polymer. Modification of layered silicates via ion exchange reactions through which quaternary alkyl ammonium

cations replace the existing cations (Ca^+, Na^+, Li^+ etc.) residing in the interlayer of the silicates help to make the layered silicates more organophilic. Non-polar polymers such as polyolefins can also be modified to where the polar maleic anhydride is grafted onto the backbone of polymers such as various polyethylenes or polypropylenes [18-21] increasing the hydrophilicity of the polymer matrix.

The next two factors which influence the level of exfoliation in a PLS nanocomposite both depend on the molecular weight of the polymer matrix, but in opposing manners. The size of a polymer chain increases as the molecular weight of the polymer sample increases. Larger polymers have more difficulty in penetrating the interlayer gap of the layered silicates whose distance from each other typically range from 15 Å to 35 Å [22]. Thus, increased molecular weight was seen to have a negative influence on exfoliating the clays in this respect as shown previously [23-30]. On the other hand, with increasing polymer molecular weight, the viscosity of the material increases as well. Increased viscosity leads to an increased amount of shear force available to be exerted by the polymer matrix onto the aggregates of nanoclay and assists in separating each individual clay platelet from one another through what has been postulated to be a "peeling" mechanism [31, 32].

Much work has been performed on the effect that varying the molecular weight of either a polymer matrix or a compatibilizer has on the dispersion of nanoclays within a given polymer [23-32]. A variety of polymers have been studied ranging from relatively non-polar polyolefins such as polyisoprene to polyamides such as nylon 6 which contain many sites for hydrogen bonding to occur. However, mixed results have been found in the literature concerning the role matrix molecular weight plays [23-32]. There are

benefits to using both a low molecular weight polymer as there are in using a high molecular weight polymer, and the extent to which these two competing factors influence the degree of clay dispersion and enhancement in mechanical properties remains unclear. Only in Kaempfer's [31] study of syndiotactic polypropylene/fluorohectorite nanocomposites and Fornes' [32] examination of nylon 6/MMT nanocomposites was it found that increasing the molecular weight of the matrix (or of maleated polypropylene compatibilizer in Kaempfer's case) increased the degree of exfoliation of the nanocomposites.

It is the purpose of this work to determine if nanoclays can be exfoliated in non-polar, unmodified HDPE of various molecular weights via single screw extrusion. The molecular weights of the HDPE used are approximately 87,000 g/mol, 155,000 g/mol, and 460,000 g/mol. This range of molecular weights is as large if not larger than has been used in past work concerning matrix molecular weight on the dispersion of nanoclays. The degree of exfoliation or intercalation is assessed by x-ray diffraction. The change in mechanical and rheological properties as a function of matrix molecular weight and MMT concentration is examined as well in order to assess the tradeoff between property enhancement and processability.

3.2 Experimental

3.2.1 Materials

Three high density polyethylene (HDPE) samples obtained from Chevron Phillips Chemical Company were designated here as "low", "middle", and "high" molecular weight samples. The $\overline{M}_W$, polydispersity (PDI) given as $\overline{M}_W / \overline{M}_N$, density (r), and melt

index (MI) of the three samples are listed in Table 3.1 as supplied by Chevron Phillips. Organically modified montmorillonite (organoclay) "Cloisite 20A" was supplied by Southern Clay Products (Gonzales, TX). The organic modifier used was a dimethyl, dihydrogenatedtallow, quaternary ammonium salt (2M2HT). The physical properties of Cloisite 20A (20A) are listed in Table 3.2

3.2.2 Melt Compounding

Prior to melt compounding, all nanocomposites were dry-mixed in a blender by combining the desired weight percent of organoclay with the desired amount of HDPE. The dry blended mixture was then placed in a vacuum oven at 105°C for a period of time between 18 to 24 hours to remove moisture. The dried clay/HDPE mixtures were then fed to a Killion single screw extruder (L/D = 18, barrel diameter of 25.25 mm, and variable screw root diameter from 16.6 mm at the feed to 21.45 mm at the exit) operating with a temperature profile of 130°C, 160°C, 160°C, and 190°C and screw speed of 20 rpm. Strands of the nanocomposites exiting the extruder die were cooled in a 1 m long water bath and fed to a pelletizer to generate pellets for further processing.

3.2.3 Determination of Actual Clay Content

Table 3.3 lists the actual compositions of the nanocomposites generated in this study. Here "organoclay" refers to the organically modified MMT used in this study, Cloisite 20A, and MMT represents pure MMT without the organically treated surface. Compositions were determined by placing nanocomposite pellets generated from extrusion onto aluminum trays in an ashing oven at 500°C for 45 minutes. The mass

fraction of actual MMT (x_{MMT}) in each nanocomposite was then taken to be the ratio of the mass of ash to the mass of nanocomposite before burning.

In order to find the mass fraction of organoclay (x_{OC}), a separate experiment was necessary to determine the fraction of organic modifier in the organoclay that degraded after being placed in the ashing oven. It was found that the weight fraction of organic modifier in the organoclay was 0.374 and this was divided into the mass of ash determined above to calculate the actual mass of organoclay in the nanocomposite. Using this mass and the mass of nanocomposite prior to burning, x_{OC} was found.

The corresponding volume fraction of the organoclay (f_{OC}) and MMT (f_{MMT}) in the nanocomposites was found by

$$f_{OC} = \left(\frac{r_{NC} \times x_{OC}}{r_{OC}} \right) \tag{3}$$

and

$$f_{MMT} = \left(\frac{r_{NC} \times x_{NC}}{r_{MMT}} \right) \tag{4}$$

where r_{NC}, r_{OC}, and r_{MMT} are the densities of the nanocomposite, organoclay and MMT, respectively. r_{OC}, and r_{MMT} were taken to be 1.77 g/cm^3 and 2.86 g/cm^3, respectively, as given by the manufacturer [22]. An upper bound on r_{NC} was estimated by using the rule of mixtures presented below:

$$r_{NC} = f_{HDPE} r_{HDPE} + f_{OC} r_{OC} . \tag{5}$$

Here f_{HDPE} and f_{OC} are the volume fractions of the HDPE matrix and organoclay, respectively. In order for r_{NC} to be calculated from Eq 5, both f_{HDPE} and f_{OC} were estimated from the initial masses of HDPE and organoclay used to generate the

nanocomposites as well as the given density values of the HDPE matrices and organoclay. These results are summarized in Table 3.4.

3.2.4 Injection Molding

The nanocomposite pellets prepared previously during extrusion were dried at 105°C in vacuum for 18 to 24 hours and then injection molded using an Arburg Allrounder Model 221-55-250 injection molder. The Arburg Allrounder has a 22 mm diameter barrel, L/D = 24, screw with variable root diameter from approximately 14.25 mm at the feed to 19.3 at the exit, a check ring non-return valve, and an insulated nozzle that is 2 mm in diameter. The composites were injection molded, using a melt temperature of 190°C, a mold temperature of 70°C, a holding pressure of 5 bars, and a screw speed of 200 rpm, into a rectangular end-gated mold with dimensions of 80 mm by 76 mm by 1.6 mm. The mold was allowed to heat for 4 hrs prior to molding to ensure thermal equilibrium.

3.2.5 X-Ray Diffraction

Wide angle x-ray diffraction (WAXD) patterns were conducted using a Scintag XDS 2000 diffractometer with CuKa radiation (wavelength = 1.542Å) at a scan rate of 0.5 deg/min on injection molded plaques.

3.2.6. Tensile Properties

The tensile properties were measured using an Instron Mechanical Tester (model 4204) following the ASTM standard D638. The test samples were cut from injection molded plaques typically in the direction of flow having dimensions of approximately 8 mm wide, 1.6 mm thick, and 80 mm in length. The load was measured with a 1 kN load

cell, and the strain was measured using an extensiometer (Instron model 2630-25), while the cross-head speed was kept at 1.27 mm/min during all tensile tests. For all tests, the average and the standard deviation were calculated from at least five samples, and data points greater than 2 standard deviations from the mean were removed. All tests were performed at ambient conditions (room temperature).

3.2.7 Dynamic Mechanical Thermal Analysis (DMTA)

Dynamic mechanical thermal analysis (DMTA) of the MMT/HDPE nanocomposites was performed using a Rheometrics RMS-800. Measurements of storage modulus (G'), loss modulus (G") and tan d were recorded as a function of temperature in the range of 30°C to 140°C at a ramp rate of 3°C/min and frequency of 1.0 Hz under a continuous nitrogen environment. To perform the tests, rectangular strips approximately 80 mm long by 8 mm wide by 1.6 mm thick were cut in the flow direction of injection molded square plaques.

3.2.8 Rheological Characterization

The dynamic rheological properties ($|h^*|$, G', G") for each nanocomposite were determined using a Rheometrics Mechanical Spectrometer Model 800 (RMS-800). The dynamic oscillatory data were collected over the range of 0.1 – 100 rad/sec using 25 mm parallel plate fixtures at a temperature of 190°C and strain amplitude of 5%. All testing was performed within an inert nitrogen atmosphere to prevent thermo-oxidative degradation. Prior to each test, samples were allowed to equilibrate at 190°C for 10 minutes between the parallel plate fixtures. Test samples were prepared by compression molding the pellets prepared previously into 25 mm diameter circular disks with

thicknesses between 1-2 mm using a Carver Laboratory Press at 190°C under nominal pressure for 10 min and allowing them to cool slowly. Samples were dried at 105°C in vacuum for 18-24 hours before pressing into the 25 mm disks and prior to rheological testing as well. Strain sweeps for the unfilled and 8 wt% nanocomposites at each molecular weight were performed at a frequency of 5.0 rad/sec and temperature of 190°C to ensure dynamic rheology was performed within the linear viscoelastic range of the material. Time sweeps were performed at 230°C, 1.0 rad/sec, and 5% strain to ensure thermal stability of nanocomposites at this temperature.

3.3 Results and Discussion

3.3.1 X-Ray Diffraction (XRD)

The XRD spectrum of MMT Cloisite 20A is presented in Figure 3.1 along with the diffraction spectra of the 8 wt% clay nanocomposites for the three molecular weight matrices used in this study. Upon characterization of injection molded plaques of the 8 wt% nanocomposites, a lowering in intensity of the diffraction peak was observed compared to the clay itself corresponding to a lowering in the concentration of clay. The d-spacing of Cloisite 20A, calculated from Bragg's Law ($d_{001} = l /2\sin q$), was found to be 24.2 Å, which was also the value given by the manufacturer, Southern Clay Products [22]. The nanocomposites each displayed two characteristic diffraction peaks: one at a smaller angle relative to that of the clay and another at a larger angle. The peaks located at the smaller angle corresponded to a larger distance separating the clay particles, namely 28.3 Å, 29.4 Å, and 33.2 Å for the LMW, MMW, and HMW samples, respectively, while the higher angle diffraction peaks were related to smaller d-spacings

of 23.0 Å, 22.0 Å, and 23.0 Å for the LMW, MMW, and HMW samples, respectively. The occurrence of these two peaks in each composite was attributed to the simultaneous expansion of the clay galleries due to intercalation of the various HDPE matrices in between the MMT platelets and collapse of the interlayer galleries during melt processing of the nanocomposites.

The reader is reminded that prior to XRD analysis, the nanocomposites were melt blended in a single screw extruder, then injection molded into plaques for testing. The thermodynamic stability of melt processed PE nanocomposites has been discussed by Alexandre et al. [34] who studied in situ polymerized nanocomposites containing 3.4 wt% unmodified hectorite clay. The initial XRD spectra of the in situ polymerized nanocomposite suggested an exfoliated morphology due to the absence of any diffraction peaks. Upon subsequent melt processing in the form of compression molding, broad diffraction peaks were observed between angles of $2q$ = 4° to 8° which the authors attributed to the reformation of repetitive clay structures due to collapse. This collapse suggested that the exfoliated nanocomposite structure was thermodynamically unfavorable for non-polar polymer such as polyethylene and polystyrene (PS) which have little to no attractive interactions with the clay itself [35].

Degradation of the organic modifier may also account for the observed decrease in d-spacing of the nanocomposites upon melt processing. Tanoue et al. [30] observed a collapse in the structures of PS/MMT nanocomposites and verified via Fourier Transform Infrared Spectroscopy (FT-IR) that thermal degradation occurred during the extrusion process in a twin screw extruder (TSE) at a temperature of 200°C and 200 rpm. Degradation of the organic modifier, which in this case was a quaternary alkyl

ammonium salt containing two methyl, one benzyl, and one hydrogenated tallow substituents, would reduce the interlayer spacing between the clay platelets because the location of the organic modifier is on the surface of the clay platelet. Other researchers have also reported the instability of organic modifiers in MMT at temperatures at 200°C or above [36-38]. Even though the results presented here were all obtained on samples melt processed at 190°C, the possibility of thermal degradation cannot be excluded due to the proximity of the processing temperature to 200°C. Furthermore the nanocomposites were subjected to two separate processing operations, i.e. extrusion and injection molding.

It was postulated that degradation of the organic modifier residing in the interlayer of the MMT used here was responsible for the observed collapse in d-spacing from 24.2 Å for the as received organically modified MMT to 23.0 Å, 22.0 Å, and 23.0 Å for the LMW, MMW, and HMW 8% nanocomposites, respectively. Each nanocomposite has been processed using identical conditions during extrusion (190°C, 20 rpm) and injection molding (190°C, 200 rpm). If the quaternary alkyl ammonium cation was in fact degrading at the conditions reported here, it would seem likely that the extent to which the organic modifier was degrading would be comparable for each nanocomposite. This statement was supported by noting the diffraction peaks corresponding to the collapsed structure for each nanocomposite were nearly identical to one another differing by 1.0 Å. On the other hand, if the interlayer collapse was due to compression of the clay galleries due to the viscous matrix, it would be expected that the more viscous HMW matrix would cause a greater decrease in the d-spacing observed by XRD than the less viscous LMW and MMW matrices. Indeed the LMW nanocomposite exhibits the same calculated

d-spacing as the HMW nanocomposite and, thus, there appears to be no effect of matrix viscosity on the thermodynamic stability of the nanoclays within the nanocomposite for this system of HDPE's.

The observed increase in the d-spacings of the 8 wt% nanocomposites was attributed to increased intercalation with increased matrix molecular weight. As the molecular weight of the polymer was increased so was the viscosity of the material, and thus, the shear force generated by means of the matrix on the clay platelets was increased and their separation and dispersion throughout the HDPE matrix was improved. Previous work has shown that increasing the molecular weight of a polymer matrix or the molecular weight of a compatibilizer can increase the separation of clay platelets as shown by XRD. Fornes et al. [32] worked with three different nylon 6 matrices of M_n = 16,400 (LMW), 22,000 (MMW), and 29,300 (HMW) g/mol and found that no diffraction peak existed for both the MMW and HMW samples, while the LMW exhibited a characteristic diffraction peak. They proposed that the higher molecular weight matrices imparted greater shear stress onto the stacks of clay platelets to separate them and achieve exfoliation while the LMW system only "skewed" the stacks rather than exfoliate them.

Kaempfer et al. [31] examined polypropylene(PP)/MMT nanocomposites where two samples of maleic anhydride grafted PP of different molecular weight were added as a compatibilizer to the PP/MMT composite. It was found that the nanocomposite containing the higher molecular weight compatibilizer (Mn=7,500 g/mol) showed a XRD peak at a smaller $2q$ angle, and hence, greater intercalation of the PP/MMT nanocomposite compared to the low molecular weight compatibilizer (Mn= 2,900 g/mol). The d-spacing for the nanocomposite containing the HMW compatibilizer was given to

be 68 Å compared to 29 Å for the LMW compatibilizer. Hence, it was concluded that increasing the shear force exerted onto MMT aggregates through increased polymer molecular weight does have a positive influence on intercalating, and in some cases exfoliating [32], polymer chains within nanoclay galleries. It was also noted that this molecular weight effect has not been shown before for unmodified HDPE. It was found that Zhong et al. [23] varied the molecular weight of a maleated HDPE compatibilizer in generating their nanocomposites. However, no change was observed in the d-spacings of their 5 wt% MMT, 5 wt% maleated HDPE, 90 wt% HDPE nanocomposites as the compatibilizer molecular weight was varied.

3.3.2 Tensile Properties

Previous work has shown that as the level of clay intercalation was increased in a PLS nanocomposite, greater improvements in mechanical properties such as the Young's modulus have been found compared to less intercalated systems of comparable clay loading [3, 33]. The tensile properties presented in the following discussion are summarized in Tables 3.5-3.7. The XRD results presented above indicated that a greater amount of intercalation occurred for the HMW nanocomposite containing 8 wt% clay, shown by a larger d-spacing compared to the LMW and MMW composites. In comparing the Young's modulus for each of the 8 wt% nanocomposites as shown in Figure 2, a greater percentage increase in the Young's modulus occurred for the HMW matrix relative to its unfilled matrix, 68%, compared to that of the LMW and MMW 8 wt% nanocomposites which exhibited 46% and 33% increases in Young's modulus, respectively. Similarly, at 4 wt% clay, a 26% increase in Young's modulus occurred for the HMW nanocomposite relative to its unfilled matrix compared to 8.3% and 20% for

the LMW and MMW nanocomposites, respectively. Greater separation of the clay platelets within a polymer matrix at a constant concentration, in this case 8 wt%, would lead to greater dispersion of the nanoclays and reduce the amount of aggregates existing within the nanocomposite. Aggregation of clay particles has been shown to reduce the amount of reinforcement that can be provided by the clays resulting in less enhancement of the Young's modulus [32].

The increased d-spacing observed for the HMW nanocomposite was postulated to be a result of the increased shear stress generated by means of both extrusion and injection molding the HMW matrix to separate the clay platelets compared to that of the less viscous LMW and MMW matrices. Kaempfer et al. [31] and Fornes et al. [32] have both reported greater levels of exfoliation with higher molecular weight polymers resulting in greater increases in the Young's modulus relative to the unfilled matrix. Fornes et al. [32] studied nylon 6/MMT nanocomposites, where the MMT was surface treated with a methyl, tallow, bis-2-hydroxyethyl, quaternary ammonium cation, and reported a 107% increase for both the MMW and HMW nanocomposites at approximately 7 wt% clay loading compared to a 74.5% increase for the LMW nanocomposite. Kaempfer et al. [31] studied maleated PP and varied the molecular weight of the maleated PP used as a compatibilizer between the clay and polymer matrix. At a 5 wt% clay content and 20 wt% compatibilizer content, it was found that the modulus of the composite containing the HMW compatibilizer increased by 128% relative to that of the unfilled matrix containing 20 wt% of the compatibilizer. In comparison, the specimen containing the LMW compatibilizer showed an increase of 102% for the Young's modulus.

Similar observations were made with the stress at 0.2% yield (Figure 3.3) with regard to clay concentration, namely, the stress required to cause a 0.2% yield increased with increasing clay content, as was the case for the Young's modulus. The stress at peak, shown in Figure 3.4, exhibited only a slight variation for the LMW and MMW nanocomposites at all clay concentrations, while the HMW nanocomposite showed a noticeably greater increase at 8 wt% clay content of 14% relative to its unfilled counterpart.

The percent elongation at break in general decreased with increasing clay content for all molecular weights as observed in Figures 3.5 and 3.6. This behavior was attributed to the nanocomposites becoming more brittle as the inorganic filler particles were added to the polymer matrix. However, a greater percentage decrease in the elongation at break was observed for the nanocomposites compounded from the LMW matrix which exhibited a 91% decrease in going from the unfilled LMW matrix to the 8 wt% nanocomposite. The MMW and HMW 8 wt% nanocomposites exhibited 80% and 23% decreases in percent strain at break relative to their corresponding unfilled matrices, respectively. The larger decrease observed in the LMW nanocomposites may be explained by the fact that more clay aggregates exist in the LMW nanocomposites due to less separation of the clay platelets due to the less viscous polymer matrix. The clay aggregates act as stress concentrators reducing the ductility of the nanocomposites. Fornes et al. [32] have shown similar observations in their work with various molecular weight nylon 6 matrices.

The stress at break in Figure 3.7 exhibits conventional behavior for the nanocomposites compounded from the LMW and MMW HDPE matrices. A decrease in

the stress at break was observed as clay was added to both these matrices indicating a weakening of the material due to unexfoliated clay particles acting as stress concentrators as was argued in accounting for the decrease in the percent elongation at break in the previous paragraph. This behavior has also been shown by other authors as well in work involving PS, HDPE, and LDPE [30, 39-40]. However, anomalous behavior was seen in the HMW nanocomposites, specifically at 8 wt% clay concentration. As the clay content was increased in the HMW nanocomposites from 0 to 4 wt%, the stress at break decreases as expected, but a dramatic rise in the stress at break occurs at a clay loading of 8 wt% where the stress at break increased from 13.8 MPa to 40.4 MPa representing a 193% increase. Although a greater interlayer separation for the 8 wt% HMW nanocomposite was observed via XRD compared to the 8 wt% LMW and MMW samples, it was not believed to be sufficient to account for such an increase in strength. It was believed that true exfoliation has not been achieved in this 8 wt% nanocomposite and, thus, it was concluded that clay aggregates must remain within the HMW HDPE matrix. It remains unclear as to the cause of such behavior.

3.3.3 Injection Molding vs. Compression Molding

The influence of the processing method on the tensile properties of the nanocomposites was examined by compression molding the 8 wt% nanocomposites at all three molecular weights and comparing their properties to those of their injection molded counterparts. It was found that the Young's moduli of the compression molded nanocomposites were significantly less than those of injection molded samples as shown in Figure 3.8. The nanocomposites compounded from the LMW and MMW HDPE matrices showed a 34% and 26% increase in Young's modulus, respectively, upon

injection molding. However, the greatest difference in modulus between compression molded and injection molded nanocomposites was found with the HMW matrix. An 81% increase in Young's modulus was shown for the HMW matrix upon injection molding. The observed increase in Young's modulus was attributed to two factors: the greater shear history imparted by injection molding where a screw speed of 200 rpm was utilized in the barrel of the injection molder prior to mold filling, as well as orientation of the nanoclay particles in the flow direction. The reader is reminded that tensile properties reported above were measured in the flow direction of the injection molded plaques to capture the effects of possible orientation. The larger percent increase in Young's modulus observed with the HMW matrix was believed to be due to the effects of shear in the barrel, during plastication, and the greater alignment of the clay particles during mold filling.

3.3.4 Anisotropy of Tensile Properties

Although we have reported tensile properties measured along the flow direction of an injection molded part, the degree of mechanical anisotropy may be significant. The anisotropy of the tensile properties was examined by comparing the tensile properties of injection molded plaques cut in the flow direction and in the direction transverse or perpendicular to flow. Table 3.8 shows the tensile properties of the unfilled HMW matrix, 8 wt% LMW, MMW, and HMW nanocomposites tested in both the transverse direction and flow directions. It was seen that as the molecular weight increased, the degree of anisotropy in tensile properties became more significant. The LMW and MMW nanocomposites exhibit nearly identical properties indicating that there was no preferred orientation of the clay particles during injection molding. The flow induced stresses, i.e.

shear and extensional, applied to the clay particles in the injection molder were not enough to align the clay particles due to the low viscosity of the matrix as will be shown later in the rheology portion of this paper. For the 8 wt% HMW nanocomposite, tensile properties measured in the transverse direction are lower than those measured in the flow direction. This behavior was attributed to alignment of the nanoclay during mold filling due to increased flow induced stress provided by the more viscous matrix, causing significantly improved tensile properties in the direction of flow.

The degree of anisotropy for the HMW nanocomposites could be attributed to the more viscous HMW matrix imparting greater amounts of stress to separate and orient the nanoclay particles in the direction of flow during the injection molding process. However, anisotropy of the HMW matrix itself could also be a substantial contributor to the tensile properties as the long polymer chains may orient during injection molding. When the tensile properties of the HMW matrix were measured in the transverse direction, it was found that anisotropy did exist in the properties of the unfilled HMW matrix. While the difference in transverse and flow properties was not as large as compared to the 8 wt% HMW nanocomposites, this distinction may account for the greater enhancements observed in the tensile properties of the HMW nanocomposites in addition to the increased stress provided by the HMW matrix during processing. Thus, it was concluded that the tensile properties of the HMW nanocomposites increased to a greater extent than the properties of the LMW and MMW nanocomposites. This behavior was attributed to the HMW matrix being able to impart greater stress onto the clay particles and orient itself as well as the clay in the direction of flow as shown by larger tensile properties in the flow direction than in the transverse direction.

3.3.5 Estimation of Young's Modulus from Theory

The observed increase in the Young's modulus with addition of layered silicates into a polymer matrix is of obvious practical benefit to many applications where improved strength and stiffness may be required. However, realizing the full potential of mechanical property increase remains unclear even when fully exfoliated nanocomposite morphologies are shown by XRD. Evaluation of the expected modulus increase for the HDPE/MMT nanocomposites presented here was based on two separate theories developed by Halpin and Tsai [43, 44] and Ji et al. [45].

The effectiveness of these two models to predict actual experimental values of Young's modulus depends on the assumptions in each theory. Halpin and Tsai's model shown below in Eq 6 assumes unidirectional orientation as well as a high degree of adhesion of the filler particles to the surrounding polymer matrix,

$$E_c = E_m \left[\frac{1 + z h f_f}{1 - h f_f} \right], \tag{6}$$

where E_c = composite modulus, E_m = unfilled matrix modulus, f_f = filler volume fraction,

$$h = \frac{E_f / E_m - 1}{E_f / E_m + z}, \tag{7}$$

$$z = 2(l / t), \tag{8}$$

E_f is the filler modulus taken to be 178 GPa for MMT [44], and l/t is the aspect ratio of MMT taken here to be approximately 100 [44]. It is noted that the high aspect ratio of 100 assumes that each MMT platelet has been fully separated or exfoliated from its initial stack of clay aggregates.

For PLS nanocomposites synthesized from non-polar polyolefins such as polyethylene the assumption of the degree of bonding between MMT and the polyethylene matrix would be invalid due to differences in the surface energies of hydrophilic MMT and hydrophobic polyethylene. The level of adhesion could be slightly increased by the use of organic modifiers such as long alkyl chains on the surface of MMT to increase the organophilic character of the nanoclay.

The model developed by Ji et al. takes into account three phases present in a PLS nanocomposite: the matrix, filler, and the interphase region between the clay platelets with the polymer matrix residing within it. Ji's model shown below in Eq 9 makes no assumption as to the state of clay orientation and so is valid for randomly oriented systems in contrast to the theory of Halpin and Tsai,

$$\frac{1}{E_c} = \frac{1-a}{E_m} + \frac{a-b}{(1-a)E_m + a(k-1)E_m/\ln k} + \frac{b}{(1-a)E_m + (a-b)(k+1)E_m/2 + E_f b}, \quad (9)$$

where

$$a = \sqrt{[2(t/t_c)+1]f_f}, \quad (10)$$

t is the thickness of the interphase region taken to be the d-spacing given by XRD analysis, t_c is the thickness of MMT taken to be approximately 1nm [14], $b = \sqrt{f_f}$, and $k = E_f/E_m$. The dependence of Ji's model on the interphase separation between clay particles further generalizes the model by making no assumption as to the state of intercalation or exfoliation of the clay platelets. If d-spacing data are available then the dependence of Young's modulus on the degree of exfoliation may be examined.

In Table 3.9 the expected moduli increase predicted by both the Halpin and Tsai correlation as well as Ji et al.'s correlation are compared to those obtained experimentally

for the nanocomposites. As seen in Table 3.9, all of the experimental Young's moduli presented are below those predicted by the Halpin-Tsai correlation. The discrepancies between experiment and theory are attributed to lack of significant bonding occurring between the polyethylene matrix and MMT, orientation of the filler particles, and complete exfoliation of the MMT [44]. The percentage deviation of the experimental modului from those predicted by the Halpin-Tsai model were observed to be greatest for the 8 wt% LMW and MMW nanocomposites in which the Halpin-Tsai model over estimated the Young's modulus by 76% and 89%, respectively. In contrast, the Halpin-Tsai model over estimated the experimental modulus of the 8 wt% HMW nanocomposite by 38%, much less than observed for both the 8 wt% LMW and MMW nanocomposites. The HMW matrix might have provided more flow induced stress to orient the clay particles during mold filling than did the LMW and MMW matrices and, thus, a closer approximation to the Halpin-Tsai theory, which is valid for unidirectionally oriented filler particles, resulted [43].

Ji et al.'s model provides a closer approximation of the Young's modulus as shown in Table 3.9. By taking into account the separation of nanoclay particles directly (i.e. degree of intercalation) in the model as well as being valid for randomly oriented particles, a more accurate prediction of Young's modulus was possible. It was observed that the theoretically predicted modulus from Ji et al.'s model was within or close to standard deviation for the experimentally obtained moduli for the 8 wt% LMW and MMW nanocomposites. However, the model of Ji et al. predicted a tensile modulus which was more than two standard deviations less than the experimentally obtained Young's modulus for the 8 wt% HMW nanocomposite. As discussed previously in this

paper, the mechanical anisotropy observed for the 8 wt% HMW nanocomposite might have accounted for this deviation as Ji et al.'s model was developed for filler particles randomly distributed in a polymer matrix [45]. It is noted that when d-spacing data was not available no attempt at determining the Young's modulus from Ji et al.'s model was made.

3.3.6 Dynamic Mechanical Thermal Analysis (DMTA)

DMTA results are presented in Figures 3.9-3.11. It was seen that for all three matrices G' increased with increasing clay content throughout the entire temperature range tested in agreement with past work [34, 44, 46]. The percentage increase in G' upon addition of clay in comparison to the unfilled matrix was greatest for the LMW matrix nanocomposites and least for the HMW matrix nanocomposites at a given temperature and clay content. Thus, the addition of clay does not affect the HMW matrix as much as the LMW and MMW matrices in the torsional deformation mode employed in DMTA. However, from the tensile properties of the nanocomposites generated in this study it was seen that the HMW nanocomposites showed the greatest percentage increase in Young's modulus particularly at the 4 wt% and 8 wt% clay concentrations. The difference in property enhancement might be due to the previously discussed anisotropic properties of the injection molded samples. It was believed that orientation of the high aspect ratio clay particles primarily occurred in the flow direction during injection molding, leading to an increase in Young's modulus for the HMW nanocomposites. Because of this mechanical anisotropy, the shear modulus, G' obtained by means of the DMTA experiments, is lower than E/3, where E is the elastic modulus. As discussed above, the HMW nanocomposites exhibited greater d-spacings than their lower molecular

weight counterparts which was attributed to greater stress available from the matrix to separate the clay platelets. The higher stress generated by the HMW matrix also induced more orientation of the nanoclays than could be done by the LMW and MMW matrices. Thus, it was postulated that injection molding and the resultant orientation of clay had a more significant impact on the tensile properties of the nanocomposites which were tested in the direction of possible clay orientation than it did on G' determined by DMTA. We note that G' is based on the contributions to the modulus from both the flow and transverse directions.

According to ASTM D648, the heat distortion temperature (HDT) is defined as the temperature at which the center of a material deflects 0.25 mm under a load of either 1.82 MPa or 0.46 MPa. As described by Scobbo [47] and used by others [44, 48], the HDT can be estimated from modulus versus temperature data obtained from DMTA. Using the equation for the center deflection of a simply supported beam shown below one estimates the elastic modulus (E) of a material necessary to provide the specified deflection ($\Delta = 0.25$ mm) under a known load (F = 1.82 MPa) [47].

$$E = FL^3 / 48I\Delta , \tag{11}$$

where L is the distance between end supports of the beam and I is the beam's moment of inertia [47]. Using the value of E calculated from Eq 11 and the assumption that E=3G' for an incompressible, elastic polymer, one can find the temperature at which the desired deflection (0.25 mm) occurs at the given load (1.82 MPa) from modulus versus temperature data. Hence, changes in HDT as a function of clay loading may be observed once the value of the storage modulus corresponding to the HDT of the unfilled matrix has been found as illustrated in Figures 3.9-3.11.

Attempts to calculate *E* from Eq 11 using actual specimen dimensions from this work proved unsuccessful as the value of *E* obtained was above the range of experimental 3G' values from DMTA due to the assumption of E=3G' being invalid for these materials. Thus, in order to facilitate the discussion presented here, the HDT of HDPE reported in the literature as 42.4°C by Gungor [49] was used as the HDT of the LMW HDPE matrix. The value of 3G' at this temperature ($7.66X10^7$ Pa), which is approximately equal to the tensile modulus, *E*, was used as the modulus corresponding to the HDT test conditions of the measured deflection and specific load applied to the test specimen from Eq 11. As shown in Table 3.10, the HDT of the nanocomposites increases as the clay content was increased at all molecular weights studied here. However, the percentage increase with respect to the unfilled matrix was highest with the LMW nanocomposites and lowest with the HMW nanocomposites. The 8 wt% LMW nanocomposite exhibited an estimated HDT of 66°C representing a 56% increase from its unfilled matrix which had a HDT of 42.4°C, while the 8 wt% HMW nanocomposite showed an 18% increase in HDT from its unfilled matrix going from 62°C to 73°C. As observed previously for the enhancement of G' from DMTA experiments, the HMW matrix was seen to dominate over the addition of the clay particles in the torsional mode of deformation leading to a lower percentage enhancement of the HDT compared to the LMW and MMW matrices. However, the HMW nanocomposites exhibit the highest estimated HDT at a given concentration relative to the LMW and MMW nanocomposites due to the influence of the HMW matrix.

3.3.7 Rheological Properties

In addition to XRD, the dynamic rheology of nanocomposites might afford information concerning the degree of dispersion of nanoclays within a polymer matrix. Various workers have shown that exfoliated PE nanocomposites, as demonstrated by XRD, have differing frequency dependence in the terminal, or low frequency region of oscillation relative to their unfilled matrices [21, 50, 51]. The nanocomposites exhibit a more non-Newtonian, or shear-thinning, behavior as shown by means of the complex viscosity, $|h^*|$, at low shear rates or frequency and a tail or plateau in G' which have been attributed to the formation of a physical network of individual layers of silicate within the PE matrix [21, 50, 51]. In the previous work with PE nanocomposites [21, 50, 51], maleic anhydride was used as a compatibilizer to increase attractive interactions between the hydrophobic PE and hydrophilic MMT. It remains unclear whether the changes in dynamic rheological properties in the low frequency region were due to the interactions of exfoliated clay platelets within the maleated PE matrix or whether crosslinking occured between the maleic anhydride groups and the hydoxylated surfaces of the silicate layers [15]. The results presented in this paper, however, utilized no such compatibilizer. Thus, the contribution of molecular weight in dispersing the nanoclays has been separated as much as possible from the effect a compatibilizer could have.

Strain sweeps were first conducted in order to ensure dynamic rheology measurements were made in the linear viscoelastic region for each HDPE matrix and their 8 wt% nanocomposites. As shown in Figure 3.12, incorporation of the nanoclay increases G' as expected. There appears to be only a slight change in the strain where G' begins to decrease for each of the matrices upon nanoclay addition. The dynamic

rheology results presented in this paper were conducted at a strain of 5% and, thus, it was shown that these measurements were made in the linear viscoelastic region of the materials studied. Furthermore, the addition of 8 wt% organically modified MMT had very little effect on the strain at which non-linear behavior occurred.

Time sweeps shown in Figure 3.13 demonstrate that the three HDPE matrices and their 8 wt% nanocomposites are thermally stable at 230°C for at least 30 min. This facilitated time-temperature superposition of $|h^*|$ and G' at a reference temperature of 190°C by performing dynamic rheometry at 230°C and ensuring test specimens would not degrade at the elevated temperature.

In Figures 3.14-3.19, master curves at a reference temperature of 190°C were generated from $|h^*|$ and G' data measured at temperatures between 190°C and 230°C. As the nanoclay was incorporated into the various molecular weight HDPE matrices, it was seen that both $|h^*|$ and G' were enhanced with increasing clay concentration as would be expected when inorganic filler particles are added to a polymer. However, there was no noticeable change in the frequency dependence in the terminal region of the data for the MMW and HMW nanocomposites in the concentration range used. Only in the LMW nanocomposites did there appear a slight deviation in $|h^*|$ and G' from the unfilled matrix as MMT was added. Thus, it seems that no significant interactions are occurring between the clay and HDPE matrix at any molecular weight or concentration used here based on dynamic rheology measurements. It was expected that little change in the dynamic rheology should be observed considering the lack of attractive interactions occurring between the clay and HDPE matrix. The behavior of the LMW nanocomposites was attributed to interactions between clay aggregates in the matrix as opposed to

interactions between individually separated silicate layers. While the MMT has been surface treated with a quaternary alkyl ammonium cation, it was obviously inadequate compared to adding maleic anhydride in inducing a change in the rheological properties as shown previously [21, 50, 51]. Furthermore, the behavior at low frequencies in which a tail in G' has been observed must be due to strong interaction between the polymer and clay surface rather than an indicator of exfoliation.

Fornes et al. [32] showed that as the molecular weight of nylon 6 matrix was increased, a greater difference in the behavior of $|h^*|$ and G' of a 3.0 wt% nanocomposite relative to that of the corresponding unfilled matrix occurred. That is, stronger non-Newtonian behavior was observed in $|h^*|$ as the molecular weight of the matrix increased. In addition, more of a terminal plateau in G' was observed with increasing molecular weight of the nylon 6 matrix. The authors attributed this behavior to the increased shear force available from the higher molecular weight matrices to "peel" and exfoliate the clay platelets apart and produce a solid-like network within nylon 6 *in addition* to the attractive interactions between the polar nylon 6 matrix and organically modified MMT. However, the differences in and magnitude of the zero shear viscosity (h_o) of the nylon 6 matrices used by Fornes et al. [32] (approximately 350 Pa*s for the LMW matrix to 2,500 Pa*s for the HMW matrix at 240°C) were not as large compared to that of the HDPE matrices used in this work (1,800 Pa*s to 112,000 Pa*s at 190°C). It was apparent from the work performed here with the non-polar and more viscous HDPE matrices that without significant interactions between the polymer and clay, a change in the frequency dependence of dynamic rheological properties, whether indicative of

exfoliation or not, cannot be achieved even with materials exerting higher stresses on the nanoclay compared with nylon 6.

3.4 Conclusions

Three HDPE matrices of various molecular weights were blended with MMT at concentrations of 2, 4, and 8 wt% in a single screw extruder. XRD measurements indicated that as the molecular weight of the matrix increased, so did the level of intercalation of the 8 wt% nanocomposites as seen by an increase in the d-spacing of the nanocomposites. However, there were no signs of an exfoliated morphology indicating that attractive interactions between the polymer matrix and nanoclay must exist in order for exfoliation to occur, and that relying solely on a high shear stress from a viscous polymer matrix was insufficient to exfoliate the nanoclays.

Despite the lack of exfoliation, tensile tests on all nanocomposites indicated that incorporation of nanoclay into HDPE improved strength and stiffness as shown by increases in their respective moduli. Significantly greater enhancement of the tensile or Young's modulus was observed for nanocomposites generated from the HMW matrix. This was attributed to greater levels of clay intercalation as shown by XRD due to flow induced orientation of the clay particles during injection molding of the test specimens because of greater amounts of shear stress being applied to the nanoclays from the HMW matrix. Larger tensile properties in injection molded test samples compared to compression molded samples, as well as larger properties of samples taken in the flow direction of injection molding compared to the transverse direction supported this conclusion.

Comparison of experimental Young's modulus with the theoretical correlations developed by Halpin and Tsai [43] and Ji et al. [45] showed that the assumptions in each model determined the accuracy of their predictions to experimentally obtained values. In the theory of Halpin and Tsai, the assumptions of significant adhesion of MMT to the HDPE matrices, exfoliated MMT particles, and unidirectionally oriented MMT particles led to an over estimation of the Young's modulus [43]. Ji et al.'s theory provided a remarkably close approximation of the Young's modulus to experimental results. This was due to the ability of the model to take into account the degree of intercalation of the nanocomposites as well as being valid for randomly oriented filler particles in a polymer matrix [45]. It was observed for the 8 wt% HMW nanocomposite that the Halpin-Tsai model over estimated the experimental Young's modulus to a lesser extent (38%) compared to the 8 wt% LMW and MMW nanocomposites in which the Halpin-Tsai model over predicted the experimental modulus by 76% and 89%, respectively. Ji et al.'s model showed an under prediction of the 8 wt% HMW nanocomposite compared to experimental results, while the model predictions for the 8 wt% LMW and MMW nanocomposites were within standard deviation of the experimental Young's modulus. The closer approximation of the Halpin-Tsai model observed for the 8 wt% HMW nanocomposite, as well as the under estimation from Ji et al's model for the 8 wt% HMW nanocomposite were both attributed to the effect the HMW matrix had on aligning the clay particles in the direction of flow during injection molding. This effect made the assumption of well oriented filler particles in the Halpin-Tsai theory more valid for the 8 wt% HMW nanocomposite and the assumption of randomly oriented filler particles in Ji et al.'s model less valid for this nanocomposite.

DMTA experiments indicated that the HDT was increased with increasing clay loading at all three molecular weights used. However, the extent of enhancement in the HDT decreased with increasing HDPE molecular weight. Addition of the inorganic MMT did not affect the torsional response of the HMW nanocomposites as much as the tensile properties which were measured in the flow direction of the injection molded bars. This was attributed to flow induced alignment of the clay particles as a result of the more viscous HMW HDPE matrix leading to greater anisotropy in the HMW nanocomposite properties.

Dynamic rheology measurements indicated that a percolated network of clay particles did not exist for any of the nanocomposites generated for this study. Attempts at elucidating changes in the terminal behavior of the nanocomposites via time-temperature superposition proved unsuccessful for the materials studied as there was no noticeable change in the frequency dependence of both $|h^*|$ and G' supporting the XRD results presented in this paper.

3.5 Acknowledgements

The authors would like to thank the National Science Foundation (Grand Number CTS-050 7995) for partial support, Chevron Phillips Chemical Company LP for donating the three HDPE matrices used in this study as well as performing the size exclusion chromatography work in determining $\overline{M}_w$, Southern Clay Products, Inc. for donating the MMT Cloisite 20A used in this study, and Quang Nguyen for performing the XRD work presented in this paper.

3.6 References

1. S. S. Ray. and M. Okamoto, *Progress in Polymer Science*, **28,** 1539 (2003).

2. A. Okada, M. Kawasumi, A. Usuki, Y. Kojima, T. Kurauchi, and O. Kamigaito. *MRS Symposium Proceedings*, **171,** 45 (1990).

3. R. A. Vaia, H. Ishii, and E. P. Gianelis, *Chem. Mater*., **5,** 1694 (1993).

4. T. G. Gopakumar, J. A. Lee, M. Kontopoulou, and J. S. Parent, *Polymer*, **43**, 5483 (2002).

5. W. Lertwimolnun and B. Vergnes, *Polymer*, **46,** 3462 (2005).

6. V. E. Yudin, G. M. Divoux, J. U. Otaigbe, and V. M. Svetlichnyi, *Polymer*, **46**, 10866 (2005).

7. T. H. Kim, S. T. Lim, C. H. Lee, H. J. Choi, and M. S. Jhon, *J. App. Polym. Sci*., **87,** 2106 (2003).

8. A. J. Hsieh, P. Moy, F. L. Beyer, P. Madison, and E. Napadensky, *Polym. Eng. Sci*, **44,** 825 (2004).

9. K. M. Lee and C. D. Han, *Polymer*, **44**, 4573 (2003).

10. G. Galgali, S. Agarwal, and A. Lele, *Polymer*, **45**, 6059 (2004).

11. M. Mehrabzadeh and M. R. Kamal, *Polym. Eng. Sci*, **44**, 152 (2004).

12. M. A. Osman, V. Mittal, M. Morbidelli, and U. W. Suter, *Macromolecules*, **36,** 9851 (2003).

13. M. A. Osman, J. E. P Rupp, and U. W. Sutter, *J. Mat. Chem*., **15,** 1298 (2005).

14. M. Valera-Zaragoza, E. Ramirez-Vargas, F. J. Melellin-Rodriquez, and B. M. Huerta-Martinez, *Poly. Deg. Stab*., **91**, 1319 (2006).

15. J. W. Gilman, C. L. Jackson, A. B. Morgan, and R. Harris Jr., *Chem. Mater*, **12,** 1866 (2000).

16. T. Pinnavaia and G. Beall, *Polymer-Clay Nanocomposites*, John Wiley & Sons, Ltd., New York, (2000).

17. M. Zanetti, S. Lomakin, and G. Camino, *Macromol. Mater. Eng.*, **279,** 1 (2000).

18. A. Usuki, M. Kato, A. Okada, and T. Kurauchi, *J. Applied Polymer Sci.*, **63**, 137 (1997).

19. M. Kawasumi, N. Hasegawa, M. Kato, A. Okada, and A. Usuki, *Macromolecule*s, **30**, 6333 (1997).

20. K. H. Wang, M. H. Choi, C. S. Koo, Y. S. Choi, and I. J. Chung, *Polymer*, **42**, 9819 (2001).

21. Y. T Lim and O. O. Park, *Rheologica Acta,* **40,** 9929 (2001).

22. Southern Clay Products Inc., Technical Data Sheets, www.nanoclay.com (2006).

23. Y. Zhong and D. De Kee, *Polym. Eng. Sci*., **45,** 469 (2005).

24. E. C. Lee, D. F. Mielewski, and R. J. Baird, *Polym. Eng. Sci*, **44,** 1773 (2004).

25. R. A. Vaia, K. D. Jandt, E. J. Kramer, and E. P. Giannelis, *Macromolecules*, **28**, 8080 (1995).

26. Z. Shen, G. P. Simon, and Y. Cheng, *Polym. Eng. Sci*., **42,** 2369 (2002).

27. H. S. Jeon and J. K. Rameshwaram, *Computational Methods in Materials Characterisation*, Computational Mechanics, Boston, MA, 255-263 (2004).

28. S. Tanoue, L. A. Utracki, A. Garcia-Rejon, J. Tatibouet, and M. R. Kamal, *Polym. Eng. Sci*, **45,** 827 (2005).

29. S. Tanoue, L. A. Utracki, A. Garcia-Rejon, P. Sammut, M-T. Ton-That, I. Pesneau, M. R. Kamal, and J. Lyngaae-Jorgensen, *Polym. Eng. Sci.*, **44,** 1061 (2004).

30. S. Tanoue, L. A. Utracki, A. Garcia-Rejon, J. Tatibouet, K. C. Cole, and M. R. Kamal, *Polym. Eng. Sci*, **44,** 1046 (2004).

31. D. Kaempfer, R. Thomann, and R. Mulhaupt, *Polymer*, **43,** 2909 (2002).

32. T. D. Fornes, P. J. Yoon, H. Keskkula, and D. R. Paul, *Polymer*, **42,** 9929 (2001).

33. J. M. Dealy, *Rheometers for Molten Plastics*, Van Nostrand Reinhold, New York (1982).

34. M. Alexandre, P. Dubois, T. Sun, J. M. Garces, and R. Jerome, *Polymer*, **43,** 2123 (2002).

35. R. Vaia and E. P. Giannelis, *Macromolecules*, **30**, 8000 (1997).

36. J. T. Yoon, W. H. Jo, M. S. Lee, and M. B. Ko, *Polymer*, **42**, 329 (2001).

37. J. Zhu, A. B. Morgan, F. J. Lamelas, and C. A. Wilkie, *Chem. Mater*., **13**, 3774 (2001).

38. D. M. Delozier, R. A. Orwoll, J. F. Cahoon, N. J. Jonston, J. G. Smith, Jr., and J. W. Connell, *Polyme*r, **43**, 813 (2002).

39. M. A. Osman, J. E. P. Rupp, and U.W. Sutter, *Polymer,* **46,** 1653 (2005).

40. J. Morawiec, A. Pawlak, M. Slouf, A. Galeski, E. Piorkowska, and N. Krasnikowa, *Eur. Polym. Journal*, **41,** 1115 (2005).

41. T. S. Ellis and J. S. D'Angelo, *J. Appl. Polym. Sci*., **90**, 1639 (2003).

42. W. S. Chow, Z. A. Mohd. Ishak, U. S. Ishiaku, J. Karger-Kocsis, and A. A. Apostolov, *J. Appl. Polym. Sci.*, **91**, 175 (2004).

43. J. C. Halpin and J. L. Kardos, *Polym. Eng. Sci*, **16**, 344 (1976).

44. T. D. Fornes and D. R. Paul, *Polymer*, **44**, 4993 (2003).

45. X. L. Ji, J. K. Jing, W. Jiang, and B. Z. Jiang, **"**Tensile modulus of polymer nanocomposites," *Polym. Eng. Sci*, **42**, 983 (2002).

46. Y. Xie, D. Yu, J. Kong, X. Fan, and W. Qiao, *J. Appl. Polym. Sci*., **100**, 4004 (2006).

47. J. J. Scobbo, Jr., *Polymer Blends, Volume 2: Performance*, Wiley, New York, 335, (2000).

48. S. Xie, S. Zhang, F. Wang, H. Liu, and M. Yang, *Polym. Eng. Sci*., **45**, 1247 (2005).

49. A. Gungor, *J. Appl. Polym. Sci*., **99**, 2438 (2006).

50. K. H Wang, M. H. Choi, C. M. Koo, M. Xu, I. J. Chung, M. C. Jang, S. W. Choi, and H. H. Song, *J. Polym. Sci. Part B: Polym. Phys*., **40,** 1454 (2002).

51. P. Mederic, T. Razafinimaro, T. Aubry, M. Moan, and M. H. Klopffer, *Macromol. Symp*., **221**, 75 (2005).

.

Table 3.1 Physical Properties of Three HDPE Samples

Name	$\overline{M}_W$ **(g/mol)**	$\overline{M}_W / \overline{M}_N$	r **(g/cm^3)**	**MI (g/10 min)**
Low Molecular Weight (LMW)	86,520	4.092	0.953	4.5
Middle Molecular Weight (MMW)	155,900	6.916	0.955	0.25
High Molecular Weight (HMW)	460,400	60.629	Unavailable	Unavailable

Table 3.2. Physical Properties of Cloisite 20A [22].

Name	**Specific gravity**	**Organic Modifier Concentration (meq/100g clay)**
Cloisite 20A	1.77	95

Table 3.3. Actual Composition of Nanocomposites

	Post-Extrusion			
	Organoclay		Montmorillonite	
Label	**Wt%**	**Vol%**	**Wt%**	**Vol%**
2 wt% LMW	1.95	1.06	1.22	0.41
4 wt% LMW	4.01	2.20	2.51	0.85
8 wt% LMW	7.50	4.19	4.69	1.62
2 wt% MMW	1.85	1.01	1.16	0.39
4 wt% MMW	3.73	2.05	2.33	0.79
8 wt% MMW	7.91	4.43	4.95	1.72
2 wt% HMW	2.13	1.17	1.33	0.45
4 wt% HMW	3.99	2.22	2.50	0.85
8 wt% HMW	7.49	4.27	4.69	1.63

Table 3.4. Estimated Density of Nanocomposites.

Label	m_{HDPE} (g)	m_{OC} (g)	V_{HDPE} (cm^3)	V_{OC} (cm^3)	f_{HDPE}	f_{OC}	r_{NC}
2 wt% LMW	98	2	102.83	1.13	0.989	0.011	0.962
4 wt% LMW	96	4	100.73	2.26	0.978	0.022	0.971
8 wt% LMW	92	8	96.54	4.52	0.955	0.045	0.990
2 wt% MMW	98	2	102.62	1.13	0.989	0.011	0.964
4 wt% MMW	96	4	100.52	2.26	0.978	0.022	0.973
8 wt% MMW	92	8	96.34	4.52	0.955	0.045	0.992
2 wt% HMW	98	2	102.08[a]	1.13	0.989	0.011	0.969
4 wt% HMW	96	4	100.00[a]	2.26	0.978	0.022	0.978
8 wt% HMW	92	8	95.83[a]	4.52	0.955	0.045	0.996

[a] actual density of HMW matrix was not given by manufacturer, therefore 0.96 g/cm3 was used as an estimate.

Table 3.5. Tensile Properties for LMW Matrix and Nanocomposites.

Organoclay Concentration (wt%)	Young's Modulus (MPa)	Stress at 0.2% Yield (MPa)	Stress at Peak (MPa)	Stress at Break (MPa)	Elongation at Break (%)
0	961.27 ± 145.17	5.85 ± 1.00	18.59 ± 1.03	12.49 ± 0.72	823.44 ± 116.10
2	1150.07 ± 72.76	6.45 ± 0.76	19.18 ± 0.07	6.50 ± 0.07	233.21 ± 40.34
4	1245.06 ± 152.77	6.73 ± 0.55	17.37 ± 0.56	5.90 ± 0.24	122.58 ± 35.91
8	1407.36 ± 142.95	7.54 ± 0.64	18.64 ± 0.60	6.37 ± 0.17	77.85 ± 31.61

Table 3.6 Tensile Properties for MMW Matrix and Nanocomposites.

Organoclay Concentration (wt%)	Young's Modulus (MPa)	Stress at 0.2% Yield (MPa)	Stress at Peak (MPa)	Stress at Break (MPa)	Elongation at Break (%)
0	1141.30 ± 129.31	8.24 ± 0.58	23.86 ± 0.61	9.72 ± 1.19	107.21 ± 34.05
2	1253.43 ± 191.87	11.56 ± 0.61	25.12 ± 0.44	8.54 ± 0.16	114.74 ± 15.46
4	1364.23 ± 160.17	8.42 ± 0.25	23.37 ± 0.82	8.08 ± 0.58	67.72 ± 12.96
8	1518. 72 ± 154.44	11.71 ± 0.35	24.66 ± 0.60	8.51 ± 0.19	12.49 ± 6.15

Table 3.7. Tensile Properties for HMW Matrix and Nanocomposites.

Organoclay Concentration (wt%)	Young's Modulus (MPa)	Stress at 0.2% Yield (MPa)	Stress at Peak (MPa)	Stress at Break (MPa)	Elongation at Break (%)
0	1331.28 ± 99.59	11.44 ± 2.63	35.54 ± 1.24	13.79 ± 1.21	11.21 ±1.19
2	1324.49 ± 115.31	14.00 ± 0.40	37.18 ± 0.82	12.96 ± 0.64	12.09 ± 1.40
4	1684.02 ± 184.10	14.03 ± 0.59	31.02 ± 1.38	10.07 ± 1.57	10.76 ± 0.31
8	2230.22 ± 117.45	14.42 ± 1.43	40.40 ± 1.15	40.42 ± 1.17	10.66 ± 1.44

Table 3.8. Comparison of Tensile Properties Taken in Transverse and Flow Directions.

Material	Test Direction	Young's Modulus (MPa)	Stress at 0.2% Yield (MPa)	Stress at Peak (MPa)	Stress at Break (MPa)
8 wt% LMW	Transverse	1468.26 ± 153.15	7.37 ± 0.68	19.13 ± 0.28	6.55 ± 0.16
	Flow	1407.36 ± 142.95	7.54 ± 0.64	18.64 ± 0.60	6.37 ± 0.17
8 wt% MMW	Transverse	1525.61 ± 116.21	8.42 ± 0.41	20.76 ± 0.53	7.54 ± 0.31
	Flow	1518.72 ± 154.44	11.71 ± 0.35	24.66 ± 0.60	8.51 ± 0.19
0 wt% HMW	Transverse	1251.40 ± 109.16	7.16 ± 0.16	22.49 ± 0.97	11.58 ± 2.16
	Flow	1331.28 ± 99.59	11.44 ± 2.63	35.54 ± 1.24	13.79 ± 1.21
8 wt% HMW	Transverse	1893.06 ± 164.35	8.95 ± 0.56	20.23 ± 0.99	6.88 ± 0.38
	Flow	2230.22 ± 117.45	14.42 ± 1.43	40.40 ± 1.15	40.42 ± 1.17

Table 3.9. Comparison of Experimental Young's Modulus with Various Theoretical Correlations.

Material	Experimental Modulus (MPa)	Ji et al. (MPa)	Halpin-Tsai (MPa)
2% LMW	1150.07 ± 72.76	N/A[a]	1340
4% LMW	1245.06 ± 152.77	N/A[a]	1750
8% LMW	1407.36 ± 142.95	1390	2470
2% MMW	1253.43 ± 191.87	N/A[a]	1530
4% MMW	1364.23 ± 160.17	N/A[a]	1930
8% MMW	1518. 72 ± 154.44	1680	2870
2% HMW	1324.49 ± 115.31	N/A[a]	1810
4% HMW	1684.02 ± 184.10	N/A[a]	2240
8% HMW	2230.22 ± 117.45	1980	3080

[a] No XRD data available.

Table 3.10. HDT as a Function of Molecular Weight and Clay Concentration.

	MMT Concentration (wt%)			
	0	**2**	**4**	**8**
LMW	42.4°C[a]	48°C	55°C	66°C
MMW	45°C	48°C	53°C	62°C
HMW	62°C	65°C	64°C	73°C

[a]As reported by Gungor [48].

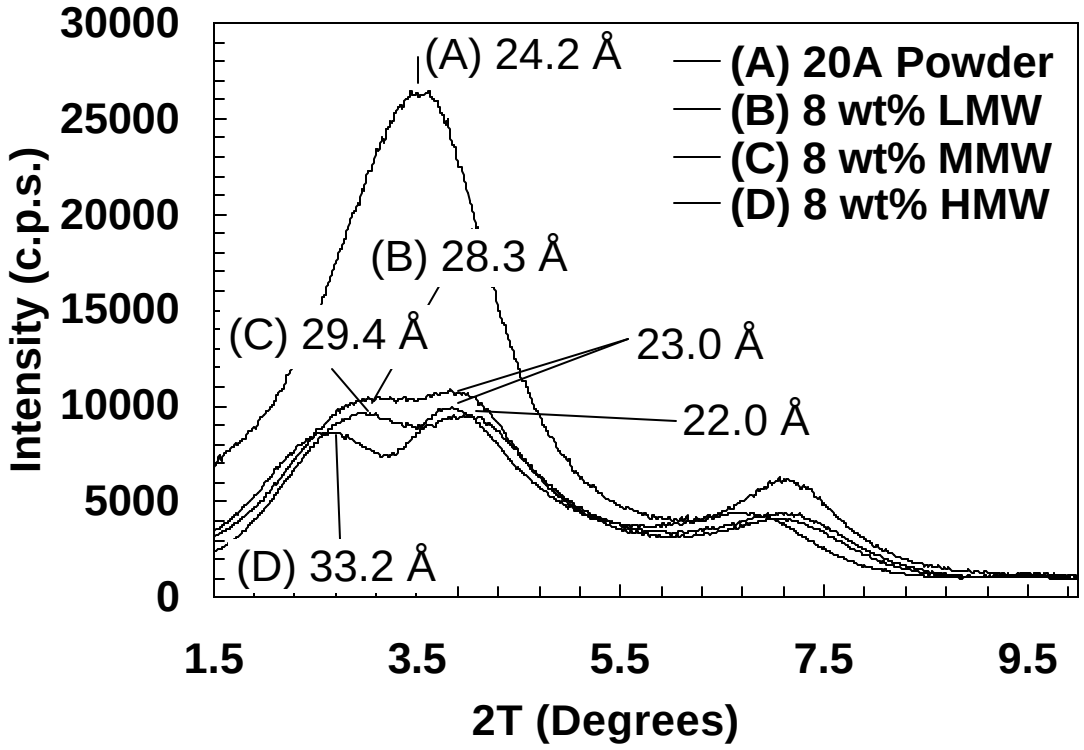

Figure 3.1. XRD Spectra of Cloisite 20A and 8 wt% Nanocomposites for LMW, MMW, and HMW Matrices.

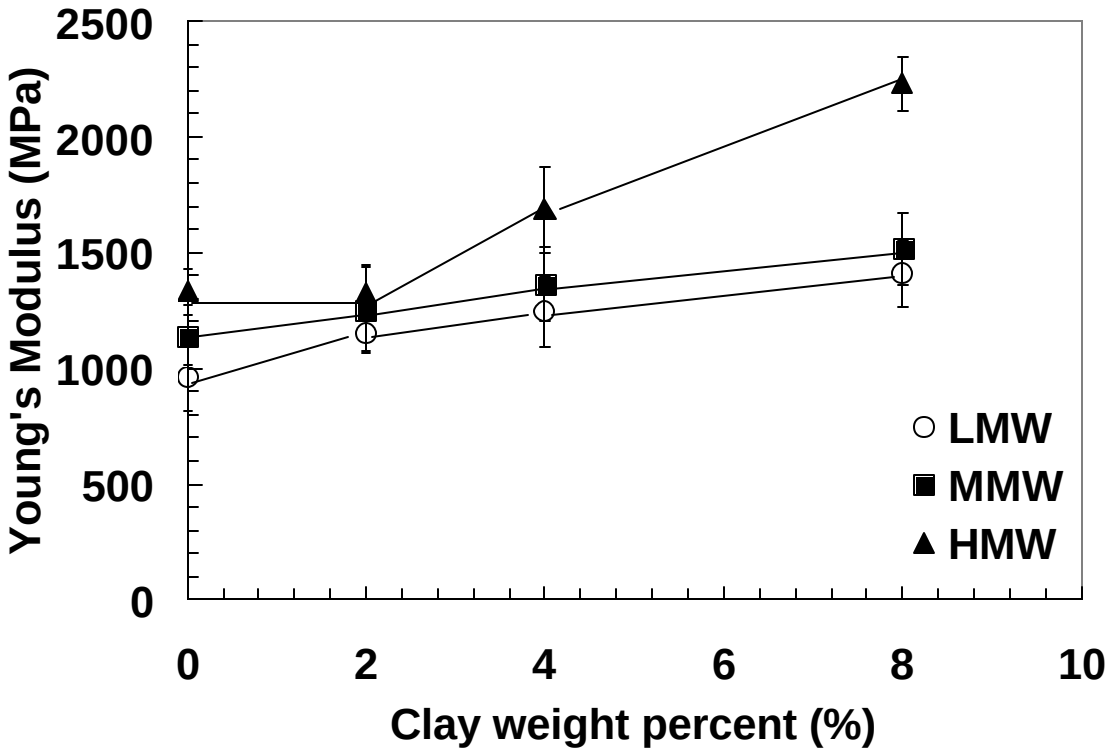

Figure 3.2. Young's Modulus as a Function of MMT Concentration for Three Molecular Weights. Connecting lines have been added to clarify trends in data.

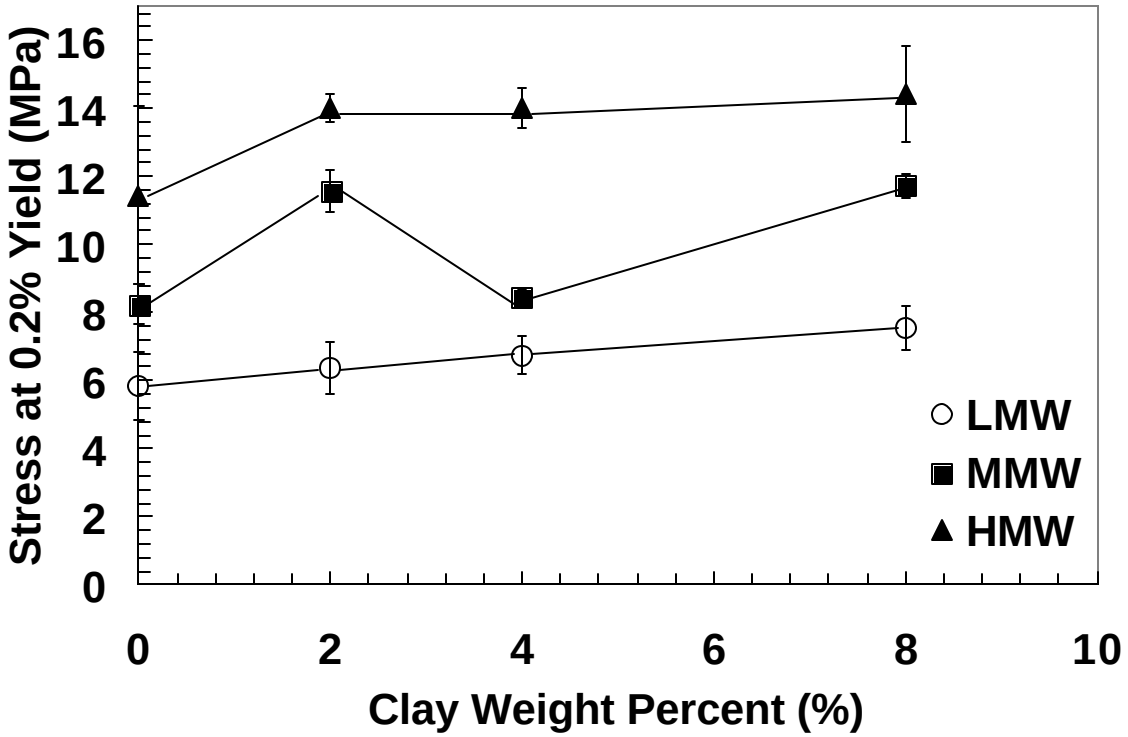

Figure 3.3. Stress at 0.2% Yield as a Function of MMT Concentration for Three Molecular Weights. Connecting lines have been added to clarify trends in data.

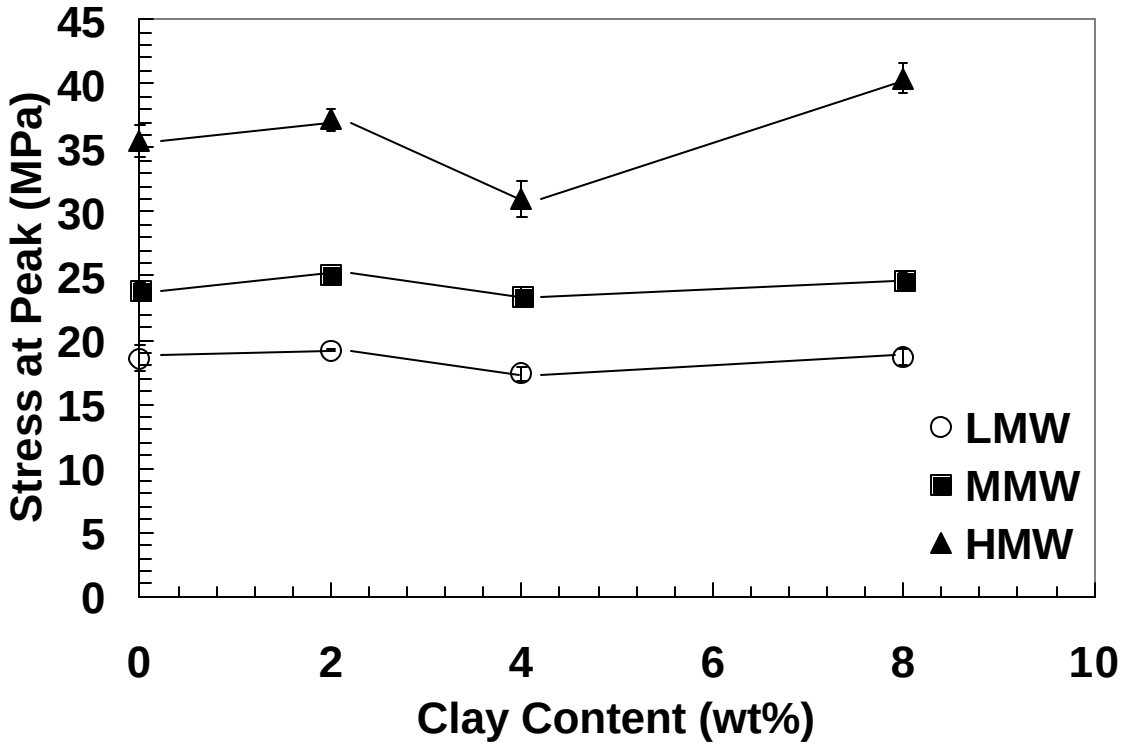

Figure 3.4. Stress at Peak as a Function of MMT Concentration for Three Molecular Weights. Connecting lines have been added to clarify trends in data.

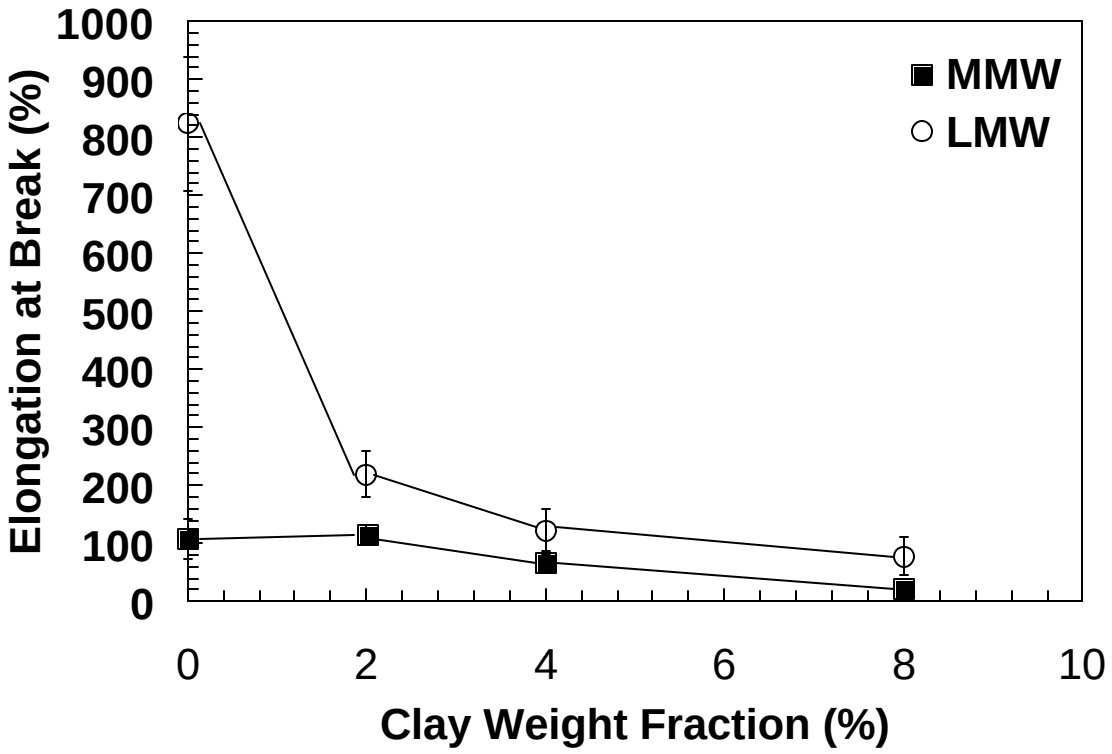

Figure 3.5. Elongation at Break as a Function of MMT Concentration for LMW and MMW Nanocomposites. Connecting lines have been added to clarify trends in data.

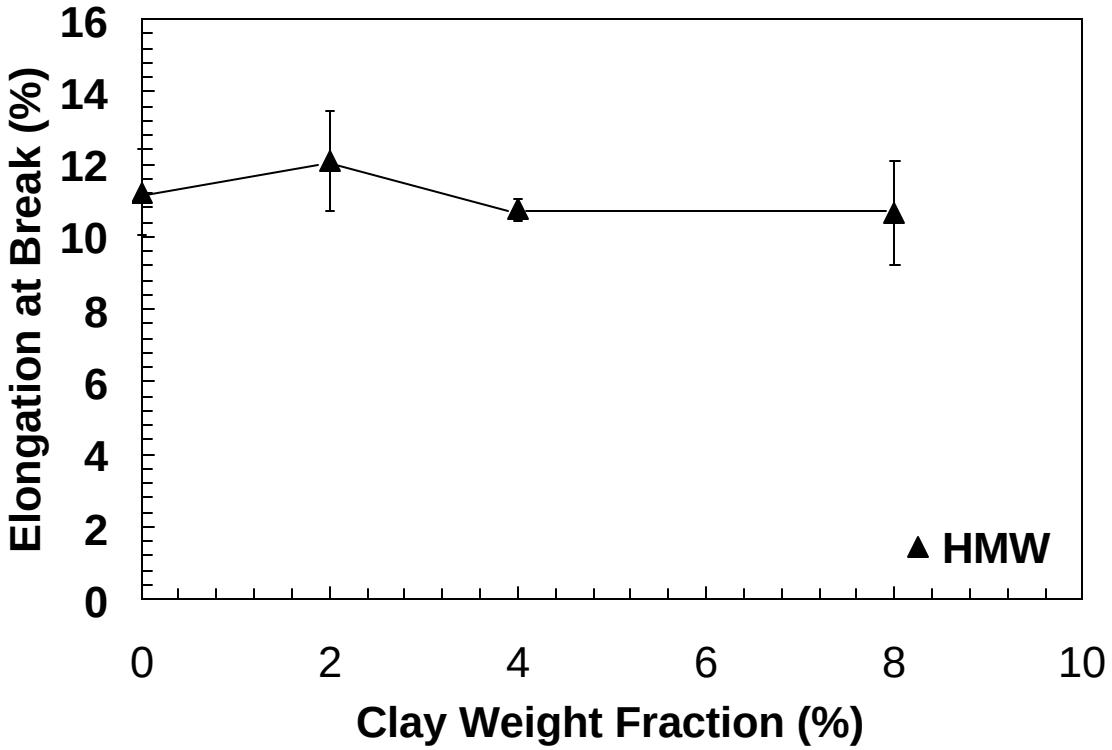

Figure 3.6. Elongation at Break as a Function of MMT Concentration for HMW Nanocomposites. Connecting lines have been added to clarify trends in data.

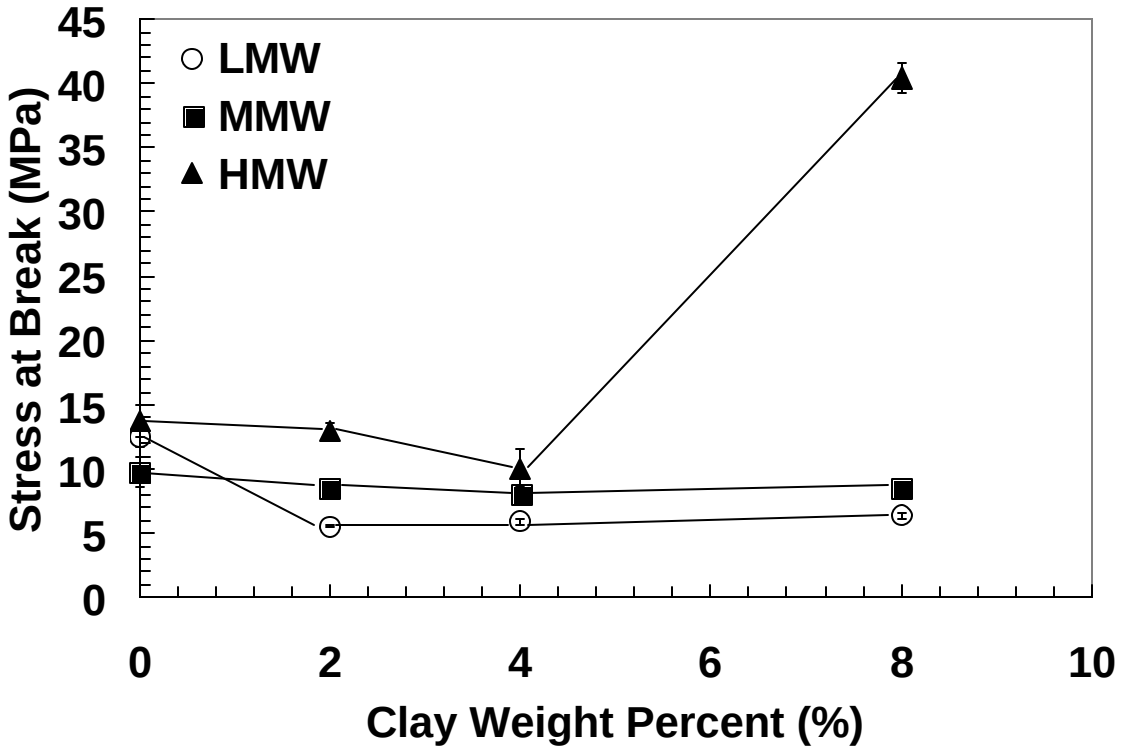

Figure 3.7. Stress at Break as a Function of MMT Concentration for Three Molecular Weights. Connecting lines have been added to clarify trends in data.

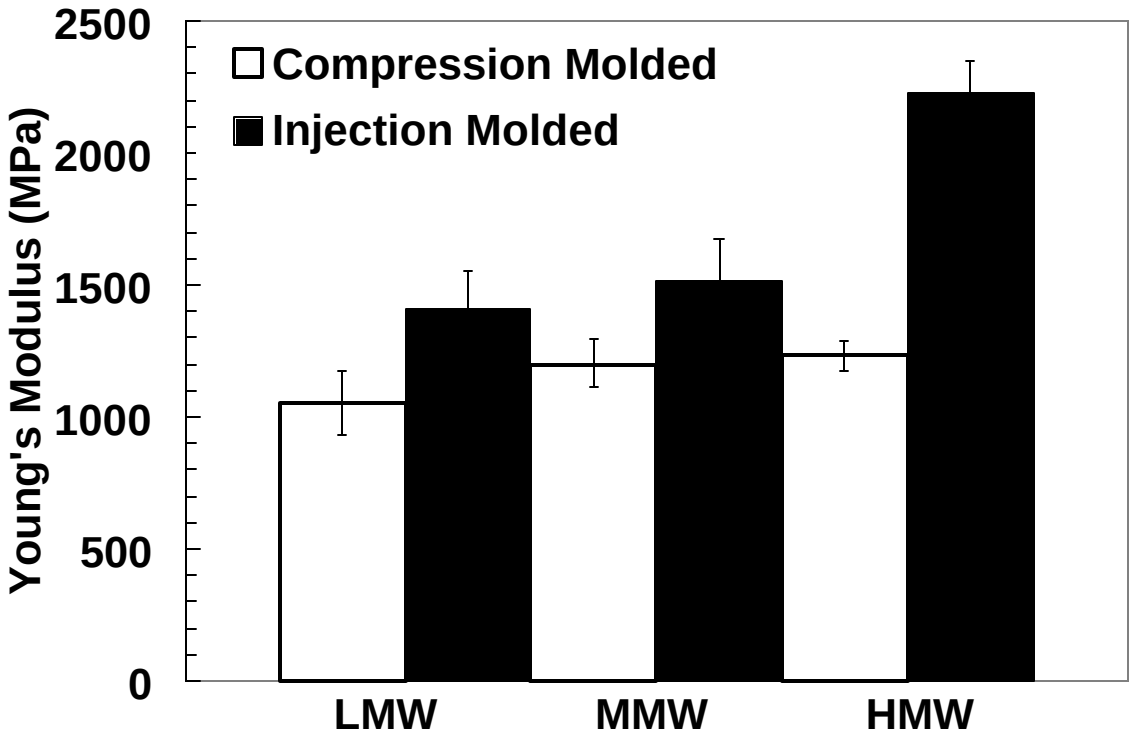

Figure 3.8. Young's Modulus of Compression Molded and Injection Molded 8 wt% Nanocomposites.

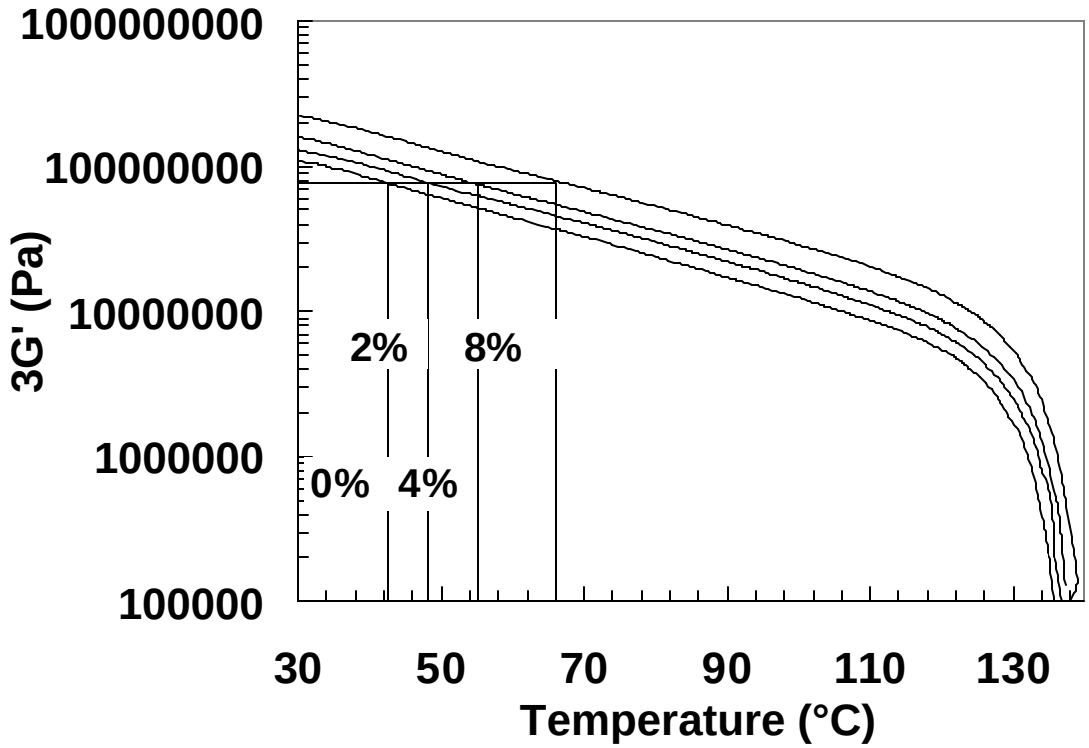

Figure 3.9. 3G' and corresponding HDT from DMTA for LMW Matrix and Nanocomposites .

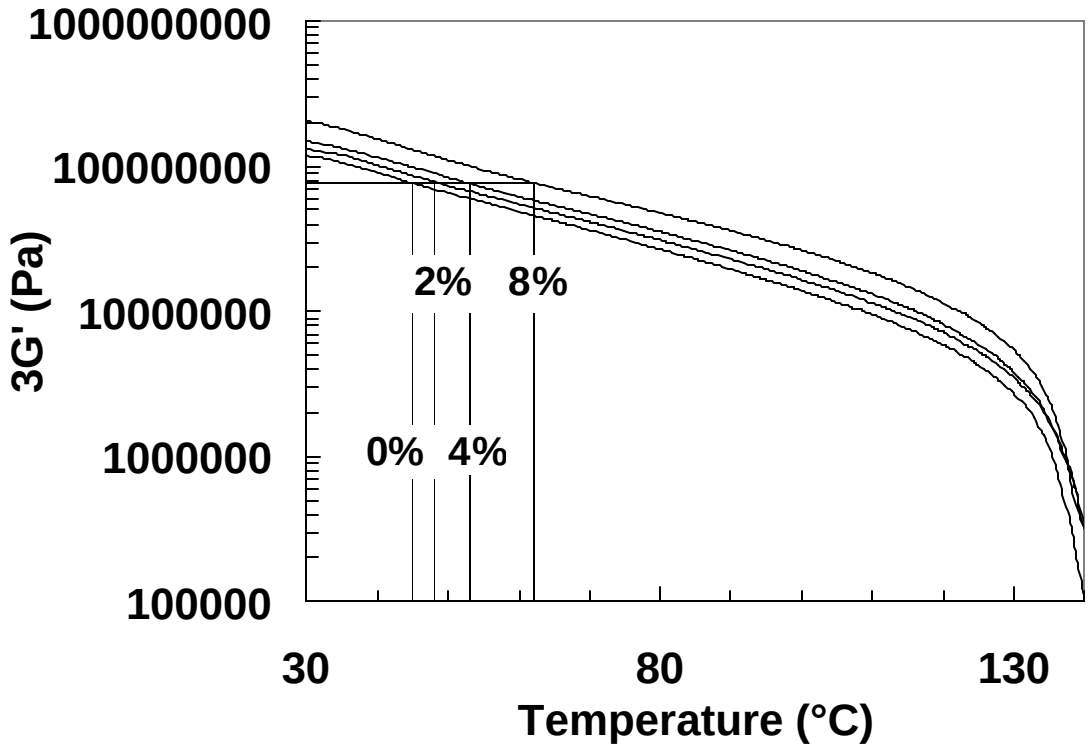

Figure 3.10. 3G' and corresponding HDT from DMTA for MMW Matrix and Nanocomposites .

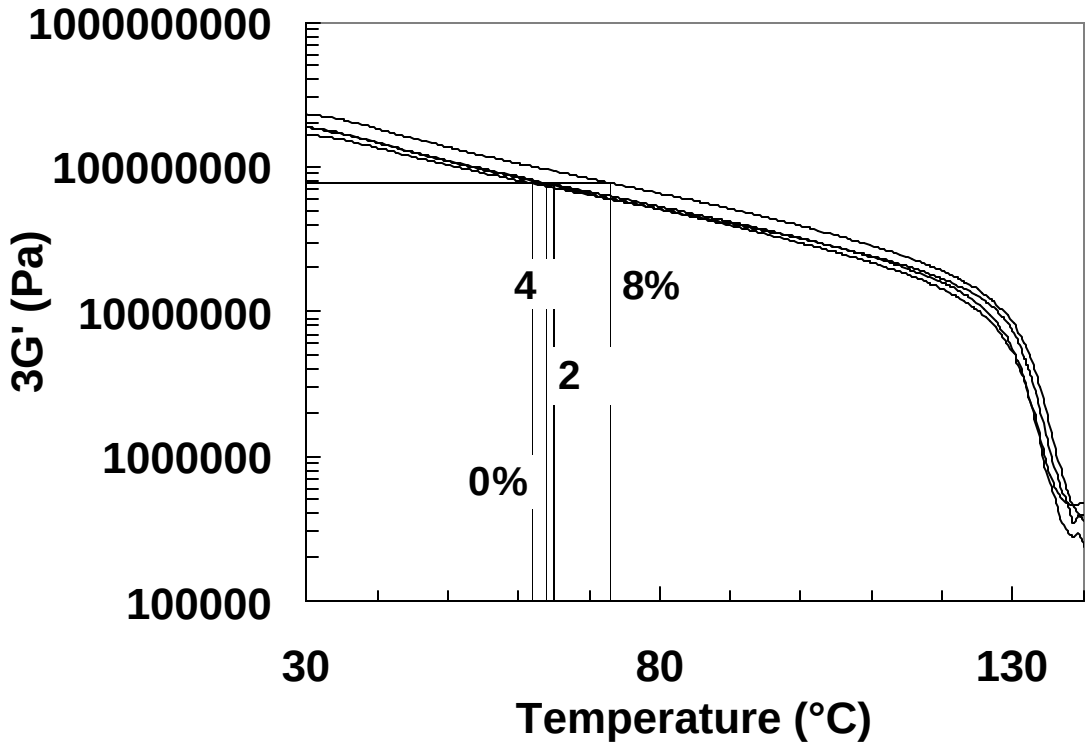

Figure 3.11. 3G’ and corresponding HDT from DMTA for HMW Matrix and Nanocomposites .

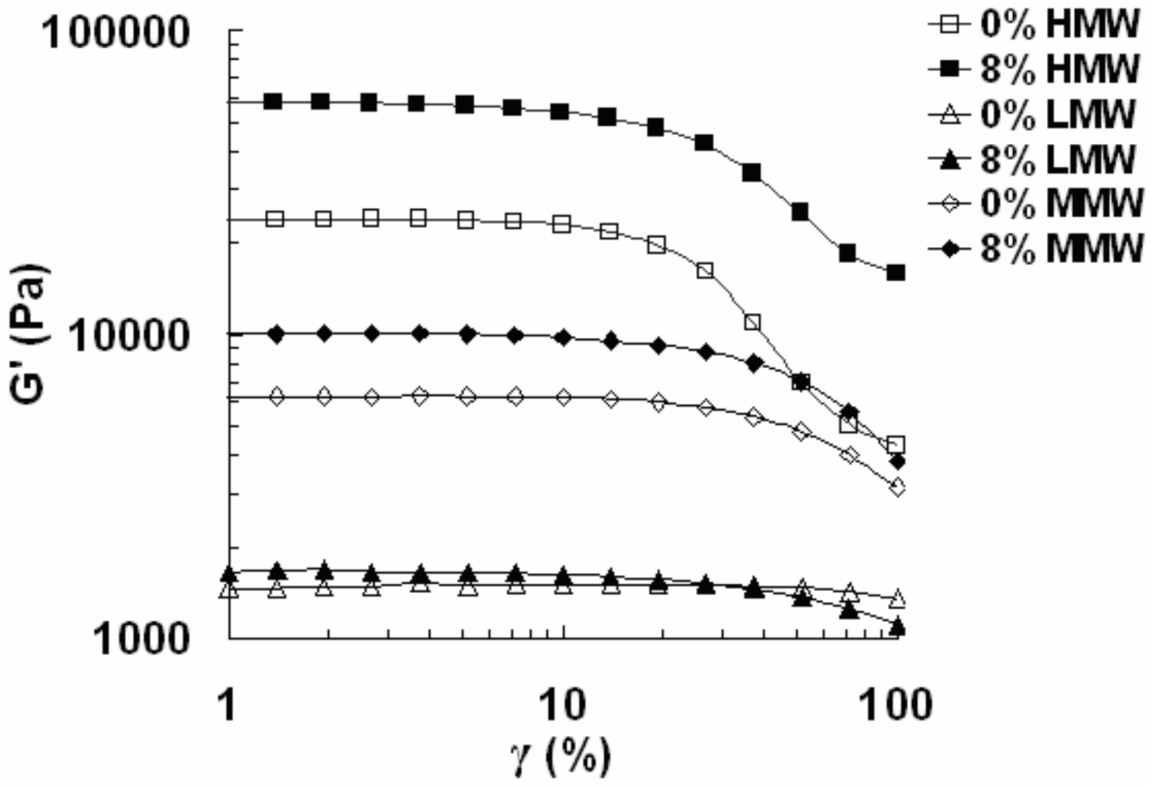

Figure 3.12. Strain Sweep of 0% and 8 wt% Nanocomposites for Three HDPE Matrices. w =5.0 rad/sec, T=190°C.

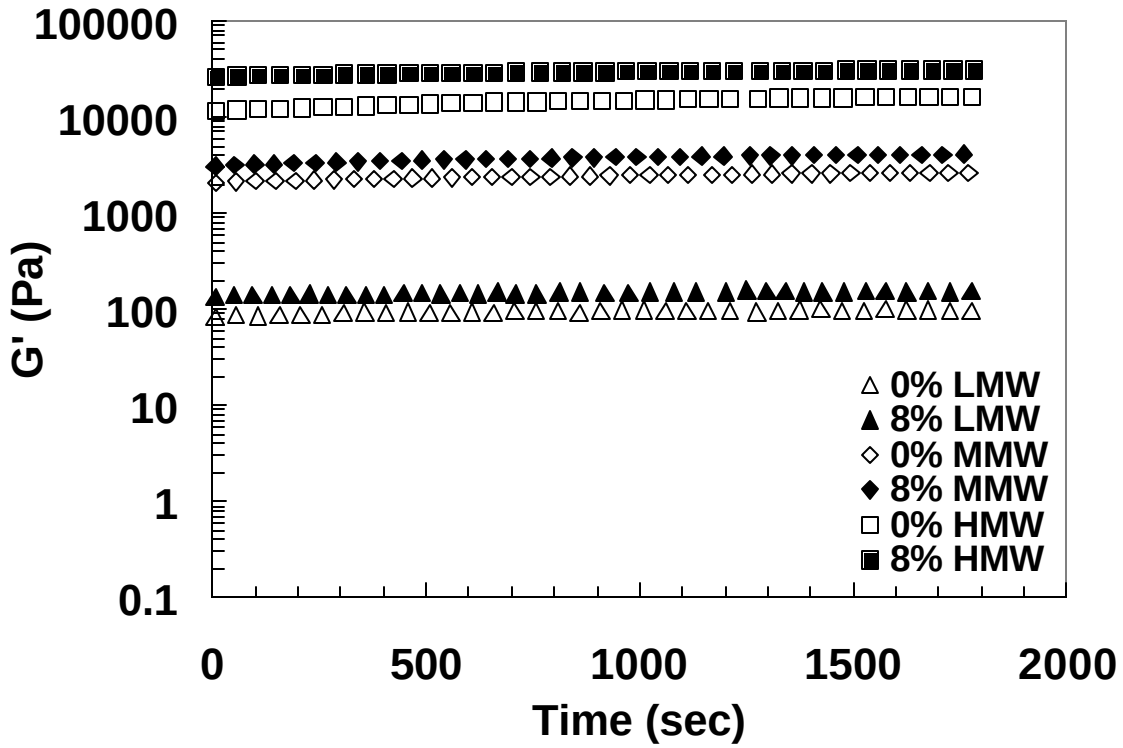

Figure 3.13. Time Sweep of 0% and 8 wt% Nanocomposites for Three HDPE Matrices. w =1.0 rad/sec, 5.0% strain, T=230°C.

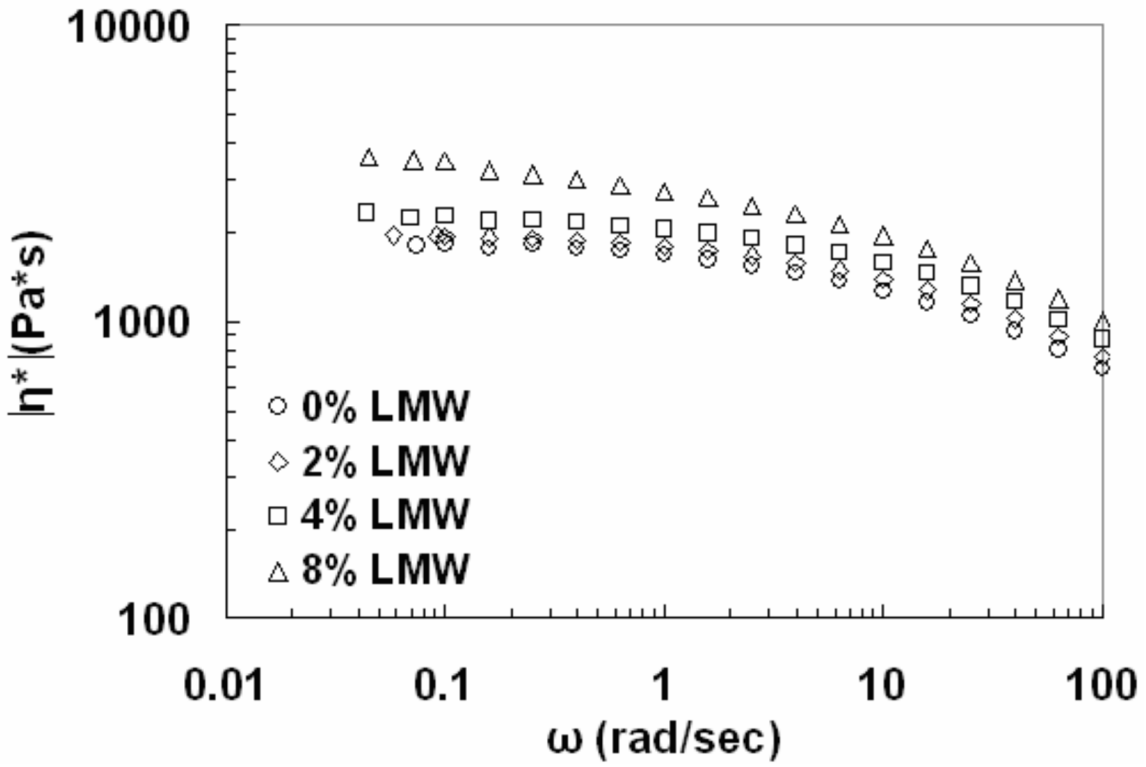

Figure 3.14. $|h^*|$ at T_{ref} = 190°C for LMW Matrix and Nanocomposites.

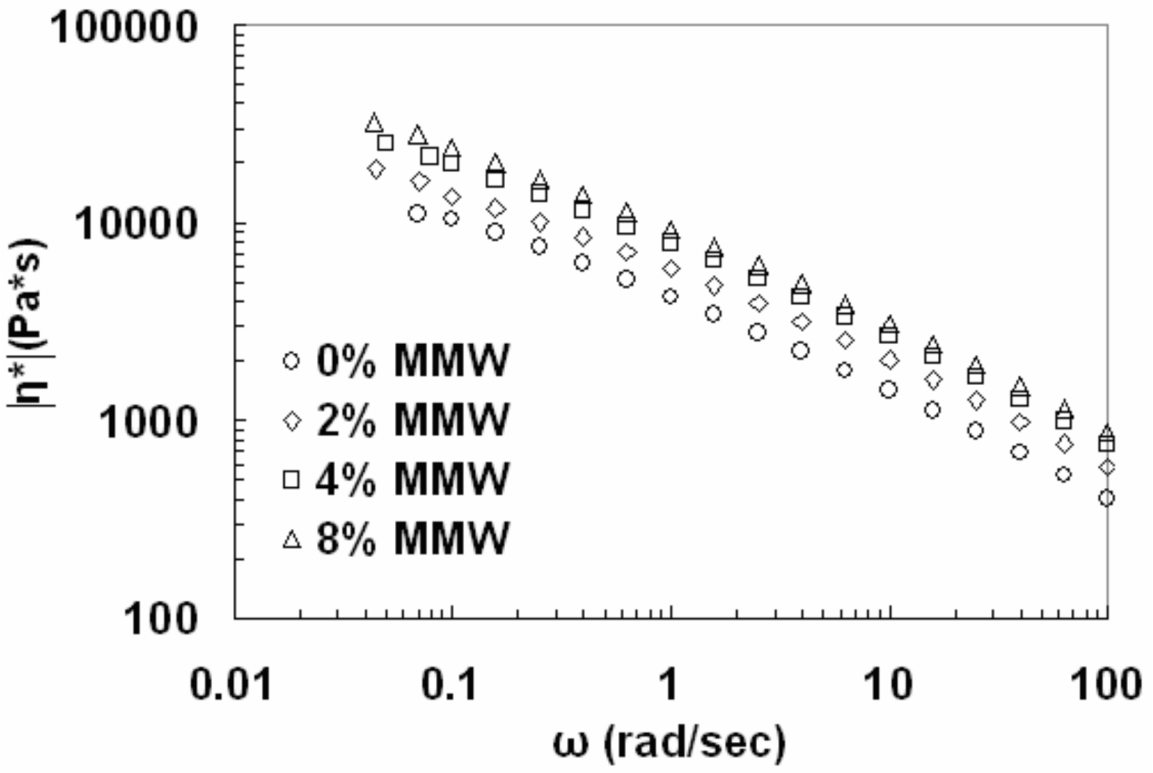

Figure 3.15. $|h^*|$ at T_{ref} = 190°C for MMW Matrix and Nanocomposites.

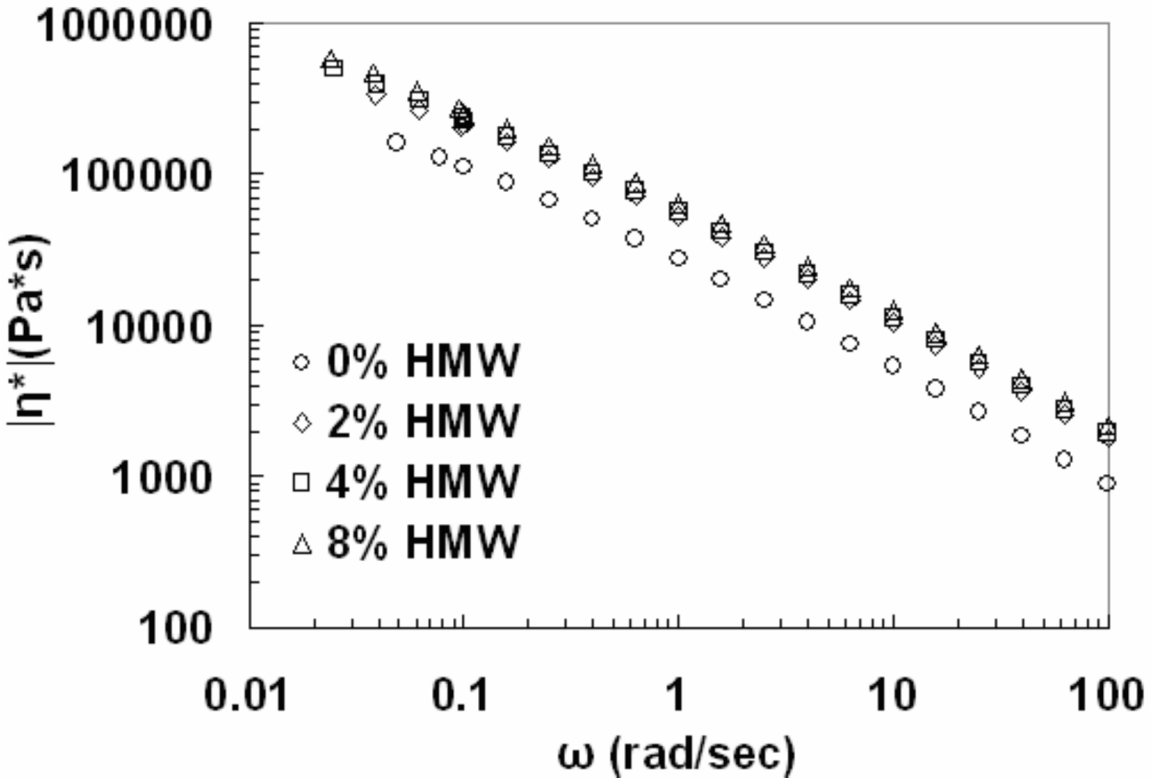

Figure 3.16. $|h^*|$ at T_{ref} = 190°C for HMW Matrix and Nanocomposites.

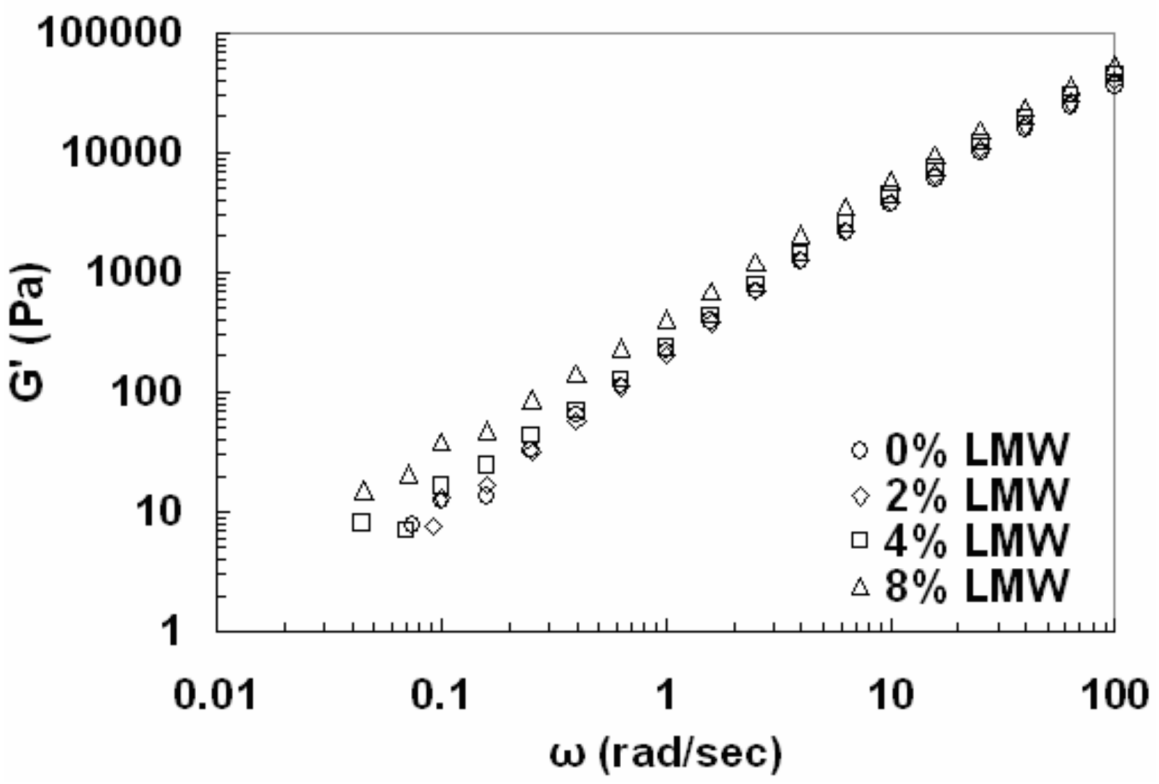

Figure 3.17. G' at T_{ref} = 190°C for LMW Matrix and Nanocomposites.

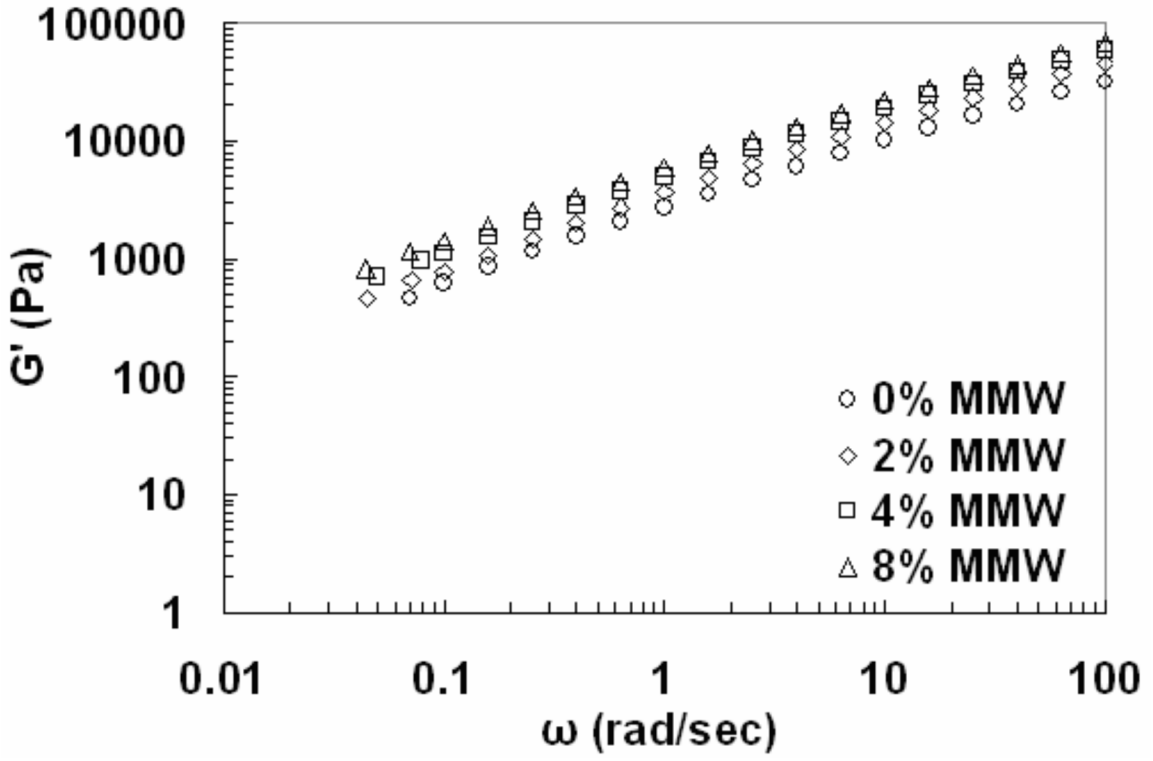

Figure 3.18. G' at T_{ref} = 190°C for MMW Matrix and Nanocomposites.

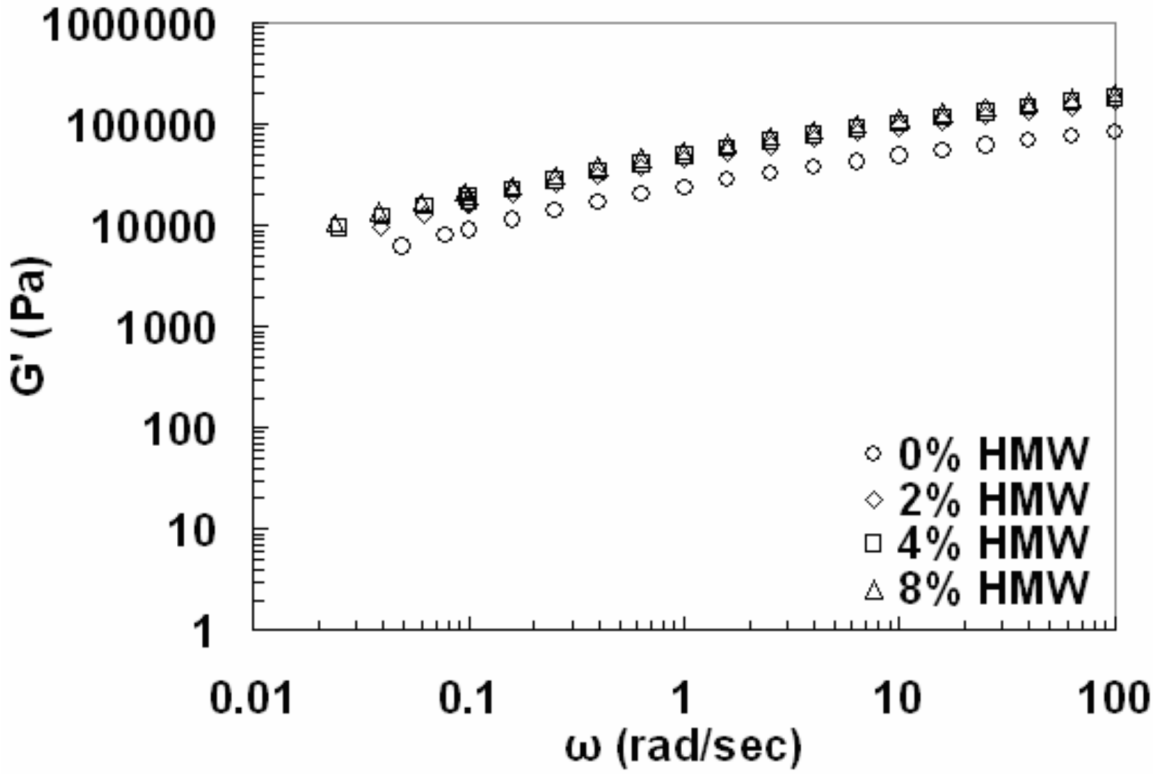

Figure 3.19. G' at T_{ref} = 190°C for HMW Matrix and Nanocomposites.

4.0 Recommendations for Future Work

1. It was shown that the HMW HDPE matrix used in this work dramatically increased the Young's modulus of HDPE/MMT nanocomposites compared to the two lower molecular weight matrices used in the *absence* of maleic anhydride as a compatibilizer. It is expected that the use of a compatibilizer between the hydrophobic HDPE and hydrophilic MMT would lead to greater attraction between the polymer and nanoclay, improving the level of adhesion of the filler to the matrix and increase mechanical properties even further. Furthermore, the degree of adhesion may be qualitatively assessed through the proximity of the experimental Young's modulus with that predicted by the Halpin-Tsai equation which assumes a good level of adhesion between filler particles and matrix. Thus, it would be beneficial to examine the effect incorporating maleic anhydride would have on the level of intercalation/exfoliation as well as the mechanical properties of the HDPE/MMT nanocomposites studied in this work.

2. Only one organically modified MMT (Cloisite 20A) was used in this work which had a modifier concentration of 95 meq/100 g clay. In order to fully optimize the properties of the HDPE/MMT nanocomposites the effect of the organoclay should be established. An organically modified MMT termed Cloisite 15A is available whose quaternary alkyl ammonium cation modifier is of the same chemical composition as Cloisite 20A but contains a higher concentration of the modifier, namely 125 meq/100 g clay. The d-spacing of Cloisite 15A was given to be 31.5 Å by the manufacturer compared to that of Cloisite 20A which was given to be 24.2 Å. The

larger d-spacing of Cloisite 15A may facilitate greater intercalation of the polymer than is observed with Cloisite 20A. However, while a larger d-spacing is observed for Cloisite 15A, the higher concentration of organic modifier residing in the interlayer of Cloisite 15A may prevent polymer chains from intercalating in between the clay galleries due to a decreased amount of space for the polymer to reside in. Thus, it would be beneficial to examine what tradeoff exists between the increased d-spacing of Cloisite 15A and the lower concentration of organic modifier residing in the interlayer of the Cloisite 20A galleries.

3. A single screw extruder was employed in this study to compound the various HDPE matrices with organically modified MMT. Other processing methods exist for generating PLS nanocomposites. Most studies have cited the use of a twin screw extruder in compounding polymer/layered silicate nanocomposites. While a greater shear force is encountered in a twin screw extruder, it is unclear whether the increased shear leads to greater separation and thus exfoliation of the high aspect ratio MMT platelets or whether the twin screw extruder simply beats the clay so much that the aspect ratio of MMT is lost. Thus, it would be beneficial to compare the levels of intercalation as well as mechanical property enhancements of HDPE/MMT nanocomposites compounded in a twin screw extruder to the nanocomposites generated in this work by a single screw extruder.

4. Additionally, supercritical carbon dioxide (SC-CO_2) has shown promise as a processing aid for PLS nanocomposite systems. SC-CO_2 acts as a polar solvent which

is able to penetrate the interlayer spacings of 2:1 phyllosilicates such as MMT. A technique is being developed by which nanoclays are mixed with SC-CO_2, the pressure is partially released to expand the particles, and then the mixture is injected into the polymer melt as it is pumped through an extruder. Because SC-CO_2 behaves as a polar organic solvent, it is believed that it readily enters the galleries of the nanoclay and swells the clay particles. When the pressure is partially released, CO_2 expands the galleries and thereby further exfoliates the clay particles. Furthermore, CO_2 is partially soluble in a number of polymers serving as a plasticizer and further facilitates the mixing process. Comparison of the rheological and mechanical properties of nanocomposites prepared using the SC-CO_2 method to nanocomposites prepared in this study would establish the utility of SC-CO_2 as a processing aid for compounding PLS nanocomposites.

5. The processing conditions utilized during nanocomposite formation may be optimized as well. The shear stress imparted to the nanoclay particles during compounding may be increased by increasing the screw speed and, hence, shear rate. The compounding temperature may also be decreased in order to increase the viscosity of the matrix. Systematically varying these two parameters, screw speed and temperature, may impart higher shear stresses onto nanoclay particles from the HDPE matrices possibly facilitating greater intercalation of the nanocomposites.

6. The highest organoclay loading used in this work was chosen to be 8 wt%. This concentration was chosen because previous literature has shown that exfoliation of

the silicate layers does not occur above 8 to 10 wt% clay loading. However, nanocomposites containing 8 wt% clay exhibited increasing tensile properties while remaining melt processable. Additionally, no solid-like network was observed in any of the nanocomposites from dynamic rheometry. It is then recommended that higher levels of nanoclay be compounded into the three HDPE matrices used to examine any additional enhancement in the tensile properties of the nanocomposites. It will also be necessary to examine the subsequent increase in viscosity of the nanocomposites containing larger amounts of clay to assure they remain melt processable.

7. Dynamic rheometry was performed in this work where the nanocomposites were subjected to an oscillatory flow field increasing in frequency. This test provided insight into the structure of the nanocomposites in that no network structure was observed due to a lack of change in the frequency dependence of $|h^*|$ and G'. Further insight may be gained concerning the structure of the nanocomposites by performing transient stress growth experiments where shear is applied to the nanocomposite and changes in the shear stress and primary normal stress difference are monitored with time. Comparison of the results from stress growth experiments for the unfilled matrices to the filled nanocomposites may provide an understanding for the effect clay has on the formation of a network within the polymer matrix. Subsequent cessation of the applied shear may provide information concerning the relaxation behavior of the clay-filled materials. Information concerning the relaxation behavior and existence of residual stresses in the nanocomposites may be used to prevent warpage of injection molded parts.

Appendix A: Mechanical Properties

Table A.1. Mechanical Properties for LMW Matrix and Nanocomposites.

Organoclay Concentration (wt%)	Young's Modulus (MPa)	Flexural Modulus (MPa)	Stress at 0.2% Yield (MPa)	Stress at Peak (MPa)	Stress at Break (MPa)	Elongation at Break (%)
0	961.27 ± 145.17	791.57 ± 51.58	5.85 ± 1.00	18.59 ± 1.03	12.49 ± 0.72	823.44 ± 116.10
2	1150.07 ± 72.76	923.31 ± 57.42	6.45 ± 0.76	19.18 ± 0.07	6.50 ± 0.07	233.21 ± 40.34
4	1245.06 ± 152.77	907.25 ± 34.34	6.73 ± 0.55	17.37 ± 0.56	5.90 ± 0.24	122.58 ± 35.91
8	1407.36 ± 142.95	906.66 ± 18.05	7.54 ± 0.64	18.64 ± 0.60	6.37 ± 0.17	77.85 ± 31.61

Table A.2. Mechanical Properties for MMW Matrix and Nanocomposites.

Organoclay Concentration (wt%)	Young's Modulus (MPa)	Flexural Modulus (MPa)	Stress at 0.2% Yield (MPa)	Stress at Peak (MPa)	Stress at Break (MPa)	Elongation at Break (%)
0	1141.30 ± 129.31	878.84 ± 49.85	8.24 ± 0.58	23.86 ± 0.61	9.72 ± 1.19	107.21 ± 34.05
2	1253.43 ± 191.87	982.71 ± 48.38	11.56 ± 0.61	25.12 ± 0.44	8.54 ± 0.16	114.74 ± 15.46
4	1364.23 ± 160.17	1079.80 ± 36.29	8.42 ± 0.25	23.37 ± 0.82	8.08 ± 0.58	67.72 ± 12.96
8	1518. 72 ± 154.44	1153.80 ± 57.22	11.71 ± 0.35	24.66 ± 0.60	11.71 ± 0.35	12.49 ± 6.15

Table A.3. Mechanical Properties for HMW Matrix and Nanocomposites.

Organoclay Concentration (wt%)	Young's Modulus (MPa)	Flexural Modulus (MPa)	Stress at 0.2% Yield (MPa)	Stress at Peak (MPa)	Stress at Break (MPa)	Elongation at Break (%)
0	1331.28 ± 99.59	1115.56 ± 53.64	11.44 ± 2.63	35.54 ± 1.24	13.79 ± 1.21	11.21 ±1.19
2	1324.49 ± 115.31	1165.89 ± 48.14	14.00 ± 0.40	37.18 ± 0.82	12.96 ± 0.64	12.09 ± 1.40
4	1684.02 ± 184.10	1093.35 ± 54.50	14.03 ± 0.59	31.02 ± 1.38	10.07 ± 1.57	10.76 ± 0.31
8	2230.22 ± 117.45	1262.33 ± 31.26	14.42 ± 1.43	40.40 ± 1.15	40.42 ± 1.17	10.66 ± 1.44

Comment on Flexural Modulus

The flexural modulus presented in Tables A.1-3 showed an increasing trend as the MMT content was increased for a given molecular weight. However, the increase was not a large compared to the enhancement observed previously in this study with the Young's modulus. A 15%, 31%, and 13% increase from the unfilled matrices were observed in the flexural modulus of the 8 wt% nanocomposites for the LMW, MMW, and HMW matrices, respectively. This was in contrast to the 46%, 33%, and 68% increase from the unfilled matrices observed in the tensile modulus for the 8 wt% nanocomposites for the LMW, MMW, and HMW matrices, respectively.

Previous studies have shown conflicting results as to the relative increases in the tensile or Young's modulus and the flexural modulus. Ellis et al. [1] observed a larger increase in the Young's modulus for a PP/MMT nanocomposite containing a 4 wt% organoclay loading than compared to the flexural modulus of the same clay content. Specifically, the Young's modulus increased from 1.97 GPa to 2.38 GPa, representing a 21% increase compared to a 12% increase in the flexural modulus from 1.89 GPa for the unfilled matrix to 2.13 GPa for the 4 wt% nanocomposite. No explanation was given to account for this behavior. XRD patterns presented for the PP matrix and the 4 wt% nanocomposite indicated slight intercalation as observed from a shift in the d-spacing of the nanoclay from 26.1 Å to 30.0 Å for the 4 wt% nanocomposite. Chow et al. [2] have shown comparable increases in the Young's and flexural moduli in a 70 wt% polyamide 6 and 30 wt% PP blend. For a 10 wt% loading of MMT modified with an octadecylamine surfactant the Young's modulus increased from 1.87 GPa for the unfilled blend to approximately 2.38 GPa representing a 27% increase. Similarly, the flexural modulus

increased from 1.73 GPa for the unfilled matrix to approximately 2.25 GPa representing a 30% increase. Chow et al. [2] argued that in the skin-core morphology of the injection molded test specimens, the skin layers contained exfoliated clay platelets aligned in the melt flow direction and it is this skin layer which is under tension/compression during flexural testing. Hence, it is believed that this accounts for the similar behavior in the Young's and flexural moduli. XRD results indicated that exfoliation was achieved by disappearance of the characteristic diffraction peak of the organoclay. The reader is reminded that only intercalated nanocomposites were observed in the XRD results presented in this paper. Thus, the lack of exfoliated nanoclay on the skin layer of the injection molded test specimens may account for the lower enhancement of the flexural modulus of the nanocomposites compared to that seen for the Young's modulus.

References

1. T. S. Ellis and J. S. D'Angelo, *J. Appl. Polym. Sci.*, **90**, 1639 (2003).

2. W. S. Chow, Z. A. Mohd. Ishak, U. S. Ishiaku, J. Karger-Kocsis, and A. A. Apostolov, *J. Appl. Polym. Sci.*, **91**, 175 (2004).

Appendix B: Dynamic Mechanical Thermal Analysis Data

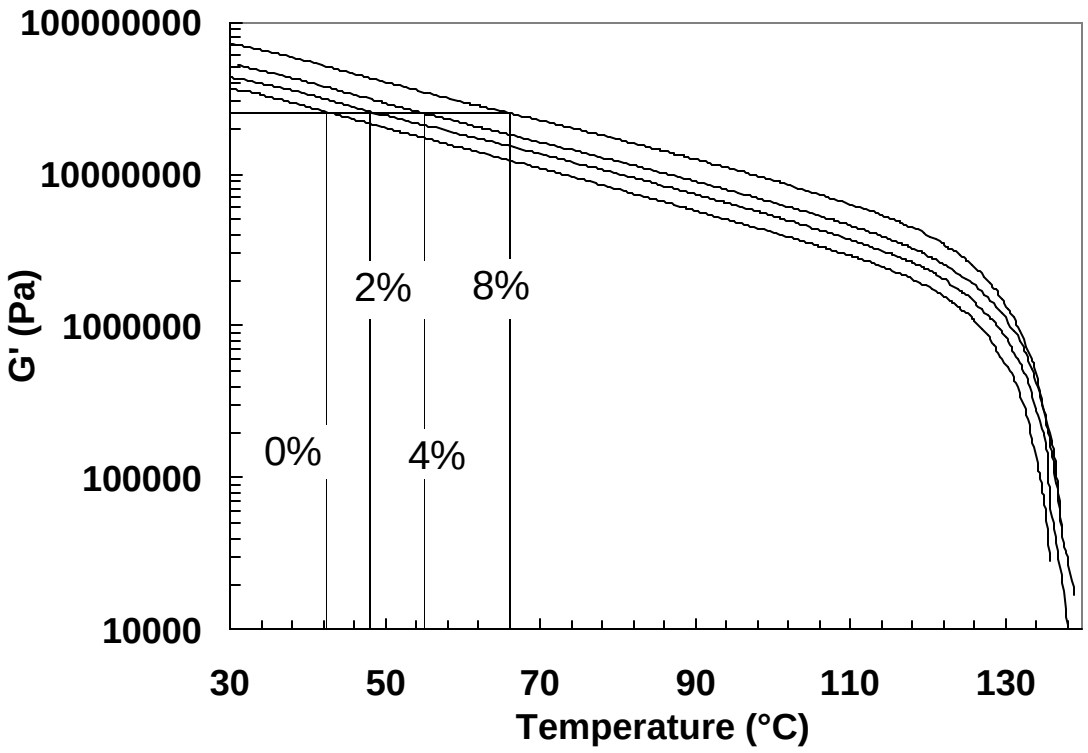

Figure B.1. G’ for LMW Matrix and Nanocomposites

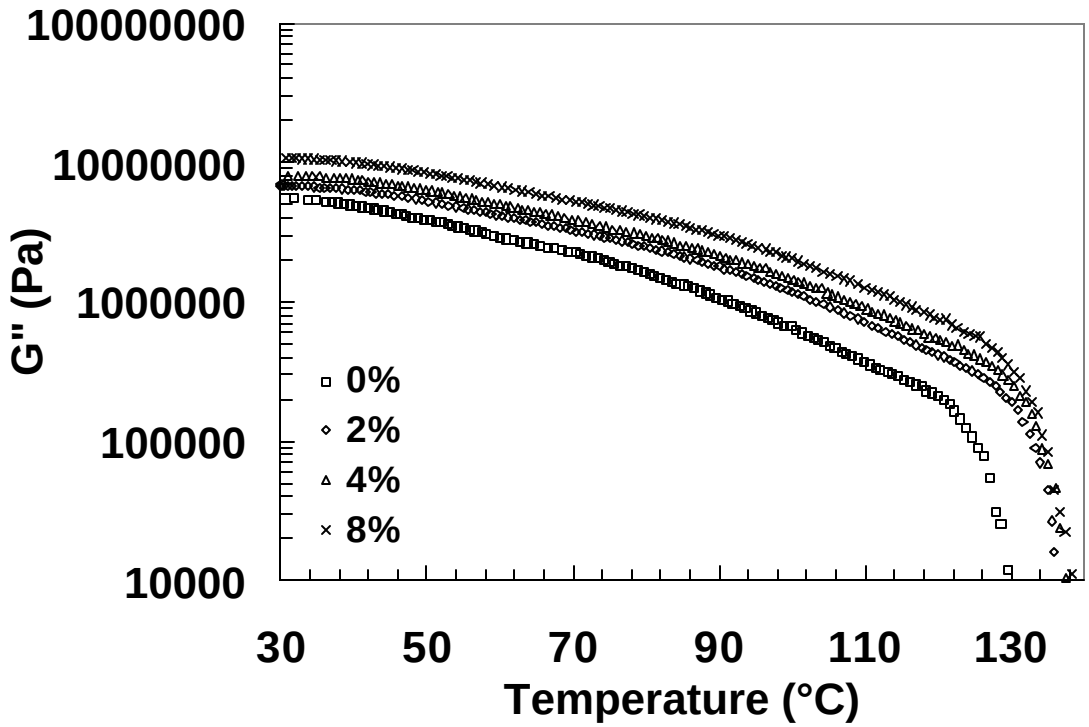

Figure B.2. G” for LMW Matrix and Nanocomposites.

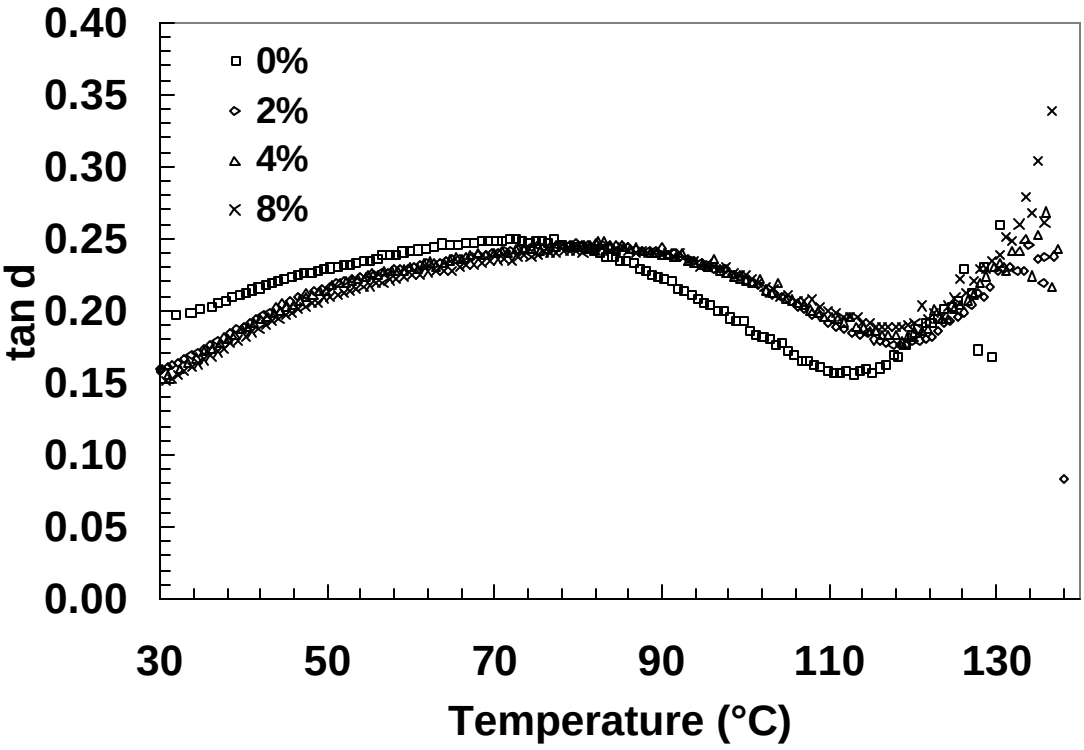

Figure B.3. Tan d for LMW Matrix and Nanocomposites.

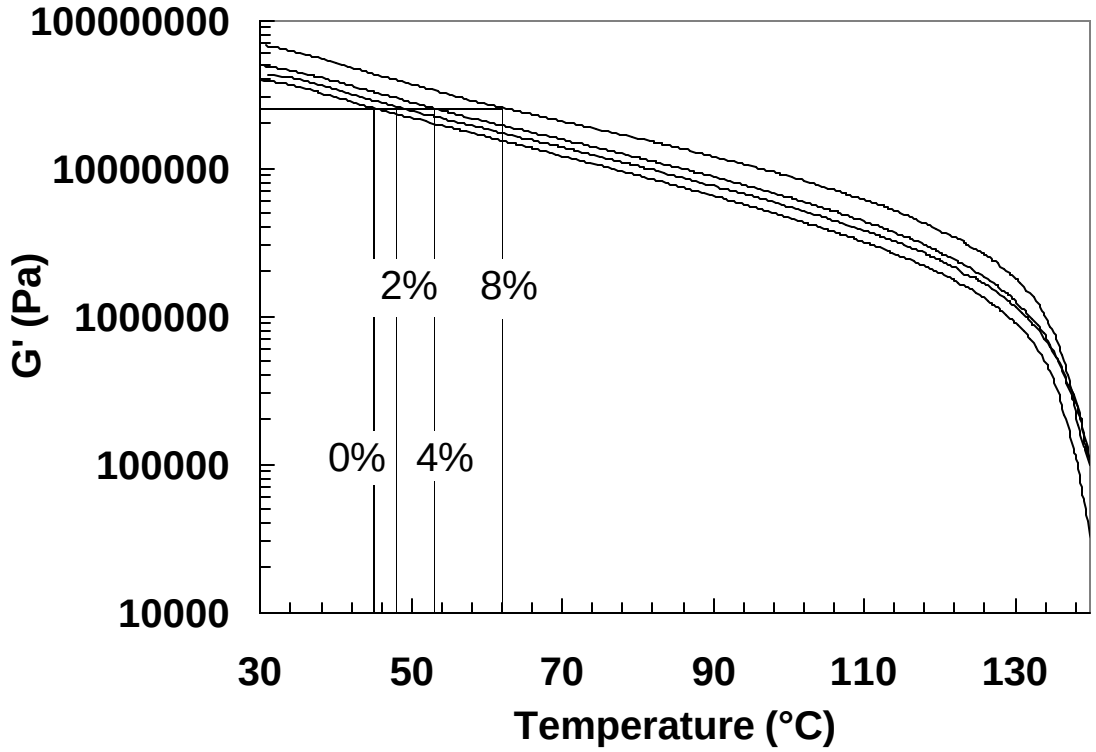

Figure B.4. G’ for MMW Matrix and Nanocomposites.

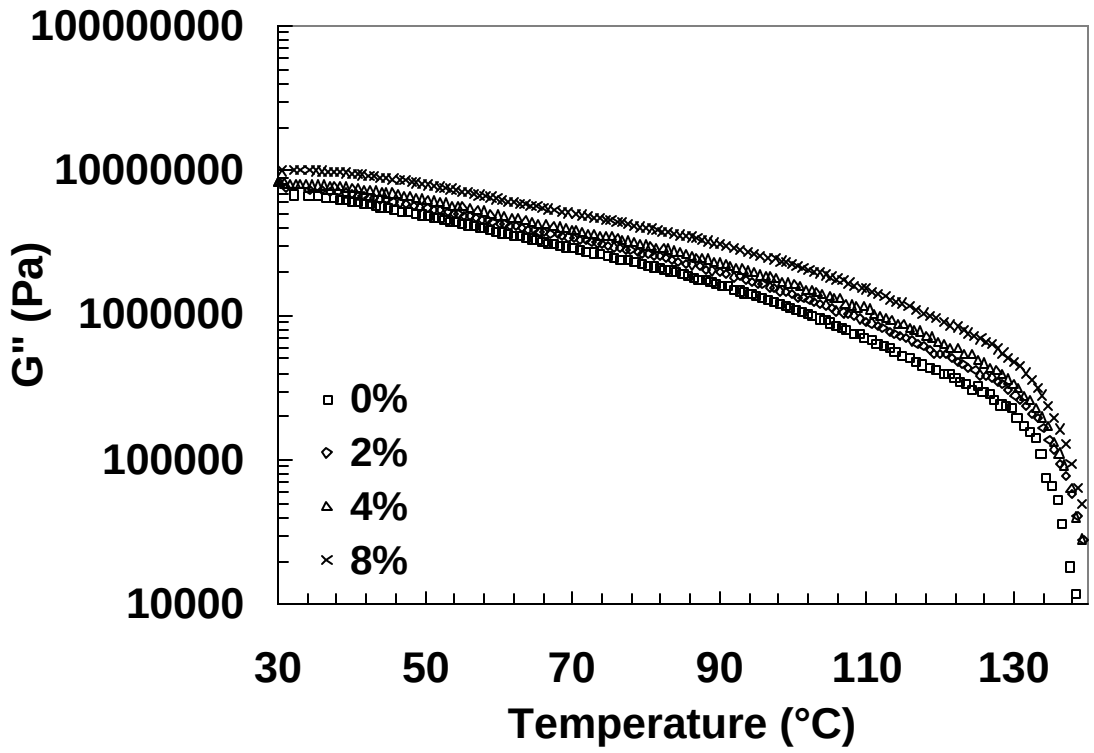

Figure B.5. G” for MMW Matrix and Nanocomposites.

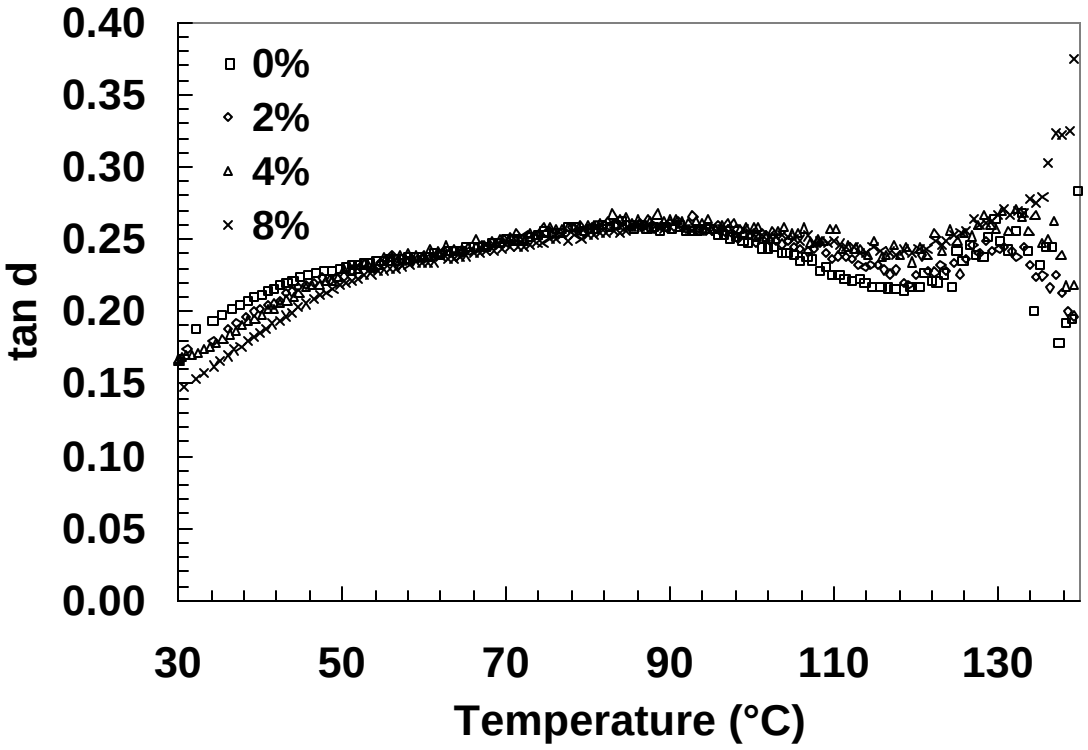

Figure B.6. Tan *d* for MMW Matrix and Nanocomposites.

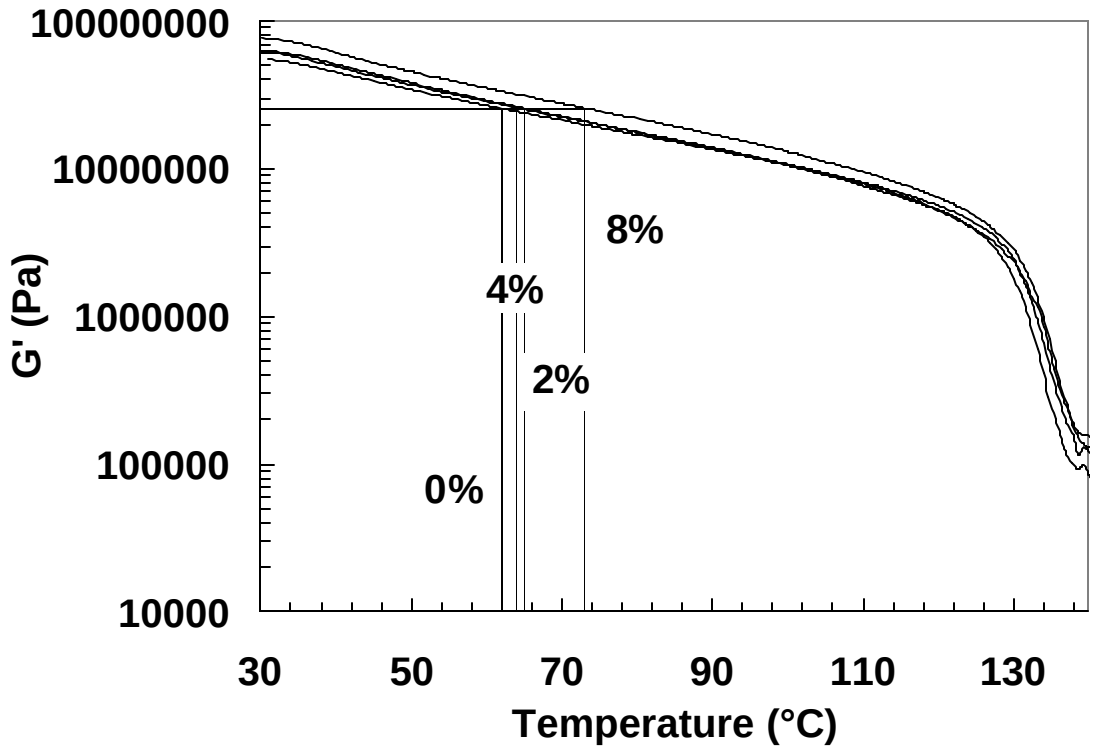

Figure B.7. G' for HMW Matrix and Nanocomposites.

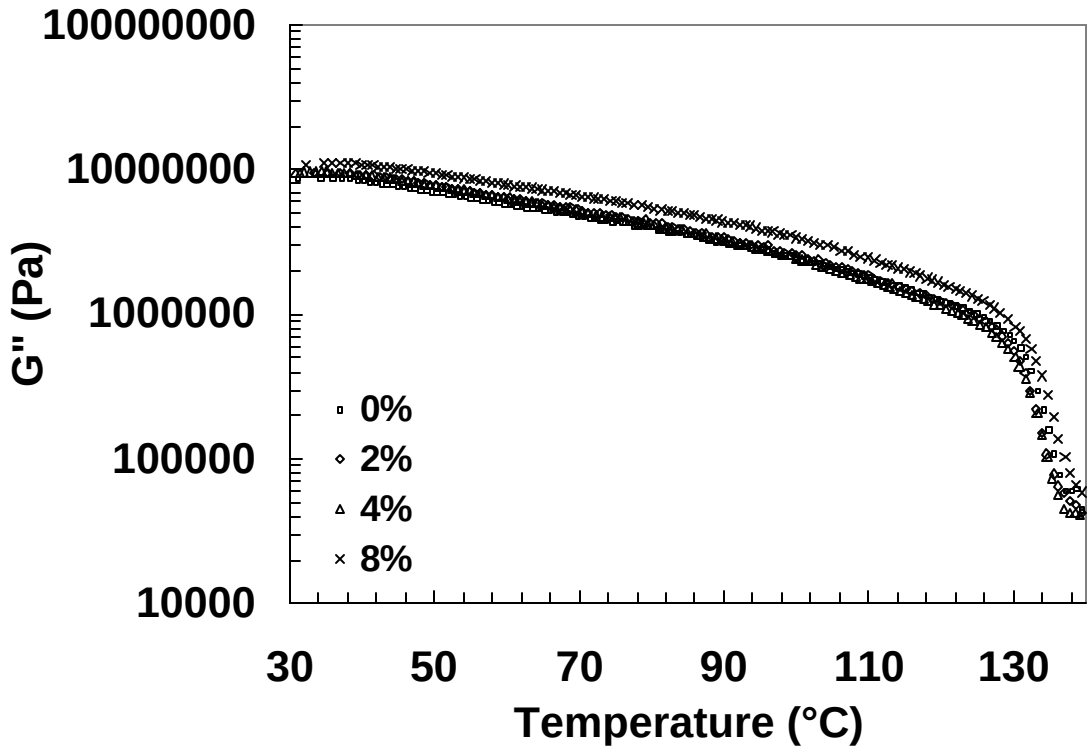

Figure B.8. G” for HMW Matrix and Nanocomposites.

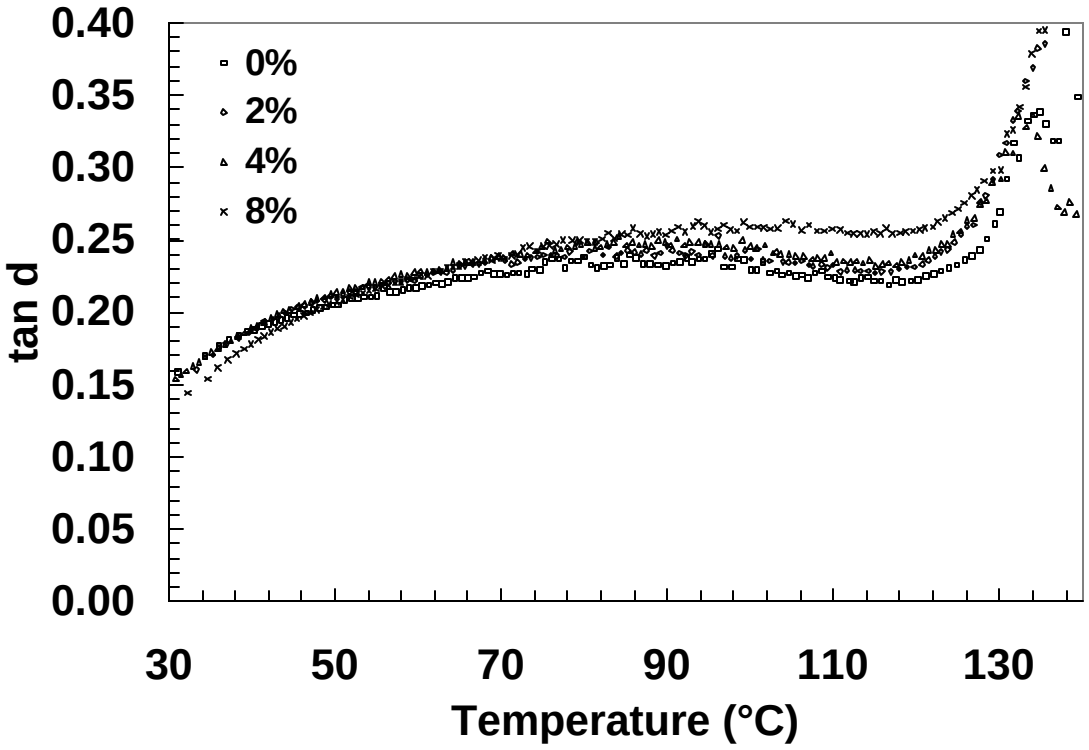

Figure B.9. Tan d for HMW Matrix and Nanocomposites.

Appendix C: Dynamic Oscillatory Rheometry Data

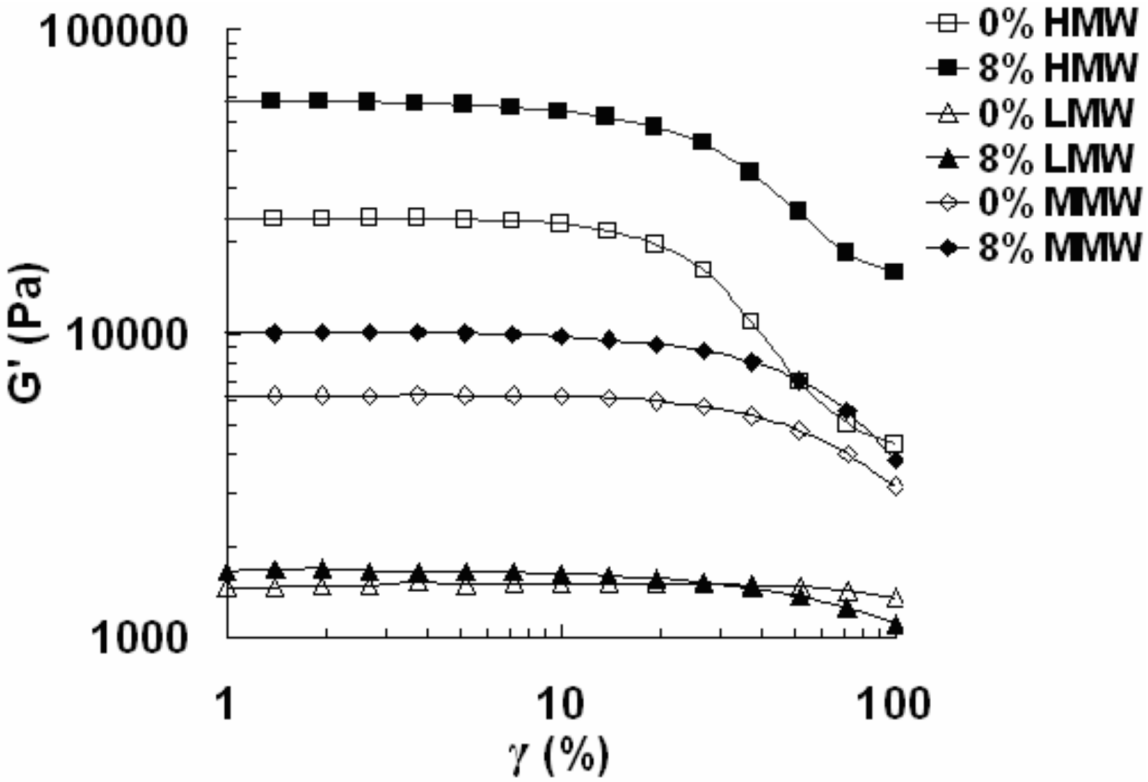

Figure C.1. Strain Sweep of 0% and 8 wt% Nanocomposites for Three HDPE Matrices. w =5.0 rad/sec, T=190°C.

Table C.1. Strain Sweep of Three unfilled HDPE Matrices. w =5.0 rad/sec, T=190°C.

0% LMW			0% MMW			0% HMW		
Strain %	**G' (Pa)**	**$\|h^*\|$ (Pa*s)**	**Strain %**	**G' (Pa)**	**$\|h^*\|$ (Pa*s)**	**Strain %**	**G' (Pa)**	**$\|h^*\|$ (Pa*s)**
0.999895	1464.5	1295.7	0.9966	6261.4	1821.8	0.99025	23750	5263.5
1.39085	1465.35	1308.8	1.3876	6267.6	1822.8	1.3782	23921	5306.7
1.93145	1475.05	1294.6	1.9301	6262.1	1826.4	1.9246	23933	5303.6
2.68495	1483.8	1304.1	2.6862	6228.4	1820.2	2.6686	23965	5312.2
3.73665	1520.15	1306.7	3.7333	6289.8	1822.6	3.7112	23955	5310
5.1877	1492.1	1308	5.1789	6269.6	1826	5.1544	23799	5281.9
7.21525	1511.65	1309.2	7.1978	6270.4	1824.6	7.1588	23499	5227.5
10.0125	1506.9	1312.9	9.9985	6214	1812.7	9.9459	22973	5120.9
13.911	1513.45	1314.5	13.89	6151.5	1794.9	13.818	21774	4880.1
19.3225	1507.55	1314.6	19.296	5988.4	1757.2	19.211	19604	4420.6
26.844	1503.7	1315.1	26.803	5753.1	1697.8	26.719	16191	3705.7
37.303	1490.3	1313.7	37.218	5364.3	1600.1	37.144	10919	2572
51.8175	1467.75	1309.4	51.624	4808.1	1461.9	51.657	6951.6	1685.4
71.929	1426.1	1300.2	71.826	4026.4	1264.3	71.818	5043.9	1228.9
99.844	1354.95	1283.3	99.848	3145.1	1042.4	99.741	4316.3	1054.9

Table C.2. Strain Sweep of 8 wt% Nanocomposites of Three HDPE Matrices. w =5.0 rad/sec, T=190°C.

8% LMW			8% MMW			8% HMW		
Strain %	**G' (Pa)**	**$\|h^*\|$ (Pa*s)**	**Strain %**	**G' (Pa)**	**$\|h^*\|$ (Pa*s)**	**Strain %**	**G' (Pa)**	**$\|h^*\|$ (Pa*s)**
1.0059	1642.4	1407.4	0.99262	10101	2941.1	0.983205	58310.5	12532
1.3949	1675.9	1396.6	1.3827	10060	2940.5	1.3614	58238.5	12547
1.9283	1690.3	1398.3	1.9262	10126	2945.5	1.8936	58072	12547
2.6831	1653.8	1400	2.6796	10135	2948.2	2.6374	57816.5	12527
3.7374	1651.2	1401.4	3.7263	10091	2947.1	3.66365	57353	12460
5.1925	1649.1	1400.2	5.1709	10047	2934.3	5.0859	56583	12337
7.2049	1643.4	1402.5	7.184	9935.4	2914	7.06475	55488.5	12147
10.018	1625.3	1397.6	9.9773	9781.7	2881.6	9.82515	53875	11869
13.908	1600.1	1389.8	13.864	9557.4	2831.3	13.6545	51541.5	11443
19.33	1564.5	1375.5	19.27	9227.9	2756.3	18.9995	47656	10804
26.84	1520.2	1352	26.768	8752.5	2646.2	26.444	42385.5	9704.9
37.293	1452.9	1319.6	37.2	8055.7	2480.6	36.8435	33816.5	7663
51.817	1367.4	1272.9	51.565	7023.1	2232.8	51.2515	25126.5	5325.5
71.786	1250.9	1208.7	71.723	5563.4	1864.1	71.3945	18401.5	4235.9
99.901	1112	1129.6	99.822	3828.6	1407.4	99.382	15868.5	5132.8

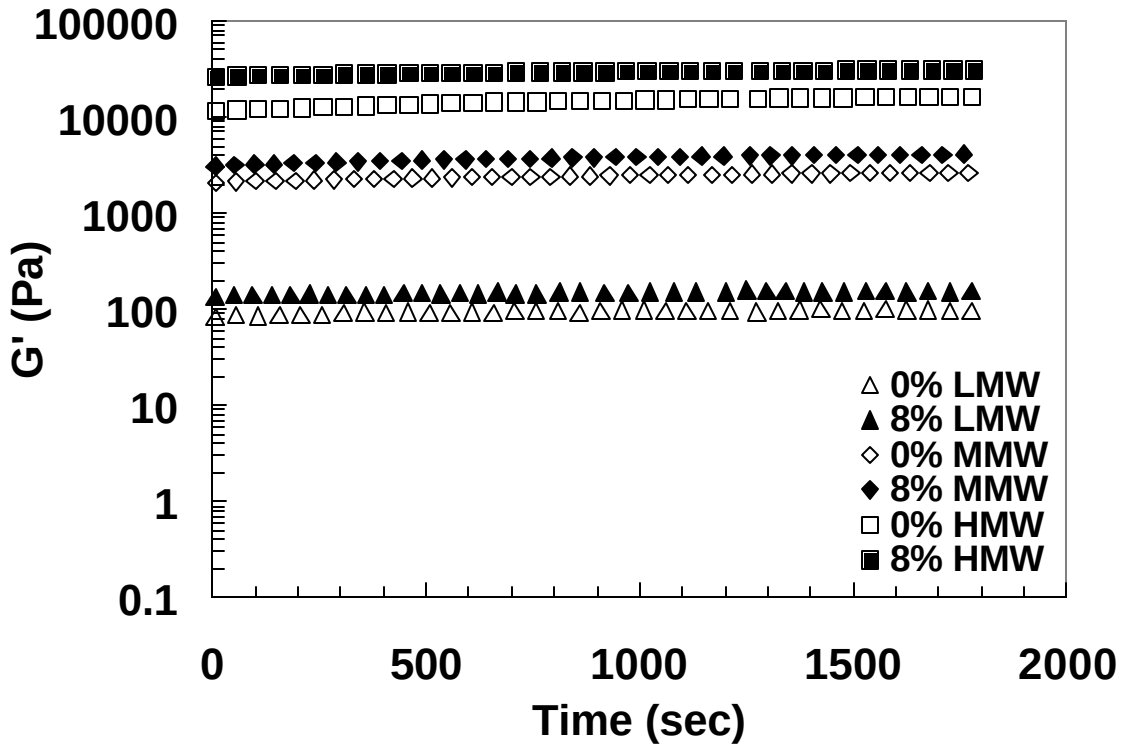

Figure C.2. Time Sweep of 0% and 8 wt% Nanocomposites for Three HDPE Matrices. w =1.0 rad/sec, 5.0% strain, T=230°C.

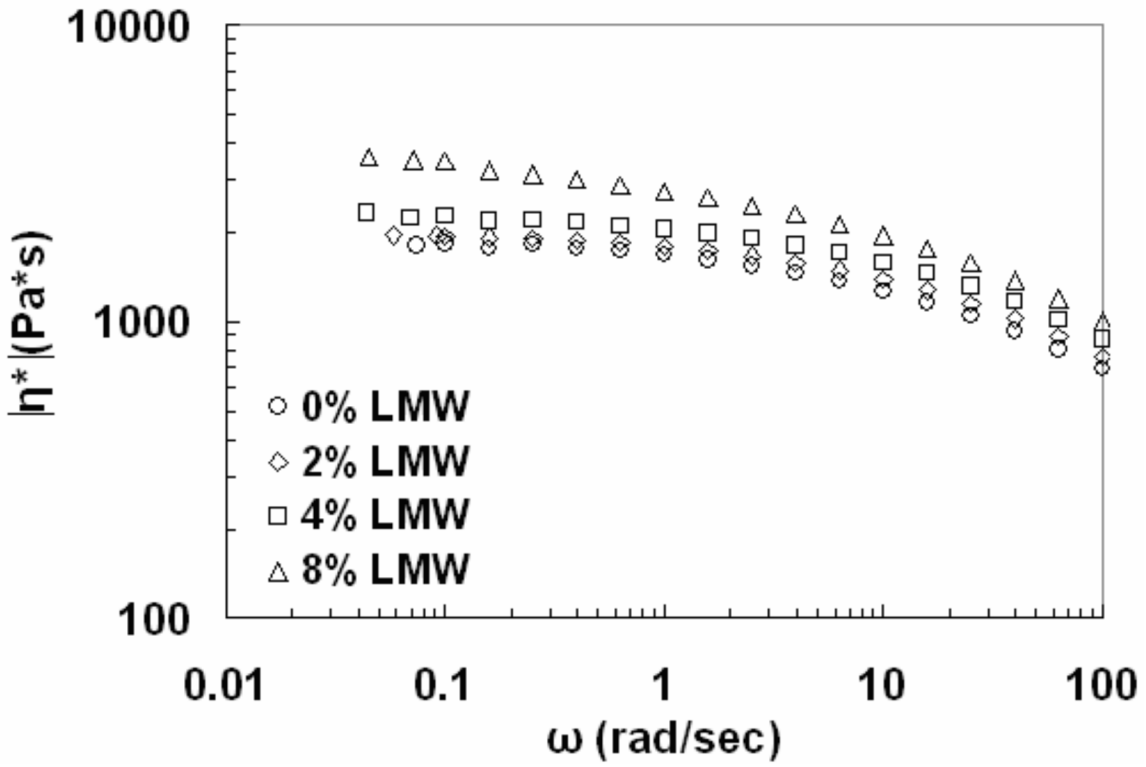

Figure C.3. Complex Viscosity Master Curve at T_{ref} = 190°C for LMW Matrix and Nanocomposites.

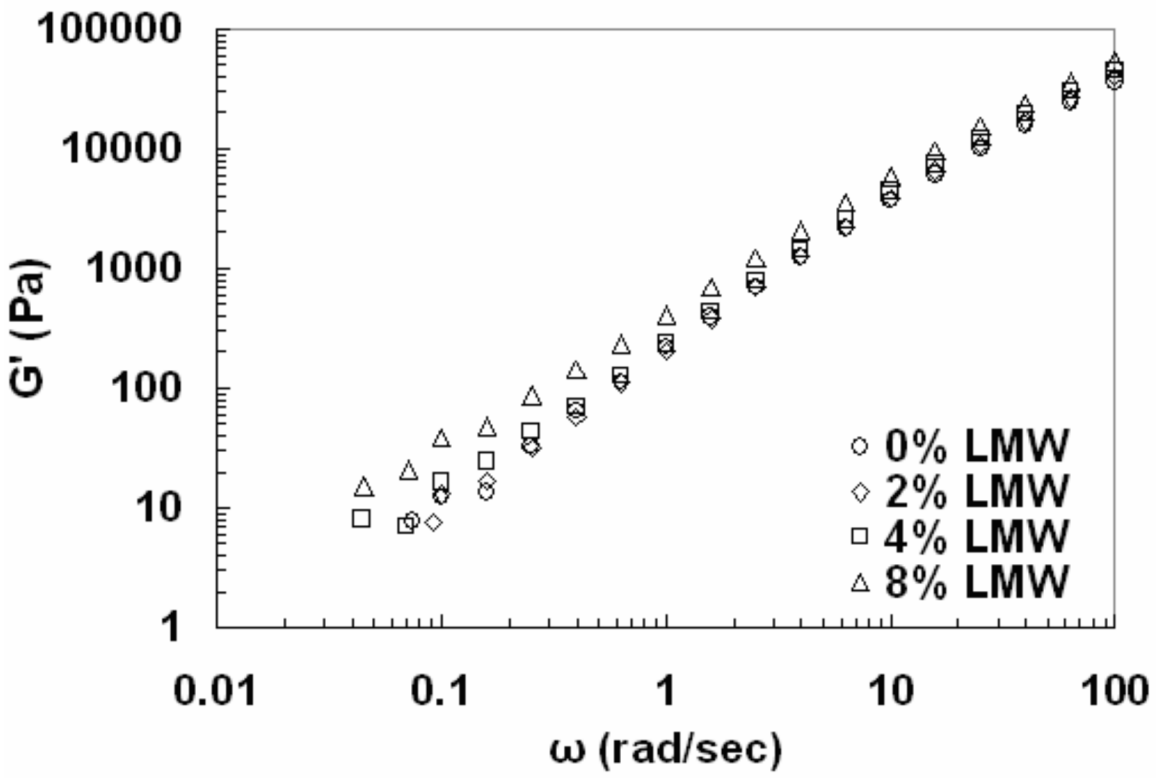

Figure C.4. Storage Modulus Master Curve at T_{ref} = 190°C for LMW Matrix and Nanocomposites.

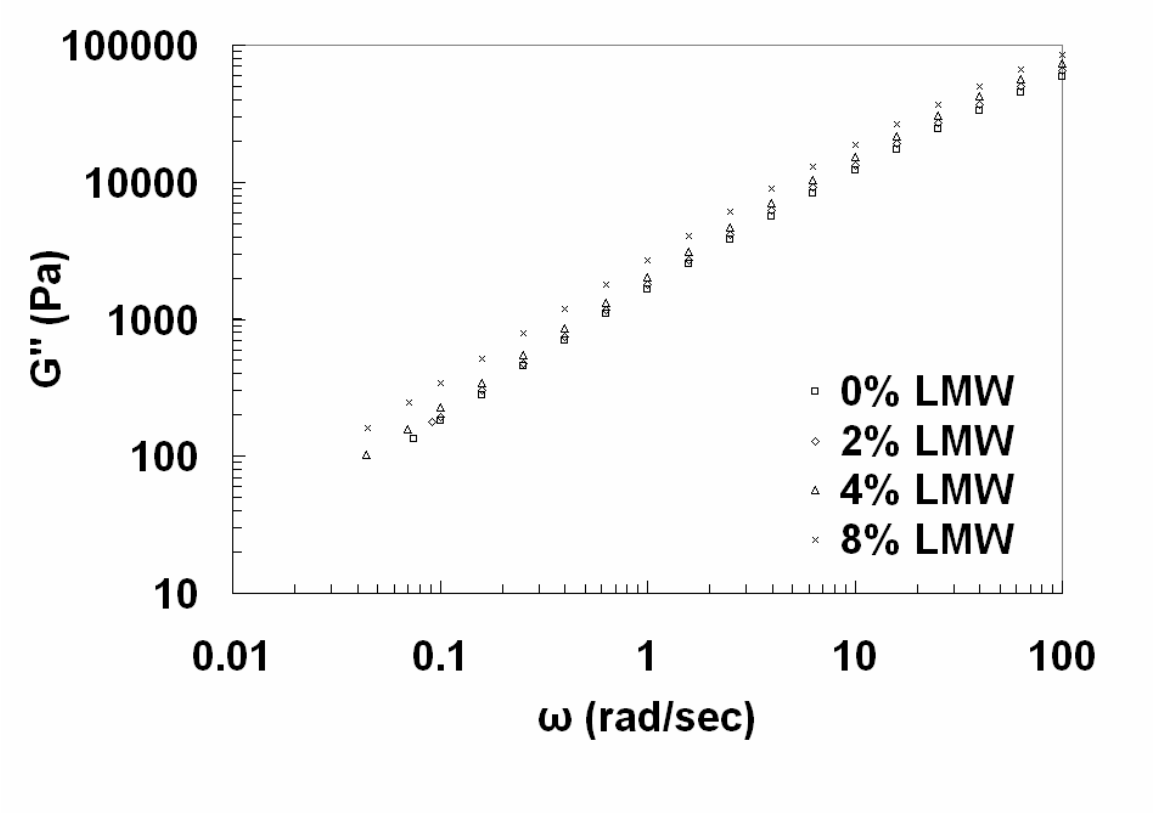

Figure C.5. Loss Modulus Master Curve at T_{ref} = 190°C for LMW Matrix and Nanocomposites.

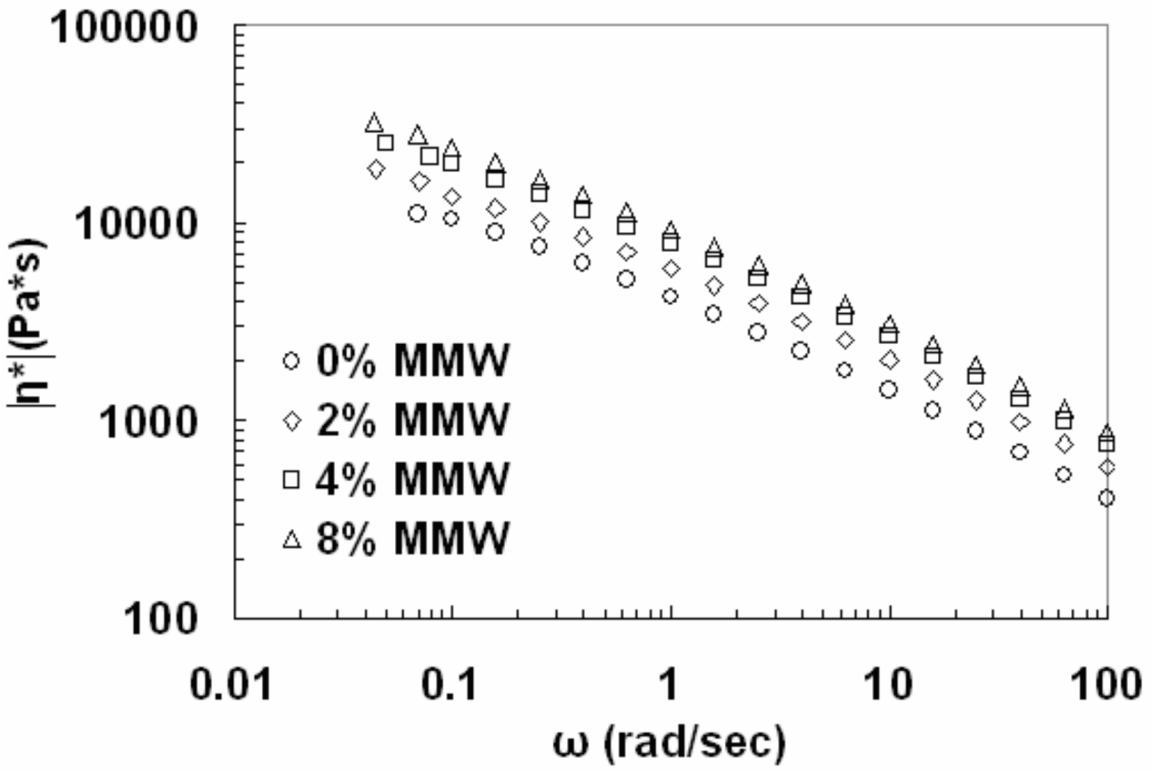

Figure C.6. Complex Viscosity Master Curve at T_{ref} = 190°C for MMW Matrix and Nanocomposites.

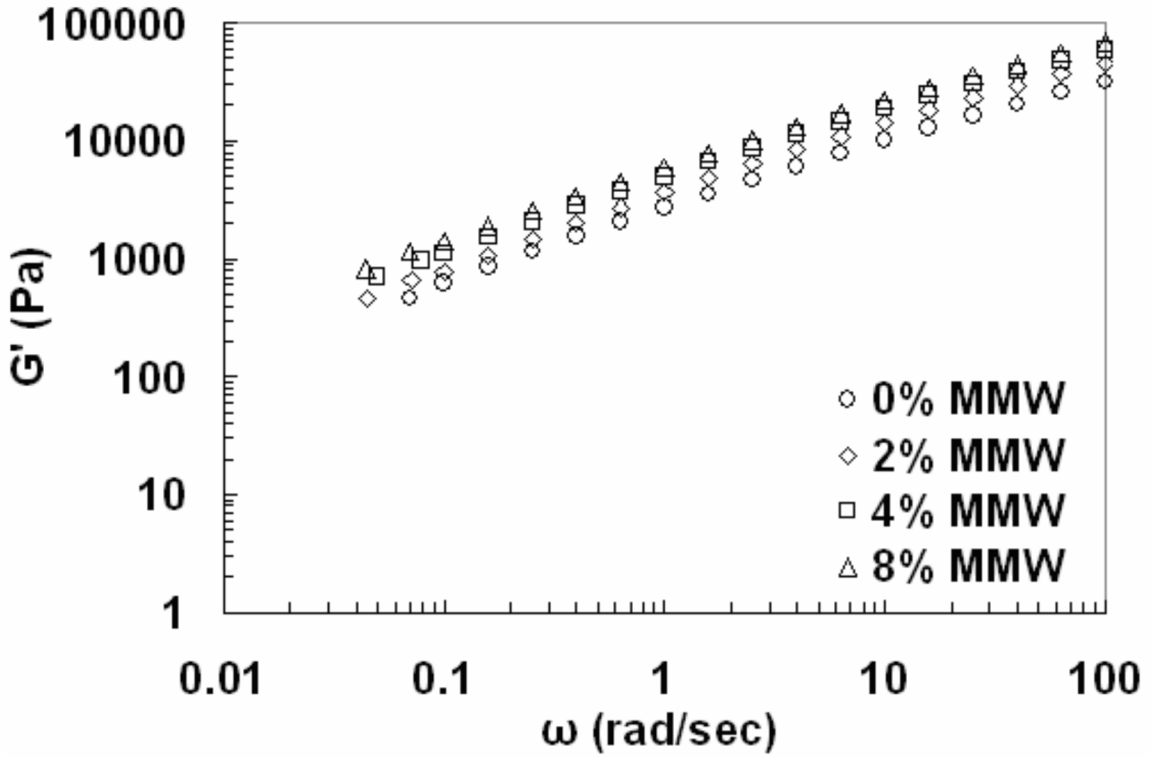

Figure C.7. Storage Modulus Master Curve at T_{ref} = 190°C for MMW Matrix and Nanocomposites.

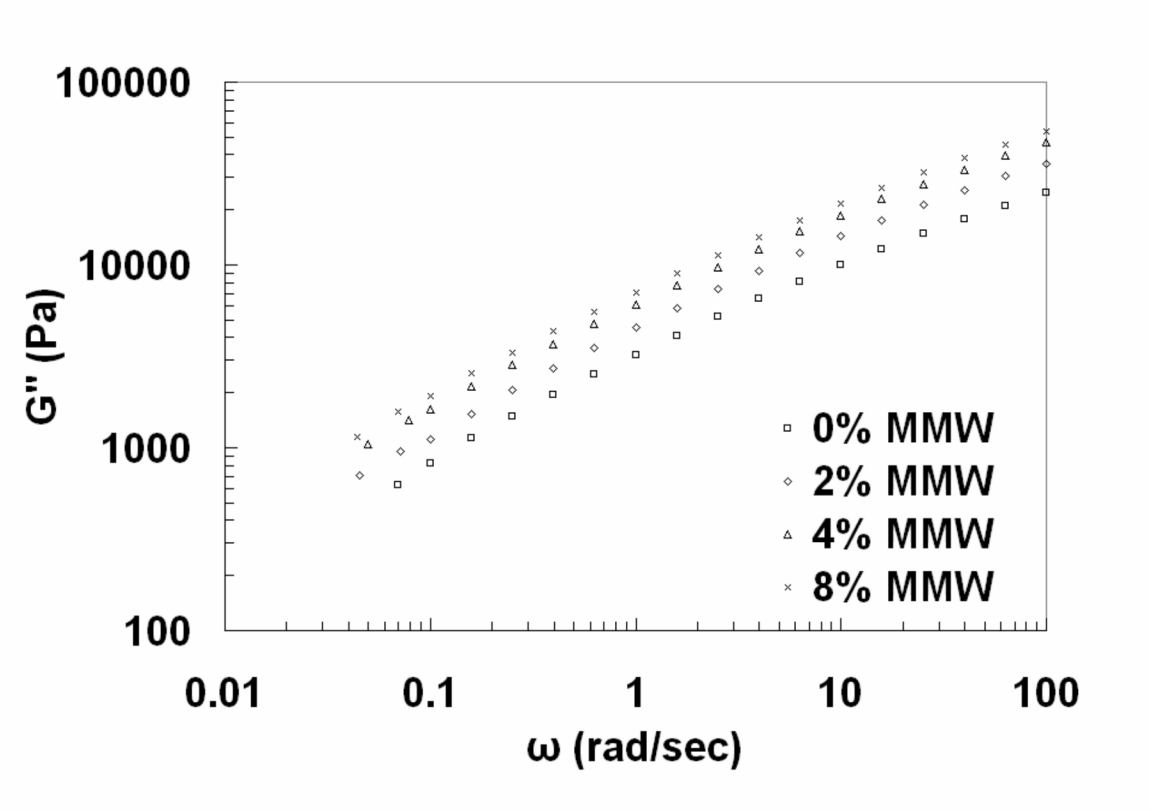

Figure C.8. Loss Modulus Master Curve at T_{ref} = 190°C for MMW Matrix and Nanocomposites.

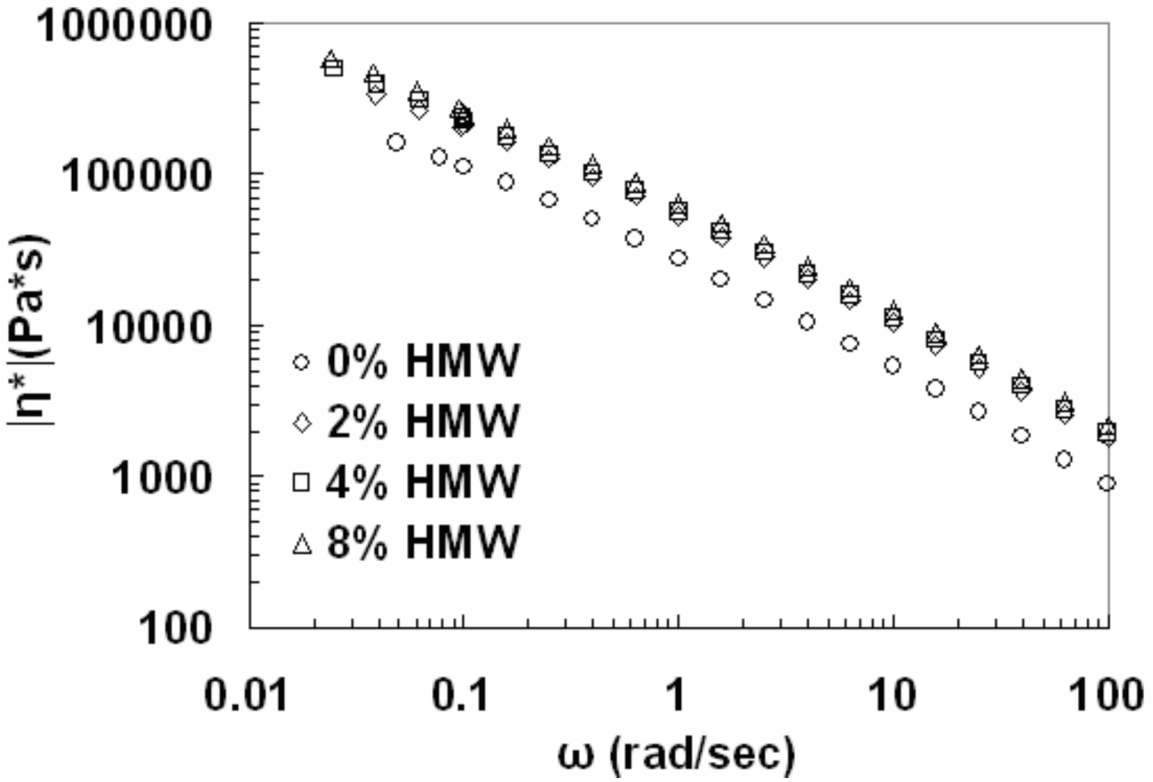

Figure C.9. Complex Viscosity Master Curve at T_{ref} = 190°C for HMW Matrix and Nanocomposites.

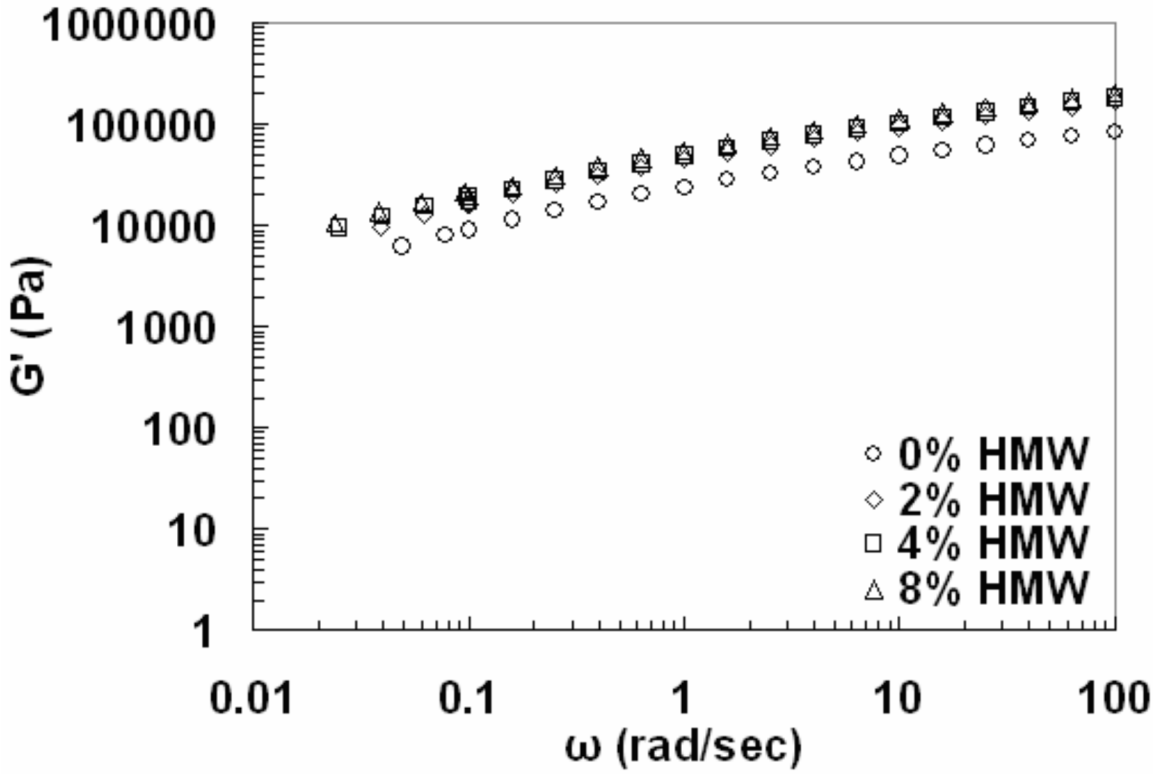

Figure C.10. Storage Modulus Master Curve at T_{ref} = 190°C for HMW Matrix and Nanocomposites.

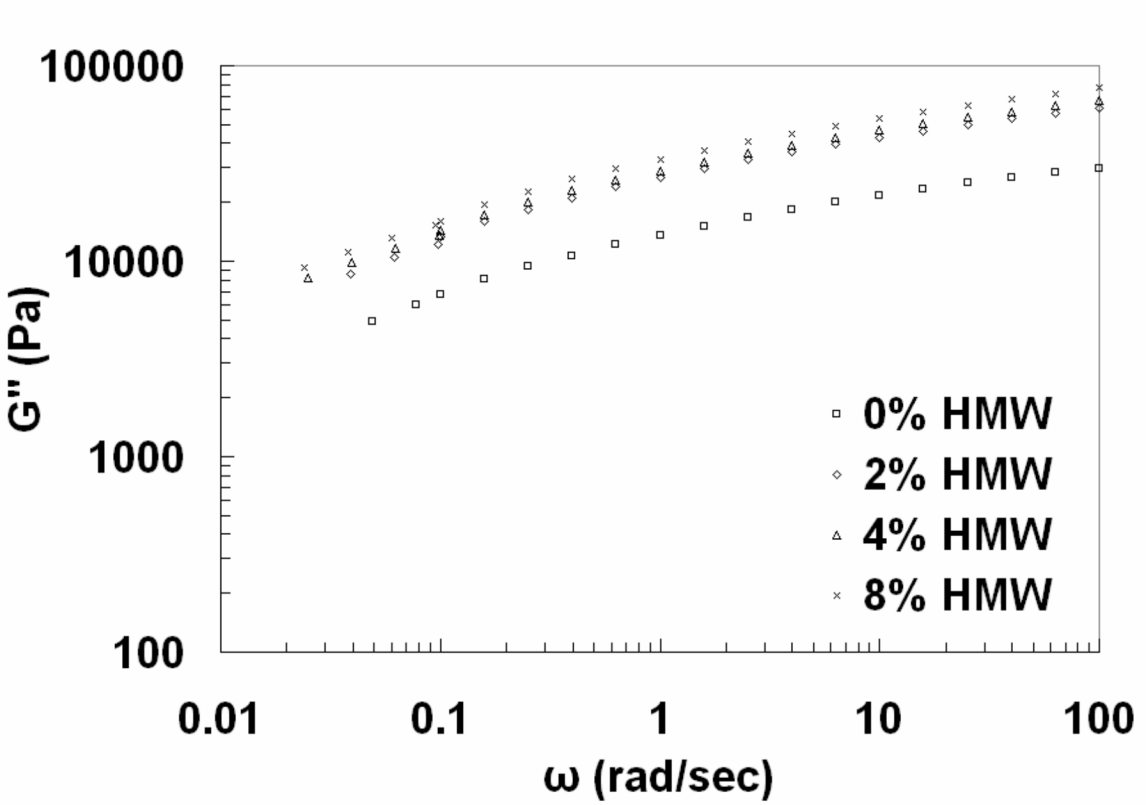

Figure C.11. Loss Modulus Master Curve at T_{ref} = 190°C for HMW Matrix and Nanocomposites.

Table C.3. Dynamic Rheology Data at 190°C and 230°C for 0% LMW.

0% LMW @ 190°C				230°C				a_t=	4.70E-01
w (rad/sec)	G'(Pa)	G"(Pa)	$\|h^*\|$ (Pa*s)	w (rad/sec)	G'(Pa)	G"(Pa)	$\|h^*\|$ (Pa*s)	$w * a_t$	$\|h^*\|/a_t$
0.100	1.21E+01	1.82E+02	1.83E+03	0.100	8.19E+00	7.87E+01	7.91E+02	0.047	1.68E+03
0.158	1.36E+01	2.80E+02	1.77E+03	0.158	7.78E+00	1.34E+02	8.48E+02	0.074	1.80E+03
0.251	3.31E+01	4.55E+02	1.82E+03	0.251	1.23E+01	2.12E+02	8.46E+02	0.118	1.80E+03
0.398	6.45E+01	7.01E+02	1.77E+03	0.398	2.38E+01	3.32E+02	8.35E+02	0.187	1.78E+03
0.631	1.13E+02	1.09E+03	1.73E+03	0.631	4.04E+01	5.20E+02	8.27E+02	0.297	1.76E+03
1.000	2.20E+02	1.66E+03	1.68E+03	1.000	7.87E+01	8.06E+02	8.10E+02	0.470	1.72E+03
1.585	3.95E+02	2.52E+03	1.61E+03	1.585	1.46E+02	1.24E+03	7.90E+02	0.745	1.68E+03
2.512	7.07E+02	3.79E+03	1.54E+03	2.512	2.72E+02	1.91E+03	7.68E+02	1.181	1.63E+03
3.981	1.25E+03	5.65E+03	1.45E+03	3.981	4.90E+02	2.89E+03	7.36E+02	1.871	1.57E+03
6.310	2.17E+03	8.33E+03	1.36E+03	6.310	8.79E+02	4.31E+03	6.97E+02	2.966	1.48E+03
10.001	3.69E+03	1.21E+04	1.27E+03	10.001	1.57E+03	6.41E+03	6.60E+02	4.700	1.40E+03
15.850	6.12E+03	1.73E+04	1.16E+03	15.850	2.69E+03	9.34E+03	6.13E+02	7.450	1.30E+03
25.121	9.92E+03	2.43E+04	1.04E+03	25.121	4.54E+03	1.34E+04	5.63E+02	11.807	1.20E+03
39.813	1.57E+04	3.34E+04	9.26E+02	39.813	7.44E+03	1.89E+04	5.10E+02	18.712	1.09E+03
63.101	2.42E+04	4.48E+04	8.07E+02	63.101	1.19E+04	2.61E+04	4.54E+02	29.657	9.66E+02
100.000	3.62E+04	5.88E+04	6.90E+02	100.000	1.84E+04	3.51E+04	3.97E+02	47.000	8.44E+02

Table C.4. Dynamic Rheology Data at 190°C and 230°C for 2% LMW

2% LMW @ 190°C				230°C				a_t=	5.80E-01
w (rad/sec)	G'(Pa)	G"(Pa)	$\|h^*\|$ (Pa*s)	w (rad/sec)	G'(Pa)	G"(Pa)	$\|h^*\|$ (Pa*s)	$w * a_t$	$\|h^*\|/a_t$
0.100	1.30E+01	1.93E+02	1.94E+03	0.100	-1.79E+00	1.13E+02	1.13E+03	0.056	2.02E+03
0.158	1.67E+01	3.03E+02	1.92E+03	0.158	7.58E+00	1.79E+02	1.13E+03	0.089	2.02E+03
0.251	3.20E+01	4.76E+02	1.90E+03	0.251	1.41E+01	2.68E+02	1.07E+03	0.141	1.91E+03
0.398	5.68E+01	7.45E+02	1.88E+03	0.398	2.50E+01	4.27E+02	1.08E+03	0.223	1.92E+03
0.631	1.11E+02	1.16E+03	1.84E+03	0.631	6.00E+01	6.65E+02	1.06E+03	0.353	1.89E+03
1.000	2.04E+02	1.78E+03	1.79E+03	1.000	1.01E+02	1.03E+03	1.04E+03	0.560	1.85E+03
1.585	3.81E+02	2.72E+03	1.73E+03	1.585	1.91E+02	1.58E+03	1.01E+03	0.888	1.80E+03
2.512	7.05E+02	4.11E+03	1.66E+03	2.512	3.50E+02	2.40E+03	9.67E+02	1.407	1.73E+03
3.981	1.26E+03	6.16E+03	1.58E+03	3.981	6.37E+02	3.66E+03	9.33E+02	2.230	1.67E+03
6.310	2.23E+03	9.14E+03	1.49E+03	6.310	1.15E+03	5.48E+03	8.87E+02	3.534	1.58E+03
10.001	3.86E+03	1.33E+04	1.39E+03	10.001	2.00E+03	8.10E+03	8.34E+02	5.601	1.49E+03
15.850	6.52E+03	1.91E+04	1.27E+03	15.850	3.44E+03	1.18E+04	7.76E+02	8.876	1.39E+03
25.121	1.07E+04	2.69E+04	1.15E+03	25.121	5.77E+03	1.69E+04	7.12E+02	14.068	1.27E+03
39.813	1.72E+04	3.70E+04	1.02E+03	39.813	9.42E+03	2.38E+04	6.43E+02	22.295	1.15E+03
63.101	2.66E+04	4.98E+04	8.95E+02	63.101	1.50E+04	3.28E+04	5.72E+02	35.337	1.02E+03
100.000	4.00E+04	6.52E+04	7.65E+02	100.000	2.32E+04	4.41E+04	4.99E+02	56.000	8.91E+02

Table C.5. Dynamic Rheology Data at 190°C and 230°C for 4% LMW

4% LMW @ 190°C				230°C				at=	4.40E-01
w (rad/sec)	G'(Pa)	G"(Pa)	$\|h^*\|$ (Pa*s)	w (rad/sec)	G'(Pa)	G"(Pa)	$\|h^*\|$ (Pa*s)	$w * a_t$	$\|h^*\|/a_t$
0.100	1.63E+01	2.26E+02	2.26E+03	0.100	7.95E+00	1.02E+02	1.03E+03	0.044	2.33E+03
0.158	2.46E+01	3.45E+02	2.18E+03	0.158	6.97E+00	1.56E+02	9.86E+02	0.070	2.24E+03
0.251	4.30E+01	5.50E+02	2.20E+03	0.251	1.59E+01	2.50E+02	9.97E+02	0.111	2.27E+03
0.398	6.99E+01	8.57E+02	2.16E+03	0.398	3.39E+01	3.88E+02	9.80E+02	0.175	2.23E+03
0.631	1.28E+02	1.32E+03	2.10E+03	0.631	4.91E+01	6.00E+02	9.55E+02	0.278	2.17E+03
1.000	2.37E+02	2.03E+03	2.05E+03	1.000	9.34E+01	9.42E+02	9.46E+02	0.440	2.15E+03
1.585	4.39E+02	3.11E+03	1.98E+03	1.585	1.71E+02	1.45E+03	9.18E+02	0.697	2.09E+03
2.512	7.96E+02	4.71E+03	1.90E+03	2.512	3.31E+02	2.21E+03	8.88E+02	1.105	2.02E+03
3.981	1.44E+03	7.05E+03	1.81E+03	3.981	5.65E+02	3.36E+03	8.55E+02	1.752	1.94E+03
6.310	2.55E+03	1.04E+04	1.70E+03	6.310	1.03E+03	5.03E+03	8.13E+02	2.776	1.85E+03
10.001	4.43E+03	1.52E+04	1.58E+03	10.001	1.80E+03	7.45E+03	7.67E+02	4.400	1.74E+03
15.850	7.45E+03	2.18E+04	1.45E+03	15.850	3.10E+03	1.09E+04	7.15E+02	6.974	1.63E+03
25.121	1.22E+04	3.06E+04	1.31E+03	25.121	5.24E+03	1.57E+04	6.57E+02	11.053	1.49E+03
39.813	1.95E+04	4.21E+04	1.17E+03	39.813	8.62E+03	2.21E+04	5.96E+02	17.518	1.35E+03
63.101	3.02E+04	5.66E+04	1.02E+03	63.101	1.38E+04	3.05E+04	5.30E+02	27.764	1.20E+03
100.000	4.52E+04	7.41E+04	8.68E+02	100.000	2.14E+04	4.10E+04	4.63E+02	44.000	1.05E+03

Table C.6. Dynamic Rheology Data at 190°C and 230°C for 8% LMW

8% LMW @ 190°C				230°C				at=	4.50E-01
w (rad/sec)	G'(Pa)	G"(Pa)	$\|h^*\|$ (Pa*s)	w (rad/sec)	G'(Pa)	G"(Pa)	$\|h^*\|$ (Pa*s)	$w * a_t$	$\|h^*\|/a_t$
0.100	3.87E+01	3.45E+02	3.47E+03	0.100	1.52E+01	1.61E+02	1.62E+03	0.047	3.44E+03
0.158	4.85E+01	5.12E+02	3.25E+03	0.158	2.09E+01	2.48E+02	1.57E+03	0.074	3.34E+03
0.251	8.79E+01	7.83E+02	3.14E+03	0.251	3.39E+01	3.78E+02	1.51E+03	0.118	3.21E+03
0.398	1.43E+02	1.19E+03	3.01E+03	0.398	5.62E+01	5.88E+02	1.48E+03	0.187	3.16E+03
0.631	2.37E+02	1.80E+03	2.87E+03	0.631	9.63E+01	9.06E+02	1.44E+03	0.297	3.07E+03
1.000	4.05E+02	2.71E+03	2.74E+03	1.000	1.65E+02	1.39E+03	1.40E+03	0.470	2.98E+03
1.585	7.03E+02	4.07E+03	2.60E+03	1.585	2.92E+02	2.12E+03	1.35E+03	0.745	2.87E+03
2.512	1.21E+03	6.05E+03	2.46E+03	2.512	5.28E+02	3.22E+03	1.30E+03	1.181	2.76E+03
3.981	2.09E+03	8.93E+03	2.30E+03	3.981	9.14E+02	4.84E+03	1.24E+03	1.871	2.63E+03
6.310	3.53E+03	1.30E+04	2.13E+03	6.310	1.60E+03	7.19E+03	1.17E+03	2.966	2.48E+03
10.001	5.89E+03	1.86E+04	1.95E+03	10.001	2.76E+03	1.06E+04	1.09E+03	4.700	2.32E+03
15.850	9.64E+03	2.63E+04	1.77E+03	15.850	4.66E+03	1.53E+04	1.01E+03	7.450	2.15E+03
25.121	1.54E+04	3.64E+04	1.58E+03	25.121	7.70E+03	2.18E+04	9.21E+02	11.807	1.96E+03
39.813	2.40E+04	4.95E+04	1.38E+03	39.813	1.25E+04	3.05E+04	8.28E+02	18.712	1.76E+03
63.101	3.64E+04	6.58E+04	1.19E+03	63.101	1.97E+04	4.17E+04	7.31E+02	29.657	1.56E+03
100.000	5.35E+04	8.52E+04	1.01E+03	100.000	3.01E+04	5.57E+04	6.33E+02	47.000	1.35E+03

Table C.7. Master Dynamic Rheology Data for LMW Matrix and Nanocomposites at T_{ref} = 190°C

Master Data0% LMW Tref=190°C				Master Data 2% LMW Tref=190°C			
w (rad/sec)	$\|h^*\|$ (Pa*s)	G' (Pa)	G" (Pa)	w (rad/sec)	$\|h^*\|$ (Pa*s)	G' (Pa)	G" (Pa)
0.047	1.68E+03	8.19E+00	7.87E+01	0.058	1.95E+03		1.13E+02
0.074	1.80E+03	7.78E+00	1.34E+02	0.092	1.95E+03	7.58E+00	1.79E+02
0.100	1.83E+03	1.21E+01	1.82E+02	0.100	1.94E+03	1.30E+01	1.93E+02
0.158	1.77E+03	1.36E+01	2.80E+02	0.158	1.92E+03	1.67E+01	3.03E+02
0.251	1.82E+03	3.31E+01	4.55E+02	0.251	1.90E+03	3.20E+01	4.76E+02
0.398	1.77E+03	6.45E+01	7.01E+02	0.398	1.88E+03	5.68E+01	7.45E+02
0.631	1.73E+03	1.13E+02	1.09E+03	0.631	1.84E+03	1.11E+02	1.16E+03
1.000	1.68E+03	2.20E+02	1.66E+03	1.000	1.79E+03	2.04E+02	1.78E+03
1.585	1.61E+03	3.95E+02	2.52E+03	1.585	1.73E+03	3.81E+02	2.72E+03
2.512	1.54E+03	7.07E+02	3.79E+03	2.512	1.66E+03	7.05E+02	4.11E+03
3.981	1.45E+03	1.25E+03	5.65E+03	3.981	1.58E+03	1.26E+03	6.16E+03
6.310	1.36E+03	2.17E+03	8.33E+03	6.310	1.49E+03	2.23E+03	9.14E+03
10.001	1.27E+03	3.69E+03	1.21E+04	10.001	1.39E+03	3.86E+03	1.33E+04
15.850	1.16E+03	6.12E+03	1.73E+04	15.850	1.27E+03	6.52E+03	1.91E+04
25.121	1.04E+03	9.92E+03	2.43E+04	25.121	1.15E+03	1.07E+04	2.69E+04
39.813	9.26E+02	1.57E+04	3.34E+04	39.813	1.02E+03	1.72E+04	3.70E+04
63.101	8.07E+02	2.42E+04	4.48E+04	63.101	8.95E+02	2.66E+04	4.98E+04
100.000	6.90E+02	3.62E+04	5.88E+04	100.000	7.65E+02	4.00E+04	6.52E+04
Master Data 4% LMW Tref=190°C				**Master Data 8% LMW Tref=190°C**			
w (rad/sec)	$\|h^*\|$ (Pa*s)	G' (Pa)	G" (Pa)	w (rad/sec)	$\|h^*\|$ (Pa*s)	G' (Pa)	G" (Pa)
0.044	2.33E+03	7.95E+00	1.02E+02	0.045	3.59E+03	1.52E+01	1.61E+02
0.070	2.24E+03	6.97E+00	1.56E+02	0.071	3.49E+03	2.09E+01	2.48E+02
0.100	2.26E+03	1.63E+01	2.26E+02	0.100	3.47E+03	3.87E+01	3.45E+02
0.158	2.18E+03	2.46E+01	3.45E+02	0.158	3.25E+03	4.85E+01	5.12E+02
0.251	2.20E+03	4.30E+01	5.50E+02	0.251	3.14E+03	8.79E+01	7.83E+02
0.398	2.16E+03	6.99E+01	8.57E+02	0.398	3.01E+03	1.43E+02	1.19E+03
0.631	2.10E+03	1.28E+02	1.32E+03	0.631	2.87E+03	2.37E+02	1.80E+03
1.000	2.05E+03	2.37E+02	2.03E+03	1.000	2.74E+03	4.05E+02	2.71E+03
1.585	1.98E+03	4.39E+02	3.11E+03	1.585	2.60E+03	7.03E+02	4.07E+03
2.512	1.90E+03	7.96E+02	4.71E+03	2.512	2.46E+03	1.21E+03	6.05E+03
3.981	1.81E+03	1.44E+03	7.05E+03	3.981	2.30E+03	2.09E+03	8.93E+03
6.310	1.70E+03	2.55E+03	1.04E+04	6.310	2.13E+03	3.53E+03	1.30E+04
10.001	1.58E+03	4.43E+03	1.52E+04	10.001	1.95E+03	5.89E+03	1.86E+04
15.850	1.45E+03	7.45E+03	2.18E+04	15.850	1.77E+03	9.64E+03	2.63E+04
25.121	1.31E+03	1.22E+04	3.06E+04	25.121	1.58E+03	1.54E+04	3.64E+04
39.813	1.17E+03	1.95E+04	4.21E+04	39.813	1.38E+03	2.40E+04	4.95E+04
63.101	1.02E+03	3.02E+04	5.66E+04	63.101	1.19E+03	3.64E+04	6.58E+04
100.000	8.68E+02	4.52E+04	7.41E+04	100.000	1.01E+03	5.35E+04	8.52E+04

Table C.8. Dynamic Rheology Data at 190°C and 230°C for 0% MMW.

0% MMW @ 190°C				230°C				a_t=	7.00E-01
w (rad/sec)	G'(Pa)	G"(Pa)	$\|h^*\|$ (Pa*s)	w (rad/sec)	G'(Pa)	G"(Pa)	$\|h^*\|$ (Pa*s)	$w * a_t$	$\|h^*\|/a_t$
0.100	6.24E+02	8.26E+02	1.04E+04	0.100	4.59E+02	6.22E+02	7.74E+03	0.070	1.11E+04
0.158	8.53E+02	1.13E+03	8.92E+03	0.158	6.45E+02	8.64E+02	6.80E+03	0.111	9.72E+03
0.251	1.15E+03	1.49E+03	7.50E+03	0.251	8.79E+02	1.16E+03	5.80E+03	0.176	8.29E+03
0.398	1.55E+03	1.94E+03	6.23E+03	0.398	1.20E+03	1.56E+03	4.94E+03	0.279	7.05E+03
0.631	2.06E+03	2.52E+03	5.15E+03	0.631	1.60E+03	2.04E+03	4.12E+03	0.442	5.88E+03
1.000	2.71E+03	3.22E+03	4.21E+03	1.000	2.14E+03	2.64E+03	3.40E+03	0.700	4.86E+03
1.585	3.57E+03	4.10E+03	3.43E+03	1.585	2.84E+03	3.39E+03	2.79E+03	1.110	3.99E+03
2.512	4.67E+03	5.18E+03	2.78E+03	2.512	3.74E+03	4.33E+03	2.28E+03	1.758	3.25E+03
3.981	6.08E+03	6.50E+03	2.24E+03	3.981	4.89E+03	5.47E+03	1.84E+03	2.787	2.63E+03
6.310	7.86E+03	8.08E+03	1.79E+03	6.310	6.39E+03	6.87E+03	1.49E+03	4.417	2.13E+03
10.001	1.01E+04	9.96E+03	1.42E+03	10.001	8.26E+03	8.56E+03	1.19E+03	7.001	1.70E+03
15.850	1.29E+04	1.22E+04	1.12E+03	15.850	1.07E+04	1.06E+04	9.47E+02	11.095	1.35E+03
25.121	1.64E+04	1.48E+04	8.78E+02	25.121	1.36E+04	1.29E+04	7.48E+02	17.585	1.07E+03
39.813	2.07E+04	1.78E+04	6.84E+02	39.813	1.73E+04	1.57E+04	5.86E+02	27.869	8.37E+02
63.101	2.58E+04	2.11E+04	5.28E+02	63.101	2.17E+04	1.88E+04	4.56E+02	44.171	6.51E+02
100.000	3.18E+04	2.47E+04	4.03E+02	100.000	2.71E+04	2.23E+04	3.51E+02	70.000	5.01E+02

Table C. 9. Dynamic Rheology Data at 190°C and 230°C for 2% MMW.

2% MMW @ 190°C				230°C				a_t=	4.50E-01
w (rad/sec)	G'(Pa)	G"(Pa)	$\|h^*\|$ (Pa*s)	w (rad/sec)	G'(Pa)	G"(Pa)	$\|h^*\|$ (Pa*s)	$w * a_t$	$\|h^*\|/a_t$
0.100	7.67E+02	1.12E+03	1.36E+04	0.100	4.60E+02	7.04E+02	8.41E+03	0.045	1.87E+04
0.158	1.07E+03	1.54E+03	1.18E+04	0.158	6.55E+02	9.56E+02	7.31E+03	0.071	1.62E+04
0.251	1.48E+03	2.06E+03	1.01E+04	0.251	8.97E+02	1.28E+03	6.22E+03	0.113	1.38E+04
0.398	2.02E+03	2.71E+03	8.49E+03	0.398	1.23E+03	1.70E+03	5.27E+03	0.179	1.17E+04
0.631	2.73E+03	3.54E+03	7.08E+03	0.631	1.66E+03	2.21E+03	4.38E+03	0.284	9.73E+03
1.000	3.66E+03	4.57E+03	5.86E+03	1.000	2.23E+03	2.87E+03	3.63E+03	0.450	8.08E+03
1.585	4.89E+03	5.84E+03	4.80E+03	1.585	2.98E+03	3.68E+03	2.99E+03	0.713	6.64E+03
2.512	6.45E+03	7.41E+03	3.91E+03	2.512	3.96E+03	4.70E+03	2.44E+03	1.130	5.43E+03
3.981	8.47E+03	9.32E+03	3.16E+03	3.981	5.21E+03	5.93E+03	1.98E+03	1.792	4.41E+03
6.310	1.10E+04	1.16E+04	2.54E+03	6.310	6.81E+03	7.46E+03	1.60E+03	2.840	3.56E+03
10.001	1.43E+04	1.44E+04	2.03E+03	10.001	8.84E+03	9.29E+03	1.28E+03	4.500	2.85E+03
15.850	1.84E+04	1.76E+04	1.61E+03	15.850	1.14E+04	1.15E+04	1.02E+03	7.133	2.27E+03
25.121	2.34E+04	2.14E+04	1.26E+03	25.121	1.46E+04	1.41E+04	8.09E+02	11.304	1.80E+03
39.813	2.96E+04	2.57E+04	9.84E+02	39.813	1.86E+04	1.72E+04	6.36E+02	17.916	1.41E+03
63.101	3.70E+04	3.06E+04	7.61E+02	63.101	2.35E+04	2.07E+04	4.96E+02	28.395	1.10E+03
100.000	4.58E+04	3.59E+04	5.82E+02	100.000	2.94E+04	2.47E+04	3.84E+02	45.000	8.52E+02

Table C.10. Dynamic Rheology Data at 190°C and 230°C for 4% MMW.

4% MMW @ 190°C				230°C				a_t=	5.00E-01
w (rad/sec)	G'(Pa)	G"(Pa)	$\|h^*\|$ (Pa*s)	w (rad/sec)	G'(Pa)	G"(Pa)	$\|h^*\|$ (Pa*s)	$w * a_t$	$\|h^*\|/a_t$
0.100	1.12E+03	1.62E+03	1.97E+04	0.100	6.99E+02	1.05E+03	1.26E+04	0.050	2.52E+04
0.158	1.53E+03	2.15E+03	1.67E+04	0.158	9.57E+02	1.42E+03	1.08E+04	0.079	2.16E+04
0.251	2.08E+03	2.84E+03	1.40E+04	0.251	1.31E+03	1.87E+03	9.09E+03	0.126	1.82E+04
0.398	2.82E+03	3.69E+03	1.17E+04	0.398	1.77E+03	2.46E+03	7.62E+03	0.199	1.52E+04
0.631	3.77E+03	4.77E+03	9.63E+03	0.631	2.40E+03	3.22E+03	6.36E+03	0.315	1.27E+04
1.000	5.02E+03	6.10E+03	7.90E+03	1.000	3.22E+03	4.16E+03	5.27E+03	0.500	1.05E+04
1.585	6.64E+03	7.75E+03	6.44E+03	1.585	4.31E+03	5.34E+03	4.33E+03	0.793	8.66E+03
2.512	8.71E+03	9.77E+03	5.21E+03	2.512	5.72E+03	6.81E+03	3.54E+03	1.256	7.08E+03
3.981	1.14E+04	1.22E+04	4.20E+03	3.981	7.53E+03	8.61E+03	2.87E+03	1.991	5.75E+03
6.310	1.47E+04	1.52E+04	3.36E+03	6.310	9.87E+03	1.08E+04	2.32E+03	3.155	4.64E+03
10.001	1.90E+04	1.87E+04	2.67E+03	10.001	1.28E+04	1.35E+04	1.86E+03	5.001	3.72E+03
15.850	2.43E+04	2.29E+04	2.10E+03	15.850	1.66E+04	1.67E+04	1.48E+03	7.925	2.97E+03
25.121	3.08E+04	2.77E+04	1.65E+03	25.121	2.13E+04	2.04E+04	1.17E+03	12.561	2.35E+03
39.813	3.87E+04	3.33E+04	1.28E+03	39.813	2.71E+04	2.48E+04	9.23E+02	19.907	1.85E+03
63.101	4.83E+04	3.96E+04	9.90E+02	63.101	3.42E+04	2.99E+04	7.19E+02	31.551	1.44E+03
100.000	5.96E+04	4.66E+04	7.57E+02	100.000	4.27E+04	3.55E+04	5.55E+02	50.000	1.11E+03

Table C.11. Dynamic Rheology Data at 190°C and 230°C for 8% MMW.

8% MMW @ 190°C				230°C				a_t=	4.40E-01
w (rad/sec)	G'(Pa)	G"(Pa)	$\|h^*\|$ (Pa*s)	w (rad/sec)	G'(Pa)	G"(Pa)	$\|h^*\|$ (Pa*s)	$w * a_t$	$\|h^*\|/a_t$
0.100	1.42E+03	1.93E+03	2.39E+04	0.100	8.26E+02	1.15E+03	1.42E+04	0.044	3.22E+04
0.158	1.90E+03	2.55E+03	2.00E+04	0.158	1.14E+03	1.57E+03	1.22E+04	0.070	2.78E+04
0.251	2.54E+03	3.32E+03	1.67E+04	0.251	1.56E+03	2.07E+03	1.03E+04	0.111	2.34E+04
0.398	3.38E+03	4.32E+03	1.38E+04	0.398	2.09E+03	2.70E+03	8.58E+03	0.175	1.95E+04
0.631	4.50E+03	5.56E+03	1.13E+04	0.631	2.79E+03	3.51E+03	7.10E+03	0.278	1.61E+04
1.000	5.94E+03	7.10E+03	9.26E+03	1.000	3.71E+03	4.50E+03	5.83E+03	0.440	1.33E+04
1.585	7.81E+03	9.02E+03	7.53E+03	1.585	4.88E+03	5.73E+03	4.75E+03	0.697	1.08E+04
2.512	1.02E+04	1.14E+04	6.08E+03	2.512	6.39E+03	7.24E+03	3.84E+03	1.105	8.74E+03
3.981	1.33E+04	1.42E+04	4.88E+03	3.981	8.33E+03	9.07E+03	3.09E+03	1.752	7.03E+03
6.310	1.71E+04	1.76E+04	3.90E+03	6.310	1.08E+04	1.13E+04	2.47E+03	2.776	5.62E+03
10.001	2.20E+04	2.17E+04	3.09E+03	10.001	1.39E+04	1.39E+04	1.96E+03	4.400	4.46E+03
15.850	2.81E+04	2.65E+04	2.44E+03	15.850	1.77E+04	1.70E+04	1.55E+03	6.974	3.52E+03
25.121	3.55E+04	3.21E+04	1.91E+03	25.121	2.25E+04	2.07E+04	1.21E+03	11.053	2.76E+03
39.813	4.47E+04	3.85E+04	1.48E+03	39.813	2.83E+04	2.49E+04	9.46E+02	17.518	2.15E+03
63.101	5.57E+04	4.58E+04	1.14E+03	63.101	3.53E+04	2.96E+04	7.31E+02	27.764	1.66E+03
100.000	6.87E+04	5.37E+04	8.72E+02	100.000	4.36E+04	3.48E+04	5.58E+02	44.000	1.27E+03

Table C.12. Master Dynamic Rheology Data for MMW Matrix and Nanocomposites at T_{ref} = 190°C

Master Data 0% MMW, Tref=190°C				**Master Data 2% MMW,Tref=190°C**			
w (rad/sec)	**$\|h^*\|$ (Pa*s)**	**G' (Pa)**	**G" (Pa)**	**w (rad/sec)**	**$\|h^*\|$ (Pa*s)**	**G' (Pa)**	**G" (Pa)**
0.070	1.11E+04	4.59E+02	6.22E+02	0.045	1.87E+04	4.60E+02	7.04E+02
0.100	1.04E+04	6.24E+02	8.26E+02	0.071	1.62E+04	6.55E+02	9.56E+02
0.158	8.92E+03	8.53E+02	1.13E+03	0.100	1.36E+04	7.67E+02	1.12E+03
0.251	7.50E+03	1.15E+03	1.49E+03	0.158	1.18E+04	1.07E+03	1.54E+03
0.398	6.23E+03	1.55E+03	1.94E+03	0.251	1.01E+04	1.48E+03	2.06E+03
0.631	5.15E+03	2.06E+03	2.52E+03	0.398	8.49E+03	2.02E+03	2.71E+03
1.000	4.21E+03	2.71E+03	3.22E+03	0.631	7.08E+03	2.73E+03	3.54E+03
1.585	3.43E+03	3.57E+03	4.10E+03	1.000	5.86E+03	3.66E+03	4.57E+03
2.512	2.78E+03	4.67E+03	5.18E+03	1.585	4.80E+03	4.89E+03	5.84E+03
3.981	2.24E+03	6.08E+03	6.50E+03	2.512	3.91E+03	6.45E+03	7.41E+03
6.310	1.79E+03	7.86E+03	8.08E+03	3.981	3.16E+03	8.47E+03	9.32E+03
10.001	1.42E+03	1.01E+04	9.96E+03	6.310	2.54E+03	1.10E+04	1.16E+04
15.850	1.12E+03	1.29E+04	1.22E+04	10.001	2.03E+03	1.43E+04	1.44E+04
25.121	8.78E+02	1.64E+04	1.48E+04	15.850	1.61E+03	1.84E+04	1.76E+04
39.813	6.84E+02	2.07E+04	1.78E+04	25.121	1.26E+03	2.34E+04	2.14E+04
63.101	5.28E+02	2.58E+04	2.11E+04	39.813	9.84E+02	2.96E+04	2.57E+04
100.000	4.03E+02	3.18E+04	2.47E+04	63.101	7.61E+02	3.70E+04	3.06E+04
				100.000	5.82E+02	4.58E+04	3.59E+04
Master Data 4% MMW, Tref=190°C				**Master Data 8% MMW, Tref=190°C**			
w (rad/sec)	**$\|h^*\|$ (Pa*s)**	**G' (Pa)**	**G" (Pa)**	**w (rad/sec)**	**$\|h^*\|$ (Pa*s)**	**G' (Pa)**	**G" (Pa)**
0.050	2.52E+04	6.99E+02	1.05E+03	0.044	3.22E+04	8.26E+02	1.15E+03
0.079	2.16E+04	9.57E+02	1.42E+03	0.070	2.78E+04	1.14E+03	1.57E+03
0.100	1.97E+04	1.12E+03	1.62E+03	0.100	2.39E+04	1.42E+03	1.93E+03
0.158	1.67E+04	1.53E+03	2.15E+03	0.158	2.00E+04	1.90E+03	2.55E+03
0.251	1.40E+04	2.08E+03	2.84E+03	0.251	1.67E+04	2.54E+03	3.32E+03
0.398	1.17E+04	2.82E+03	3.69E+03	0.398	1.38E+04	3.38E+03	4.32E+03
0.631	9.63E+03	3.77E+03	4.77E+03	0.631	1.13E+04	4.50E+03	5.56E+03
1.000	7.90E+03	5.02E+03	6.10E+03	1.000	9.26E+03	5.94E+03	7.10E+03
1.585	6.44E+03	6.64E+03	7.75E+03	1.585	7.53E+03	7.81E+03	9.02E+03
2.512	5.21E+03	8.71E+03	9.77E+03	2.512	6.08E+03	1.02E+04	1.14E+04
3.981	4.20E+03	1.14E+04	1.22E+04	3.981	4.88E+03	1.33E+04	1.42E+04
6.310	3.36E+03	1.47E+04	1.52E+04	6.310	3.90E+03	1.71E+04	1.76E+04
10.001	2.67E+03	1.90E+04	1.87E+04	10.001	3.09E+03	2.20E+04	2.17E+04
15.850	2.10E+03	2.43E+04	2.29E+04	15.850	2.44E+03	2.81E+04	2.65E+04
25.121	1.65E+03	3.08E+04	2.77E+04	25.121	1.91E+03	3.55E+04	3.21E+04
39.813	1.28E+03	3.87E+04	3.33E+04	39.813	1.48E+03	4.47E+04	3.85E+04
63.101	9.90E+02	4.83E+04	3.96E+04	63.101	1.14E+03	5.57E+04	4.58E+04
100.000	7.57E+02	5.96E+04	4.66E+04	100.000	8.72E+02	6.87E+04	5.37E+04

Table C. 13 Dynamic Rheology Data at 190°C and 230°C for 0% HMW.

0% HMW @ 190°C				230°C				at=	4.90E-01
w (rad/sec)	G'(Pa)	G"(Pa)	$\|h^*\|$ (Pa*s)	w (rad/sec)	G'(Pa)	G"(Pa)	$\|h^*\|$ (Pa*s)	$w * a_t$	$\|h^*\|/a_t$
0.100	9.02E+03	6.72E+03	1.12E+05	0.100	6.20E+03	4.89E+03	7.90E+04	0.049	1.61E+05
0.158	1.14E+04	8.04E+03	8.81E+04	0.158	8.03E+03	6.01E+03	6.33E+04	0.078	1.29E+05
0.251	1.41E+04	9.34E+03	6.73E+04	0.251	1.01E+04	7.12E+03	4.92E+04	0.123	1.00E+05
0.398	1.70E+04	1.07E+04	5.05E+04	0.398	1.24E+04	8.24E+03	3.73E+04	0.195	7.61E+04
0.631	2.03E+04	1.21E+04	3.75E+04	0.631	1.49E+04	9.42E+03	2.79E+04	0.309	5.70E+04
1.000	2.40E+04	1.36E+04	2.76E+04	1.000	1.77E+04	1.07E+04	2.07E+04	0.490	4.22E+04
1.585	2.81E+04	1.51E+04	2.01E+04	1.585	2.09E+04	1.19E+04	1.52E+04	0.777	3.10E+04
2.512	3.26E+04	1.67E+04	1.46E+04	2.512	2.45E+04	1.33E+04	1.11E+04	1.231	2.26E+04
3.981	3.75E+04	1.83E+04	1.05E+04	3.981	2.85E+04	1.47E+04	8.05E+03	1.951	1.64E+04
6.310	4.29E+04	1.99E+04	7.50E+03	6.310	3.28E+04	1.62E+04	5.80E+03	3.092	1.18E+04
10.001	4.88E+04	2.17E+04	5.34E+03	10.001	3.76E+04	1.77E+04	4.16E+03	4.900	8.48E+03
15.850	5.52E+04	2.34E+04	3.78E+03	15.850	4.28E+04	1.93E+04	2.96E+03	7.767	6.04E+03
25.121	6.19E+04	2.51E+04	2.66E+03	25.121	4.84E+04	2.08E+04	2.10E+03	12.309	4.28E+03
39.813	6.91E+04	2.68E+04	1.86E+03	39.813	5.44E+04	2.24E+04	1.48E+03	19.508	3.01E+03
63.101	7.67E+04	2.85E+04	1.30E+03	63.101	6.08E+04	2.40E+04	1.04E+03	30.919	2.11E+03
100.000	8.43E+04	2.99E+04	8.95E+02	100.000	6.73E+04	2.53E+04	7.19E+02	49.000	1.47E+03

Table C.14. Dynamic Rheology Data at 190°C and 230°C for 2% HMW.

2% HMW @ 190°C				230°C				at=	3.90E-01
w (rad/sec)	G'(Pa)	G"(Pa)	$\|h^*\|$ (Pa*s)	w (rad/sec)	G'(Pa)	G"(Pa)	$\|h^*\|$ (Pa*s)	$w * a_t$	$\|h^*\|/a_t$
0.100	1.63E+04	1.34E+04	2.11E+05	0.100	9.83E+03	8.61E+03	1.31E+05	0.039	3.35E+05
0.158	2.08E+04	1.59E+04	1.65E+05	0.158	1.28E+04	1.04E+04	1.04E+05	0.062	2.67E+05
0.251	2.58E+04	1.85E+04	1.26E+05	0.251	1.61E+04	1.22E+04	8.06E+04	0.098	2.07E+05
0.398	3.16E+04	2.12E+04	9.54E+04	0.398	1.99E+04	1.42E+04	6.14E+04	0.155	1.57E+05
0.631	3.81E+04	2.40E+04	7.13E+04	0.631	2.43E+04	1.62E+04	4.63E+04	0.246	1.19E+05
1.000	4.54E+04	2.68E+04	5.27E+04	1.000	2.92E+04	1.84E+04	3.45E+04	0.390	8.84E+04
1.585	5.35E+04	2.98E+04	3.86E+04	1.585	3.48E+04	2.06E+04	2.55E+04	0.618	6.54E+04
2.512	6.24E+04	3.29E+04	2.81E+04	2.512	4.10E+04	2.29E+04	1.87E+04	0.980	4.79E+04
3.981	7.23E+04	3.62E+04	2.03E+04	3.981	4.79E+04	2.54E+04	1.36E+04	1.553	3.49E+04
6.310	8.31E+04	3.95E+04	1.46E+04	6.310	5.55E+04	2.79E+04	9.84E+03	2.461	2.52E+04
10.001	9.49E+04	4.29E+04	1.04E+04	10.001	6.38E+04	3.06E+04	7.08E+03	3.900	1.81E+04
15.850	1.08E+05	4.64E+04	7.40E+03	15.850	7.29E+04	3.33E+04	5.06E+03	6.182	1.30E+04
25.121	1.21E+05	5.00E+04	5.23E+03	25.121	8.28E+04	3.61E+04	3.60E+03	9.797	9.22E+03
39.813	1.36E+05	5.36E+04	3.68E+03	39.813	9.35E+04	3.90E+04	2.55E+03	15.527	6.53E+03
63.101	1.52E+05	5.73E+04	2.57E+03	63.101	1.05E+05	4.19E+04	1.79E+03	24.609	4.59E+03
100.000	1.68E+05	6.08E+04	1.79E+03	100.000	1.17E+05	4.46E+04	1.25E+03	39.000	3.21E+03

Table C.15. Dynamic Rheology Data at 190°C and 230°C for 4% HMW.

4% HMW @ 190°C				230°C				at=	2.50E-01
w (rad/sec)	G'(Pa)	G"(Pa)	$\|h^*\|$ (Pa*s)	w (rad/sec)	G'(Pa)	G"(Pa)	$\|h^*\|$ (Pa*s)	$w * a_t$	$\|h^*\|/a_t$
0.100	1.75E+04	1.45E+04	2.27E+05	0.100	9.44E+03	8.18E+03	1.25E+05	0.025	5.00E+05
0.158	2.23E+04	1.72E+04	1.78E+05	0.158	1.23E+04	9.87E+03	9.94E+04	0.040	3.98E+05
0.251	2.78E+04	2.00E+04	1.36E+05	0.251	1.55E+04	1.16E+04	7.71E+04	0.063	3.09E+05
0.398	3.39E+04	2.29E+04	1.03E+05	0.398	1.91E+04	1.34E+04	5.87E+04	0.100	2.35E+05
0.631	4.10E+04	2.59E+04	7.69E+04	0.631	2.33E+04	1.54E+04	4.42E+04	0.158	1.77E+05
1.000	4.89E+04	2.90E+04	5.68E+04	1.000	2.79E+04	1.74E+04	3.29E+04	0.250	1.31E+05
1.585	5.77E+04	3.22E+04	4.17E+04	1.585	3.31E+04	1.95E+04	2.42E+04	0.396	9.69E+04
2.512	6.73E+04	3.57E+04	3.03E+04	2.512	3.89E+04	2.17E+04	1.77E+04	0.628	7.09E+04
3.981	7.80E+04	3.92E+04	2.19E+04	3.981	4.54E+04	2.40E+04	1.29E+04	0.995	5.16E+04
6.310	8.97E+04	4.28E+04	1.57E+04	6.310	5.25E+04	2.64E+04	9.31E+03	1.578	3.72E+04
10.001	1.02E+05	4.65E+04	1.12E+04	10.001	6.03E+04	2.89E+04	6.68E+03	2.500	2.67E+04
15.850	1.16E+05	5.03E+04	7.99E+03	15.850	6.88E+04	3.14E+04	4.77E+03	3.963	1.91E+04
25.121	1.31E+05	5.43E+04	5.65E+03	25.121	7.80E+04	3.40E+04	3.39E+03	6.280	1.36E+04
39.813	1.47E+05	5.83E+04	3.97E+03	39.813	8.80E+04	3.68E+04	2.40E+03	9.953	9.58E+03
63.101	1.64E+05	6.25E+04	2.78E+03	63.101	9.87E+04	3.94E+04	1.68E+03	15.775	6.73E+03
100.000	1.81E+05	6.64E+04	1.93E+03	100.000	1.10E+05	4.20E+04	1.18E+03	25.000	4.70E+03

Table C.16. Dynamic Rheology Data at 190°C and 230°C for 8% HMW.

8% HMW @ 190°C				230°C				at=	2.40E-01
w (rad/sec)	G'(Pa)	G"(Pa)	$\|h^*\|$ (Pa*s)	w (rad/sec)	G'(Pa)	G"(Pa)	$\|h^*\|$ (Pa*s)	$w * a_t$	$\|h^*\|/a_t$
0.100	1.93E+04	1.61E+04	2.51E+05	0.100	1.06E+04	9.26E+03	1.41E+05	0.020	7.05E+05
0.158	2.50E+04	1.95E+04	2.00E+05	0.158	1.37E+04	1.12E+04	1.11E+05	0.032	5.57E+05
0.251	3.14E+04	2.27E+04	1.54E+05	0.251	1.72E+04	1.32E+04	8.62E+04	0.050	4.31E+05
0.398	3.84E+04	2.62E+04	1.17E+05	0.398	2.13E+04	1.52E+04	6.57E+04	0.080	3.28E+05
0.631	4.64E+04	2.97E+04	8.74E+04	0.631	2.58E+04	1.74E+04	4.94E+04	0.126	2.47E+05
1.000	5.52E+04	3.33E+04	6.45E+04	1.000	3.10E+04	1.97E+04	3.68E+04	0.200	1.84E+05
1.585	6.51E+04	3.71E+04	4.72E+04	1.585	3.69E+04	2.21E+04	2.71E+04	0.317	1.36E+05
2.512	7.59E+04	4.10E+04	3.43E+04	2.512	4.33E+04	2.46E+04	1.98E+04	0.502	9.91E+04
3.981	8.78E+04	4.51E+04	2.48E+04	3.981	5.05E+04	2.72E+04	1.44E+04	0.796	7.21E+04
6.310	1.01E+05	4.93E+04	1.78E+04	6.310	5.84E+04	3.00E+04	1.04E+04	1.262	5.20E+04
10.001	1.15E+05	5.37E+04	1.27E+04	10.001	6.71E+04	3.28E+04	7.47E+03	2.000	3.73E+04
15.850	1.30E+05	5.82E+04	9.01E+03	15.850	7.66E+04	3.57E+04	5.33E+03	3.170	2.67E+04
25.121	1.47E+05	6.28E+04	6.36E+03	25.121	8.68E+04	3.87E+04	3.78E+03	5.024	1.89E+04
39.813	1.65E+05	6.75E+04	4.47E+03	39.813	9.79E+04	4.18E+04	2.67E+03	7.963	1.34E+04
63.101	1.84E+05	7.22E+04	3.13E+03	63.101	1.10E+05	4.49E+04	1.88E+03	12.620	9.40E+03
100.000	2.03E+05	7.68E+04	2.17E+03	100.000	1.22E+05	4.78E+04	1.31E+03	20.000	6.56E+03

Table C.17. Master Dynamic Rheology Data for HMW Matrix and Nanocomposites at T_{ref} = 190°C

Master Data 0% HMW, Tref=190°C				**Master Data 2% HMW, Tref=190°C**			
w (rad/sec)	**$\|h^*\|$ (Pa*s)**	**G' (Pa)**	**G" (Pa)**	**w (rad/sec)**	**$\|h^*\|$ (Pa*s)**	**G' (Pa)**	**G" (Pa)**
0.049	1.61E+05	6.20E+03	4.89E+03	0.039	3.35E+05	9.83E+03	8.61E+03
0.078	1.29E+05	8.03E+03	6.01E+03	0.062	2.67E+05	1.28E+04	1.04E+04
0.100	1.12E+05	9.02E+03	6.72E+03	0.098	2.07E+05	1.61E+04	1.22E+04
0.158	8.81E+04	1.14E+04	8.04E+03	0.100	2.11E+05	1.63E+04	1.34E+04
0.251	6.73E+04	1.41E+04	9.34E+03	0.158	1.65E+05	2.08E+04	1.59E+04
0.398	5.05E+04	1.70E+04	1.07E+04	0.251	1.26E+05	2.58E+04	1.85E+04
0.631	3.75E+04	2.03E+04	1.21E+04	0.398	9.54E+04	3.16E+04	2.12E+04
1.000	2.76E+04	2.40E+04	1.36E+04	0.631	7.13E+04	3.81E+04	2.40E+04
1.585	2.01E+04	2.81E+04	1.51E+04	1.000	5.27E+04	4.54E+04	2.68E+04
2.512	1.46E+04	3.26E+04	1.67E+04	1.585	3.86E+04	5.35E+04	2.98E+04
3.981	1.05E+04	3.75E+04	1.83E+04	2.512	2.81E+04	6.24E+04	3.29E+04
6.310	7.50E+03	4.29E+04	1.99E+04	3.981	2.03E+04	7.23E+04	3.62E+04
10.001	5.34E+03	4.88E+04	2.17E+04	6.310	1.46E+04	8.31E+04	3.95E+04
15.850	3.78E+03	5.52E+04	2.34E+04	10.001	1.04E+04	9.49E+04	4.29E+04
25.121	2.66E+03	6.19E+04	2.51E+04	15.850	7.40E+03	1.08E+05	4.64E+04
39.813	1.86E+03	6.91E+04	2.68E+04	25.121	5.23E+03	1.21E+05	5.00E+04
63.101	1.30E+03	7.67E+04	2.85E+04	39.813	3.68E+03	1.36E+05	5.36E+04
100.000	8.95E+02	8.43E+04	2.99E+04	63.101	2.57E+03	1.52E+05	5.73E+04
				100.000	1.79E+03	1.68E+05	6.08E+04
Master Data 4% HMW, Tref=190°C				**Master Data 8% HMW, Tref=190°C**			
w (rad/sec)	**$\|h^*\|$ (Pa*s)**	**G' (Pa)**	**G" (Pa)**	**w (rad/sec)**	**$\|h^*\|$ (Pa*s)**	**G' (Pa)**	**G" (Pa)**
0.025	5.00E+05	9.44E+03	8.18E+03	0.024	5.87E+05	1.06E+04	9.26E+03
0.040	3.98E+05	1.23E+04	9.87E+03	0.038	4.64E+05	1.37E+04	1.12E+04
0.063	3.09E+05	1.55E+04	1.16E+04	0.060	3.59E+05	1.72E+04	1.32E+04
0.100	2.35E+05	1.91E+04	1.34E+04	0.096	2.74E+05	2.13E+04	1.52E+04
0.100	2.27E+05	1.75E+04	1.45E+04	0.100	2.51E+05	1.93E+04	1.61E+04
0.158	1.78E+05	2.23E+04	1.72E+04	0.158	2.00E+05	2.50E+04	1.95E+04
0.251	1.36E+05	2.78E+04	2.00E+04	0.251	1.54E+05	3.14E+04	2.27E+04
0.398	1.03E+05	3.39E+04	2.29E+04	0.398	1.17E+05	3.84E+04	2.62E+04
0.631	7.69E+04	4.10E+04	2.59E+04	0.631	8.74E+04	4.64E+04	2.97E+04
1.000	5.68E+04	4.89E+04	2.90E+04	1.000	6.45E+04	5.52E+04	3.33E+04
1.585	4.17E+04	5.77E+04	3.22E+04	1.585	4.72E+04	6.51E+04	3.71E+04
2.512	3.03E+04	6.73E+04	3.57E+04	2.512	3.43E+04	7.59E+04	4.10E+04
3.981	2.19E+04	7.80E+04	3.92E+04	3.981	2.48E+04	8.78E+04	4.51E+04
6.310	1.57E+04	8.97E+04	4.28E+04	6.310	1.78E+04	1.01E+05	4.93E+04
10.001	1.12E+04	1.02E+05	4.65E+04	10.001	1.27E+04	1.15E+05	5.37E+04
15.850	7.99E+03	1.16E+05	5.03E+04	15.850	9.01E+03	1.30E+05	5.82E+04
25.121	5.65E+03	1.31E+05	5.43E+04	25.121	6.36E+03	1.47E+05	6.28E+04
39.813	3.97E+03	1.47E+05	5.83E+04	39.813	4.47E+03	1.65E+05	6.75E+04
63.101	2.78E+03	1.64E+05	6.25E+04	63.101	3.13E+03	1.84E+05	7.22E+04
100.000	1.93E+03	1.81E+05	6.64E+04	100.000	2.17E+03	2.03E+05	7.68E+04

Appendix D. Capillary Rheometry Data

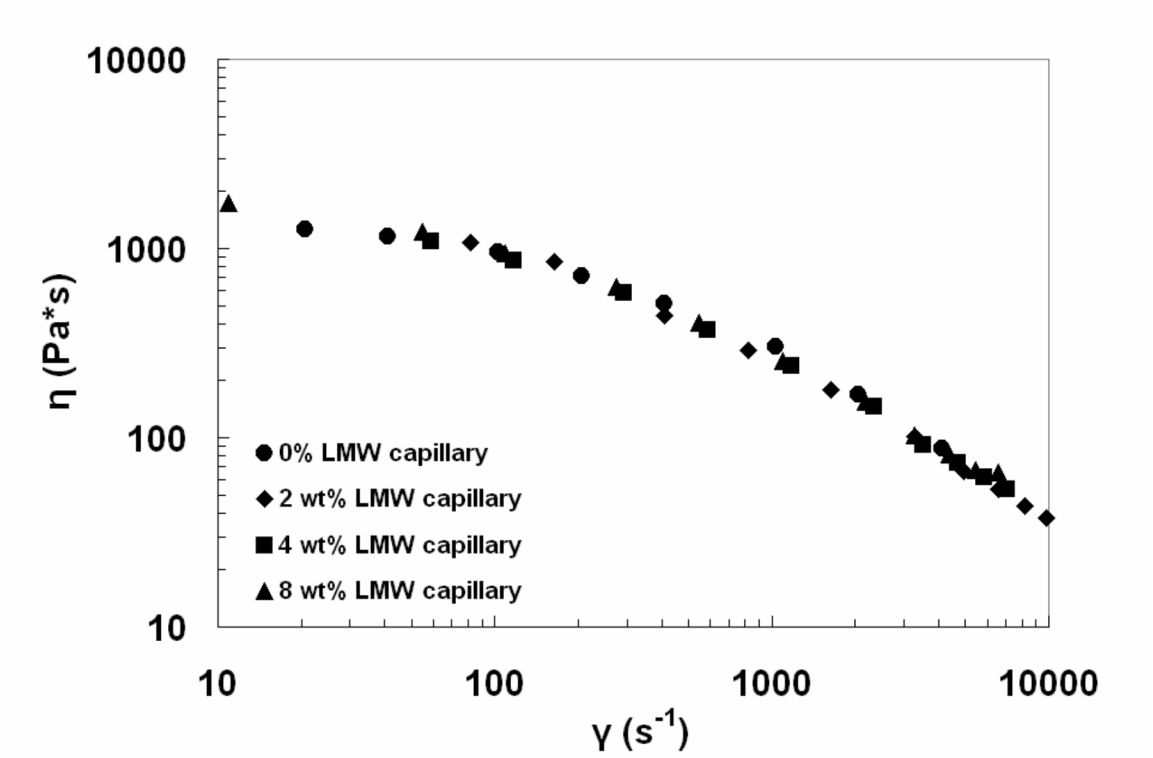

Figure D.1. True Steady Shear Viscosity for LMW Matrix and Nanocomposites at 190°C from Capillary Rheometer. L/D=30.

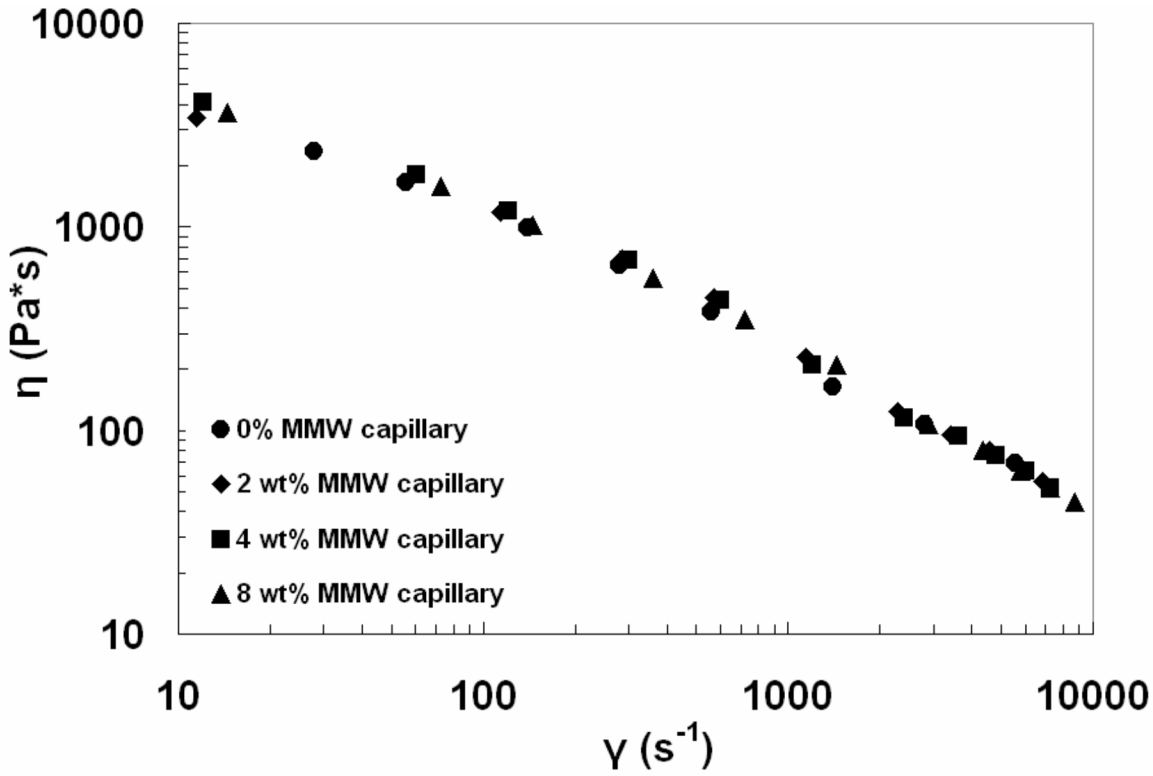

Figure D.2. True Steady Shear Viscosity for MMW Matrix and Nanocomposites at 190°C from Capillary Rheometer. L/D=30.

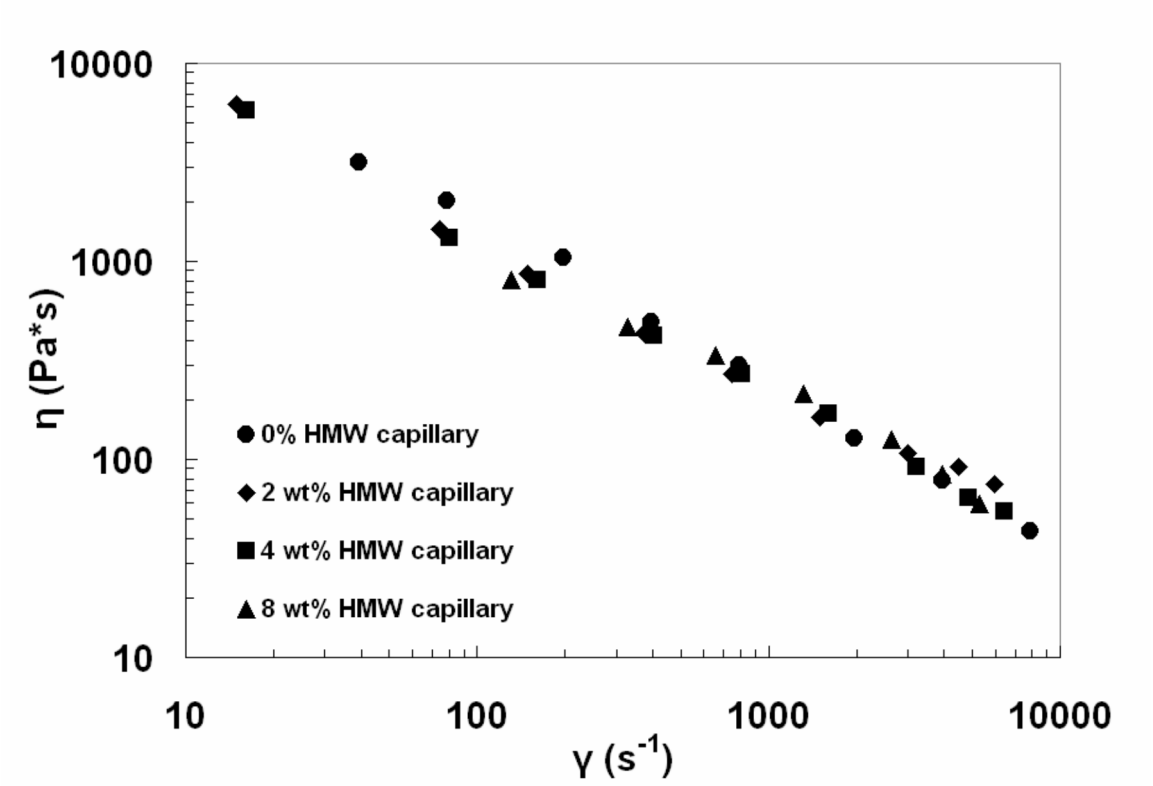

Figure D.3. True Steady Shear Viscosity for HMW Matrix and Nanocomposites at 190°C from Capillary Rheometer. L/D=30.

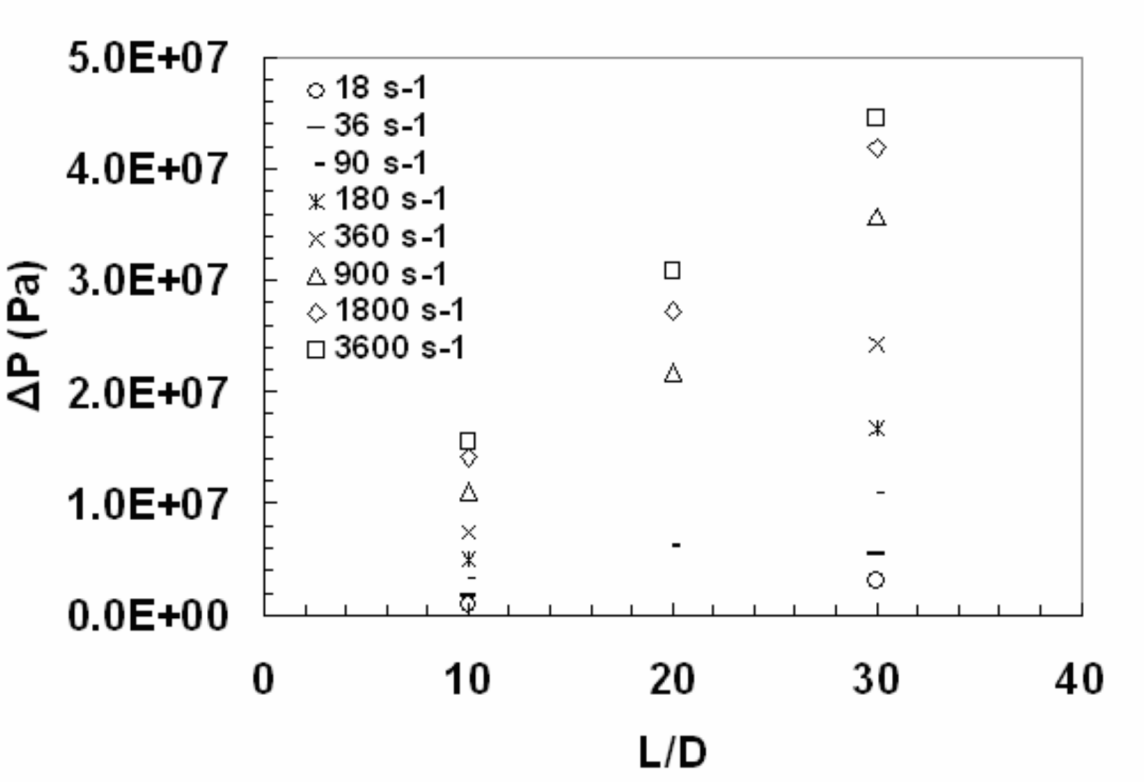

Figure D.4. Bagley Plot for 0% LMW at 190°C.

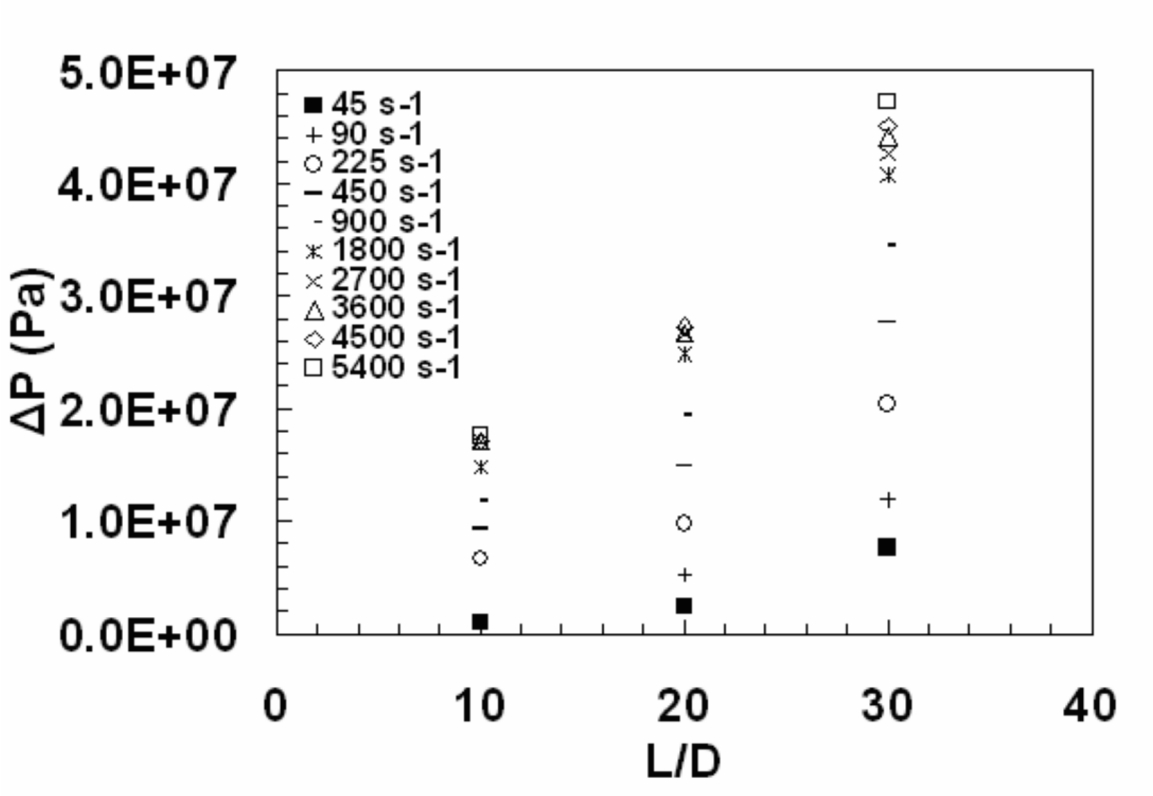

Figure D.5. Bagley Plot for 2% LMW at 190°C.

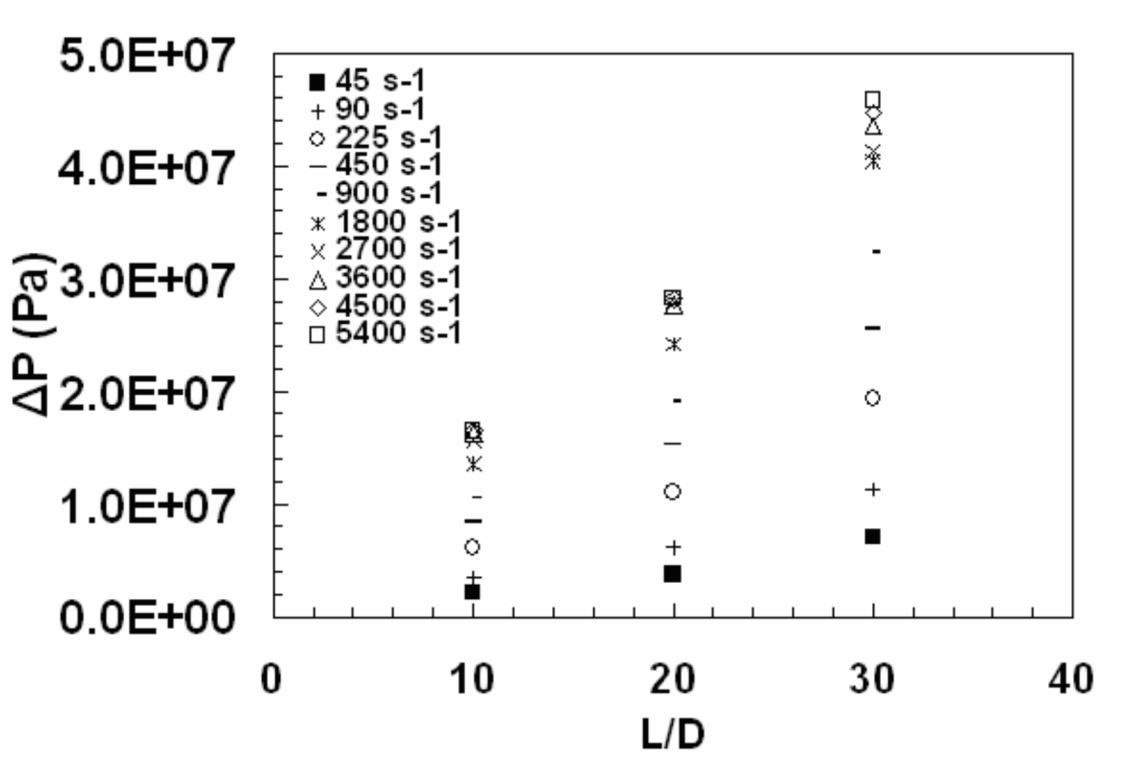

Figure D.6. Bagley Plot for 4% LMW at 190°C.

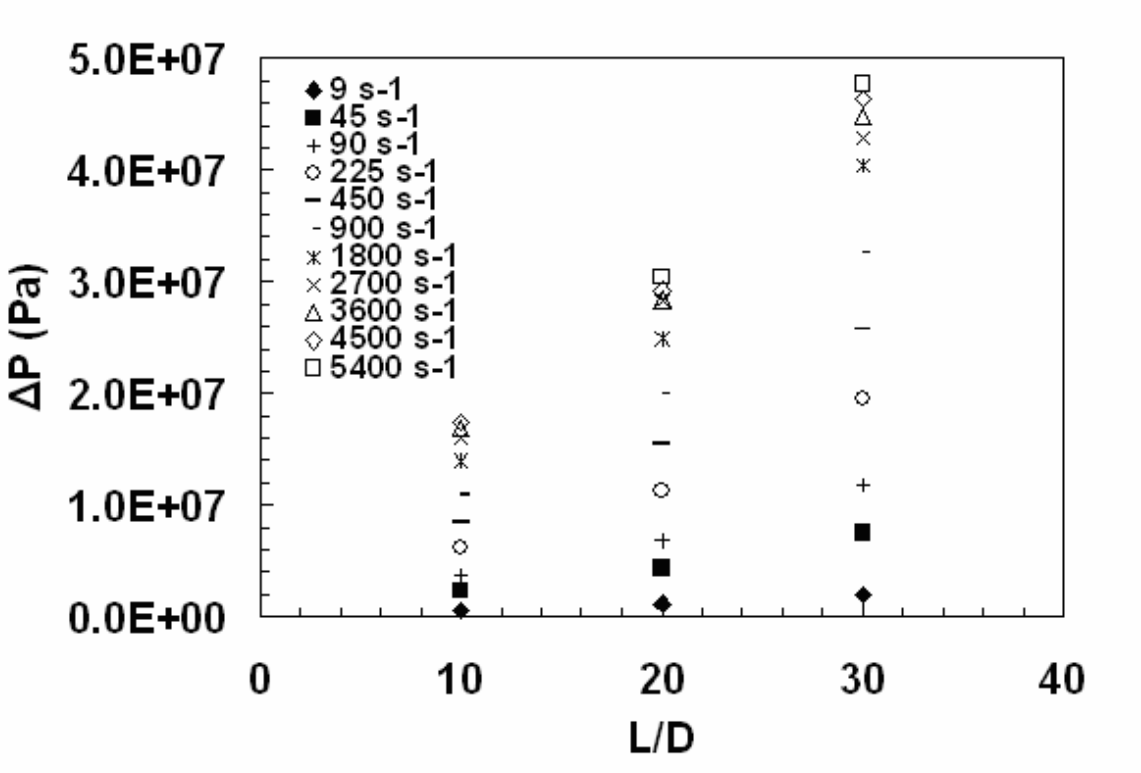

Figure D.7. Bagley Plot for 8% LMW at 190°C.

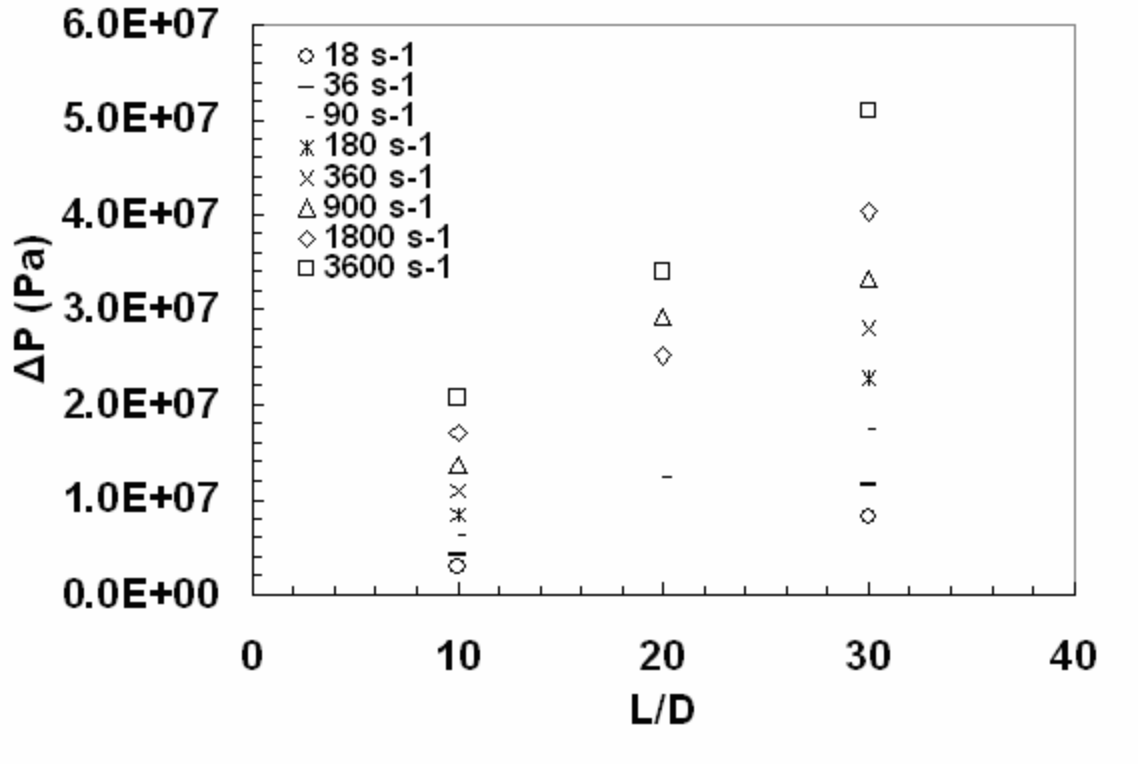

Figure D.8. Bagley Plot for 0% MMW at 190°C.

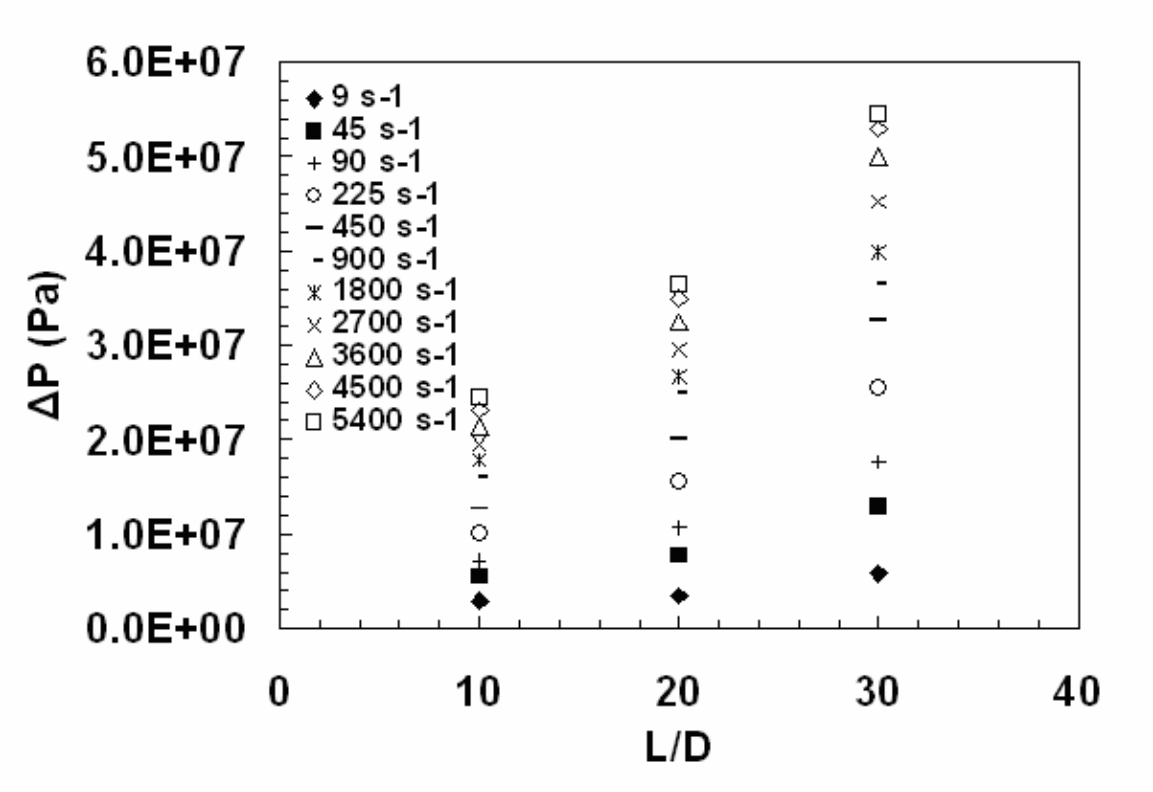

Figure D.9. Bagley Plot for 2% MMW at 190°C.

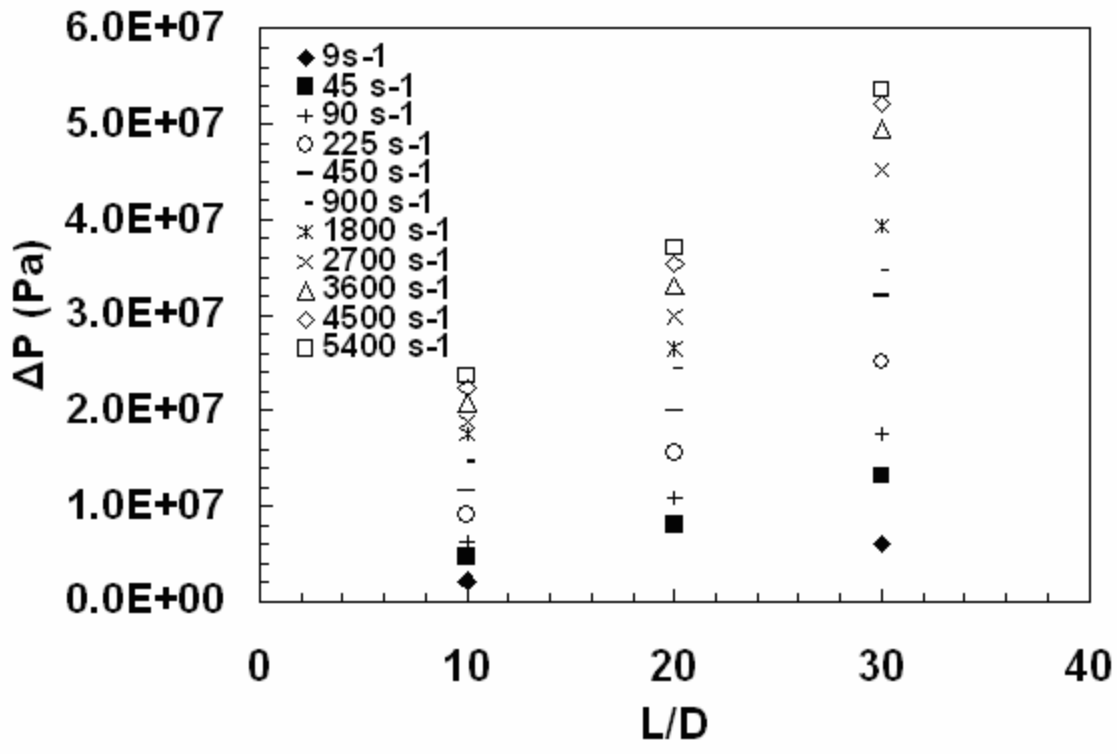

Figure D.10. Bagley Plot for 4% MMW at 190°C.

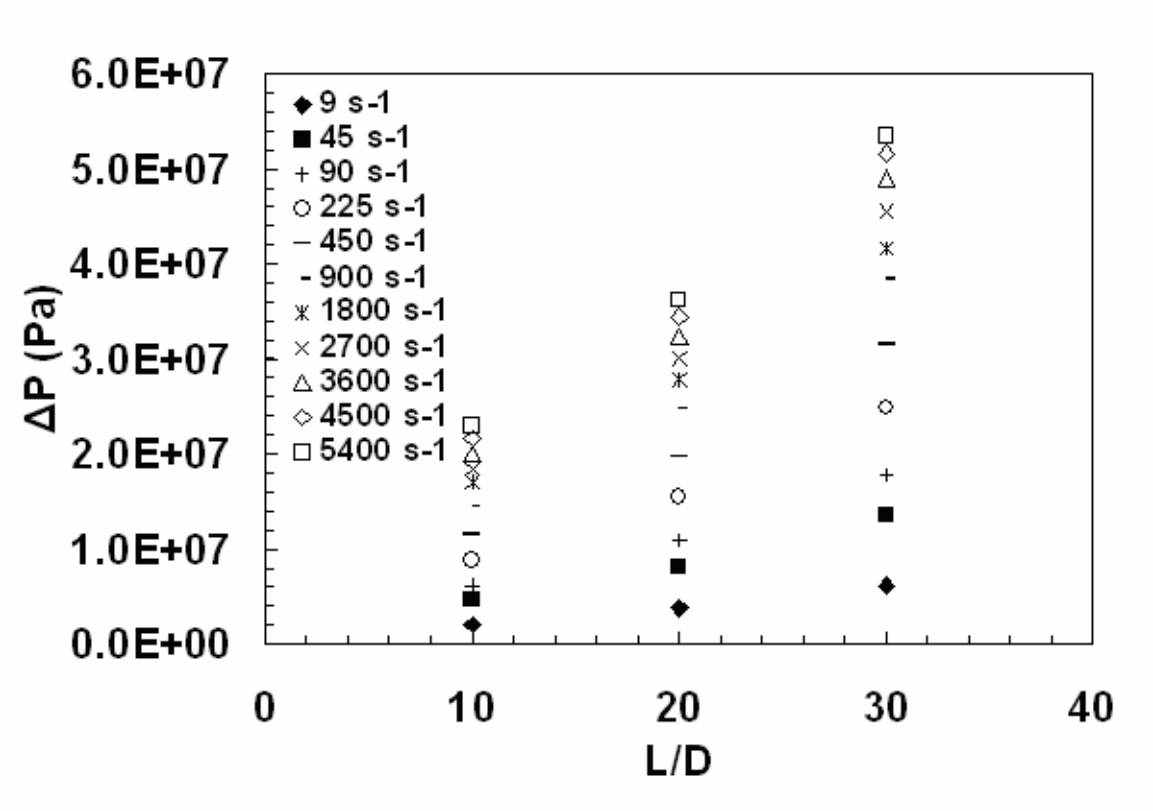

Figure D.11. Bagley Plot for 8% MMW at 190°C.

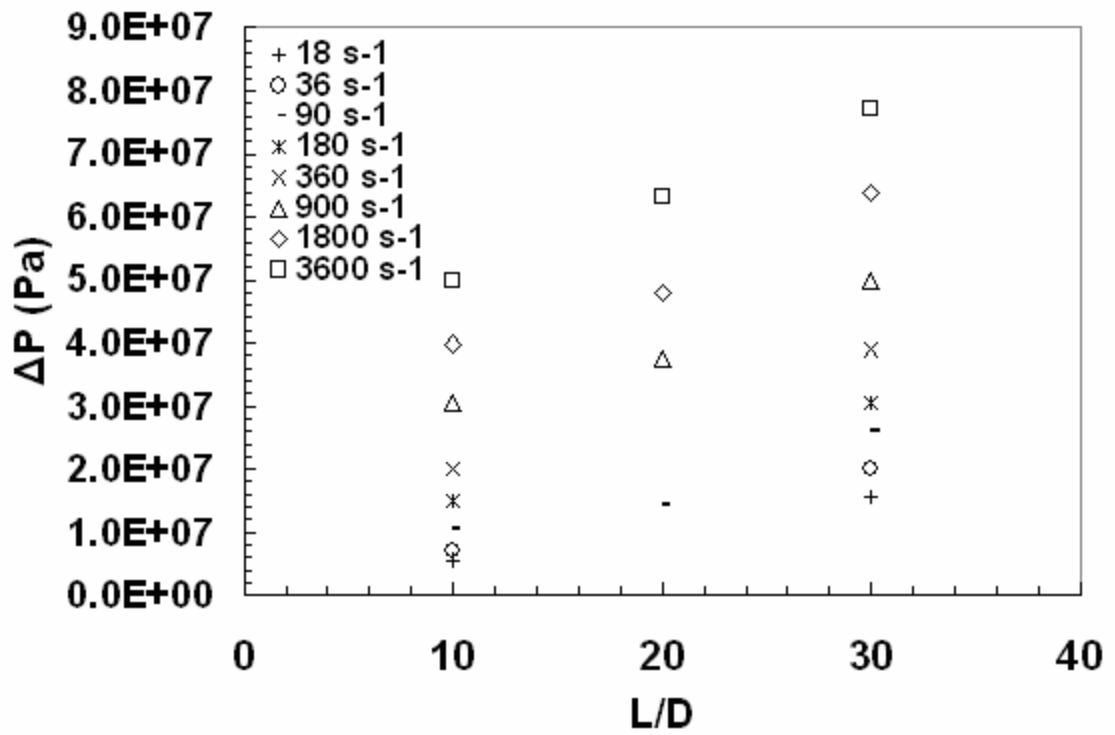

Figure D.12. Bagley Plot for 0% HMW at 190°C.

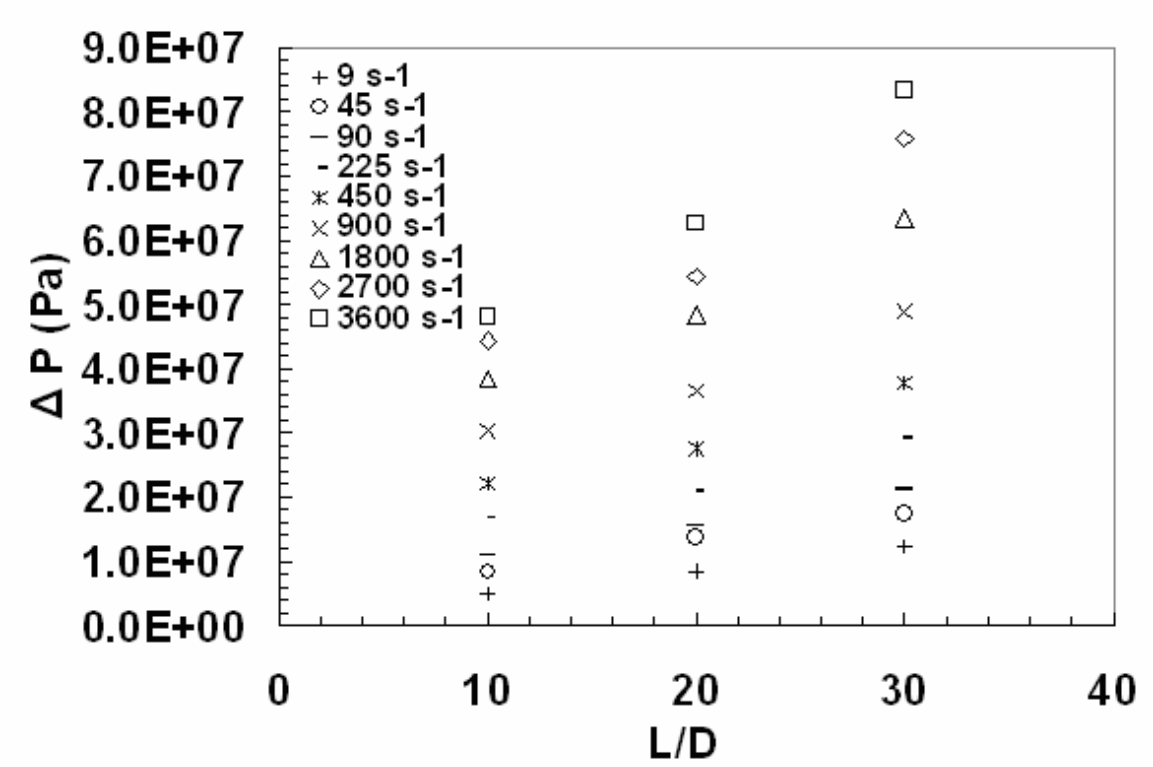

Figure D.13. Bagley Plot for 2% HMW at 190°C.

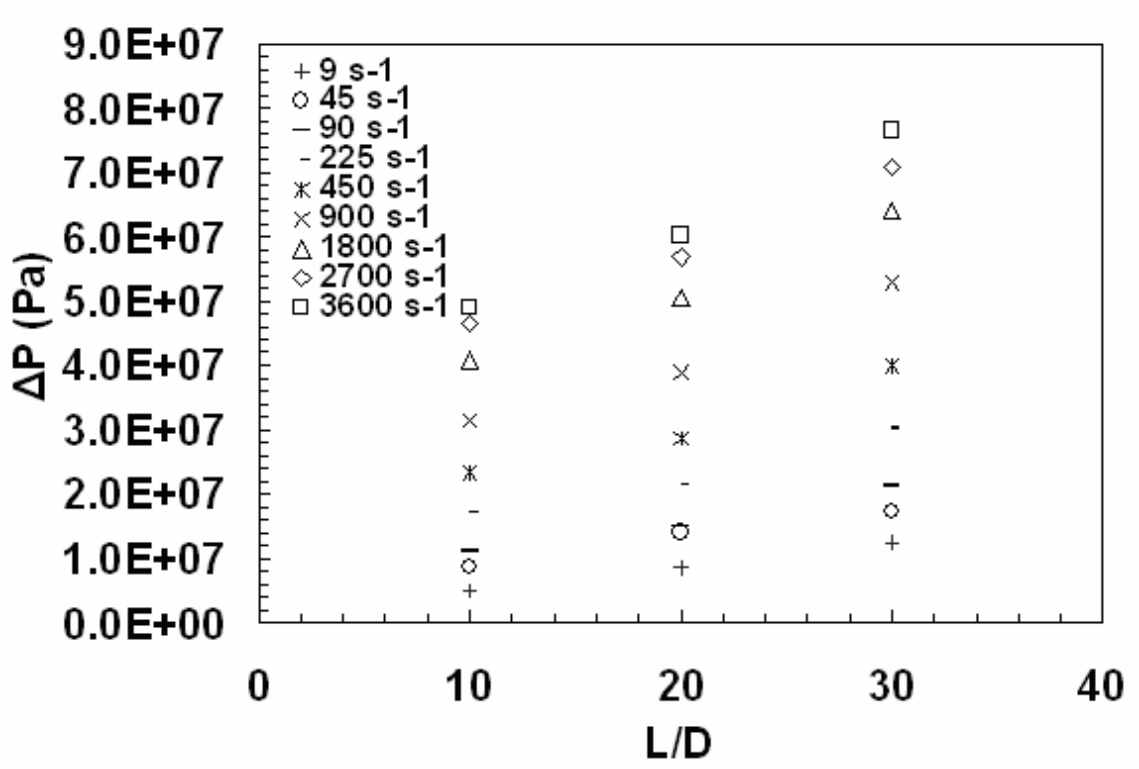

Figure D.14. Bagley Plot for 4% HMW at 190°C.

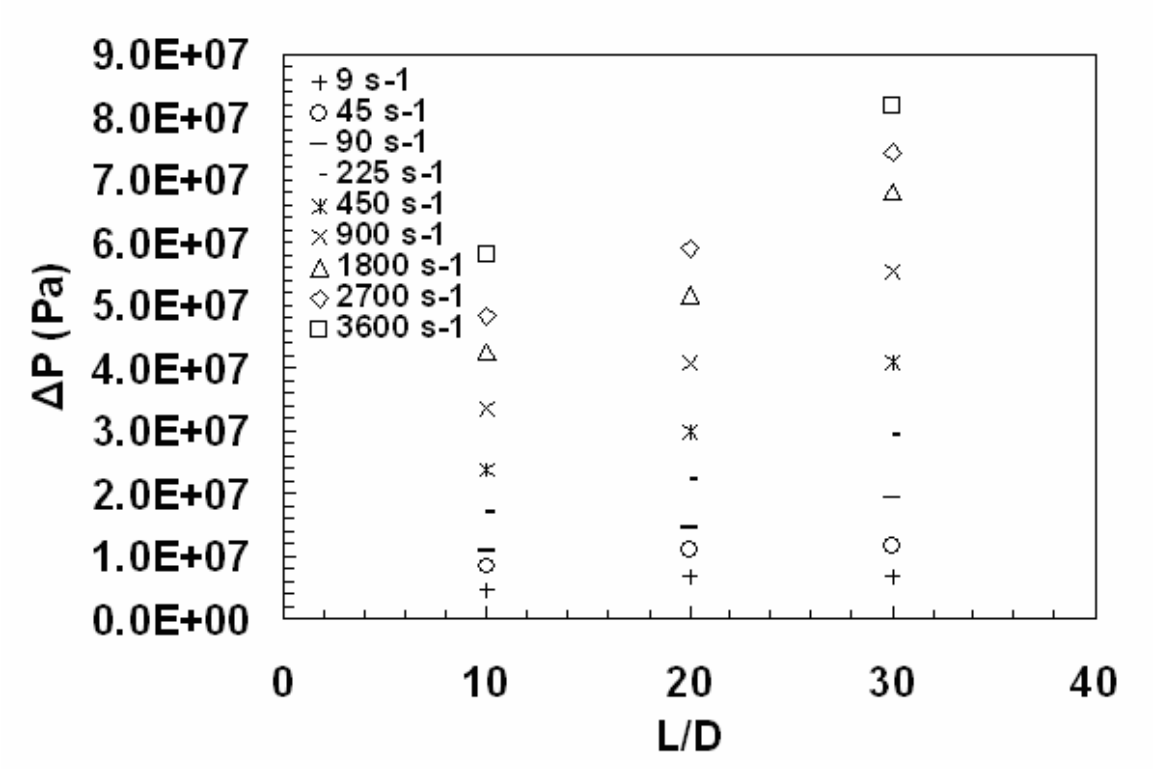

Figure D.15. Bagley Plot for 8% HMW at 190°C.

Table D.1. 0% LMW Capillary Data.

L/D=10							
ΔP(Pa)	**$\dot{\gamma}_{app}$(s^{-1})**	**τ_{app}(Pa)**	**η_{app}(Pa*s)**	**ΔP_{end} (Pa)**	**τ_{true}(Pa)**	**$\dot{\gamma}_{true}$(s^{-1})**	**η_{true} (Pa*s)**
9.277E+05	18	2.319E+04	1288.47	-1.160E+05	2.609E+04	20.53	1270.66
1.660E+06	36	4.150E+04	1152.78	-2.565E+05	4.791E+04	41.07	1166.63
3.222E+06	90	8.055E+04	895.00	-9.037E+05	1.031E+05	102.67	1004.58
4.980E+06	180	1.245E+05	691.67	-9.100E+05	1.473E+05	205.35	717.08
7.385E+06	360	1.846E+05	512.85	-1.058E+06	2.111E+05	410.69	513.95
1.105E+07	900	2.763E+05	306.94	-1.837E+06	3.222E+05	1026.73	313.79
1.417E+07	1800	3.543E+05	196.81	1.667E+04	3.538E+05	2053.45	172.31
1.552E+07	3600	3.880E+05	107.78	1.313E+06	3.552E+05	4106.91	86.48

L/D=20							
ΔP(Pa)	**$\dot{\gamma}_{app}$(s^{-1})**	**τ_{app}(Pa)**	**η_{app}(Pa*s)**	**ΔP_{end} (Pa)**	**τ_{true}(Pa)**	**$\dot{\gamma}_{true}$(s^{-1})**	**η_{true} (Pa*s)**
9.765E+05	9	1.221E+04	1356.25		1.221E+04	11.57	1055.08
3.808E+06	45	4.760E+04	1057.78		4.760E+04	57.85	822.89
6.201E+06	90	7.751E+04	861.25	-9.037E+05	8.881E+04	115.69	767.64
1.123E+07	225	1.404E+05	623.89		1.404E+05	289.23	485.35
1.612E+07	450	2.015E+05	447.78		2.015E+05	578.45	348.34
2.177E+07	900	2.721E+05	302.36	-1.837E+06	2.951E+05	1156.90	255.07
2.725E+07	1800	3.406E+05	189.24	1.667E+04	3.404E+05	2313.80	147.12
3.085E+07	2700	3.856E+05	142.82		3.856E+05	3470.71	111.11
3.084E+07	3600	3.855E+05	107.08	1.313E+06	3.691E+05	4627.61	79.76
3.095E+07	4500	3.869E+05	85.97		3.869E+05	5784.51	66.88
3.221E+07	5400	4.026E+05	74.56		4.026E+05	6941.41	58.00

L/D=30							
ΔP(Pa)	**$\dot{\gamma}_{app}$(s^{-1})**	**τ_{app}(Pa)**	**η_{app}(Pa*s)**	**ΔP_{end} (Pa)**	**τ_{true}(Pa)**	**$\dot{\gamma}_{true}$(s^{-1})**	**η_{true} (Pa*s)**
3.015E+06	18	2.513E+04	1395.83	-1.160E+05	2.609E+04	20.58	1267.89
5.493E+06	36	4.578E+04	1271.53	-2.565E+05	4.791E+04	41.16	1164.12
1.090E+07	90	9.083E+04	1009.26	-9.037E+05	9.836E+04	102.89	955.98
1.676E+07	180	1.397E+05	775.93	-9.100E+05	1.473E+05	205.79	715.54
2.427E+07	360	2.023E+05	561.81	-1.058E+06	2.111E+05	411.58	512.83
3.574E+07	900	2.978E+05	330.93	-1.837E+06	3.131E+05	1028.94	304.33
4.194E+07	1800	3.495E+05	194.17	1.667E+04	3.494E+05	2057.88	169.77
4.449E+07	3600	3.708E+05	102.99	1.313E+06	3.598E+05	4115.76	87.42

Table D.2. 2% LMW Capillary Data.

L/D=10							
ΔP(Pa)	**$\dot{\gamma}_{app}$(s^{-1})**	**τ_{app}(Pa)**	**η_{app}(Pa*s)**	**ΔP_{end} (Pa)**	**τ_{true}(Pa)**	**$\dot{\gamma}_{true}$(s^{-1})**	**η_{true} (Pa*s)**
9.033E+05	9	2.258E+04	2509.17	-3.011E+06	2.258E+04	16.85	1339.95
9.643E+05	45	2.411E+04	535.72	-4.860E+06	9.938E+04	84.27	1179.38

9.765E+05	90	2.441E+04	271.25	-1.432E+06	1.459E+05	168.53	865.78
6.677E+06	225	1.669E+05	741.89	-1.020E+06	2.027E+05	421.33	481.15
9.350E+06	450	2.338E+05	519.44	-7.400E+05	2.593E+05	842.66	307.66
1.182E+07	900	2.955E+05	328.33	9.100E+05	3.140E+05	1685.33	186.31
1.484E+07	1800	3.710E+05	206.11	3.273E+06	3.483E+05	3370.66	103.32
1.711E+07	2700	4.278E+05	158.43	2.250E+06	3.459E+05	5055.98	68.42
1.711E+07	3600	4.278E+05	118.82	1.867E+06	3.715E+05	6741.31	55.11
1.712E+07	4500	4.280E+05	95.11	2.655E+06	3.813E+05	8426.64	45.25
1.752E+07	5400	4.380E+05	81.11	-3.011E+06	3.716E+05	10111.97	36.75

L/D=20							
ΔP(Pa)	**g_{app}(s^{-1})**	**t_{app}(Pa)**	**h_{app}(Pa*s)**	**ΔP_{end} (Pa)**	**t_{true}(Pa)**	**g_{true}(s^{-1})**	**h_{true} (Pa*s)**
0.000E+00	9	0.000E+00	0.00	-3.011E+06	0.000E+00	15.63	0.00
2.343E+06	45	2.929E+04	650.83	-4.860E+06	6.693E+04	78.13	856.60
5.273E+06	90	6.591E+04	732.36	-1.432E+06	1.267E+05	156.26	810.60
9.777E+06	225	1.222E+05	543.17	-1.020E+06	1.401E+05	390.64	358.67
1.492E+07	450	1.865E+05	414.44	-7.400E+05	1.993E+05	781.29	255.03
1.936E+07	900	2.420E+05	268.89	9.100E+05	2.513E+05	1562.57	160.79
2.485E+07	1800	3.106E+05	172.57	3.273E+06	2.993E+05	3125.15	95.76
2.670E+07	2700	3.338E+05	123.61	2.250E+06	2.928E+05	4687.72	62.47
2.663E+07	3600	3.329E+05	92.47	1.867E+06	3.048E+05	6250.30	48.76
2.728E+07	4500	3.410E+05	75.78	2.655E+06	3.177E+05	7812.87	40.66

L/D=30							
ΔP(Pa)	**g_{app}(s^{-1})**	**t_{app}(Pa)**	**h_{app}(Pa*s)**	**ΔP_{end} (Pa)**	**t_{true}(Pa)**	**g_{true}(s^{-1})**	**h_{true} (Pa*s)**
1.953E+05	9	1.628E+03	180.83	-3.011E+06	1.628E+03		
7.617E+06	45	6.348E+04	1410.56	-4.860E+06	8.857E+04	82.05	1079.37
1.188E+07	90	9.900E+04	1100.00	-1.432E+06	1.395E+05	164.11	850.05
2.039E+07	225	1.699E+05	755.19	-1.020E+06	1.819E+05	410.27	443.24
2.769E+07	450	2.308E+05	512.78	-7.400E+05	2.393E+05	820.54	291.58
3.443E+07	900	2.869E+05	318.80	9.100E+05	2.931E+05	1641.08	178.59
4.074E+07	1800	3.395E+05	188.61	3.273E+06	3.319E+05	3282.16	101.13
4.266E+07	2700	3.555E+05	131.67	2.250E+06	3.282E+05	4923.24	66.67
4.416E+07	3600	3.680E+05	102.22	1.867E+06	3.493E+05	6564.32	53.20
4.508E+07	4500	3.757E+05	83.48	2.655E+06	3.601E+05	8205.40	43.89
4.725E+07	5400	3.938E+05	72.92	-3.011E+06	3.716E+05	9846.48	37.74

Table D.3. 4% LMW Capillary Data.

L/D=10							
ΔP(Pa)	**g_{app}(s^{-1})**	**t_{app}(Pa)**	**h_{app}(Pa*s)**	**ΔP_{end} (Pa)**	**t_{true}(Pa)**	**g_{true}(s^{-1})**	**h_{true} (Pa*s)**
2.148E+06	45	5.370E+04	1193.33	-6.023E+05	6.876E+04	59.09	1163.54
3.503E+06	90	8.758E+04	973.06	-7.973E+05	1.075E+05	118.19	909.64
6.079E+06	225	1.520E+05	675.44	-1.128E+06	1.802E+05	295.47	609.80
8.435E+06	450	2.109E+05	468.61	-7.200E+05	2.289E+05	590.94	387.31
1.055E+07	900	2.638E+05	293.06	-1.140E+06	2.923E+05	1181.87	247.28

1.356E+07	1800	3.390E+05	188.33	-7.967E+05	3.589E+05	2363.74	151.84
1.563E+07	2700	3.908E+05	144.72	2.643E+06	3.247E+05	3545.61	91.57
1.625E+07	3600	4.063E+05	112.85	1.847E+06	3.601E+05	4727.48	76.17
1.650E+07	4500	4.125E+05	91.67	1.567E+06	3.733E+05	5909.35	63.18
1.650E+07	5400	4.125E+05	76.39	8.933E+05	3.902E+05	7091.23	55.02
1.738E+07	6300	4.345E+05	68.97				

L/D=20							
ΔP(Pa)	**g_{app}(s^{-1})**	**t_{app}(Pa)**	**h_{app}(Pa*s)**	**ΔP_{end} (Pa)**	**t_{true}(Pa)**	**g_{true}(s^{-1})**	**h_{true} (Pa*s)**
2.929E+05	9	3.661E+03	406.81				
3.735E+06	45	4.669E+04	1037.50	-6.023E+05	5.422E+04	57.57	941.75
6.176E+06	90	7.720E+04	857.78	-7.973E+05	8.717E+04	115.14	757.05
1.102E+07	225	1.378E+05	612.22	-1.128E+06	1.519E+05	287.85	527.54
1.524E+07	450	1.905E+05	423.33	-7.200E+05	1.995E+05	575.70	346.54
1.914E+07	900	2.393E+05	265.83	-1.140E+06	2.535E+05	1151.39	220.17
2.419E+07	1800	3.024E+05	167.99	-7.967E+05	3.123E+05	2302.78	135.63
2.795E+07	2700	3.494E+05	129.40	2.643E+06	3.163E+05	3454.18	91.58
2.764E+07	3600	3.455E+05	95.97	1.847E+06	3.224E+05	4605.57	70.00
2.822E+07	4500	3.528E+05	78.39	1.567E+06	3.332E+05	5756.96	57.87
2.828E+07	5400	3.535E+05	65.46	8.933E+05	3.423E+05	6908.35	49.55

L/D=30							
ΔP(Pa)	**g_{app}(s^{-1})**	**t_{app}(Pa)**	**h_{app}(Pa*s)**	**ΔP_{end} (Pa)**	**t_{true}(Pa)**	**g_{true}(s^{-1})**	**h_{true} (Pa*s)**
9.765E+04	9	8.138E+02	90.42				
7.067E+06	45	5.889E+04	1308.70	-6.023E+05	6.391E+04	58.62	1090.20
1.129E+07	90	9.408E+04	1045.37	-7.973E+05	1.007E+05	117.25	859.11
1.936E+07	225	1.613E+05	717.04	-1.128E+06	1.707E+05	293.11	582.48
2.557E+07	450	2.131E+05	473.52	-7.200E+05	2.191E+05	586.23	373.72
3.238E+07	900	2.698E+05	299.81	-1.140E+06	2.793E+05	1172.46	238.25
4.041E+07	1800	3.368E+05	187.08	-7.967E+05	3.434E+05	2344.91	146.44
4.127E+07	2700	3.439E+05	127.38	2.643E+06	3.219E+05	3517.37	91.51
4.355E+07	3600	3.629E+05	100.81	1.847E+06	3.475E+05	4689.83	74.10
4.476E+07	4500	3.730E+05	82.89	1.567E+06	3.599E+05	5862.29	61.40
4.580E+07	5400	3.817E+05	70.68	8.933E+05	3.742E+05	7034.74	53.20

Table D.4. 8% LMW Capillary Data.

L/D=10							
ΔP(Pa)	**g_{app}(s^{-1})**	**t_{app}(Pa)**	**h_{app}(Pa*s)**	**ΔP_{end} (Pa)**	**t_{true}(Pa)**	**g_{true}(s^{-1})**	**h_{true} (Pa*s)**
5.615E+05	9	1.404E+04	1559.72	-2.277E+05	1.973E+04	10.96	1800.13
2.270E+06	45	5.675E+04	1261.11	-5.293E+05	6.998E+04	54.80	1277.01
3.723E+06	90	9.308E+04	1034.17	-6.470E+05	1.093E+05	109.60	996.78
6.140E+06	225	1.535E+05	682.22	-1.020E+06	1.790E+05	274.01	653.27
8.496E+06	450	2.124E+05	472.00	-6.887E+05	2.296E+05	548.02	419.00
1.093E+07	900	2.733E+05	303.61	-5.467E+05	2.869E+05	1096.03	261.78

1.396E+07	1800	3.490E+05	193.89	-3.333E+04	3.498E+05	2192.07	159.59
1.597E+07	2700	3.993E+05	147.87	2.123E+06	3.462E+05	3288.10	105.28
1.687E+07	3600	4.218E+05	117.15	2.090E+06	3.695E+05	4384.13	84.28
1.738E+07	4500	4.345E+05	96.56	2.003E+06	3.844E+05	5480.16	70.15

L/D=20							
ΔP(Pa)	**$g_{app}(s^{-1})$**	**t_{app}(Pa)**	**h_{app}(Pa*s)**	**ΔP_{end} (Pa)**	**t_{true}(Pa)**	**$g_{true}(s^{-1})$**	**h_{true} (Pa*s)**
1.171E+06	9	1.464E+04	1626.39	-2.277E+05	1.748E+04	10.93	1599.64
4.296E+06	45	5.370E+04	1193.33	-5.293E+05	6.032E+04	54.65	1103.70
6.787E+06	90	8.484E+04	942.64	-6.470E+05	9.293E+04	109.30	850.20
1.132E+07	225	1.415E+05	628.89	-1.020E+06	1.543E+05	273.25	564.51
1.547E+07	450	1.934E+05	429.72	-6.887E+05	2.020E+05	546.49	369.60
1.994E+07	900	2.493E+05	276.94	-5.467E+05	2.561E+05	1092.98	234.30
2.490E+07	1800	3.113E+05	172.92	-3.333E+04	3.117E+05	2185.97	142.58
2.827E+07	2700	3.534E+05	130.88	2.123E+06	3.268E+05	3278.95	99.68
2.841E+07	3600	3.551E+05	98.65	2.090E+06	3.290E+05	4371.93	75.25
2.927E+07	4500	3.659E+05	81.31	2.003E+06	3.408E+05	5464.91	62.37
3.043E+07	5400	3.804E+05	70.44	-4.070E+06	4.313E+05	6557.90	65.76

L/D=30							
ΔP(Pa)	**$g_{app}(s^{-1})$**	**t_{app}(Pa)**	**h_{app}(Pa*s)**	**ΔP_{end} (Pa)**	**t_{true}(Pa)**	**$g_{true}(s^{-1})$**	**h_{true} (Pa*s)**
2.050E+06	9	1.708E+04	1898.15	-2.277E+05	1.898E+04	10.95	1733.27
7.482E+06	45	6.235E+04	1385.56	-5.293E+05	6.676E+04	54.75	1219.28
1.181E+07	90	9.842E+04	1093.52	-6.470E+05	1.038E+05	109.51	947.94
1.947E+07	225	1.623E+05	721.11	-1.020E+06	1.708E+05	273.77	623.69
2.576E+07	450	2.147E+05	477.04	-6.887E+05	2.204E+05	547.54	402.53
3.265E+07	900	2.721E+05	302.31	-5.467E+05	2.766E+05	1095.09	252.62
4.042E+07	1800	3.368E+05	187.13	-3.333E+04	3.371E+05	2190.18	153.92
4.289E+07	2700	3.574E+05	132.38	2.123E+06	3.397E+05	3285.27	103.41
4.481E+07	3600	3.734E+05	103.73	2.090E+06	3.560E+05	4380.36	81.27
4.639E+07	4500	3.866E+05	85.91	2.003E+06	3.699E+05	5475.45	67.55
4.768E+07	5400	3.973E+05	73.58	-4.070E+06	4.313E+05	6570.54	65.63

Table D.5. 0% MMW Capillary Data.

L/D=10							
ΔP(Pa)	**$g_{app}(s^{-1})$**	**t_{app}(Pa)**	**h_{app}(Pa*s)**	**ΔP_{end} (Pa)**	**t_{true}(Pa)**	**$g_{true}(s^{-1})$**	**h_{true} (Pa*s)**
2.929E+06	18	7.323E+04	4068.06	3.105E+05	6.546E+04	27.23	2404.24
4.162E+06	36	1.041E+05	2890.28	4.780E+05	9.210E+04	54.46	1691.28
6.152E+06	90	1.538E+05	1708.89	7.760E+05	1.344E+05	136.14	987.22
8.386E+06	180	2.097E+05	1164.72	1.184E+06	1.801E+05	272.28	661.27
1.090E+07	360	2.725E+05	756.94	2.325E+06	2.144E+05	544.56	393.67
1.363E+07	900	3.408E+05	378.61	5.697E+06	1.983E+05	1361.39	145.68
1.700E+07	1800	4.250E+05	236.11	4.170E+06	3.208E+05	2722.79	117.80
2.073E+07	3600	5.183E+05	143.96	4.983E+06	3.937E+05	5445.58	72.29

L/D=20							
ΔP(Pa)	γ_{app}(s^{-1})	τ_{app}(Pa)	η_{app}(Pa*s)	ΔP_{end} (Pa)	τ_{true}(Pa)	γ_{true}(s^{-1})	η_{true} (Pa*s)
4.113E+06	9	5.141E+04	5712.50		5.141E+04	15.53	3311.52
9.069E+06	45	1.134E+05	2519.17		1.134E+05	77.63	1460.35
1.228E+07	90	1.535E+05	1705.56	7.760E+05	1.438E+05	155.25	926.23
1.773E+07	225	2.216E+05	985.00		2.216E+05	388.13	571.00
2.296E+07	450	2.870E+05	637.78		2.870E+05	776.27	369.72
2.921E+07	900	3.651E+05	405.69	5.697E+06	2.939E+05	1552.54	189.31
2.517E+07	1800	3.146E+05	174.79	4.170E+06	2.625E+05	3105.07	84.54
3.071E+07	2700	3.839E+05	142.18		3.839E+05	4657.61	82.42
3.395E+07	3600	4.244E+05	117.88	4.983E+06	3.621E+05	6210.14	58.31
3.670E+07	4500	4.588E+05	101.94		4.588E+05	7762.68	59.10
3.885E+07	5400	4.856E+05	89.93		4.856E+05	9315.21	52.13

L/D=30							
ΔP(Pa)	γ_{app}(s^{-1})	τ_{app}(Pa)	η_{app}(Pa*s)	ΔP_{end} (Pa)	τ_{true}(Pa)	γ_{true}(s^{-1})	η_{true} (Pa*s)
8.166E+06	18	6.805E+04	3780.56	3.105E+05	6.546E+04	27.96	2341.67
1.153E+07	36	9.608E+04	2668.98	4.780E+05	9.210E+04	55.91	1647.26
1.728E+07	90	1.440E+05	1600.00	7.760E+05	1.375E+05	139.78	983.94
2.279E+07	180	1.899E+05	1055.09	1.184E+06	1.801E+05	279.56	644.06
2.805E+07	360	2.338E+05	649.31	2.325E+06	2.144E+05	559.11	383.42
3.332E+07	900	2.777E+05	308.52	5.697E+06	2.302E+05	1397.78	164.68
4.033E+07	1800	3.361E+05	186.71	4.170E+06	3.013E+05	2795.55	107.79
5.096E+07	3600	4.247E+05	117.96	4.983E+06	3.831E+05	5591.10	68.53

Table D.6. 2% MMW Capillary Data.

L/D=10							
ΔP(Pa)	γ_{app}(s^{-1})	τ_{app}(Pa)	η_{app}(Pa*s)	ΔP_{end} (Pa)	τ_{true}(Pa)	γ_{true}(s^{-1})	η_{true} (Pa*s)
2.929E+06	9	7.323E+04	8136.11	1.138E+06	4.478E+04	11.62	3853.23
5.480E+06	45	1.370E+05	3044.44	1.258E+06	1.056E+05	58.10	1816.68
7.189E+06	90	1.797E+05	1996.94	1.372E+06	1.454E+05	116.20	1251.49
1.005E+07	225	2.513E+05	1116.67	1.560E+06	2.123E+05	290.50	730.63
1.273E+07	450	3.183E+05	707.22	1.893E+06	2.709E+05	581.01	466.30
1.600E+07	900	4.000E+05	444.44	5.247E+06	2.688E+05	1162.01	231.34
1.785E+07	1800	4.463E+05	247.92	6.090E+06	2.940E+05	2324.03	126.50
1.954E+07	2700	4.885E+05	180.93	5.787E+06	3.438E+05	3486.04	98.63
2.144E+07	3600	5.360E+05	148.89	6.060E+06	3.845E+05	4648.05	82.72
2.314E+07	4500	5.785E+05	128.56	7.233E+06	3.977E+05	5810.06	68.45
2.449E+07	5400	6.123E+05	113.38	8.477E+06	4.003E+05	6972.08	57.42

L/D=20							
ΔP(Pa)	γ_{app}(s^{-1})	τ_{app}(Pa)	η_{app}(Pa*s)	ΔP_{end} (Pa)	τ_{true}(Pa)	γ_{true}(s^{-1})	η_{true} (Pa*s)
3.417E+06	9	4.271E+04	4745.83	1.138E+06	2.849E+04	10.98	2594.65
7.714E+06	45	9.643E+04	2142.78	1.258E+06	8.070E+04	54.90	1470.04

1.066E+07	90	1.333E+05	1480.56	1.372E+06	1.161E+05	109.79	1057.44
1.552E+07	225	1.940E+05	862.22	1.560E+06	1.745E+05	274.48	635.74
2.008E+07	450	2.510E+05	557.78	1.893E+06	2.273E+05	548.97	414.12
2.490E+07	900	3.113E+05	345.83	5.247E+06	2.457E+05	1097.93	223.75
2.669E+07	1800	3.336E+05	185.35	6.090E+06	2.575E+05	2195.86	117.27
2.958E+07	2700	3.698E+05	136.94	5.787E+06	2.974E+05	3293.80	90.29
3.244E+07	3600	4.055E+05	112.64	6.060E+06	3.298E+05	4391.73	75.08
3.496E+07	4500	4.370E+05	97.11	7.233E+06	3.466E+05	5489.66	63.13
3.645E+07	5400	4.556E+05	84.38	8.477E+06	3.497E+05	6587.59	53.08

L/D=30							
ΔP(Pa)	**g_{app}(s^{-1})**	**t_{app}(Pa)**	**h_{app}(Pa*s)**	**ΔP_{end} (Pa)**	**t_{true}(Pa)**	**g_{true}(s^{-1})**	**h_{true} (Pa*s)**
5.859E+06	9	4.883E+04	5425.00	1.138E+06	3.934E+04	11.43	3442.06
1.293E+07	45	1.078E+05	2394.44	1.258E+06	9.727E+04	57.15	1702.00
1.765E+07	90	1.471E+05	1634.26	1.372E+06	1.357E+05	114.30	1186.82
2.552E+07	225	2.127E+05	945.19	1.560E+06	1.997E+05	285.74	698.76
3.266E+07	450	2.722E+05	604.81	1.893E+06	2.564E+05	571.49	448.64
3.658E+07	900	3.048E+05	338.70	5.247E+06	2.611E+05	1142.97	228.45
3.991E+07	1800	3.326E+05	184.77	6.090E+06	2.818E+05	2285.94	123.29
4.519E+07	2700	3.766E+05	139.48	5.787E+06	3.284E+05	3428.91	95.76
5.001E+07	3600	4.168E+05	115.76	6.060E+06	3.663E+05	4571.88	80.11
5.291E+07	4500	4.409E+05	97.98	7.233E+06	3.806E+05	5714.85	66.61
5.449E+07	5400	4.541E+05	84.09	8.477E+06	3.834E+05	6857.82	55.91

.**Table D.7.** 4% MMW Capillary Data.

L/D=10							
ΔP(Pa)	**g_{app}(s^{-1})**	**t_{app}(Pa)**	**h_{app}(Pa*s)**	**ΔP_{end} (Pa)**	**t_{true}(Pa)**	**g_{true}(s^{-1})**	**h_{true} (Pa*s)**
2.148E+06	9	5.370E+04	5966.67	1.705E+05	4.944E+04	11.91	4150.73
4.638E+06	45	1.160E+05	2576.67	1.347E+05	1.126E+05	59.55	1890.48
6.274E+06	90	1.569E+05	1742.78	2.553E+05	1.505E+05	119.11	1263.31
9.057E+06	225	2.264E+05	1006.33	4.760E+05	2.145E+05	297.76	720.45
1.158E+07	450	2.895E+05	643.33	7.100E+05	2.718E+05	595.53	456.32
1.464E+07	900	3.660E+05	406.67	4.540E+06	2.525E+05	1191.06	212.00
1.756E+07	1800	4.390E+05	243.89	6.000E+06	2.890E+05	2382.11	121.32
1.882E+07	2700	4.705E+05	174.26	4.857E+06	3.491E+05	3573.17	97.69
2.082E+07	3600	5.205E+05	144.58	5.757E+06	3.766E+05	4764.22	79.04
2.237E+07	4500	5.593E+05	124.28	6.857E+06	3.878E+05	5955.28	65.12
2.363E+07	5400	5.908E+05	109.40	8.160E+06	3.868E+05	7146.33	54.12

L/D=20							
ΔP(Pa)	**g_{app}(s^{-1})**	**t_{app}(Pa)**	**h_{app}(Pa*s)**	**ΔP_{end} (Pa)**	**t_{true}(Pa)**	**g_{true}(s^{-1})**	**h_{true} (Pa*s)**
0.000E+00	9	0.000E+00	0.00	1.705E+05	-2.131E+03	6.75	-315.74
8.032E+06	45	1.004E+05	2231.11	1.347E+05	9.872E+04	62.90	1569.36
1.087E+07	90	1.359E+05	1509.72	2.553E+05	1.327E+05	125.81	1054.67
1.556E+07	225	1.945E+05	864.44	4.760E+05	1.886E+05	314.51	599.50

1.993E+07	450	2.491E+05	553.61	7.100E+05	2.403E+05	629.03	381.94
2.434E+07	900	3.043E+05	338.06	4.540E+06	2.475E+05	1258.05	196.73
2.646E+07	1800	3.308E+05	183.75	6.000E+06	2.558E+05	2516.11	101.65
2.983E+07	2700	3.729E+05	138.10	4.857E+06	3.122E+05	3774.16	82.71
3.305E+07	3600	4.131E+05	114.76	5.757E+06	3.412E+05	5032.21	67.80
3.541E+07	4500	4.426E+05	98.36	6.857E+06	3.569E+05	6290.26	56.74
3.706E+07	5400	4.633E+05	85.79	8.160E+06	3.613E+05	7548.32	47.86

L/D=30							
ΔP(Pa)	**g_{app}(s^{-1})**	**t_{app}(Pa)**	**h_{app}(Pa*s)**	**ΔP_{end} (Pa)**	**t_{true}(Pa)**	**g_{true}(s^{-1})**	**h_{true} (Pa*s)**
6.103E+06	9	5.086E+04	5650.93	1.705E+05	4.944E+04	12.03	4111.06
1.309E+07	45	1.091E+05	2424.07	1.347E+05	1.080E+05	60.13	1795.54
1.760E+07	90	1.467E+05	1629.63	2.553E+05	1.445E+05	120.25	1201.94
2.518E+07	225	2.098E+05	932.59	4.760E+05	2.059E+05	300.64	684.77
3.206E+07	450	2.672E+05	593.70	7.100E+05	2.613E+05	601.27	434.49
3.464E+07	900	2.887E+05	320.74	4.540E+06	2.508E+05	1202.55	208.58
3.935E+07	1800	3.279E+05	182.18	6.000E+06	2.779E+05	2405.10	115.55
4.527E+07	2700	3.773E+05	139.72	4.857E+06	3.368E+05	3607.65	93.35
4.953E+07	3600	4.128E+05	114.65	5.757E+06	3.648E+05	4810.20	75.83
5.216E+07	4500	4.347E+05	96.59	6.857E+06	3.775E+05	6012.75	62.79
5.355E+07	5400	4.463E+05	82.64	8.160E+06	3.783E+05	7215.30	52.42

Table D.8. 8% MMW Capillary Data.

L/D=10							
ΔP(Pa)	**g_{app}(s^{-1})**	**t_{app}(Pa)**	**h_{app}(Pa*s)**	**ΔP_{end} (Pa)**	**t_{true}(Pa)**	**g_{true}(s^{-1})**	**h_{true} (Pa*s)**
2.062E+06	9	5.155E+04	5727.78	-1.067E+05	5.422E+04	14.54	3728.57
4.626E+06	45	1.157E+05	2570.00	-1.730E+05	1.200E+05	72.70	1650.18
6.152E+06	90	1.538E+05	1708.89	-3.400E+04	1.547E+05	145.41	1063.55
8.886E+06	225	2.222E+05	987.33	4.047E+05	2.120E+05	363.52	583.28
1.146E+07	450	2.865E+05	636.67	8.433E+05	2.654E+05	727.04	365.06
1.446E+07	900	3.615E+05	401.67	1.907E+06	3.138E+05	1454.09	215.83
1.704E+07	1800	4.260E+05	236.67	4.250E+06	3.198E+05	2908.17	109.95
1.843E+07	2700	4.608E+05	170.65	4.183E+06	3.562E+05	4362.26	81.65
2.005E+07	3600	5.013E+05	139.24	4.860E+06	3.798E+05	5816.34	65.29
2.163E+07	4500	5.408E+05	120.17	5.907E+06	3.931E+05	7270.43	54.07
2.303E+07	5400	5.758E+05	106.62	7.113E+06	3.979E+05	8724.52	45.61
2.403E+07	6300	6.008E+05	95.36				

L/D=20							
ΔP(Pa)	**g_{app}(s^{-1})**	**t_{app}(Pa)**	**h_{app}(Pa*s)**	**ΔP_{end} (Pa)**	**t_{true}(Pa)**	**g_{true}(s^{-1})**	**h_{true} (Pa*s)**
3.808E+06	9	4.760E+04	5288.89	-1.067E+05	4.893E+04	14.40	3398.04
8.117E+06	45	1.015E+05	2254.72	-1.730E+05	1.036E+05	72.00	1439.19
1.093E+07	90	1.366E+05	1518.06	-3.400E+04	1.371E+05	144.00	951.71
1.545E+07	225	1.931E+05	858.33	4.047E+05	1.881E+05	360.01	522.39
1.971E+07	450	2.464E+05	547.50	8.433E+05	2.358E+05	720.02	327.54

2.478E+07	900	3.098E+05	344.17	1.907E+06	2.859E+05	1440.05	198.55
2.781E+07	1800	3.476E+05	193.13	4.250E+06	2.945E+05	2880.09	102.25
3.001E+07	2700	3.751E+05	138.94	4.183E+06	3.228E+05	4320.14	74.73
3.232E+07	3600	4.040E+05	112.22	4.860E+06	3.433E+05	5760.18	59.59
3.446E+07	4500	4.308E+05	95.72	5.907E+06	3.569E+05	7200.23	49.57
3.614E+07	5400	4.518E+05	83.66	7.113E+06	3.628E+05	8640.28	41.99

L/D=30							
ΔP(Pa)	**g_{app}(s^{-1})**	**t_{app}(Pa)**	**h_{app}(Pa*s)**	**ΔP_{end} (Pa)**	**t_{true}(Pa)**	**g_{true}(s^{-1})**	**h_{true} (Pa*s)**
6.188E+06	9	5.157E+04	5729.63	-1.067E+05	5.246E+04	14.50	3618.81
1.357E+07	45	1.131E+05	2512.96	-1.730E+05	1.145E+05	72.48	1580.17
1.782E+07	90	1.485E+05	1650.00	-3.400E+04	1.488E+05	144.95	1026.43
2.489E+07	225	2.074E+05	921.85	4.047E+05	2.040E+05	362.38	563.07
3.151E+07	450	2.626E+05	583.52	8.433E+05	2.556E+05	724.76	352.61
3.845E+07	900	3.204E+05	356.02	1.907E+06	3.045E+05	1449.53	210.09
4.161E+07	1800	3.468E+05	192.64	4.250E+06	3.113E+05	2899.05	107.39
4.559E+07	2700	3.799E+05	140.71	4.183E+06	3.451E+05	4348.58	79.35
4.897E+07	3600	4.081E+05	113.36	4.860E+06	3.676E+05	5798.11	63.40
5.163E+07	4500	4.303E+05	95.61	5.907E+06	3.810E+05	7247.63	52.57
5.346E+07	5400	4.455E+05	82.50	7.113E+06	3.862E+05	8697.16	44.41

Table D.9. 0% HMW Capillary Data.

L/D=10							
ΔP(Pa)	**g_{app}(s^{-1})**	**t_{app}(Pa)**	**h_{app}(Pa*s)**	**ΔP_{end} (Pa)**	**t_{true}(Pa)**	**g_{true}(s^{-1})**	**h_{true} (Pa*s)**
5.597E+06	18	6.996E+04	3886.81	5.955E+05	1.250E+05	38.90	3214.74
7.128E+06	36	8.910E+04	2475.00	6.970E+05	1.608E+05	77.79	2066.78
1.047E+07	90	1.309E+05	1454.17	1.367E+06	2.276E+05	194.48	1170.20
1.502E+07	180	1.878E+05	1043.06	7.215E+06	1.951E+05	388.95	501.67
2.016E+07	360	2.520E+05	700.00	1.077E+07	2.348E+05	777.90	301.77
3.045E+07	900	3.806E+05	422.92	1.978E+07	2.668E+05	1944.75	137.16
3.990E+07	1800	4.988E+05	277.08	2.660E+07	3.325E+05	3889.50	85.49
4.990E+07	3600	6.238E+05	173.26	3.620E+07	3.425E+05	7779.01	44.03

L/D=20							
ΔP(Pa)	**g_{app}(s^{-1})**	**t_{app}(Pa)**	**h_{app}(Pa*s)**	**ΔP_{end} (Pa)**	**t_{true}(Pa)**	**g_{true}(s^{-1})**	**h_{true} (Pa*s)**
1.430E+07	90	1.192E+05	1324.07	1.367E+06	1.617E+05	186.36	867.48
3.746E+07	900	3.122E+05	346.85	1.978E+07	2.210E+05	1863.59	118.59
4.803E+07	1800	4.003E+05	222.36	2.660E+07	2.679E+05	3727.18	71.87
6.318E+07	3600	5.265E+05	146.25	3.620E+07	3.373E+05	7454.36	45.24

L/D=30							
ΔP(Pa)	**g_{app}(s^{-1})**	**t_{app}(Pa)**	**h_{app}(Pa*s)**	**ΔP_{end} (Pa)**	**t_{true}(Pa)**	**g_{true}(s^{-1})**	**h_{true} (Pa*s)**
1.560E+07	18	3.900E+05	21666.67	5.955E+05	1.250E+05	39.53	3163.38
1.999E+07	36	4.998E+05	13881.94	6.970E+05	1.608E+05	79.05	2033.76

2.604E+07	90	6.510E+05	7233.33	1.367E+06	2.056E+05	197.63	1040.35
3.063E+07	180	7.658E+05	4254.17	7.215E+06	1.951E+05	395.27	493.65
3.895E+07	360	9.738E+05	2704.86	1.077E+07	2.348E+05	790.53	297.06
4.996E+07	900	1.249E+06	1387.78	1.978E+07	2.515E+05	1976.33	127.26
6.392E+07	1800	1.598E+06	887.78	2.660E+07	3.110E+05	3952.66	78.68
7.709E+07	3600	1.927E+06	535.35	3.620E+07	3.408E+05	7905.32	43.10

Table D.10. 2% HMW Capillary Data.

L/D=10							
ΔP(Pa)	**g_{app}(s^{-1})**	**t_{app}(Pa)**	**h_{app}(Pa*s)**	**ΔP_{end} (Pa)**	**t_{true}(Pa)**	**g_{true}(s^{-1})**	**h_{true} (Pa*s)**
4.980E+06	9	1.245E+05	13833.33	1.197E+06	9.458E+04	14.60	6477.45
8.398E+06	45	2.100E+05	4665.56	4.244E+06	1.039E+05	73.00	1422.54
1.101E+07	90	2.753E+05	3058.33	5.713E+06	1.324E+05	146.01	906.98
1.672E+07	225	4.180E+05	1857.78	9.790E+06	1.733E+05	365.02	474.64
2.220E+07	450	5.550E+05	1233.33	1.361E+07	2.148E+05	730.03	294.16
3.024E+07	900	7.560E+05	840.00	1.990E+07	2.585E+05	1460.07	177.05
3.842E+07	1800	9.605E+05	533.61	2.505E+07	3.343E+05	2920.13	114.46
4.433E+07	2700	1.108E+06	410.46	2.665E+07	4.420E+05	4380.20	100.91
4.799E+07	3600	1.200E+06	333.26	2.932E+07	4.668E+05	5840.27	79.92
5.389E+07	4500	1.347E+06	299.39		1.347E+06	7300.33	184.55

L/D=20							
ΔP(Pa)	**g_{app}(s^{-1})**	**t_{app}(Pa)**	**h_{app}(Pa*s)**	**ΔP_{end} (Pa)**	**t_{true}(Pa)**	**g_{true}(s^{-1})**	**h_{true} (Pa*s)**
8.471E+06	9	1.059E+05	11765.28	1.197E+06	9.093E+04	15.76	5769.06
1.374E+07	45	1.718E+05	3816.67	4.244E+06	1.187E+05	78.80	1506.27
1.552E+07	90	1.940E+05	2155.56	5.713E+06	1.226E+05	157.61	777.80
2.095E+07	225	2.619E+05	1163.89	9.790E+06	1.395E+05	394.02	354.04
2.756E+07	450	3.445E+05	765.56	1.361E+07	1.744E+05	788.04	221.28
3.659E+07	900	4.574E+05	508.19	1.990E+07	2.086E+05	1576.08	132.37
4.832E+07	1800	6.040E+05	335.56	2.505E+07	2.909E+05	3152.16	92.28
5.430E+07	2700	6.788E+05	251.39	2.665E+07	3.456E+05	4728.24	73.10
6.269E+07	3600	7.836E+05	217.67	2.932E+07	4.171E+05	6304.33	66.16

L/D=30							
ΔP(Pa)	**g_{app}(s^{-1})**	**t_{app}(Pa)**	**h_{app}(Pa*s)**	**ΔP_{end} (Pa)**	**t_{true}(Pa)**	**g_{true}(s^{-1})**	**h_{true} (Pa*s)**
1.240E+07	9	1.033E+05	11481.48	1.197E+06	9.336E+04	14.93	6251.06
1.730E+07	45	1.442E+05	3203.70	4.244E+06	1.088E+05	74.67	1457.00
2.121E+07	90	1.768E+05	1963.89	5.713E+06	1.291E+05	149.35	864.70
2.923E+07	225	2.436E+05	1082.59	9.790E+06	1.620E+05	373.37	433.89
3.776E+07	450	3.147E+05	699.26	1.361E+07	2.013E+05	746.74	269.50
4.893E+07	900	4.078E+05	453.06	1.990E+07	2.419E+05	1493.48	161.98
6.342E+07	1800	5.285E+05	293.61	2.505E+07	3.198E+05	2986.96	107.05
7.584E+07	2700	6.320E+05	234.07	2.665E+07	4.099E+05	4480.44	91.49
8.334E+07	3600	6.945E+05	192.92	2.932E+07	4.502E+05	5973.92	75.36

Table D.11. 4% HMW Capillary Data.

L/D=10							
ΔP(Pa)	$\dot{\gamma}_{app}$(s^{-1})	τ_{app}(Pa)	η_{app}(Pa*s)	ΔP_{end} (Pa)	τ_{true}(Pa)	$\dot{\gamma}_{true}$(s^{-1})	η_{true} (Pa*s)
4.992E+06	9	1.248E+05	13866.67	1.220E+06	9.430E+04	15.80	5969.47
8.691E+06	45	2.173E+05	4828.33	4.681E+06	1.003E+05	78.99	1269.22
1.114E+07	90	2.785E+05	3094.44	5.670E+06	1.368E+05	157.97	865.67
1.707E+07	225	4.268E+05	1896.67	9.727E+06	1.836E+05	394.93	464.83
2.327E+07	450	5.818E+05	1292.78	1.398E+07	2.323E+05	789.85	294.04
3.146E+07	900	7.865E+05	873.89	1.973E+07	2.933E+05	1579.70	185.64
4.080E+07	1800	1.020E+06	566.67	2.856E+07	3.060E+05	3159.41	96.85
4.656E+07	2700	1.164E+06	431.11	3.385E+07	3.178E+05	4739.11	67.05
4.893E+07	3600	1.223E+06	339.79	3.429E+07	3.660E+05	6318.82	57.92

L/D=20							
ΔP(Pa)	$\dot{\gamma}_{app}$(s^{-1})	τ_{app}(Pa)	η_{app}(Pa*s)	ΔP_{end} (Pa)	τ_{true}(Pa)	$\dot{\gamma}_{true}$(s^{-1})	η_{true} (Pa*s)
8.593E+06	9	1.074E+05	11934.72	1.220E+06	9.216E+04	16.82	5480.28
1.398E+07	45	1.748E+05	3883.33	4.681E+06	1.162E+05	84.09	1382.37
1.489E+07	90	1.861E+05	2068.06	5.670E+06	1.153E+05	168.17	685.31
2.136E+07	225	2.670E+05	1186.67	9.727E+06	1.454E+05	420.43	345.87
2.868E+07	450	3.585E+05	796.67	1.398E+07	1.838E+05	840.86	218.53
3.896E+07	900	4.870E+05	541.11	1.973E+07	2.404E+05	1681.71	142.93
5.051E+07	1800	6.314E+05	350.76	2.856E+07	2.744E+05	3363.42	81.58
5.686E+07	2700	7.108E+05	263.24	3.385E+07	2.876E+05	5045.13	57.01
6.026E+07	3600	7.533E+05	209.24	3.429E+07	3.246E+05	6726.85	48.26

L/D=30							
ΔP(Pa)	$\dot{\gamma}_{app}$(s^{-1})	τ_{app}(Pa)	η_{app}(Pa*s)	ΔP_{end} (Pa)	τ_{true}(Pa)	$\dot{\gamma}_{true}$(s^{-1})	η_{true} (Pa*s)
1.245E+07	9	1.038E+05	11527.78	1.220E+06	9.358E+04	16.11	5809.24
1.735E+07	45	1.446E+05	3212.96	4.681E+06	1.056E+05	80.55	1310.73
2.122E+07	90	1.768E+05	1964.81	5.670E+06	1.296E+05	161.09	804.40
3.023E+07	225	2.519E+05	1119.63	9.727E+06	1.709E+05	402.74	424.25
3.991E+07	450	3.326E+05	739.06	1.398E+07	2.161E+05	805.47	268.26
5.281E+07	900	4.401E+05	488.98	1.973E+07	2.757E+05	1610.94	171.12
6.401E+07	1800	5.334E+05	296.34	2.856E+07	2.954E+05	3221.88	91.69
7.078E+07	2700	5.898E+05	218.46	3.385E+07	3.078E+05	4832.82	63.68
7.656E+07	3600	6.380E+05	177.22	3.429E+07	3.523E+05	6443.76	54.67

Table D.12. 8% HMW Capillary Data.

L/D=10							
ΔP(Pa)	$\dot{\gamma}_{app}$(s^{-1})	τ_{app}(Pa)	η_{app}(Pa*s)	ΔP_{end} (Pa)	τ_{true}(Pa)	$\dot{\gamma}_{true}$(s^{-1})	η_{true} (Pa*s)
4.504E+06	9	1.126E+05	12511.11	3.788E+06	1.790E+04	13.04	1372.68

8.398E+06	45	2.100E+05	4665.56	7.151E+06	3.118E+04	65.20	478.14
1.085E+07	90	2.713E+05	3013.89	6.503E+06	1.087E+05	130.40	833.39
1.708E+07	225	4.270E+05	1897.78	1.067E+07	1.603E+05	326.00	491.56
2.381E+07	450	5.953E+05	1322.78	1.443E+07	2.345E+05	652.01	359.66
3.352E+07	900	8.380E+05	931.11	2.135E+07	3.043E+05	1304.02	233.32
4.246E+07	1800	1.062E+06	589.72	2.838E+07	3.520E+05	2608.04	134.97
4.827E+07	2700	1.207E+06	446.94	3.450E+07	3.443E+05	3912.06	88.00
5.814E+07	3600	1.454E+06	403.75	4.415E+07	3.498E+05	5216.07	67.05

L/D=20

ΔP(Pa)	g_{app}(s^{-1})	t_{app}(Pa)	h_{app}(Pa*s)	ΔP_{end} (Pa)	t_{true}(Pa)	g_{true}(s^{-1})	h_{true} (Pa*s)
6.628E+06	9	8.285E+04	9205.56	3.788E+06	3.550E+04	13.49	2631.08
1.094E+07	45	1.368E+05	3038.89	7.151E+06	4.736E+04	67.46	702.05
1.457E+07	90	1.821E+05	2023.61	6.503E+06	1.008E+05	134.93	747.36
2.214E+07	225	2.768E+05	1230.00	1.067E+07	1.434E+05	337.31	425.05
2.982E+07	450	3.728E+05	828.33	1.443E+07	1.924E+05	674.63	285.16
4.071E+07	900	5.089E+05	565.42	2.135E+07	2.420E+05	1349.26	179.36
5.151E+07	1800	6.439E+05	357.71	2.838E+07	2.891E+05	2698.52	107.14
5.904E+07	2700	7.380E+05	273.33	3.450E+07	3.068E+05	4047.77	75.78
6.336E+07	3600	7.920E+05	220.00	4.415E+07	2.401E+05	5397.03	44.49

L/D=30

ΔP(Pa)	g_{app}(s^{-1})	t_{app}(Pa)	h_{app}(Pa*s)	ΔP_{end} (Pa)	t_{true}(Pa)	g_{true}(s^{-1})	h_{true} (Pa*s)
6.640E+06	9	5.533E+04	6148.15	3.788E+06	2.377E+04	13.17	1804.44
1.154E+07	45	9.617E+04	2137.04	7.151E+06	3.658E+04	65.86	555.38
1.923E+07	90	1.603E+05	1780.56	6.503E+06	1.061E+05	131.71	805.23
2.923E+07	225	2.436E+05	1082.59	1.067E+07	1.547E+05	329.28	469.71
4.088E+07	450	3.407E+05	757.04	1.443E+07	2.204E+05	658.56	334.69
5.537E+07	900	4.614E+05	512.69	2.135E+07	2.835E+05	1317.12	215.24
6.811E+07	1800	5.676E+05	315.32	2.838E+07	3.311E+05	2634.25	125.68
7.431E+07	2700	6.193E+05	229.35	3.450E+07	3.318E+05	3951.37	83.96
8.173E+07	3600	6.811E+05	189.19	4.415E+07	3.132E+05	5268.49	59.44

Comment on Capillary Rheometry

Capillary rheometry was performed as well for each molecular weight and concentration. Previous studies involving steady shear, capillary measurements have shown that as clay is incorporated into a polymer matrix, the shear viscosity can be enhanced relative to the unfilled polymer [1, 2]. However, other researchers have shown that the steady shear viscosities of an unfilled polymer and its corresponding nanocomposite can overlap due to shear induced alignment of the nanoclay particles in the flow direction during capillary measurements [3, 4]. Fornes et al. [4] observed that only in their HMW and MMW systems where both exfoliation and higher levels of shear stress were achieved did the capillary viscosities of unfilled nylon 6 and its 3 wt% MMT nanocomposites overlap. Their LMW 3 wt% nanocomposite showed a steady shear viscosity higher than its unfilled matrix. Zhong et al. [3] observed overlapping capillary viscosities for both an exfoliated and intercalated system indicating that shear induced alignment of clay tactoids may occur as long as the shear force imparted to them is high enough. The approximate zero shear viscosity of the unfilled matrix of Zhong et al.'s intercalated system was 3,500 Pa*s while that of Fornes et al. was 350 Pa*s, thus it appears that there is a minimum viscosity, and thus, shear force required to induce alignment of clay tactoids during processing in a capillary rheometer.

The results from capillary rheometry presented in Figures D.1-3 agree with the work of Zhong et al. where the steady shear viscosity of the polymer overlaps with its corresponding nanocomposites. It should be noted that in the previous studies mentioned above [1-4], the capillary viscosity of only one concentration of nanocomposite was presented in each work with the clay loading varying from between 3 wt% to 5 wt%. The

results presented in this paper show that nanocomposites containing between 2 wt% to 8 wt% clay content at all three molecular weights exhibit possible shear induced alignment of unexfoliated clay tactoids. Even though XRD indicated that no exfoliation occurred, the viscosities of the HDPE matrices used in this study were sufficiently high so as to induce alignment of clay particles and process all nanocomposites through a 1 mm diameter capillary die without any significant increase in the pressure required to force the materials through the die. Typical industrial applications such as extrusion and injection molding operate at high shear rates equivalent to those used in this capillary study, thus the results presented here indicate that materials with improved mechanical and thermal properties as shown previously in this paper can be processed at the same conditions as their unfilled counterparts at the high shear rates encountered in common manufacturing operations.

References

1. N. Artzi, Y. Nir, M. Narkis, and A. Siegmann, *J. Polym. Sci. Part B: Polym. Phys*., **40**, 1741 (2002).
2. W. S. Chow, A. Abu Bakar, Z. A. Mohd Ishak, J. Karger-Kocsis, and U. S. Ishiaku, *Eur. Polym. Journal*, **41**, 687 (2005).
3. Y. Zhong, D. De Kee, *Polym. Eng. Sci*., **45,** 469 (2005).
4. T. D. Fornes, P. J. Yoon, H. Keskkula, D. R. Paul, *Polymer*, **42,** 9929 (2001).

Appendix E: Determination of Actual Clay Concentration

Table E.1 lists the actual compositions of the nanocomposites generated in this study. Here "organoclay" refers to the organically modified MMT used in this study, Cloisite 20A, and MMT represents pure MMT without the organically treated surface. Compositions were calculated by placing nanocomposite pellets generated from extrusion onto aluminum trays in an ashing oven at 500°C for 45 minutes. The actual weight fraction of organoclay in the nanocomposite (x_{OC}) was found from the following formula

$$x_{OC} = \left(\frac{m_{MMT} / x_{MMT\ burned}}{m_{NC}} \right) \tag{E.1}$$

where m_{MMT} is the mass of MMT actually in the nanocomposite which was taken to be the mass of ash remaining in the tray after being placed in the ashing oven, m_{NC} is the mass of the nanocomposite before being placed in the ashing oven, and $x_{MMT\ burned}$ is the mass fraction of MMT in the organoclay. $x_{MMT\ burned}$ was determined in a separate experiment where the organoclay itself was burned in the ashing oven and the ratio of the amount of MMT remaining (again taken to be the mass of ash left in the tray) to the original mass of organoclay prior to burning was found. By dividing this ratio (0.626) into the m_{MMT} described above, the original amount of organoclay in the nanocomposite can be calculated. It is noted that 0.626 represents the actual weight fraction of MMT or ash contained in the organoclay. The weight fraction of organic modifier (2M2HT) contained in the organoclay is then 0.374.

The actual weight fraction of MMT (x_{MMT}) in the nanocomposite was determined by the following formula

$$x_{MMT} = \left(\frac{m_{MMT}}{m_{NC}} \right) \tag{E.2}$$

where m_{ash} and m_{NC} were determined in the same manner as described above. The corresponding volume fraction of the organoclay (f_{OC}) and MMT (f_{MMT}) in the nanocomposites were found from the following equations

$$f_{OC} = \left(\frac{r_{NC} \times x_{OC}}{r_{OC}} \right) \tag{E.3}$$

and

$$f_{MMT} = \left(\frac{r_{NC} \times x_{NC}}{r_{MMT}} \right) \tag{E.4}$$

where r_{NC}, r_{OC}, and r_{MMT} are the densities of the nanocomposite, organoclay and MMT, respectively. r_{OC}, and r_{MMT} were taken to be 1.77 g/cm^3 and 2.86 g/cm^3, respectively, from the manufacturer. An upper bound on r_{NC} was estimated by using the rule of mixtures presented below:

$$r_{NC} = f_{HDPE} r_{HDPE} + f_{OC} r_{OC}. \tag{E.5}$$

Here f_{HDPE} and f_{OC} are the volume fractions of the HDPE matrix and organoclay, respectively. In order for r_{NC} to be calculated from Eq E.5, both f_{HDPE} and f_{OC} were estimated from the initial masses of HDPE and organoclay used to generate the nanocomposites as well as the given density values of the HDPE matrices and organoclay. These results are summarized in Table E.2.

Table E.1. Actual Composition of Nanocomposites.

	Post-Extrusion			
	Organoclay		Montmorillonite	
Label	**Wt%**	**Vol%**	**Wt%**	**Vol%**
2 wt% LMW	1.95	1.06	1.22	0.41
4 wt% LMW	4.01	2.20	2.51	0.85
8 wt% LMW	7.50	4.19	4.69	1.62
2 wt% MMW	1.85	1.01	1.16	0.39
4 wt% MMW	3.73	2.05	2.33	0.79
8 wt% MMW	7.91	4.43	4.95	1.72
2 wt% HMW	2.13	1.17	1.33	0.45
4 wt% HMW	3.99	2.22	2.50	0.85
8 wt% HMW	7.49	4.27	4.69	1.63

Table E.2. Estimated Density of Nanocomposites.

Label	m_{HDPE} **(g)**	m_{OC} **(g)**	V_{HDPE} **(cm^3)**	V_{OC} **(cm^3)**	f_{HDPE}	f_{OC}	r_{NC}
2 wt% LMW	98	2	102.83	1.13	0.989	0.011	0.962
4 wt% LMW	96	4	100.73	2.26	0.978	0.022	0.971
8 wt% LMW	92	8	96.54	4.52	0.955	0.045	0.990
2 wt% MMW	98	2	102.62	1.13	0.989	0.011	0.964
4 wt% MMW	96	4	100.52	2.26	0.978	0.022	0.973
8 wt% MMW	92	8	96.34	4.52	0.955	0.045	0.992
2 wt% HMW	98	2	102.08[a]	1.13	0.989	0.011	0.969
4 wt% HMW	96	4	100.00[a]	2.26	0.978	0.022	0.978
8 wt% HMW	92	8	95.83[a]	4.52	0.955	0.045	0.996

[a] actual density of HMW matrix was not given by manufacturer, therefore 0.96 g/cm3 was used as an estimate.

Vita

David Chu was born and raised in Atlanta, GA. He attended Tucker High School and subsequently enrolled at Georgia Institute of Technology to pursue his Bachelor's degree in chemical engineering which was awarded in August 2003 cum laude. Upon graduation from Georgia Tech the David worked in the field of environmental consulting with GeoSierra in Atlanta, GA before enrolling at Virginia Tech in August 2004 to pursue his Master's degree in chemical engineering. Under the guidance of Dr. Baird, the David began his graduate research in the area of polymer processing. His Master's degree was awarded in the Summer of 2006. After graduation the David was offered and accepted a job offer from BASF with his first assignment located in Wyandotte, MI.

David Chu